N O T I C E

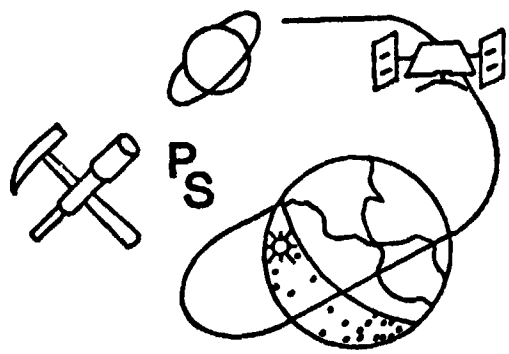
THIS DOCUMENT HAS BEEN REPRODUCED FROM MICROFICHE. ALTHOUGH IT IS RECOGNIZED THAT CERTAIN PORTIONS ARE ILLEGIBLE, IT IS BEING RELEASED IN THE INTEREST OF MAKING AVAILABLE AS MUCH INFORMATION AS POSSIBLE

N82-22131

(NASA-CP-168732) SPECTROSCOPIC STUDIES OF WATER AND WATER/REGOLITH MIXTURES ON PLANETARY SURFACES AT LOW TEMPERATURES Ph.D. Thesis (Hawaii Univ.) 340 p HC A15/MF A01 CSCL 03B G3/91 Unclas 18216

UNIVERSITY OF HAWAII

PLANETARY SCIENCES



ACCESSIONING, REPRODUCTION AND DISTRIBUTION
BY OR FOR NASA PERMITTED

HAWAII INSTITUTE OF GEOPHYSICS

2525 CORREA ROAD

HONOLULU, HAWAII 96822

REPRODUCTION RESTRICTIONS OVERRIDDEN

NASA Scientific and Technical Information Facility

ACCESSIONING, REPRODUCTION AND DISTRIBUTION
BY OR FOR NASA PERMITTED

SPECTROSCOPIC STUDIES OF WATER AND WATER/REGOLITH MIXTURES ON PLANETARY SURFACES AT LOW TEMPERATURES

ACCESSIONING, REPRODUCTION AND DISTRIBUTION BY OR FOR NASA PERMITTED

by

© ROGER NELSON CLARK

REPRODUCTION RESTRICTIONS OVERRIDDEN
NASA Scientific and Technical Information Facility

SPECTROSCOPIC STUDIES OF WATER and WATER/REGOLITH MIXTURES ON PLANETARY SURFACES AT LOW TEMPERATURES

by

© ROGER NELSON CLARK

B.S. (Physics) Seattle University (1975)

SUBMITTED IN PARTIAL FULFILLMENT
OF THE REQUIREMENTS FOR THE
DEGREE OF

DOCTOR OF PHILOSOPHY

MASSACHUSETTS INSTITUTE OF TECHNOLOGY

January 1980

Signature of Author Roger Nelson Clark
Department of Earth and Planetary Sciences, January 23, 1980

Certified by Thomas B. McCord
Thesis Supervisor

Accepted by _____
Chairman, Departmental Committee on Graduate Students

SPECTROSCOPIC STUDIES OF WATER AND WATER/REGOLITH MIXTURES ON PLANETARY SURFACES AT LOW TEMPERATURES

by

ROGER NELSON CLARK

Submitted to the
Department of Earth and Planetary Science on
January 23, 1980 in partial fulfillment of the
requirements for the degree of Ph.D.

ABSTRACT

New reflectance spectra of Ganymede, Europa, Callisto, Io, Saturn's rings, and Mars were obtained in the 0.65- to 2.5-μm spectral region. These spectra show several previously unreported features, and represent the best available data for determining the composition of these objects. The new data is combined with data covering other spectral regions for compositional interpretation.

To analyze these data, the spectral properties of water and mixtures of water plus other minerals were studied in the laboratory at the low temperatures typical of Mars, the Galilean satellites, and Saturn's rings. High precision reflectance spectra of water ice are studied showing the 2.0-, 1.65-, 1.5-, 1.25-,1.04-,0.90-, and 0.81-μm absorptions. The strengths of the absorptions are grain size dependent and the relative band depths are different for frost layers on thick ice than for pure frost. The higher overtones appear stronger relative to the lower overtones for frost on ice as compared to pure frost.

The spectral studies of minerals with bound water show that the bound water absorptions which occur at 1.4 and 1.9 μm do not shift appreciably in wavelength ($\lesssim$100Å) over a temperature range from 273 K to 150 K, and are distinguishable from the broader water ice absorptions at 1.5 and 2.0 μm.

Laboratory studies show that the decrease in reflectance at visible wavelengths seen in planetary reflectance spectra and containing water ice absorptions can be explained by water-mineral mixtures, mineral grains on frost, or frost on mineral grains. Mineral grains on frost are detectable in very small quantities (fractional areal coverage $\lesssim$0.005) depending on the mineral reflectance features, while it takes a thick layer of frost ($\gtrsim$1mm) to mask other mineral reflectance

properties at wavelengths shortward of 1.4 μm, again depending on the mineral reflectance features. Frost on a very dark surface (reflectance ∿6%) is easily seen, however a dark material mixed with water ice could completely mask water absorptions shortward of 2.5 μm.

The laboratory spectral studies were used to help determine the composition of the icy Galilean satellites, Saturn's rings, and Mars. The spectra of the icy Galilean satellites are characteristic of water ice or frost on ice rather than pure water frost, and the decrease in reflectance at visible wavelengths is characteristic of other mineral grains in the surface. No water is seen on Io. The spectra of Saturn's rings are more characteristic of water frost (rather than frost on ice) with some other mineral grains in the frost. The impurity grains on the icy Galilean satellites and Saturn's rings appear to have reflectance spectra typical of minerals containing Fe^{3+}. Ganymede is found to have more water ice on the surface than previously thought (∿90%) as is Callisto (30-60%). The surface of Europa has a vast frozen water surface with only a few percent impurities. Saturn's rings also have only a few percent impurities. There is very little bound water on these objects (5±5%). A new absorption feature is identified in the spectra of Ganymede, Callisto, and probably Europa at 1.15 μm which is also seen in spectra of Io, but not in Saturn's rings. This feature has not been seen in laboratory studies and its cause is unknown.

Spectra of the martian north residual polar cap confirms the results of the Viking IRTM and MAWD experiments which indicate that the cap is composed of water ice. Other absorptions in the spectrum indicate that hydrated minerals are also present. Spectra of other martian surface regions indicate the presence of small amounts of water ice and hydrated minerals in the bright albedo regions. Less water and hydrated minerals are seen in the dark albedo regions.

Thesis supervisor: Thomas B. McCord, professor of Planetary Geology

ACKNOWLEDGEMENTS

The many phases of this thesis required the assistance of a number of people. First among these is Tom McCord who provided support, help and encouragement throughout all the phases. I had many useful discussions about the interpretation of reflectance spectra and mineralogy in general with Mike Gaffey, Robert Huguenin, Fraser Fanale, Roger Burns, John Adams, and Robert Singer. I have greatly benefited from the professors at M.I.T.: John Lewis, Ronald Prinn, Irwin Shapiro, Jin Au Kong, and at the University of Hawaii: David Morrison, Dale Cruikshank, and Carl Pilcher. Discussion with Carle Pieters, Lucy McFadden, and Ray Hawke also proved useful in helping me to complete this work.

I would like to thank Mike Brookes and Jeffrey Bosel for their electronics and engineering assistance and Terry Jones and Richard Capps for sharing their knowledge of infrared dewar and indium antimonide detector technology. Sandra Ostrowski, Pam Owensby, Mark Rognstad, and Zeny Cocson provided technical and administrative support.

I would like to give my wife, Susan, my special thanks for her companionship, constant encouragement, and for always listening and helping me through stressful times. To my parents I give my appreciation for their concern, encouragement, and unfailing interest. To all

those forgotten in print but not in spirit I give my appreciation and thanks for their help. Finally, I would like to thank my dog, Kelly, for our long relaxing walks.

Table of Contents

	Page
Abstract	2
Acknowledgements	4
Introduction	8
Section I: Telescopic Studies	15
Chapter 1: The Galilean Satellites: New Near-Infrared Spectral Reflectance Measurements (0.65 - 2.5 μm) and a 0.325 - 5 μm Summary	16
Chapter 2: The Rings of Saturn: New Near-Infrared Reflectance Measurements and a 0.326 - 4.08 μm Summary	64
Chapter 3: Mars: Near-Infrared Reflectance Spectra of Surface Regions and Compositional Implications	92
Section II: Laboratory Studies	131
Chapter 1: Water Frost and Ice: The Near-Infrared Spectral Reflectance 0.65 - 2.5 μm	132
Chapter 2: The Spectral Reflectance of Water-Mineral Mixtures at Low Temperatures	178

		Page
Section III: Interpretation of Present Data		229
Chapter 1:	Mars Residual North Polar Cap: Earth-Based Spectroscopic Confirmation of Water Ice as a Major Constituent and Evidence for Hydrated Minerals	230
Chapter 2:	Ganymede, Europa, Callisto, and Saturn's Rings: Compositional Analysis from Reflectance Spectroscopy	251
Appendix A:	A Large Scale Interactive One Dimensional Array Processing System	309
Appendix B:	Atmospheric Extinction 0.65 - 2.50 μm Above Mauna Kea	331

Introduction

The purpose of this study is to determine the composition of icy solar system objects using spectrophotometric remote sensing techniques. This is done in three phases: (1) by acquiring the high quality telescopic data necessary for interpretation, (2) performing laboratory studies necessary to interpret the data, and (3) to apply the knowledge gained from the laboratory studies and remote sensing techniques in general to the interpretation of the data. The laboratory program was designed to fill a large gap in our understanding of the spectral properties of water and mixtures of water and other minerals so that the knowledge may be applied to present and future studies.

The thesis is organized in three sections: Telescopic Studies, Laboratory Studies, and the Interpretation of Present Data. The first section is primarily a presentation of telescopic results and includes only a small amount of interpretation. Telescopic data of sufficient quality to be analyzed were obtained on Mars, the Galilean satellites, and Saturn's rings, all of which show spectral signatures of water in varying degrees. In the case of Mars, however, the water signatures are weak (except for the polar cap) and thus the data warrant only the minimum interpretation given in section I, chapter 3. The martian north polar cap has a stronger

water signature and the interpretation is presented in section III.

Spectroscopic studies by other investigators have shown the presence of water ice on Saturn's satellites (Rhea, Dione, Tethys, Iapetus, Enceladus, and Hyperion), and the satellites of Uranus (Umbrial, Titania, and Oberon). However, due to the faintness of the objects, the spectroscopic data is not of sufficient quality to indicate the presence or absence of other minerals besides water ice, except in some cases where a decrease in reflectance toward visible wavelengths indicates surfaces which are not pure water ice. These objects were not studied in this thesis, however, it is hoped that the laboratory results will be of use when adequate data become available.

Section II presents the laboratory studies in a general manner. The laboratory section is an extended survey of the spectral properties water ice and other minerals in mixtures. The laboratory studies were designed to answer specific and general questions concerning the spectra of icy surfaces. Some of these questions are: (1) Why are the relative band depth ratios of the solid water features on the Galilean satellites and Saturn's rings different from laboratory spectra of water frost and from each other? (2) How does the presence of water affect the absorption bands and continua of other minerals? (3) Can the presence

of other minerals produce the decrease in reflectance at visible wavelengths observed on the Galilean satellites and Saturn's rings? (4) How does the presence of other minerals affect the shapes and depths of the water ice absorptions? The answers to these questions were found, at least in part, but due to the complexity of the mixture studies, many more years of research are needed to fully solve the problem.

Section III draws on the laboratory results in interpreting the existing telescopic data. The combination of the high quality telescopic data and the laboratory results has added significantly to our understanding of the composition of the Galilean satellites and Saturn's rings.

Due to the topics of the thesis and the arrival of the Voyager spacecrafts at Jupiter and Pioneer at Saturn, it was felt that the results should be made available to the investigating teams as soon as possible. For this reason, I elected to make each chapter a paper which has been or is to be submitted for publication and distributed to the scientific community. This has given both this study and myself advantages. I have learned and benefitted from other scientists in discussions relating to the results of the thesis. Each chapter stands on its own scientific merit, while collectively they present a complete research program. However, some duplication of of effort resulted due to the necessity of including

those sections dealing with instrument description and observation in each telescopic and laboratory paper. If, when reading this thesis, the reader wishes to skip the observations section of each individual paper, the general points and results will not be missed. For those particularly interested in observational technique, subtle differences can be found between papers. Additionally, differences may also be found between the experimental equipment and calibration sections of the laboratory papers. This duplication represents approximately one dozen pages of text (out of ∿240).

This thesis was completed in absentia from MIT at the University of Hawaii, where the work was performed at the Institute for Astronomy, the Hawaii Institute of Geophysics and the Mauna Kea Observatory 2.2-meter telescope. Working on this thesis in absentia also had some advantages and disadvantages. I experienced the workings of other groups and organizations, and met many other scientists working in this field. However, some time was lost in the major move of household and laboratory which could have been spent doing science. When moving the laboratory to Hawaii, everything had to be reorganized and set up again. Our software for data analysis needed rewriting. Although this was an annoying delay at times, it provided a greater understanding of how a laboratory is organized and is run. Thus the delay was well worth the experience, overall.

Due partly to the circumstances of the work in absentia but mostly to the opportunities made available to me by Tom McCord, this thesis represents a complete research program which included instrument design, implementation, software development, telescopic observations, laboratory studies and finally interpretation and synthesis. When I first arrived at MIT, I began work on a new infrared spectrometer using an Indium Antimonide solid state detector, a circular variable filter (covering the range 0.6 - 2.6 μm), and a sophisticated digital control system. The system was completed in approximately 8 months during which time I learned much about electronics and the importance of teamwork in designing and building the instrument. Over one month of testing at the 24-inch telescope at Wallace Observatory followed. As we started to obtain data, I wrote a few simple routines to analyze the data. Our first major observing run was on the 2.2-meter telescope on Mauna Kea in April of 1976 which turned out to be a major success. This observing run was our first in this spectral region and thus required the development of a new set of standards. In my naivety, I reduced the data in the way astronomers normally correct photometric data for atmospheric extinction. Due to our careful extinction measurements the data was excellent even in the 1.4- and 1.9-μm telluric water bands. Later, several astronomers informed us that observations could not be made through those absorption bands. On succeeding

observing runs, we continued to take data through these absorptions with good results. This method of obtaining data is described in Appendix B and it is now considered a standard technique to observe in this region by other groups.

At the time of the move to Hawaii, we decided to improve our system by cooling the circular variable filter and apertures. A new dewar was designed and built which employed a lower noise detector. The sensitivity of the system was increased by over a factor of 50. Due to the relocation to Hawaii, we lacked the software for a general data reduction and analysis facility. I set out to modify the routines used on the MIT Wallace Observatory computer and wrote a general interactive processing and analysis system that is now over 19,000 lines of FORTRAN in length. This is described in Appendix A and is in general use at the Planetary Sciences laboratory in Hawaii. All data in this thesis were analyzed using this system.

In order to interpret the telescopic data, a laboratory system had to be designed and built. The goniometer section was designed primarily by Robert B. Singer while I primarily designed the environmental chamber. The telescopic instrumentation was used on the laboratory system and thus provided the state-of-the-art in photometric precision.

This experience showed me the value and necessity of teamwork without which a research program such as this cannot succeed. I would like to thank Tom McCord again for his help and for the unusual opportunities which he made available to me.

SECTION I

TELESCOPIC STUDIES

SECTION I

CHAPTER 1

The Galilean Satellites: New Near-Infrared Spectral Reflectance Measurements (0.65-2.5 μm) and a 0.325-5 μm Summary

This chapter has been accepted for publication by the journal Icarus. Authors: R.N. Clark and T.B. McCord.

Abstract

New near-infrared (0.65 - 2.5 μm) reflectance spectra of the Galilean satellites with 1½% spectral resolution and ∿2% intensity precision are presented. These spectra more precisely define the water ice absorption features previously identified on Europa, Ganymede, and Callisto at 1.35 and 2.0 μm. In addition, previously unreported spectral features due to water ice are seen at 1.25, 1.06, 0.90, and 0.81 μm on Europa, and at 1.25, 1.04, and possibly 0.71 μm on Ganymede. Unreported absorption features in Callisto's spectrum occur at 1.2 μm, probably due to H_2O, and a weak, broad band extending from 0.75 to 0.95 μm, due possibly to other minerals. The spectrum of Io has only weak absorption features at 1.15 μm and between 0.8 and 1.0 μm. No water absorptions are positively identified in the Io spectra, incidating an upper limit of areal water frost coverage of 2% (leading and trailing sides). It is found for Callisto, Ganymede, and Europa that the water ice absorption features are due to free water and not to water bound or absorbed onto minerals. The areal coverage of water frost is ∿100% on Europa (trailing side), ∿65% on Ganymede (leading side) and 20-30% on Callisto (leading side). An upper limit of ∿5% bound water (in addition to the 20-30% ice) may be present on Callisto, based on the strong 3 μm band seen by other investigators. A summary of spectra of the

satellites from 0.325 to about 5 μm to aid in laboratory and interpretation studies is also presented.

Introduction

Water is the only material that has been positively identified on the surfaces of the Galilean satellites Europa, Ganymede and Callisto, and sulfur dioxide frost is the only material that has been identified on Io. Pilcher et al. (1972) determined that 5 to 25% of Callisto's surface, 20 to 65% of Ganymede's surface, and 50 to 100% of Europa's surface is covered by water ice. No water has been identified on Io. Lebofsky (1977) reported the presence of water frost on Callisto and Ganymede, but the results were based on only a few data points in the 3 μm region. More recently, Pollack et al. (1978), using data obtained on the Kuiper Airborne Observatory, reported that most of the water on Callisto is bound to minerals. They also found that the trailing side of Ganymede is 50±15% water ice, and the leading sides of Ganymede and Europa are 65±15% and greater than 85%, respectively. Their interpretation was based largely on theoretical spectra.

Nash and Fanale (1977) performed extensive laboratory studies to determine a compositional model for Io that was consistent with the then available full disk reflectance spectra. Their results indicated that the dominant mineral phases are free sulfur and sulfates. Their best match consisted of a fine-grained particulate mixture of free sulfur (55 vol. %), dehydrated bloedite

[$Na_2Mg(SO_4)_2 \cdot x\ H_2O$] (30 vol. %), ferric sulfate [$Fe_2(SO_4)_3\ x\ H_2O$] (15 vol. %), and trace amounts of hematite [Fe_2O_3]. Recently Fanale et al. (1979) identified SO_2 frost on Io based on the 4.08 μm band. However, SO_2 frost cannot account for the decrease in the visible reflectance indicating that free sulfur and sulfates probably still play a role.

It has been difficult to interpret the existing Galilean satellite spectra since they contain gaps (e.g. Pilcher et al., 1972; Fink et al., 1973) in spectral regions of telluric water absorption, or the photometric quality is much lower (5 - 10%) than is typical of laboratory data (∿1%). In order to best interpret reflectance spectra, they should be at least equivalent in quality to the laboratory data. We present here new satellite reflectance spectra in an attempt to provide the required data for compositional interpretation.

Observations

These measurements were obtained at Mauna Kea Observatory using the 2.2-m telescope during two observing runs (table 1). A continuously scanning circular variable filter (CVF) spectrometer and an indium antimonide detector were used. The spectral resolution is approximately 1½%. The spectrometer scans from 0.6 to 2.7 μm every 10 seconds. The spectra were coadded on successive scans and then written onto magnetic tape after 10 scans (100 seconds), which we call a run. The spectrum is made up of 120 data points (separate spectral channels). During the accumulation of data for each channel, the sky was subtracted (by chopping twice between sky and satellite) using a mirrored chopper rotating at 24 Hz. A sky-sky measurement was taken every few minutes. This residual signal (plus detector noise) was less than 1 - 2% (mostly being due to detector noise) of the satellite signal and was subtracted later by computer. The final analysis was completed using an interactive spectrum processing computer program (Clark, 1980a). The instrument and data reduction procedure are further discussed in McCord et al. (1978, 1980a, b).

In order to obtain accurate reflectance measurements, we compared the flux from the satellites with that from the star Beta Gemini and/or a lunar area in Mare

Serenatatis. The reflectance of this lunar area (called MS2) has been calibrated by laboratory and telescopic measurements of the Apollo 16 landing site surface material (McCord et al., 1972; Nygard, 1975; Adams and McCord, 1973; McCord et al., 1980a). The spectral flux of Beta Gemini was calibrated by using the derived MS2 reflectance. Thermal emission effects (which are less than 5% at 2.5 μm and negligible below 2 μm) from the MS2 and Apollo 16 calibrations have been removed using the analysis of Clark (1979). Color variations due to lunar phase angle effects may introduce slope errors of up to 5% in the derived reflectance. Residual lunar absorption features in this calibration procedure are less than about 1%. The reflectance of a solar system object is then calculated with the equation

$$R_{obj} = C \frac{I_{obj}}{I_{MS2}} R_{MS2}$$

where C is a scaling constant, R_{MS2} is the previously measured reflectance of MS2, I_{obj} is the intensity of the object measured at the telescope and I_{MS2} is the intensity of MS2 measured at the telescope. In order to calibrate for the effects of the earth's atmosphere, I_{obj} and I_{MS2} must be measured at, or calculated to, the same air mass. The standard (MS2 or Beta Gemini) was measured throughout each night and an extinction

analysis was performed (see McCord and Clark, 1979 for details). This resulted in high quality observations even in the strong telluric water bands at 1.4 and 1.9 μm.

The wavelength of each spectral channel was calibrated in the laboratory with a monochrometer and the calibration was checked with a narrowband 0.951-μm filter at the telescope. The absolute wavelength of each channel is accurate to better than 0.004 μm for the wavelength region 0.6 to 13.5 μm (channels 1-60) and to 0.008 μm for 1.32 to 2.6 μm (channels 61-120). The relative wavelength spacing between adjacent channels is accurate to approximately 0.001 μm.

The indium antimonide detector, CVF, apertures, and relay lenses were all operated at solid nitrogen temperature to minimize detector noise. The signal-to-detector noise for Ganymede was about 100 for each channel in one run (10 coadded scans at 10 seconds per scan). However, seeing degraded this somewhat so that many runs were averaged together. The error bars on our data represent ±1 standard deviation of the mean of the average. Table I shows the observing parameters for the satellite and standard observations. The final data have been averaged into leading and/or trailing side spectra for each satellite. The lunar area MS2 was the primary calibration on Dec. 18, while

Beta Gemini was the standard on Jan. 2 and 3 UT. Beta Gemini was calibrated to the sun via the MS2 data from Dec. 18 and was verified with calibrations derived on previous observing runs which also used the moon. The Beta Gemini/Sun ratio from Dec. 18 agrees well with our previous calibrations of Beta Gemini.

Results

The Galilean satellite reflectance spectra obtained from the three nights are shown in figure 1 along with data from McFadden et al. (1980) for comparison in the very near infrared. The data of McFadden et al. agree in general with those of Johnson and McCord (1970), Wamsteker (1972), and Nelson and Hapke (1978). Some differences occur among all these data sets, most of which are due to differences in orbital and solar phase angles at which the data were taken. The spectra obtained are shown in figure 2. The spectrum of Io from 0.65 to 2.5 μm has relatively weak features, while Europa and Ganymede show several strong features. Callisto appears to have spectral features intermediate between Io and Ganymede. We briefly discuss the features present, then compare our measurements with others, and finally discuss the interpretation.

The most prominent absorption (in this spectral region) in the Io spectrum occurs at 1.15 μm, with a band depth of 5%. The trailing and leading side spectra are nearly identical. Shortward of this band is a broad weak feature (2.5 - 3%) extending from 0.8 to 1.0 μm. The spectrum has a relative peak at 1.4 μm. The reflectance then drops 5 to 7% from 1.4 to 1.5 μm. Beyond 1.5 μm, the spectrum is essentially featureless, decreasing slowly to 2.5 μm. The small rise at 1.9 μm

in the trailing spectrum is due to a slight error in telluric water removal which may also affect the 1.4-μm region. Note that the error bars are slightly larger at 1.4 and 1.9 μm due to the uncertainty in telluric water removal. The leading side spectrum shows no rise at 1.9 μm.

Europa's trailing side spectrum shows much stronger bands than any other Galilean satellite spectrum in this data set. There are two very broad, deep asymmetric features at 1.53 and 2.0 μm, and there is a small weak feature at 1.65 μm. Absorption features which have not been identified before in the literature are at 1.25 μm (10-11% depth), 1.06 μm (4% depth), 0.91 μm (4% depth), and 0.81 μm (2.5%).

Ganymede shows absorption bands similar to Europa except that the 1.53- and 2.0-μm bands are more symmetric. The bands are at 2.0 μm (46% depth), 1.65 μm (7-8% depth), and 2.53 μm (43% depth). Bands not reported previously in the literature are at 1.26 μm (11-12% depth), and 1.03 μm (3%), and a broad (2-3%) feature extending from just below 0.8 μm to just below 1.0 μm. There may be a weak (3%) band at 0.81 μm at the short side of this broad band.

Callisto has a 2.0-μm absorption band (12% depth) and a 1.53-μm band (18% depth) which were identified previously, but they were poorly defined (Pollack et al., 1978). Bands which have not been identified before are

at 1.2 μm (7% depth) and a weak, broad feature (5% depth) extending from 0.75 to 0.95 μm. This last band may be a composite of two bands at 0.84 and 0.91 μm.

Comparison With Other Data

Comparison of our data with other published data in this spectral region are shown in figures 3-6. The Hansen (1975), Lee (1972) and Moroz (1965) data are not available separated into leading and trailing side measurements. The Io spectra (figure 3) show a major discrepancy between our results and those of Pollack et al. (1978), and also possibly Lee (1972) and Hansen (1975). However, the Moroz (1965) data agree quite well with ours. The results for Europa and Ganymede (figures 4 and 5) all agree quite well. The Callisto (figure 6) spectra show a discrepancy similar to that for the Io spectra.

It is puzzling that measurements for some objects agree while for others they do not. Two possible explanations occurred to us: (1) the spectra of the bodies change with time, or (2), the calibration procedure was different for different objects. For example, Pollack et al., used several standard stars (α Leo, β Gemini, and Polaris). Pollack et al. (1978) used α Leo and Polaris for the calibration of the Io trailing spectrum, Polaris and β Gemini for Io leading, Polaris for Europa trailing, Polaris for Ganymede leading, and α Leo and Polaris for

the Callisto leading side spectrum (Pollack 1979, private communication). It was then assumed that α Leo was a black body of 12,000 K and Polaris a black body of 5600 K. The spectra of Pollack et al. (1978) which do not agree with ours are those in which α Leo was used in the calibration. We measured α Leo in April 1976 at Mauna Kea on the 2.2-m telescope and have plotted the resulting calculation, α Leo/12,000 K black body in figure 7 at the wavelengths of Pollack et al. Applying this "correction" spectrum to the Pollack et al. leading side spectrum of Io produces the result in figure 8. The agreement with our data is now much better. Similar results were obtained with the Io trailing side and both Callisto spectra, although the corrected Io trailing spectrum would be slightly low beyond about 1.7 μm. Also, Polaris may not be a good standard since it is a known variable star with a variable period (Kukarkin et al., 1969). Pollack (1979 - private communication) believes this could introduce a slope uncertainty of up to approximately 5%.

Figure 1 compares our data with the visible data of McFadden et al. (1980). In general, the region of overlap agrees quite well. The 0.9-μm feature is apparent in both sets of data for the leading and trailing sides of Io. The Europa data sets show the 0.9-μm band well, but the overall match is not as good as the matches for Io, Ganymede, and Callisto. The Ganymede data overlap nicely

but the "visible" data do not show the 0.8-μm band. The Callisto data agree well but the rise in our data in the short wavelength limit appears spurious. See McFadden et al. (1980) for a summary of visible reflectance data.

Laboratory spectra of water frost for several grain sizes are shown in figure 9 (Clark 1980b). The absorption features at 2.02, 1.65, 1.53, 1.25 μm are well known and are commonly seen in laboratory ice spectra (e.g. Ockman, 1958; Fink and Larson, 1975). Higher overtones identified by Clark (1980b) are located at 1.04, 0.90, and 0.81 μm. All of these features can be seen in the Europa and Ganymede spectra (figure 2). The 1.53-, 2.02-μm, and possibly the 1.65-μm ice bands are seen in Callisto. There is a strong band at 1.20 μm in the Callisto spectrum that appears similar to the 1.25-μm ice band, but shifted shortward. However, the 1.20-μm band depth in Callisto is much stronger (relative to the 1.5- and 2-μm bands) than in water ice. There is also an indication of 0.90- and 0.81-μm bands. Bound water bands occur at 1.4 and 1.9 μm (Hunt and Salisbury, 1970, 1971; Hunt et al., 1971a, b; 1972; 1973) at room temperature, and Clark (1980c) has shown that these bands shift less than 0.01 μm when the temperature is lowered to 150 K. Therefore, it is not difficult to distinguish free water ice from bound water (Clark, 1980c). We see no evidence based on the 1.53- and 2.02-μm bands in Europa, Ganymede, and Callisto for bound water. The 1.2-μm band in Callisto is unusual compared to a pure water ice spectrum, but it is similar to features seen in spectra of Mars (McCord et al., 1978, 1980b) and in Io (figure 2). The Io

absorption is even shorter in wavelength (1.15 μm), however, and may not be related to water since there is no 3-μm band as on Europa, Ganymede, and Callisto (Pollack et al., 1978). Pollack et al. (1978) reported that most of the water reported on Callisto is bound. Comparison of their Callisto spectra with ours (figure 6) shows that their water bands are at shorter wavelengths than for ice. Their features are similar to features obtained when the earth's atmospheric water content in the line of observation for the satellite is different than that for the standard star, resulting in improper calibration of the earth's atmospheric water absorption. This explanation seems unlikely, however, since the data were obtained with the Kuiper Airborne Observatory where the absorption due to telluric water at 1.4 and 1.9 μm is typically 2% (Pollack, 1979 - private communication). Although the bands are shifted to shorter wavelengths than in ice, they are at longer wavelengths than those common in minerals (Hunt and Salisbury, 1970, 1971; Hunt et al., 1971a, b, 1972, 1973; Clark 1980c) and may be due to some other calibration difference.

The Io spectra (figure 2) are more puzzling. The only major absorption is the 1.15-μm band. A weaker broad feature occurs near 0.9 μm. There is a curious rise in the spectrum from 1.2 to 1.45 μm which we believe is a property of the satellite spectrum. The

drop beyond 1.45 μm is not typical of a water ice or hydroxyl absorption; with no 3-μm fundamental present (Pollack et al., 1978), H_2O or OH seems ruled out.

Composite Spectra 0.3 - 5 μm

In order to interpret properly the reflectance spectrum of an object to determine composition, it is desirable to have the greatest wavelength coverage possible. Thus composite spectra of the Galilean satellites from 0.325 to approximately 5 μm using data from the literature were prepared.

The composite spectra of Io are shown in figures 10 and 11. Absorption features not discussed (in this paper) previously are at 2.5 and 4.08 μm. However, the reality of the 2.5-μm band is questionable, especially since two independent measurements are joined at 2.5 μm and there are apparent calibration differences (see figure 3a). In defense of the 2.5-μm band, we point out that the Pollack et al. spectrum which bridges this region does appear to show the band but the precision of the data appears to be near the magnitude of the band. Pollack et al. (Pollack, 1979- private communication) have other unpublished Io data which confirm the existence of the 2.5-μm band. Also our reflectance spectrum is decreasing with increasing wavelength as might be expected for the wing of an absorption band. The trailing side spectrum of Io (figure 10b) shows the possibility of the 2.5-μm feature, although there may be some differences compared to the leading side. Cruikshank (1980) has measured Io at many orbital phase

angles to produce a higher resolution and higher photometric quality spectrum than Pollack et al. (1978). His spectrum was used in making the composite shown in Figure 11. In addition to the absorption band at 4.08 μm, originally reported by Cruikshank et al. (1978), the Cruikshank data show absorptions at 3.80, 3.18 and 2.95 μm. Recently, Fanale et al. (1979) reported that the 4.08-μm band was due to sulfur dioxide frost and that the 3.18-μm band may be due to H_2S absorbed in the surface. In addition, the reflectance spectrum of SO_2 frost is nearly featureless in the 0.65- to 2.5-μm region and has a downward slope similar to the spectrum of Io. The two weak bands at 2.95 and 3.18 μm are at similar wavelengths to the water fundamentals ν_1(∿3.11 μm) and ν_3(∿2.94 μm). If these bands are the water fundamentals, the amount of water present on the surface is very small ($\lesssim 10^{-3}$% based on studies of bound water by Pollack et al. (1978) or ≲2% areal frost coverage). However, these bands could be due to incomplete removal of telluric water bands in this region and the measurements should be confirmed. The limit of detectable water band strength in the 1.5- to 2-μm region is 1-2%, indicating an upper limit from these bands of ≲2% for the areal coverage of water ice. This limit is the same as for the 3-μm band because the data are of higher precision, although sensitivity is less by approximately a factor of 1.5.

The composite spectrum of Europa is shown in Figure 17. The region beyond 2.5 μm is dominated by water absorptions and Europa appears essentially black from 3 to 5 μm (Pollack et al., 1978).

The composite spectrum of Ganymede (Figure 13) shows the O-H stretch fundamental at 3 μm in addition to the features already discussed. The rise in the reflectance beyond 3 μm is due to minerals other than water frost (e.g. Pollack et al., 1978). The fractional areal coverage of water frost is approximately 65% based on the water ice reflectance spectra in figure 9. This agrees well with Pollack et al. (1978).

The composite spectrum of Callisto (Figure 14) shows the 3-μm water fundamental, but the relative reflectance is higher than for Ganymede. The shape of the 3-μm band is questionable since there are differences in the Pollack et al. 1.4- and 1.9-μm absorption features, as discussed previously (see figure 6). Based on the 12 and 15% band depths of the 2- and 1.5-μm water bands, respectively, in our new data, the areal coverage of water frost is found to be 20 to 30% from the observed band depth range of the water frost spectra in figure 9. The limit of bound water on Callisto is about 5 ± 5%, based on the absence of absorptions at 1.4 and 1.9 μm. However 5% bound water could strongly effect the 3-μm band explaining the conclusion of Pollack et al. (1978) that all of the water on Callisto is bound.

Conclusions

New reflectance data for the Galilean satellites have been obtained in the 0.65- to 2.5-μm region which clearly define water ice absorptions on Europa, Ganymede, Callisto and which reveal previously unreported absorption bands on all four satellites. No evidence is found for bound water in the 0.3- to 2.5-μm region for any of the satellites, rather, the water on Europa, Ganymede, and Callisto appears to be in the form of ice patches (e.g. frost, puddles, lakes). Although a few percent bound water may be on the surface, it is small compared to the amount of free water present. The water ice signature on the trailing side of Europa is so strong that it must be covered almost completely by water ice with a grain size of several millimeters or greater. The depth, in order to be optically thick, must then be a centimeter or more. The areal coverage of water frost on Io is $\lesssim$2%, on Callisto 20-30% and on Ganymede approximately 65%.

The spectra presented here are currently undergoing a detailed analysis and the results will be presented in a future paper (Clark, 1980d) along with implications from the Voyager spacecraft results.

Acknowledgements

We thank Pamela Owensby, Jeffrey Bell and Mark Rognstad for helping with the observations. We had helpful discussions with Fraser Fanale, Dale Cruikshank, and James Pollack. This research was supported by NASA grants NSG 7323 and NSG 7312.

References

ADAMS, J.B., and MCCORD, T.B. (1973). Vitrification darkening in the lunar highlands and identification of the Descartes material at the Apollo 16 site. Proc. 4th Lunar Sci. Conf., 1, 163-177.

CLARK, R.N. (1979). Planetary reflectance measurements in the region of planetary thermal emission. Icarus 40, 94-103.

CLARK, R.N. (1980a). A large scale interactive one-dimensional array processing system. P.A.S.P., submitted. Thesis App A

CLARK, R.N. (1980b). Water frost and ice: The near-infrared reflectance 0.65 - 2.5 μm. J. Geophys. Res., submitted. Thesis II Ch1

CLARK, R.N. (1980c). The spectral reflectance of water-mineral mixtures at low temperatures. J. Geophys. Res., submitted. Thesis II Ch2

CLARK, R.N. (1980d). Ganymede, Europa, Callisto, and Saturn's rings: Compositional analysis from reflectance spectroscopy. Icarus, submitted. Thesis III Ch2

CRUISKHANK, D.P. (1980). Infrared spectrum of Io, 2.8 - 5.3 μm. Icarus, in press.

CRUIKSHANK, D.P., JONES, T.J., and PILCHER, C.B. (1978). Absorption bands in the spectrum of Io. Astrophys. J. Lett. 225, L89-192.

FANALE, F.P., BROWN, R.H., CRUIKSHANK, D.P., and CLARK, R.N. (1979). Significance of absorption features in Io's infrared reflectance spectrum. Nature 30, 761-763.

FINK, U., DEKKERS, N.H., and LARSON, H.P. (1973). Infrared spectra of the Galilean satellites of Jupiter. Astrophys. J. Lett. 179, L155-L1159.

FINK, U., and LARSON, H.P. (1975). Temperature dependence of the water ice spectrum between 1 and 4 microns: Application to Europa, Ganymede and Saturn's rings. Icarus 24, 411-420.

HANSEN, O.L. (1975). Infrared albedos and rotation curves of the Galilean satelliites. Icarus 26, 24-29.

HUNT, G.R., and SALISBURY, J.W. (1970). Visible and near-infrared spectra of minerals and rocks: I. Silicate minerals. Mod. Geol. 1, 283-300.

HUNT, G.R., and SLIASBURY, J.W. (1971). Visible and near-infrared spectra of minerals and rocks: II. Carbonates. Mod. Geol. 2, 23-30.

HUNT, G.R., SALISBURY, J.W., and LENHOFF, C.J. (1971a). Visible and near-infrared spectra of minerals and rocks: III. Oxides and hydroxides. Mod. Geol. 2, 195-205.

HUNT, G.R., SALISBURY, J.W., and LENHOFF, C.J. (1971b). Visible and near-infrared spectra of minerals and rocks: IV. Sulphides and sulphates. Mod. Geol. 3, 1-14.

HUNT, G.R., SALISBURY, J.W., and LENHOFF, C.J. (1972). Visible and near-infrared spectra of minerals and rocks: V. Halides, phosphates, arsenates, vanadates, and borates. Mod. Geol. 3, 121-132.

HUNT, G.R., SALISBURY, J.W., and LENHOFF, C.J. (1973). Visible and near-infrared spectra of minerals and rocks: VII. Acidic igneous rocks. Mod. Geol. 4, 217-224.

JOHNSON, T.V., and MCCORD, T.B. (1970). Galilean satellites - the spectral reflectivity 0.30-1.10 micron. Icarus 13, 37-42.

KUKARKIN, B.V., KHOLOPOV, R.N., EFREMOV, Y.N., KUKARKINA, N.P., KUROCHKIN, N.E., MEDVEDEVA, G.I. PEROVA, N.B., FEDOROVICH, V.P., and FROLOV, M.S. (1969). General Catalog of Variable Stars V.2. Academy of Sciences, Moscow.

LEBOFSKY, L. (1977). Identification of water frost on Callisto. Nature 269, 785-787.

LEE, T. (1972). Spectral albedos of the Galilean satellites. Comm. Lunar Planet. Lab. 9, 179-180.

MCCORD, T.B., CHARETTE, M.P., JOHNSON, T.V., LEBOFSKY, L.A., and PIETERS, C. (1972). Lunar spectral types. J. Geophys. Res. 77, 1349-1359.

MCCORD, T.B., and CLARK, R.N. (1979). Atmospheric extinction 0.65 - 2.50 μm above Mauna Kea. P.A.S.P. 91, 571-576. Thesis App B

MCCORD, T.B., CLARK, R.N., and HUGUENIN, R.L. (1978). Mars: Near-infrared spectral reflectance and compositional implication. J. Geophys. Res. 83, 5433-5441.

MCCORD, T.B., CLARK, R.N., MCFADDEN, L.A., PIETERS, C.M., OWENSBY, P.D., and ADAMS, J.B. (1980). Moon: Near-infrared spectral reflectance, a first good look. J. Geophys. Res., submitted.

MCCORD, T.B., CLARK, R.N., SINGER, R.B., and HUGUENIN, R.L. (1980). Mars: Near-infrared reflectance spectra of surface regions and compositional implications. J. Geophys. Res., to be submitted. Thesis I Ch 3

MCFADDEN, L.A., BELL, J., and MCCORD, T.B. (1980). Visible spectral reflectance measurements 0.3 - 1.1 μm of the Galilean satellites at many orbital phase angles 1977-1978. To be submitted to Icarus.

MOROZ, V.I. (1965). Infrared spectrophotometry of satellites: The moon and the Galilean satellites of Jupiter. Astron. Zh. 42, 1287; trans. in Soviet Astron. - AJ 9, 999-1006.

NASH, D.B., and FANALE, F.P. (1977). Io's surface composition based on reflectance spectra of sulfur/salt mixtures and proton-irradion experiments. Icarus 31, 40-80.

NELSON, R.M., and HPAKE, B.W. (1978). Spectral reflectivities of the Galilean satellites and Titan 0.32 to 0.86 micrometers. Icarus 36, 304-329.

NYGARD, S. (1975). Alpha Lyrae/sun flux ratios for use in standard star calibration: Results of three techniques. Masters Thesis, Massachusetts Institute of Technology, Cambridge.

OCKMAN, N. (1958). The infrared and Raman spectra of ice. Advan. Phys. 7, 199-220.

PILCHER, C.B., RIDGWAY, S.T., and MCCORD, T.B. (1972). Galilean satellites: Identification of water frost. Science 178, 1087-1089.

POLLACK, J.B., WITTEBORN, F.C., EDWIN, F.E., STRECKER, D.W., BALDWIN, J.B., and BUNCH, B.E. (1978). Near-infrared spectra of the Galilean satellites: Observation and compositional implications. Icarus 36, 271-303.

WAMSTEKER, W. (1972). Narrow band photometry of the Galilean satellites. Comm. Lunar Planet. Lab., No. 167, 171-177.

Figure Captions

Figure 1: The spectra of McFadden et al., 1980 are compared with the data from this study in the overlap region of the two data sets. In general, the agreement is excellent.

Figure 2: The reflectance of spectra of the Galilean satellites obtained during the nights listed in Table 1. The geometric albedos at 1 μm are 0.90 (Io - leading), 0.85 (Io - trailing), 0.23 (Callisto - leading), 0.53 (Ganymede - leading) and 0.60 (Europa - trailing).

Figure 3: (A) A comparison of the spectra of the leading side of Io. The Hansen (1975), Lee (1972) and Moroz (1965) data were not presented as leading or trailing sides and are the same in both (A) and (B). (B) The comparison of the Io trailing spectra.

Figure 4: A comparison of the spectra of the trailing side of Europa. It is not known if the Hansen, Lee, and Moroz data are of the trailing or leading side.

Figure 5: The comparison of leading side spectra of Ganymede. The Hansen, Lee, and Moroz data are of unknown sides.

Figure 6: (A) The spectra of the leading side of Callisto are compared along with the Callisto

spectra of Hansen (1975) and Lee (1972). The unusual absorption in the Pollack et al. data at 1.5 μm appears somewhat like an error in telluric water removal which we occasionally encounter in our own measurements of solar system objects, although it is not certain if this is the cause (see text). (B) The spectra of mixed sides of Callisto are compared. The Pollack et al. spectrum may have residual telluric water at 1.4 and 1.9 μm.

Figure 7: The spectrum of Alpha Leonis divided by a 12,000 K black body and convolved from our CVF measurement to the wavelengths of the Pollack et al. Io leading side spectrum.

Figure 8: The spectrum of the leading side of Io by Pollack et al. (1978) and multiplied by the Alpha Leo/12,200 K black body spectrum in figure 9 is compared to our measurements.

Figure 9: The spectral reflectance of water frost of different grain sizes (from Clark, 1980b). Halon is a white reflectance standard. These data were taken with the same CVF spectrometer as the Galilean satellite spectra presented in this paper. The phase angle is 10° with normal incidence. The fine grained frost is approximately 30 micrometers and the coarse is several millimeters.

Figure 10: The composite spectra of Io for the (A) leading side, (B) trailing side.

Figure 11: The composite spectrum of the leading side of Io except for the Cruikshank data which are mixed orbital phases.

Figure 12: The composite spectrum of the trailing side of Europa. The reflectance of Europa longward of 4.2 μm is essentially black (Pollack et al., 1978).

Figure 13: The composite spectrum of the leading side of Ganymede.

Figure 14: The composite spectrum of the leading side of Callisto.

Table 1

Galilean Satellite Observations

Object	Date (UT)	UT Time	Airmass Range	# Scans	Orbital Phase Angle (in degrees)
J1 (leading)	12/18/78	12:21 - 13:15	1.000 - 1.028	80	118.1 - 125.7
J3 (leading)	12/18/78	13:30 - 15:02	1.001 - 1.099	140	92.5 - 95.7
Beta Gemini	12/18/78	13:01 - 15:31	1.023 - 1.390	30	---
MS2	12/18/78	12:11 - 15:47	1.006 - 1.270	170	---
J1 (trailing)	01/02/79	9:41 - 10:38	1.088 - 1.244	150	269.1 - 277.2
J2 (trailing)	01/02/79	11:11 - 14:44	1.037 - 1.217	250	236.1 - 249.8
J4 (leading)	01/02/79	7:59 - 12:40	1.000 - 2.024	210	122.0 - 126.2
Beta Gemini	01/02/79	7:32 - 12:57	1.013 - 1.910	560	---
J1 (leading)	01/03/79	7:57 - 11:18	1.024 - 1.984	230	98.2 - 126.6
J4 (leading)	01/03/79	9:16 - 12:16	1.000 - 1.333	400	144.2 - 147.3
Beta Gamini	01/03/79	6:44 - 11:33	1.011 - 2.168	520	---

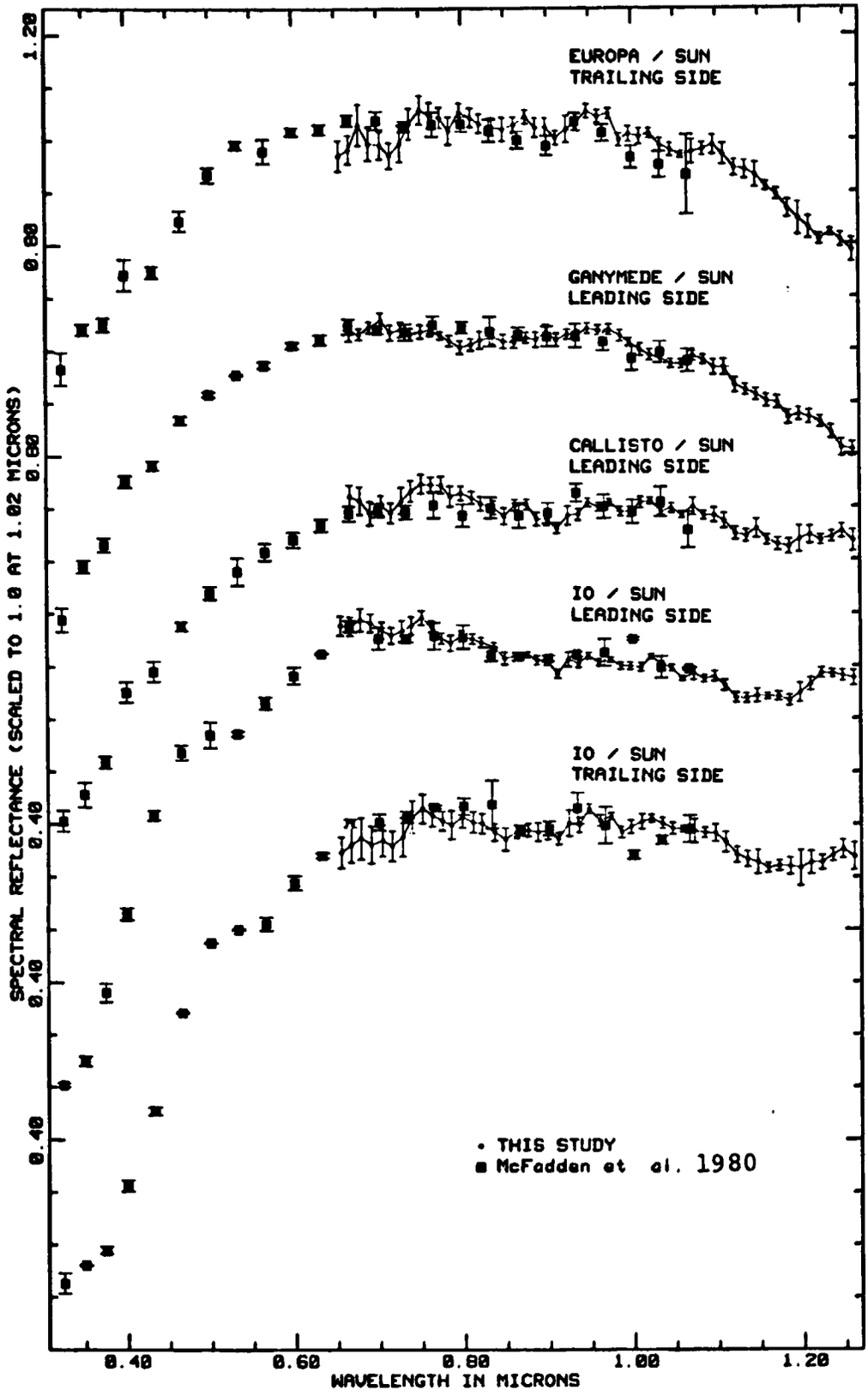

EUROPA / SUN
TRAILING SIDE
GANYMEDE / SUN
LEADING SIDE
CALLISTO / SUN
LEADING SIDE
IO / SUN
LEADING SIDE
IO / SUN
TRAILING SIDE
• THIS STUDY
■ McFadden et al. 1980
SPECTRAL REFLECTANCE (SCALED TO 1.0 AT 1.02 MICRONS)
WAVELENGTH IN MICRONS
0.40
0.60
0.80
1.00
1.20

Figure 1

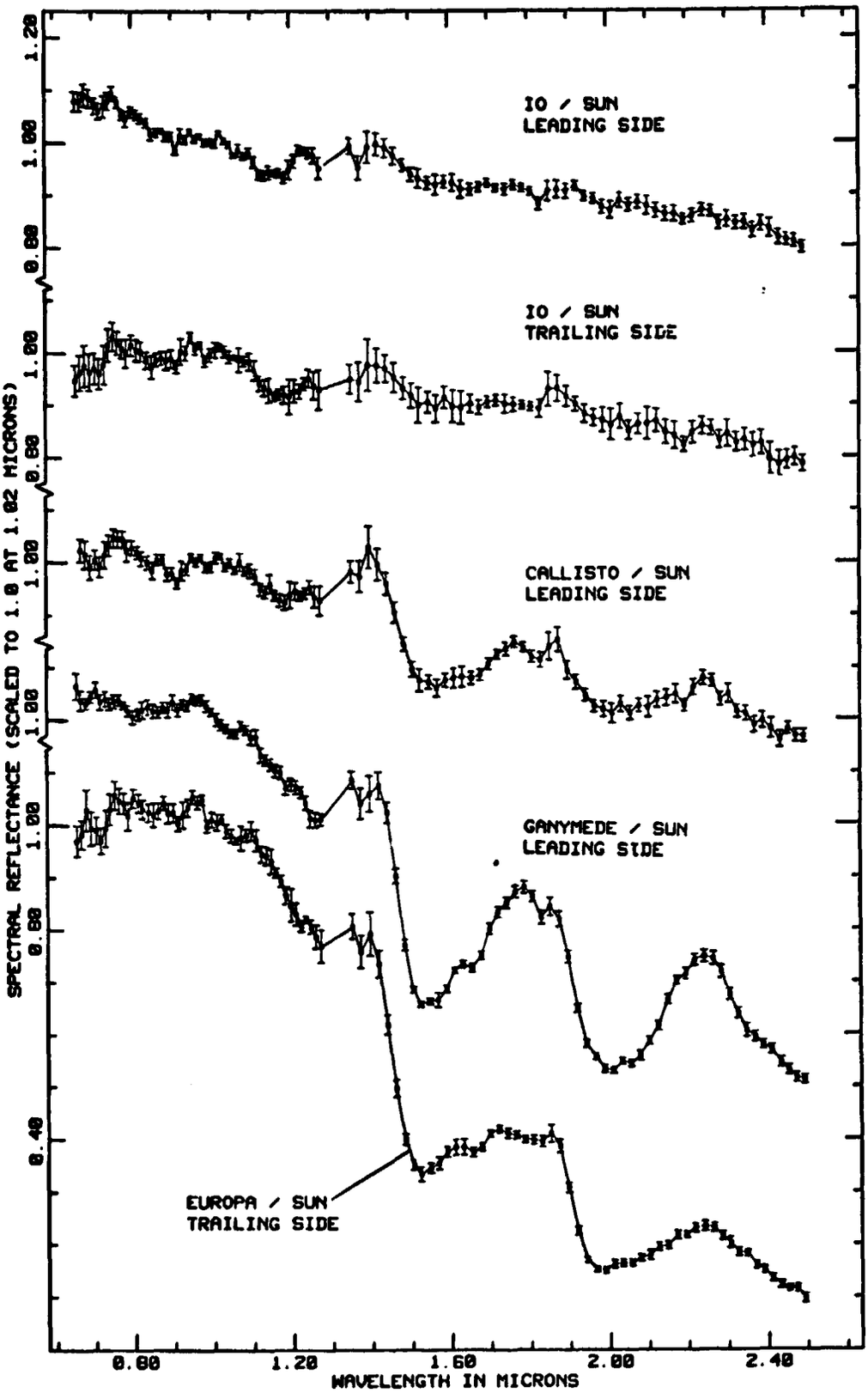

IO / SUN
LEADING SIDE
IO / SUN
TRAILING SIDE
CALLISTO / SUN
LEADING SIDE
GANYMEDE / SUN
LEADING SIDE
EUROPA / SUN
TRAILING SIDE
SPECTRAL REFLECTANCE (SCALED TO 1.0 AT 1.02 MICRONS)
1.20
1.00
0.80
1.00
0.80
1.00
1.00
0.80
0.40
0.00
1.20
1.60
2.00
2.40
WAVELENGTH IN MICRONS

Figure 2

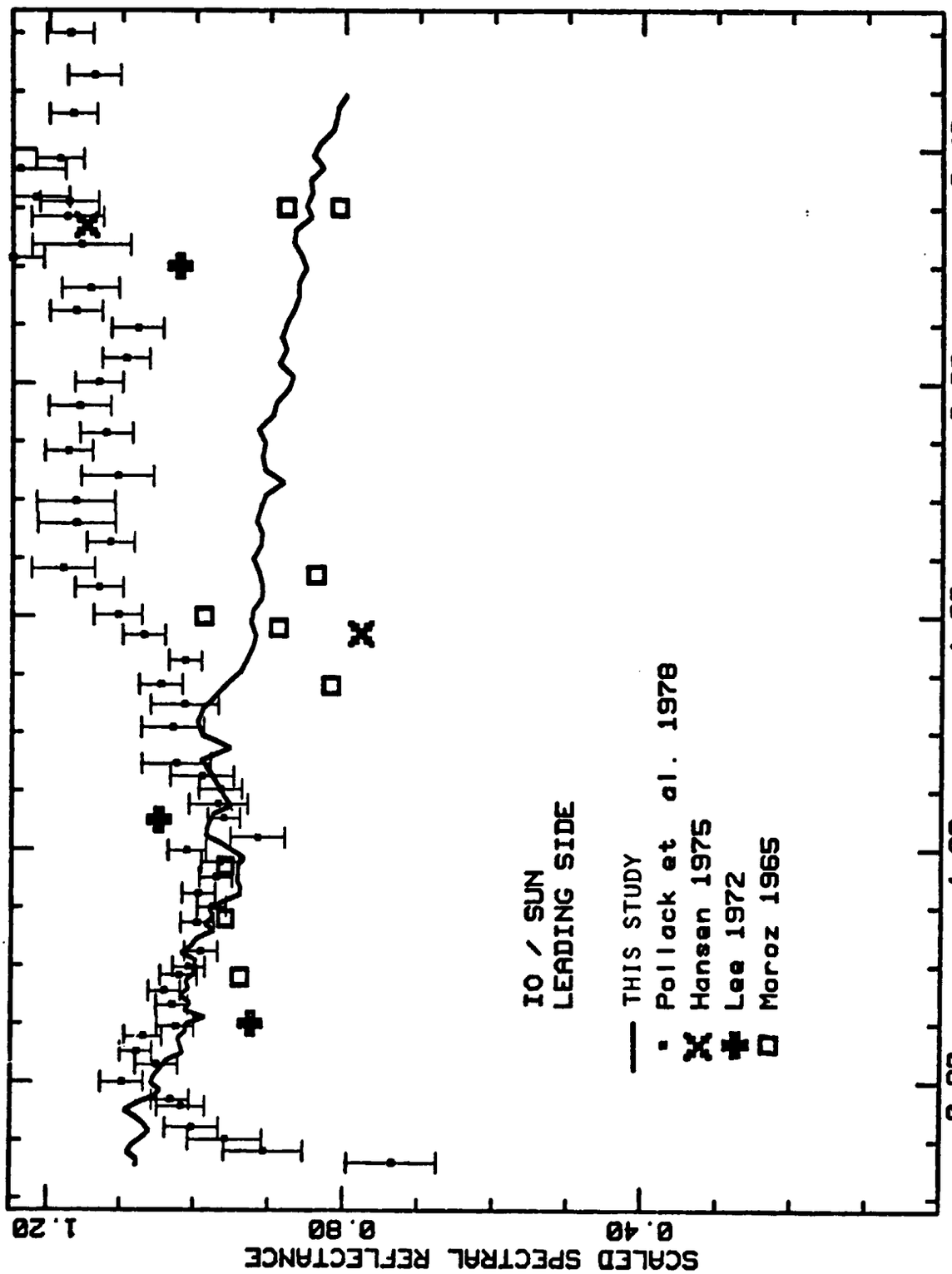

IO / SUN
LEADING SIDE
THIS STUDY
Pollack et al. 1978
Hansen 1975
Lee 1972
Moroz 1965
SCALED SPECTRAL REFLECTANCE
0.40
0.80
1.20
WAVELENGTH IN MICRONS
0.80
1.20
1.60
2.00
2.40

Figure 3A

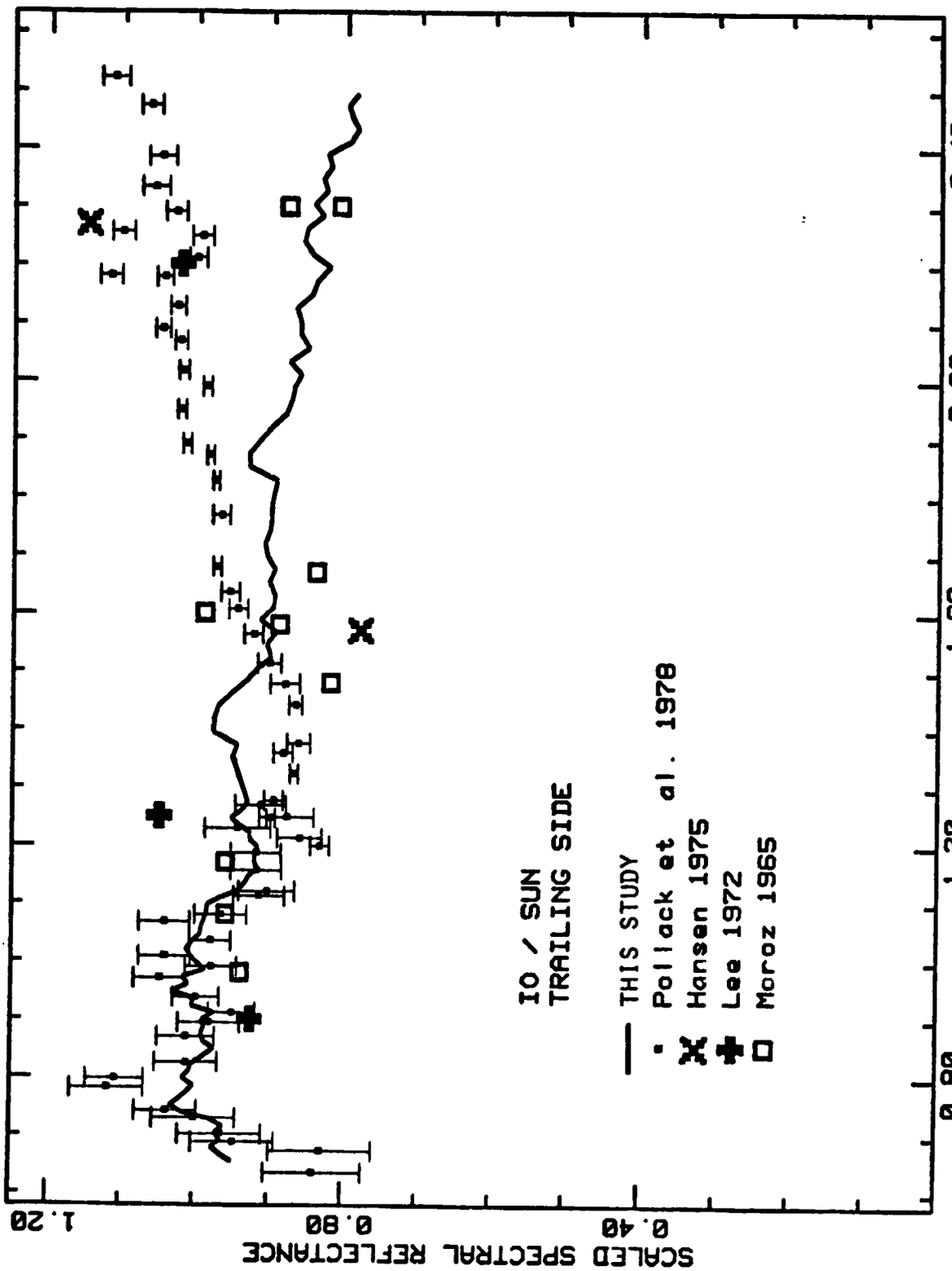

SCALED SPECTRAL REFLECTANCE
0.40
0.80
1.20
WAVELENGTH IN MICRONS
0.80
1.20
1.60
2.00
2.40
IO / SUN
TRAILING SIDE
THIS STUDY
Pollack et al. 1978
Hansen 1975
Lee 1972
Moroz 1965

Figure 3B.

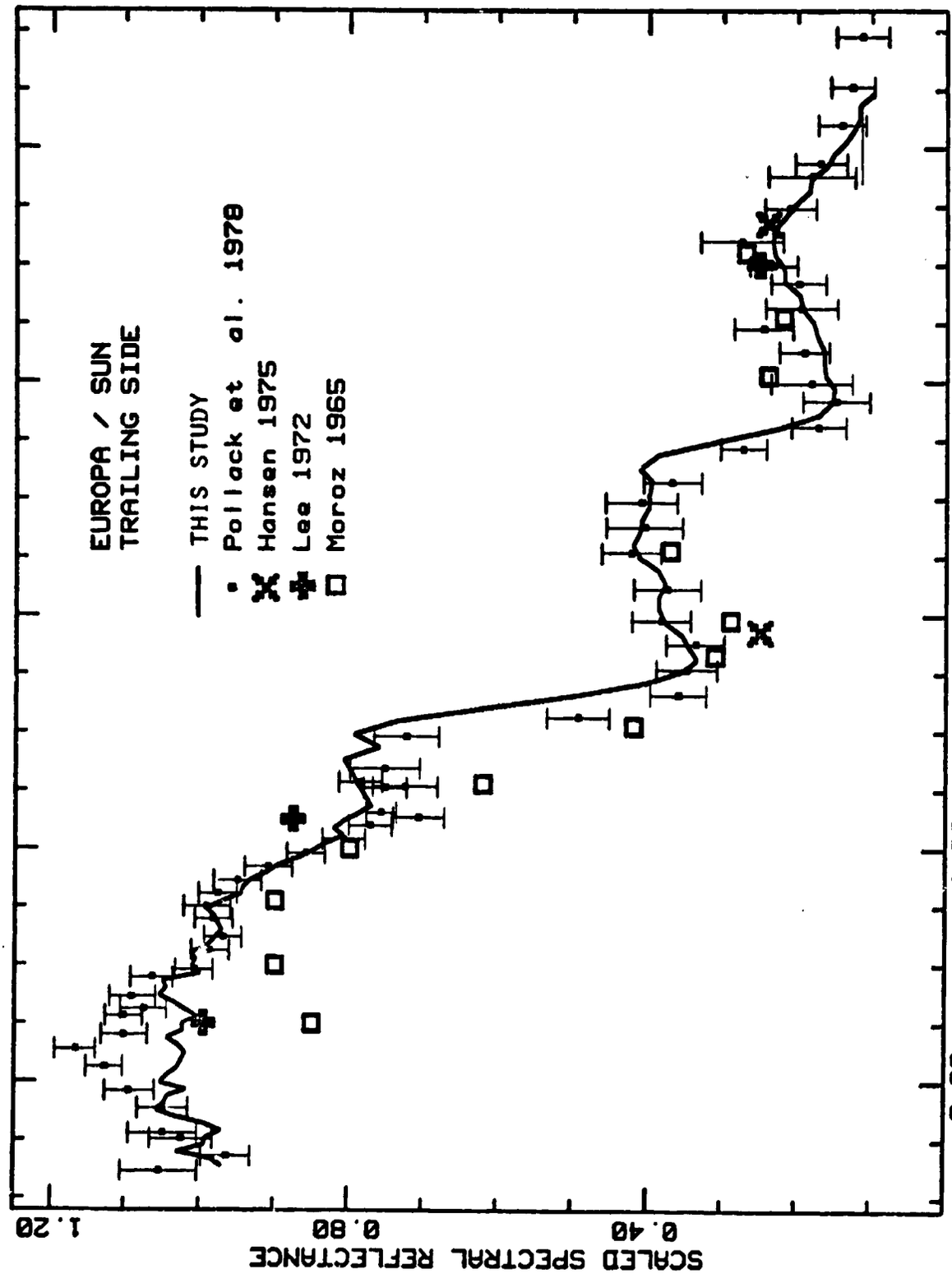

EUROPA / SUN
TRAILING SIDE
THIS STUDY
Pollack et al. 1978
Hansen 1975
Lee 1972
Moroz 1965
SCALED SPECTRAL REFLECTANCE
0.40
0.80
1.20
WAVELENGTH IN MICRONS
0.80
1.20
1.60
2.00
2.40

Figure 4

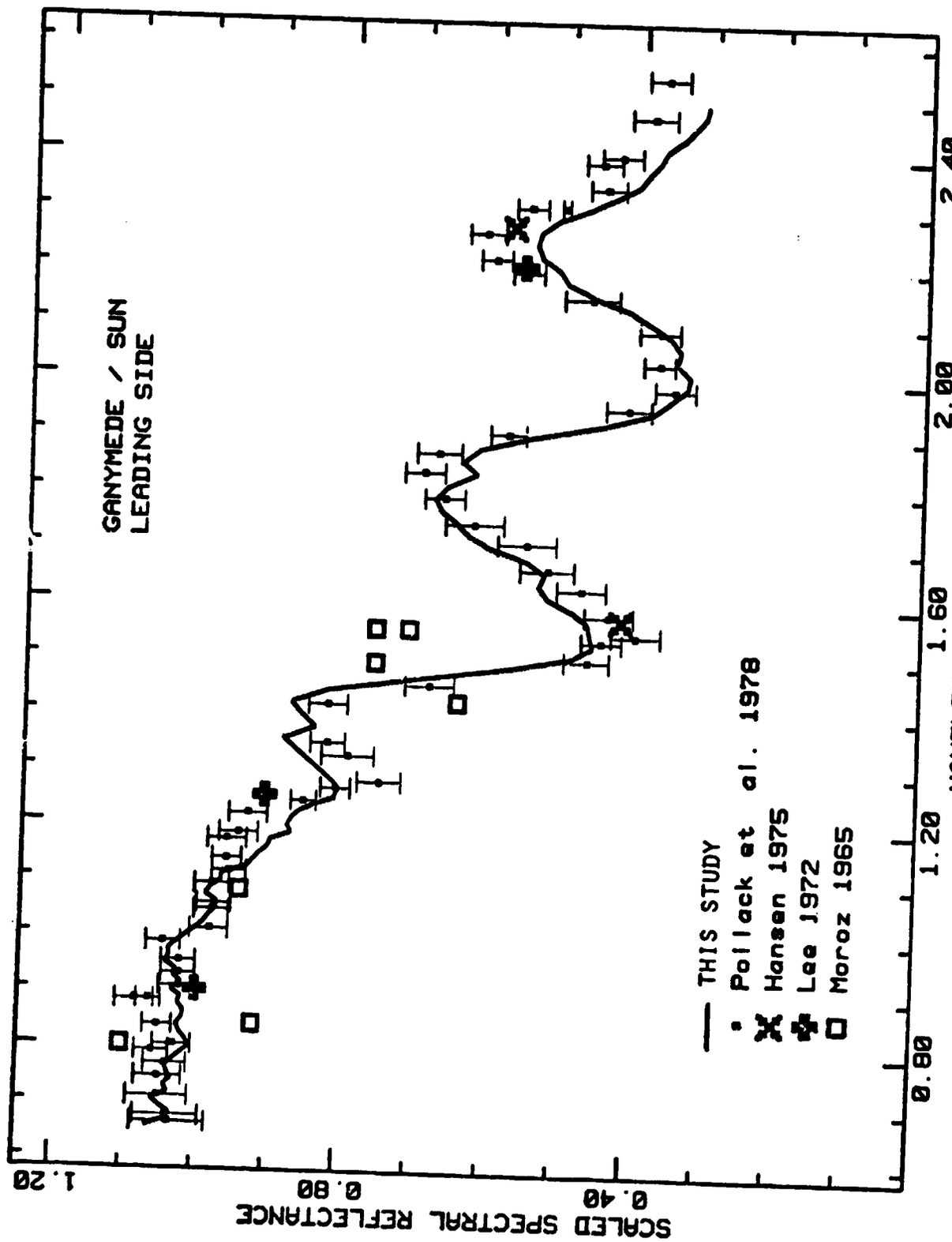

GANYMEDE / SUN
LEADING SIDE
THIS STUDY
Pollack et al. 1978
Hansen 1975
Lee 1972
Moroz 1965
SCALED SPECTRAL REFLECTANCE
0.40
0.80
1.20
WAVELENGTH IN MICRONS
0.80
1.20
1.60
2.00
2.40

Figure 5

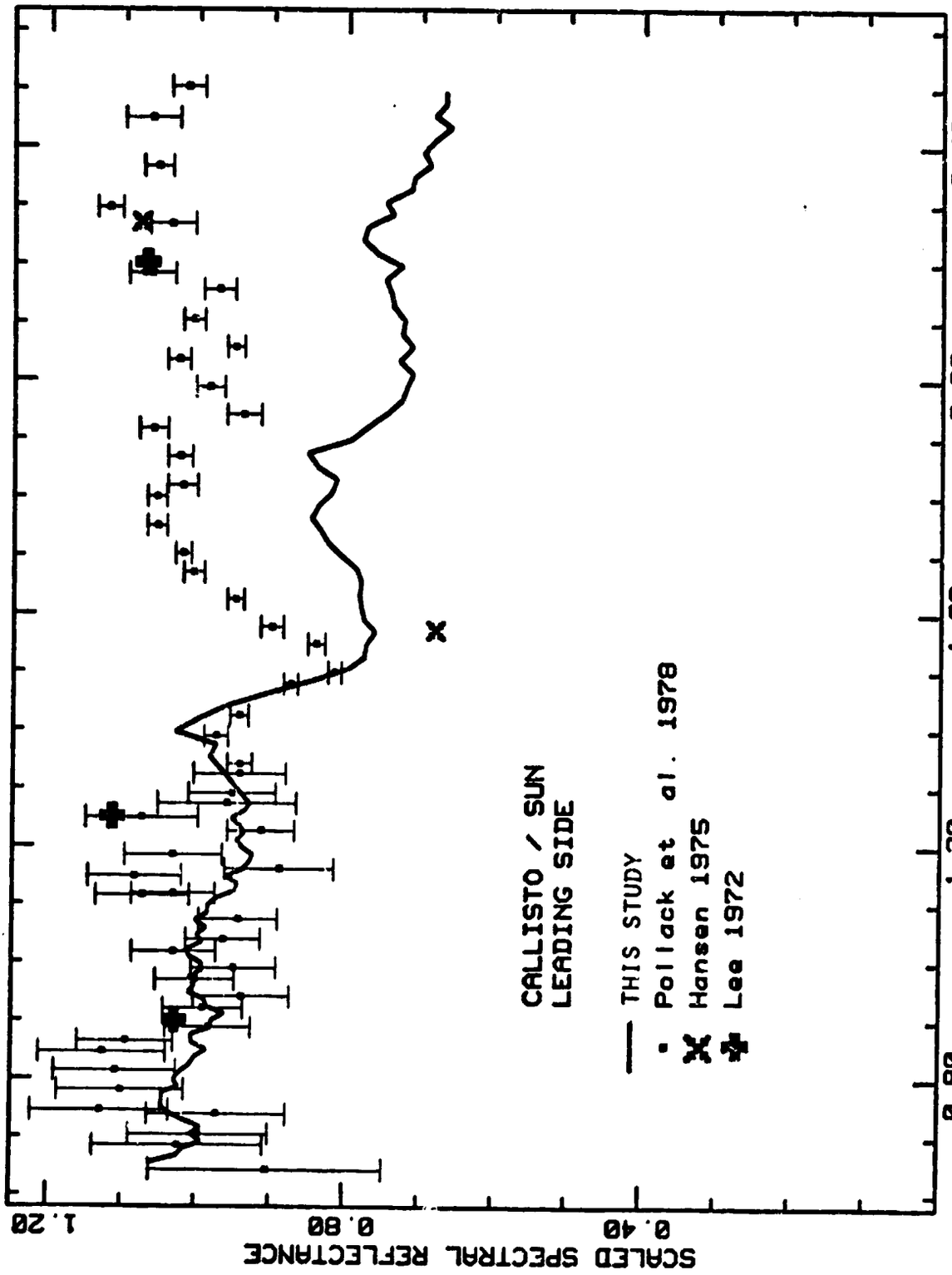

CALLISTO / SUN
LEADING SIDE
THIS STUDY
Pollack et al. 1978
Hansen 1975
Lee 1972
SCALED SPECTRAL REFLECTANCE
0.40
0.80
1.20
WAVELENGTH IN MICRONS
0.80
1.20
1.60
2.00
2.40

Figure 6A

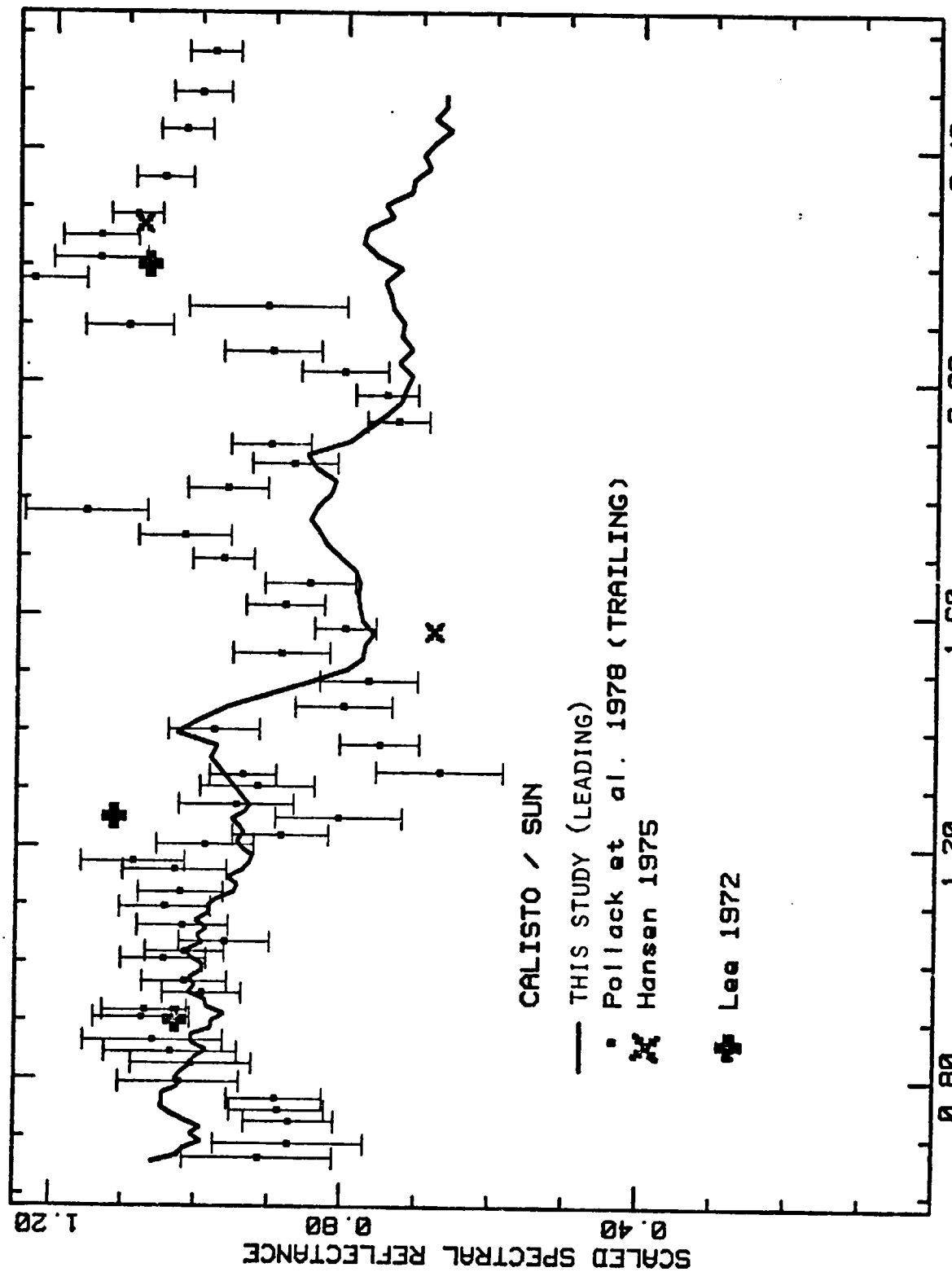

CALISTO / SUN
THIS STUDY (LEADING)
Pollack et al. 1978 (TRAILING)
Hansen 1975
Lee 1972
SCALED SPECTRAL REFLECTANCE
0.40
0.80
1.20
WAVELENGTH IN MICRONS
0.80
1.20
1.60
2.00
2.40

Figure 6B

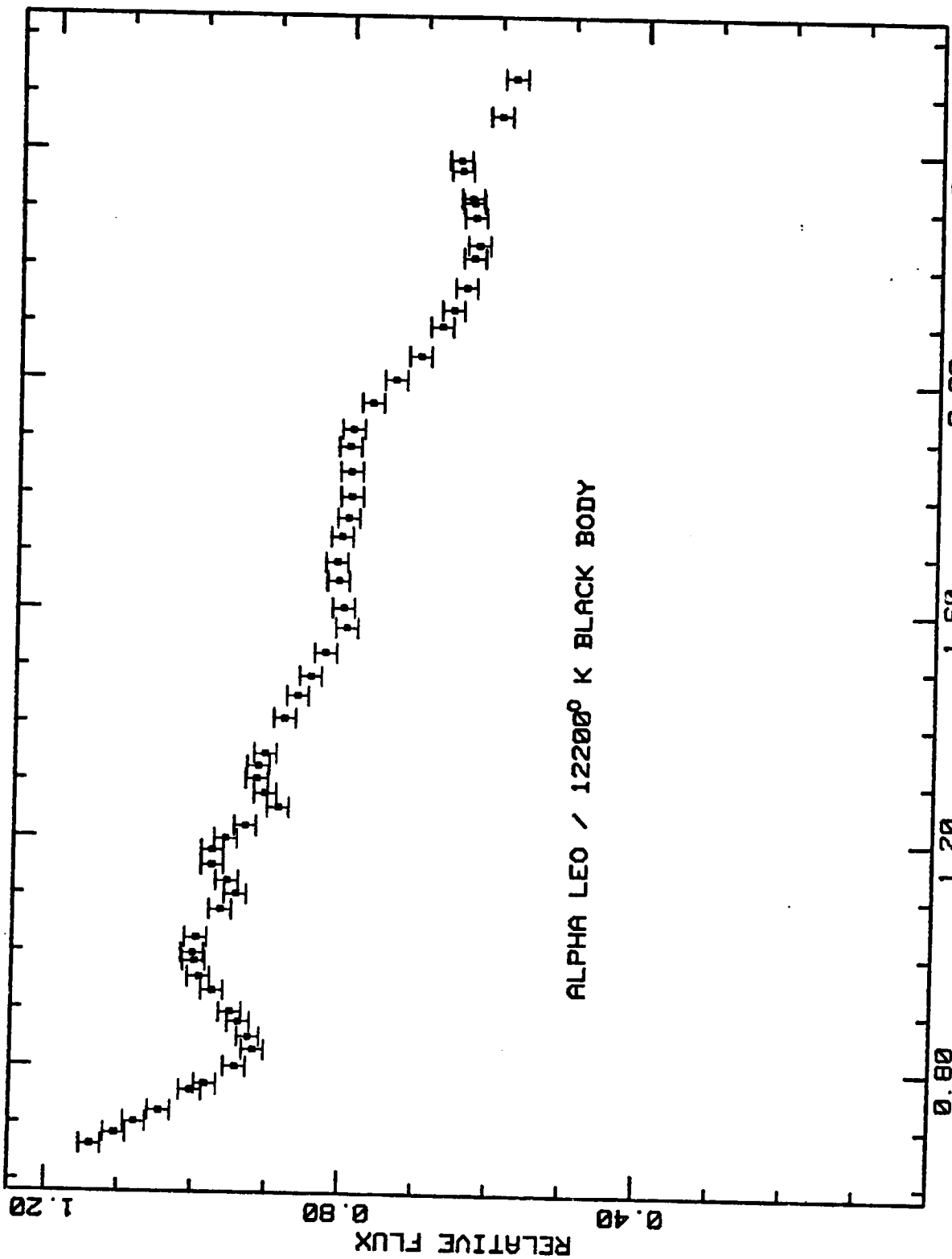

ALPHA LEO / 12200° K BLACK BODY
RELATIVE FLUX
0.40
0.80
1.20
WAVELENGTH IN MICRONS
0.80
1.20
1.60
2.00
2.40

Figure 7

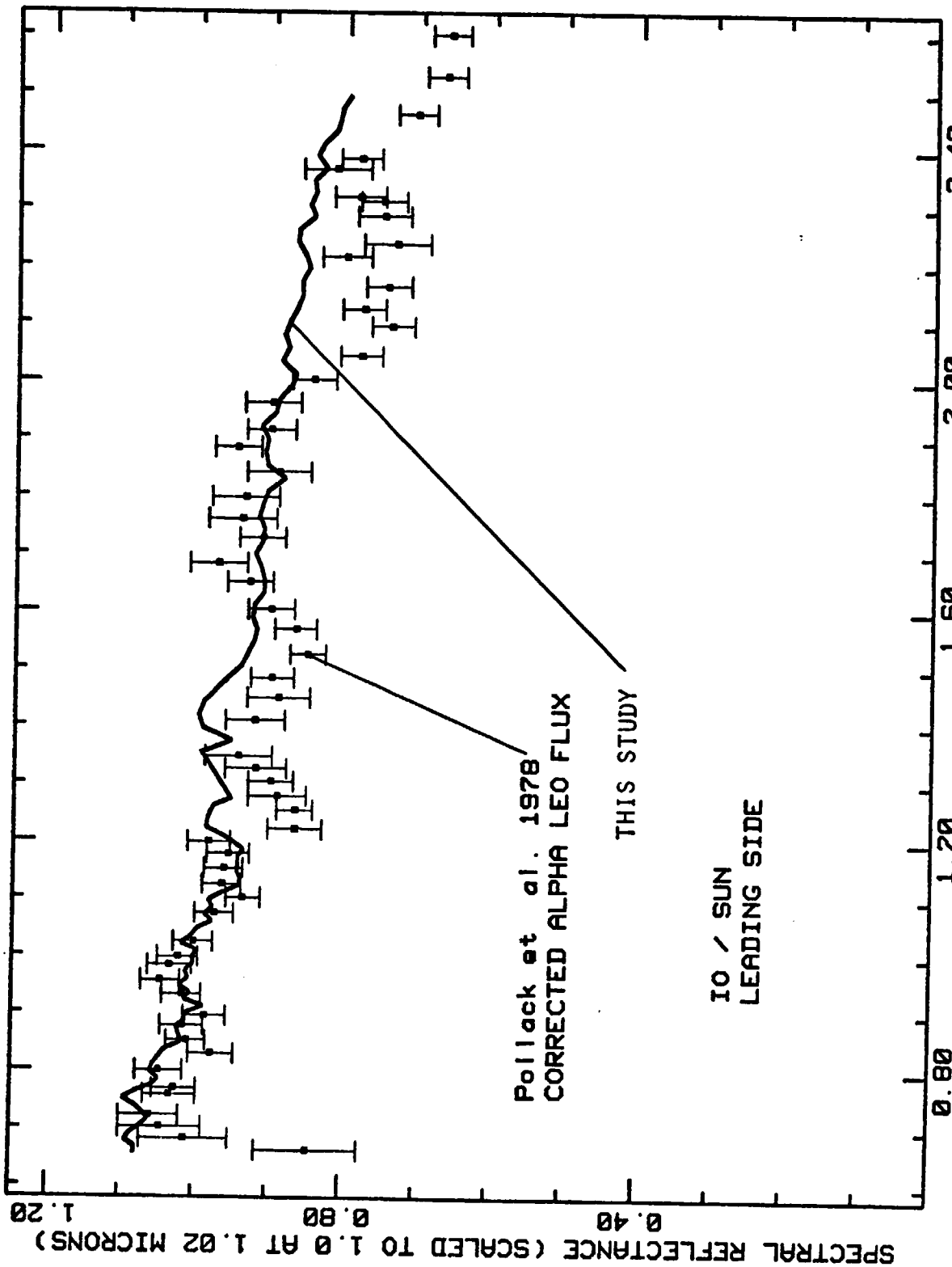

SPECTRAL REFLECTANCE (SCALED TO 1.0 AT 1.02 MICRONS)
0.40
0.80
1.20
0.80
1.60
2.00
2.40
WAVELENGTH IN MICRONS
IO / SUN
LEADING SIDE
THIS STUDY
Pollack et al. 1978
CORRECTED ALPHA LEO FLUX

Figure 8

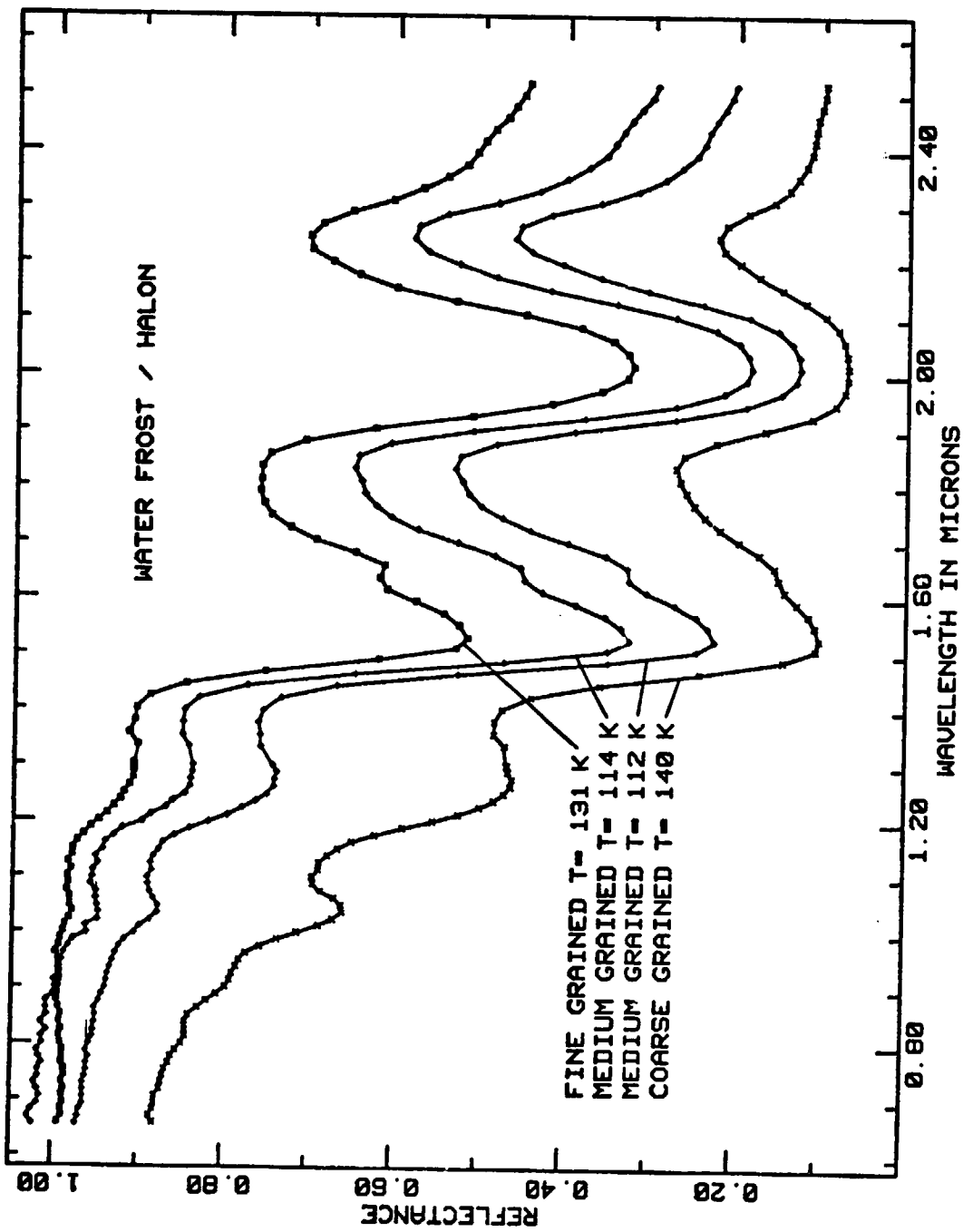

WATER FROST / HALON
FINE GRAINED T= 131 K
MEDIUM GRAINED T= 114 K
MEDIUM GRAINED T= 112 K
COARSE GRAINED T= 140 K
REFLECTANCE
0.20
0.40
0.60
0.80
1.00
WAVELENGTH IN MICRONS
0.80
1.20
1.60
2.00
2.40

Figure 9

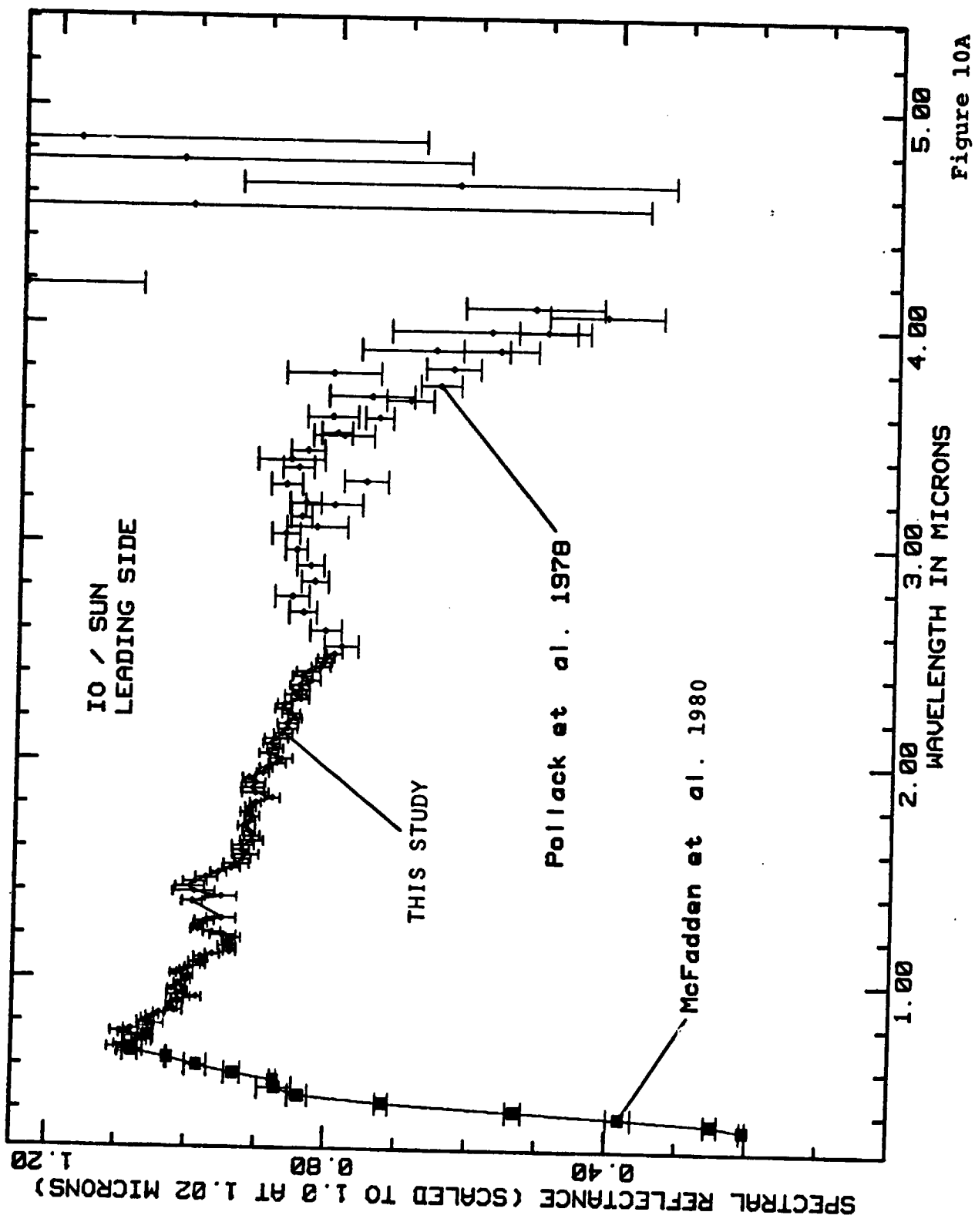

IO / SUN
LEADING SIDE
THIS STUDY
Pollack et al. 1978
McFadden et al. 1980
SPECTRAL REFLECTANCE (SCALED TO 1.0 AT 1.02 MICRONS)
0.40
0.80
1.20
1.00
2.00
3.00
4.00
5.00
WAVELENGTH IN MICRONS

Figure 10A

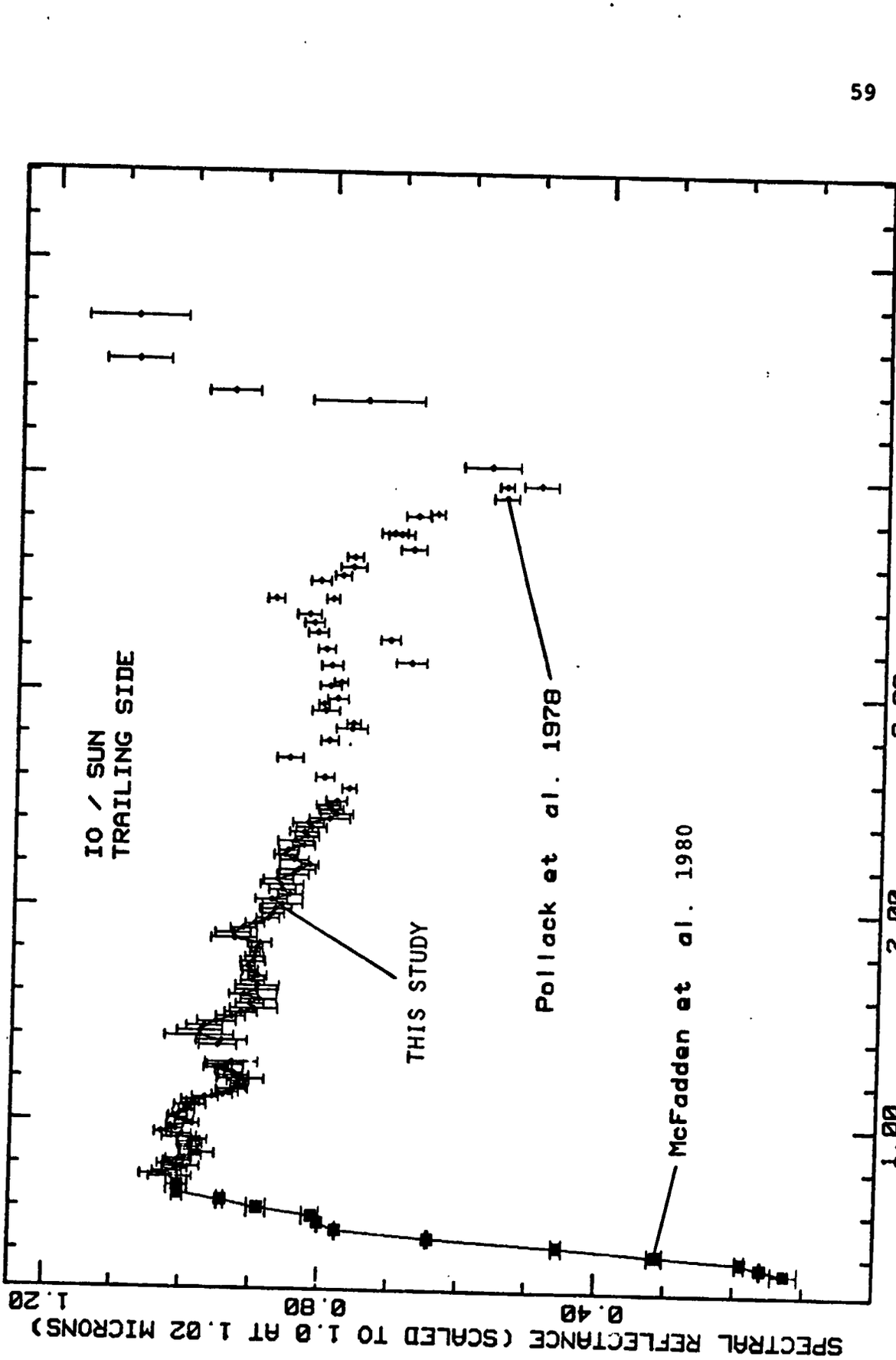

IO / SUN
TRAILING SIDE
THIS STUDY
Pollack et al. 1978
McFadden et al. 1980
SPECTRAL REFLECTANCE (SCALED TO 1.0 AT 1.02 MICRONS)
0.40
0.80
1.20
1.00
2.00
3.00
4.00
5.00
WAVELENGTH IN MICRONS

Figure 10B

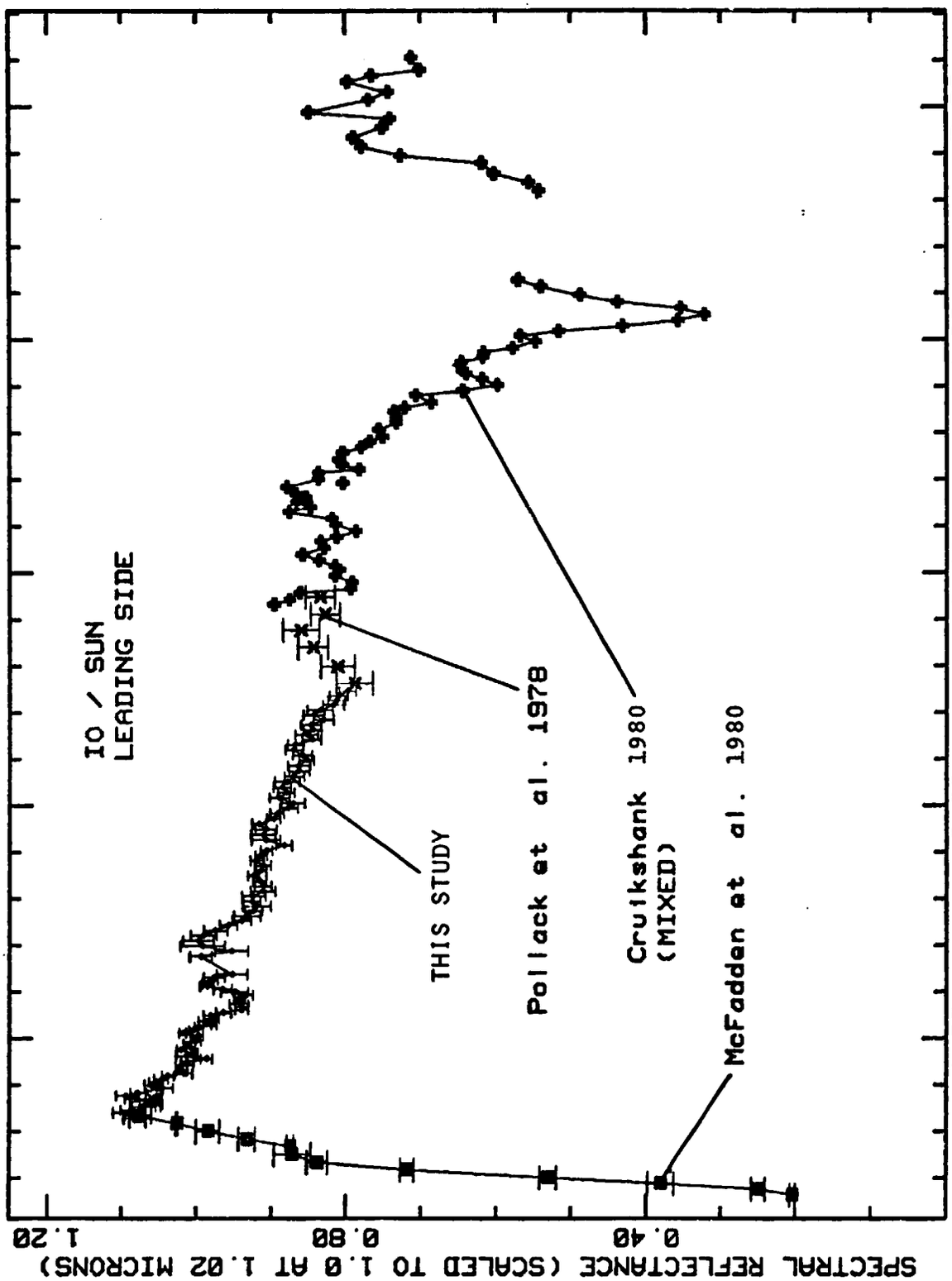

IO / SUN
LEADING SIDE
THIS STUDY
Pollack et al. 1978
Crukshank 1980
(MIXED)
McFadden et al. 1980
SPECTRAL REFLECTANCE (SCALED TO 1.0 AT 1.02 MICRONS)
0.40
0.80
1.20
1.00
2.00
3.00
4.00
5.00
WAVELENGTH IN MICRONS

Figure 11

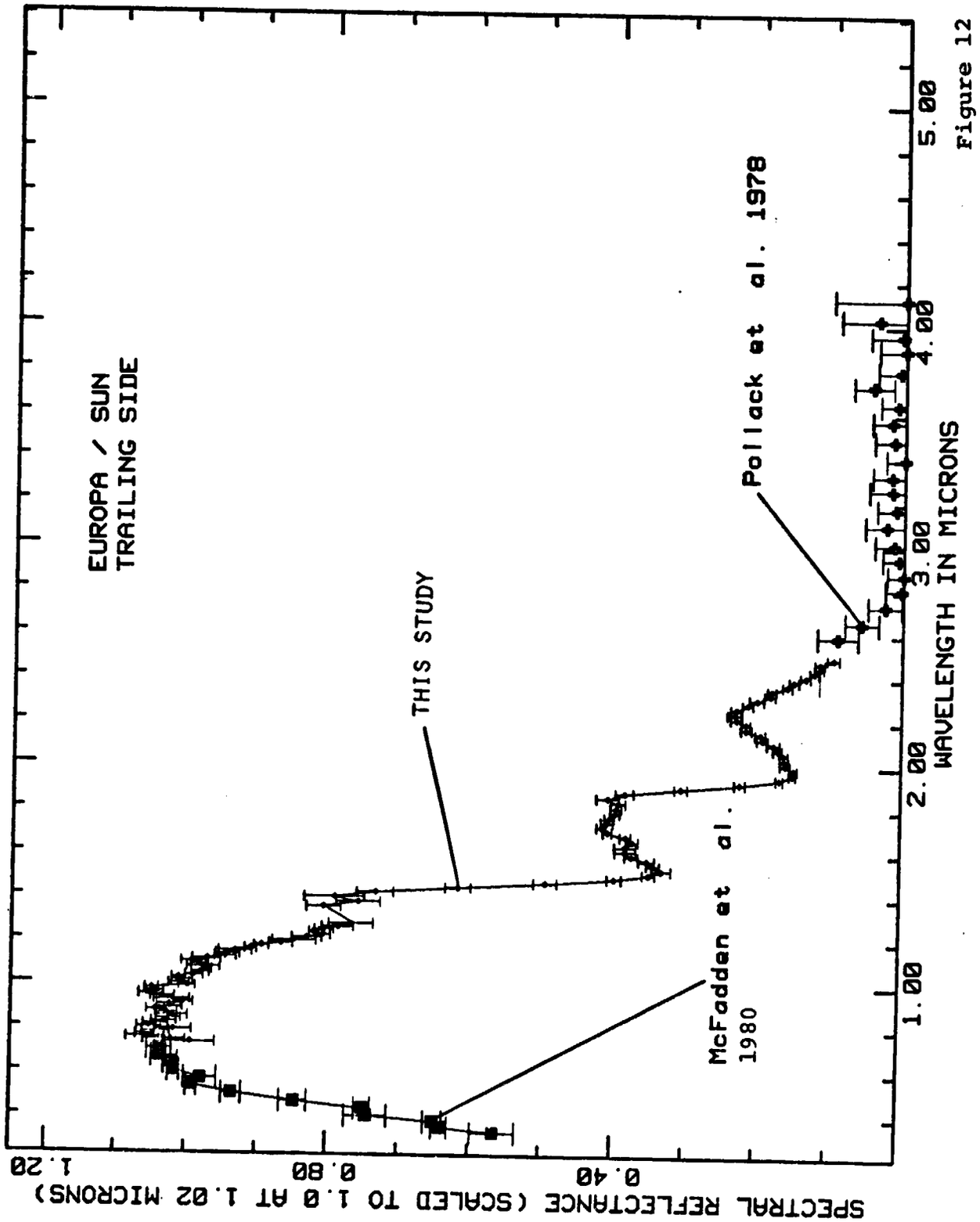

EUROPA / SUN
TRAILING SIDE
THIS STUDY
Pollack et al. 1978
McFadden et al.
1980
SPECTRAL REFLECTANCE (SCALED TO 1.0 AT 1.02 MICRONS)
0.40
0.80
1.20
1.00
2.00
3.00
4.00
5.00
WAVELENGTH IN MICRONS

Figure 12

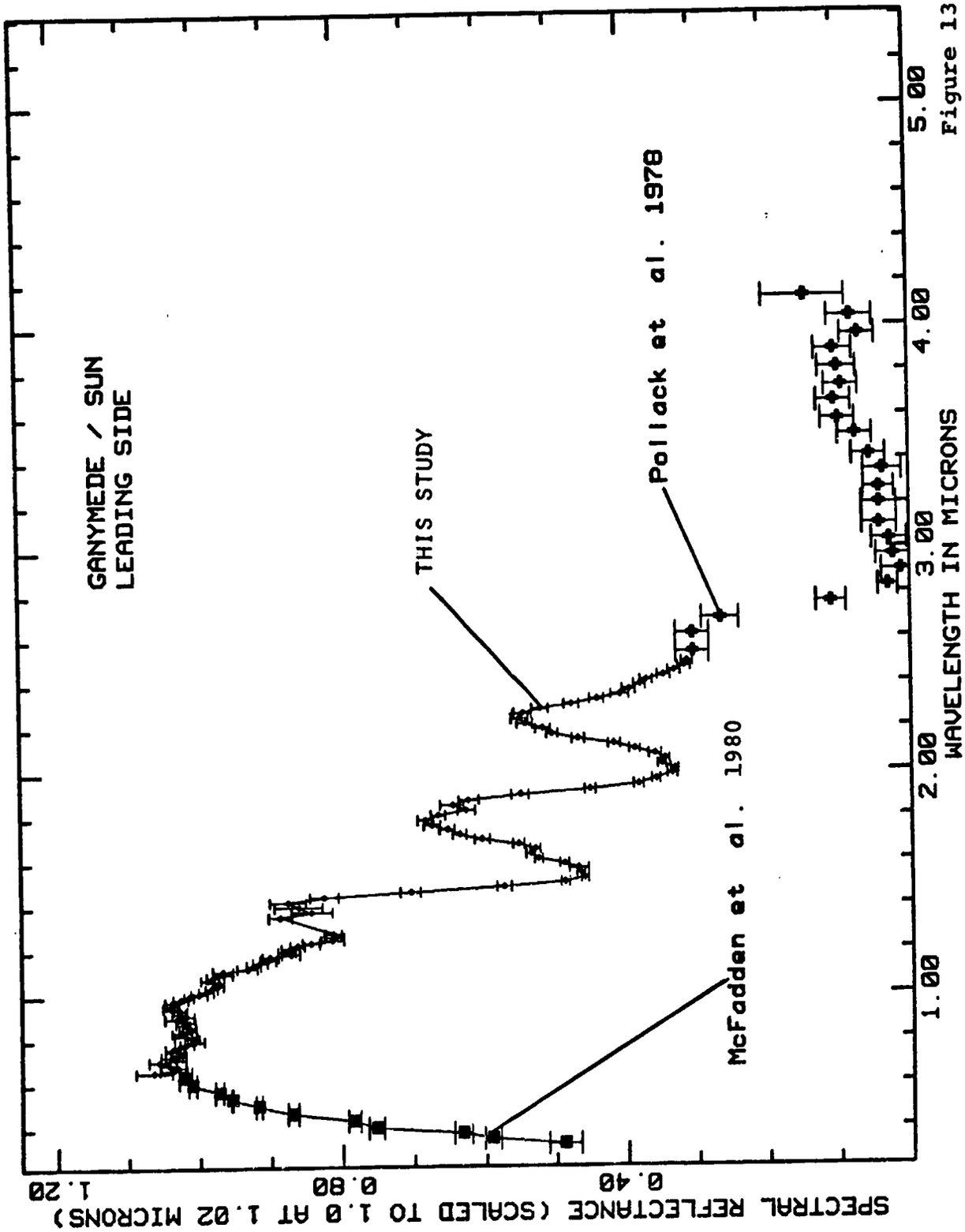

GANYMEDE / SUN
LEADING SIDE
THIS STUDY
Pollack et al. 1978
McFadden et al. 1980
SPECTRAL REFLECTANCE (SCALED TO 1.0 AT 1.02 MICRONS)
0.40
0.80
1.20
1.00
2.00
3.00
4.00
5.00
WAVELENGTH IN MICRONS

Figure 13

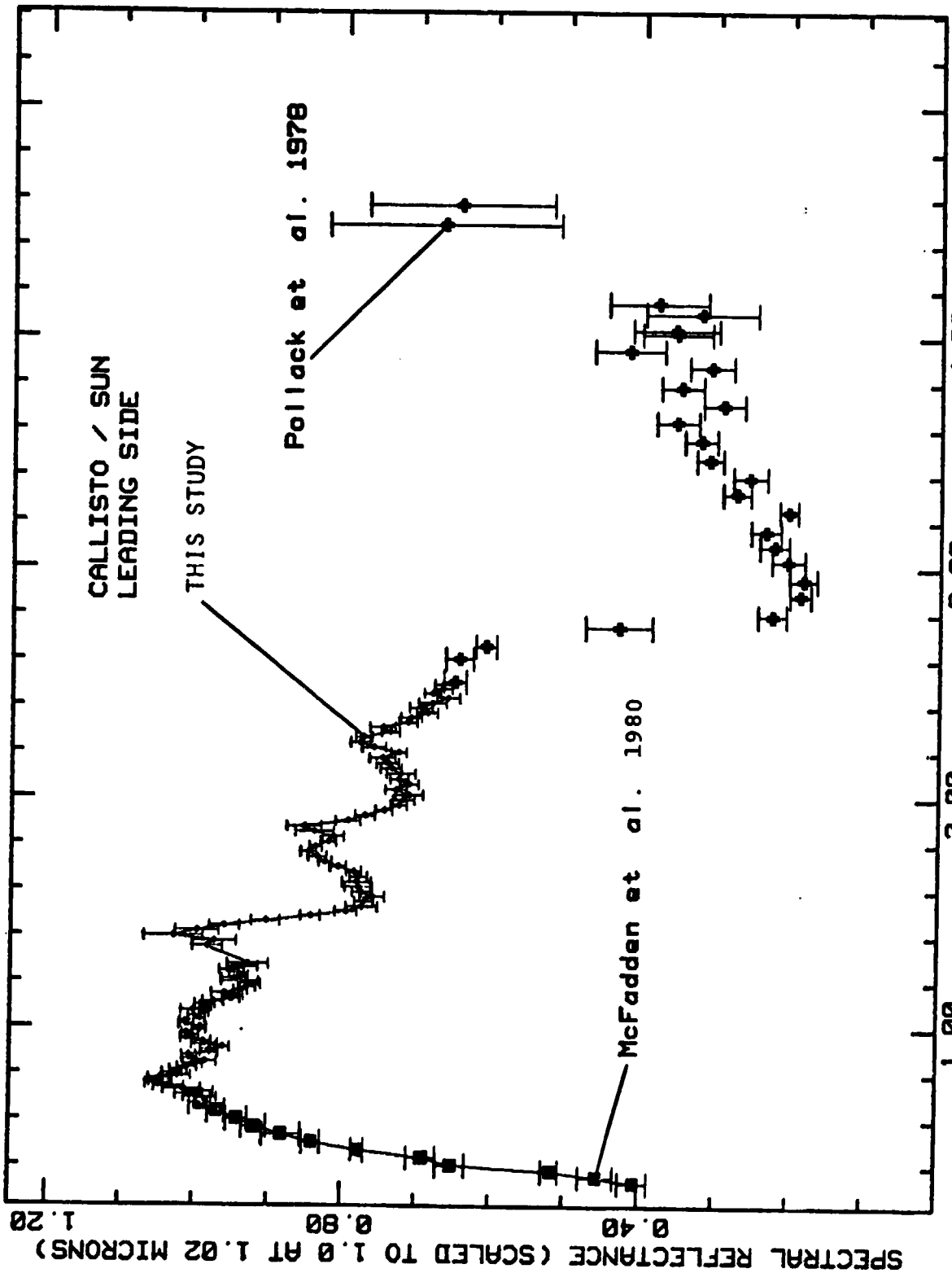

CALLISTO / SUN
LEADING SIDE
THIS STUDY
Pollack et al. 1978
McFadden et al. 1980
SPECTRAL REFLECTANCE (SCALED TO 1.0 AT 1.02 MICRONS)
0.40
0.80
1.20
1.00
2.00
3.00
4.00
5.00
WAVELENGTH IN MICRONS

Figure 14

SECTION I

CHAPTER 2

The Rings of Saturn: New Near-Infrared Reflectance Measurements and a 0.326-4.08 μm Summary

This chapter has been submitted for publication to the journal Icarus. Authors: R.N. Clark and T.B. McCord.

Abstract

A new high photometric precision reflectance spectrum of Saturn's rings covering the 0.65 to 2.5-μm spectral region is presented and three previously unreported absorption features at 1.25, 1.04 and 0.85μm are identified. The 1.25 and 1.04-μm absorptions are due to water ice. The 0.85-μm feature may be due to a combination of 0.81- and 0.90-μm ice absorptions but this feature appears too strong relative to the 1.04-μm band to be completely explained by water ice. Another possibility is that the 0.85-μm band is due to an iron oxide in an ice-mineral mixture. This explanation could also account for the drop in the visible and ultraviolet reflectance and the rise in reflectance around 3.6μm. Finally, a composite spectrum from 0.325 to 4.08μm is presented which will be useful for future analysis and laboratory studies.

Introduction

Infrared spectral (1 - 2.5μm) of the rings of Saturn (Kuiper et al., 1970) have been used to establish that water ice is a major component of the ring material (Pilcher et al., 1970; Fink et al., 1976). The decrease in reflectivity from the visible to the ultraviolet indicates something other than pure water is present (Lebofsky et al., 1970; Irvine and Lane, 1973). The reflectance spectrum further into the ifnrared (2 - 4μm) indicates essentially pure water ice (Puetter and Russell, 1977). Fink et al. (1976) recently published a high quality relfectance spectrum of the rings, from 1.0 to 2.5μm but the spectrum contained gaps in the regions of telluric water absorptions. A new spectrum of the rings of Saturn is presented with high photometric precison (≲1%) and 1 % spectral resoltuion in the 0.65 to 2.5μm region and with no gaps due to telluric water absorption.

Observations

The data presented here resulted from ten nights of observations of the west (astronomical east) ansae of the combined Saturn A and B rings. The 2.2-meter telescope on Mauna Kea was used. Table I shows the observational parameters. A continuously scanning circular variable filter (CVF) spectrometer and an indium antimonide detector were used. The spectral resolution is approximately 1½%. The spectrum is made up of 120 data points (separate spectral channels) and the spectrometer scans from 0.65 to 2.4μm every 10 seconds. The spectra were coadded on successive scans and then written onto magnetic tape after 10 scans (100 seconds), which we call a run. During the accumulation of data for each channel, the background was subtracted by chopping twice between a black reference and the rings using a chopper rotating at 24 Hz. A sky minus black reference measurement was taken immediately before or after each ring measurement. This residual signal was less than 1-2% of the ring signal and was later subtracted by computer. The indium antimonide detector was operated at liquid nitrogen temperature (77°K). The CVF and aperture were at ambient temperature for the 1976 and 1977

runs but were cooled to LN_2 temperature for the 1978 run. The aperture consists of an aluminized plate mounted 45° to the optical axis located at the cassegrain focus with the aperture hole drilled in the center. This enabled us to determine the precise area being measured as a dark spot in the field of view. A beam splitter in the viewing optics allowed simultaneous photographs to be made. Excellent seeing of $\leq$1 arcsec prevailed throughout most of these observations, and this made possible accurate placement of the aperture on the desired ring area. We are confident that no contamination from the disk of Saturn is present in these ring spectra because placement of the aperture next to the disk but off the rings resulted in a signal indistinguishable from measurements of sky far from Saturn. The data were processed on our laboratory computer using an interactive spectral analysis program (Clark, 1979a). The instrument and data reduction procedure are further discussed in McCord et al. (1978, 1980a).

In order to obtain accurate reflectance measurements, the flux from the rings was compared with that from the star Beta Geminorium and/or a lunar area in Mare Serenatatis. The reflectance

of this area (called MS2) has been calibrated by laboratory and telescopic measurements to the Apollo 16 landing site surface material (McCord et al., 1972; Nygard, 1975; Adams and McCord, 1973; McCord et al., 1980a). The spectral flux of Beta Geminorium was calibrated by using the derived MS2 reflectance. Color variations due to lunar phase angle effects may introduce slope errors of up to 5% in the derived reflectance. Residual lunar absorption in this calibration procedure are less than about 1%. The reflectance is then calculated by the equation

$$R_{obj} = C \frac{I_{obj}}{I_{MS2}} R_{MS2}$$

where C is a scaling constant, R_{MS2} is the previously measured reflectance of MS2, I_{obj} is the intensity of the object measured at the telescope and I_{MS2} is the intensity of MS2 measured at the telescope. In order to calibrate out the effects of the earth's atmosphere, I_{obj} and I_{MS2} must be measured or calculated to the same air mass. The standard (MS2 or Beta Geminorium) was measured throughout each night and an extinction analysis was performed (see McCord and Clark, 1979). This resulted in high quality observations even in the

strong telluric water bands at 1.4 and 1.9μm.

The wavelength of each spectral channel was calibrated in the laboratory with a monochrometer and the calibration was checked with a narrowband 0.951μm filter at the telescope. The absolute wavelength of each channel is accurate to better than 0.004μm for the wavelength region 0.6 to 1.35 (channels 1-60) and 0.008μm for 1.32 to 2.6μm (channels 61-120) and the relative wavelength spacing to adjacent channels is accurate to approximately 0.001μm.

The error bars on our data represent approximately ±2 standard deviations of the mean, however, there may be systematic errors of about 1% in the calibration procedure (see McCord et al. (1980a).

Results

The spectrum of Saturn's combined A and B rings obtained after 1,190 scans is shown in Figure 1. The major water ice features previously identified (Pilcher et al., 1970; Fink et al., 1976) are apparent at 2.02μm, 1.65μm and 1.53μm.

Pollack et al. (1973) performed theoretical calculations for water frost and determined the mean particle radius of between 25 and 125 micrometers from the shape of the 1.53- and 2.0-μm ice bands. Their best-fit theoretical spectrum is shown in Figure 2 (24-micrometer mean radius). The match to our data is reasonably good, however, the theoretical spectrum below 1.4μm seems anomalously high.

Clark (1980b) has measured the spectral reflectance of frosts in a laboratory environment chamber with the same instrument used for the telescopic ring data. The spectral contrast varies considerably with grain size as shown in Figure 3. The spectrum of pure ice is very

similar to the ring spectrum beyond about 0.9μm. Also, note that the ice and ring spectra are so similar that even a small inflection at 2.43μm in the ice spectra also appears in the ring spectrum. Clark (1980b) has identified overtone features in laboratory water ice reflectance spectra shortward of 1.4μm at 1.25, 1.04, 0.90 and 0.81μm.

The 1.25-μm band is readily apparent in the Saturn's rings spectrum. The 1.04-μm band is also present but it is weak. There is an apparently complex band extending from 0.78 to 0.92μm. Water ice has weak features at 0.90 and 0.81-μm but these are several times weaker than the 1.04-μm band in pure water frost (Clark, 1980b). However, there is evidence that higher overtone water ice bands may become enhanced as is seen on Callisto, Europa, Ganymede and Mars (Clark and McCord, 1980; McCord et al., 1978; McCord et al., 1980). These solar system bodies display different water ice band depth ratios (e.g. 1.53/2.0-μm, 1.25/1.53-μm, 1.03/1.53-μm band ratios) than in the reflectance spectra of pure water frost.

The 0.85-μm band in Saturn's rings appear particularly deep compared to the 1.04- and 1.25-μm bands indicating other minerals with absorptions

in the 0.85-μm region are probably present. Iron oxide has bands in the 0.85-μm region and also has a strong decrease in reflectivity in the visible and ultraviolet. A mixture of iron oxide and water frost might then account for the obbserved spectrum of the rings. If there is a thin contaminating layer of iron oxide (≲ a few micrometers) the visible radiation would be strongly influenced by the iron oxide causing the decrease in reflectivity at shorter wavelengths and the infrared radiation would be minimally absorbed by the oxide resulting in the strong water ice spectral features.

There is no evidence for bound water in the ring spectrum. Bound water bands occur near 1.4 and 1.9μm (Hunt and Salisbury, 1970, 1972; Hunt et al., 1971a, b, 1972 and 1973) and do not shift in wavelength significantly (≲100Å) from 300° to 150°K (Clark, 1980c). It has been found (Clark, 1980c) that bound water bands are distinctive even in the presence of very strong water ice bands. This then rules out clay minerals such as montmorillionite and kaolinite as a major constitutent of the rings.

Comparison with Other Data

A comparison of the spectrum presented in this paper with previously published visible and near IR data is shown in Figure 4. In general, most of the previous data agree with our new data, within the errors. Some of the differences are probably due to the way the data were obtained. The Lebofsky and Fegley (1976) data are of ring B only and are corrected from the original measurement of Lebofsky et al. (1970) using a better standard star calibration. The discrepancies could indicate real differences between the A and B rings. The data of Irvine and Lane (1973) were obtained in a complicated manner using photometry of the entire Saturn + Ring system and then subtracting the disk component. The data agree reasonably well except for the two values at 0.86 and 1.06μm. The data of Singer (1977) agree very well and were derived by integrating regions on multispectral images obtained with a silicon diode vidicon imaging system. Nearly the same area of rings A and B were used in the computation of the spectrum as with our data. The Singer data were taken on the night of February 4, 1977, in the middle of one of our observing runs.

Puetter and Russell (1977) obtained a 2- to 4-μm spectrum of the rings of Saturn (Also the west side). Their results are compared with ours in Figure 5. The agreement is very good. They report that their data in the 3- to 4-μm region are consistent with a pure H_2O ice with a particle size of $\leq$50 m but they could not rule out small amounts of CH_4 clathrate. This was due to the apparent higher reflectance of the rings in the 3- to 4-μm region than laboratory measurements of pure water frost. Pollack et al. (1978), using theoretical studies, found the reflectance of the 3- to 4-μm region could be rasied by the addition of a mineral to the frost. The addition of a mineral to pure frost might then give a better fit to the 3- to 4-μm region of the ring spectrum. This is consistent with the drop in reflectance in the visible and with the existence of a 0.85μm band, neither of which can be explained by a pure H_2O ice.

A composite spectrum of the rings from 0.325 to 4.08μm is presented in Figure 6. This nearly complete spectrum will be useful for future laboratory studies and for comparison with spectra of other solar system objects. There is

a need for measurements in the 2.5 to 2.8μm region as this is where there is a steep drop in reflectance due to the ν_1 and ν_3 water ice fundamentals.

ACKNOWLEDGEMENTS

This research was supported by NASA Grants NSG 7323 and NSG 7312.

REFERENCES

Adams, J.B. and McCord, T.B. (1973). Vitrification darkening in the lunar highlands and identification of descartes material at the Apollo 16 site. Proceedings of the Fourth Lunar Science Conf. 1, 163-177.

Clark, R.N. (1980a). A large scale interactive one dimensional array processing system. Submitted to Pub. A.S.P. Thesis App A

Clark, R.N. (1980b). Water frost and ice: The near-infrared spectral reflectance 0.65-2.5μm. J. Geophys. Res. submitted. Thesis II Ch1

Clark, R.N. (1980c). The spectral reflectance of water-mineral mixtures at low temperatures. J. Geophys. Res. submitted. Thesis II Ch2

Clark, R.N. and McCord, T.B. (1980). The Galilean Satellites: New near-infrared spectral reflectance measurement (0.65-2.5μm) and 0.325-5μm summary. Icarus submitted. Thesis I Ch1

Fink, U., Larson, H.P., Gautier, T.N. III and Treffers, R.R. (1976). Infrared spectra of the satellites of Saturn: Identification of water ice on Iapetus, Rhea, Dione and Tethys. Asophys. J. 207, L63-67.

Hunt, G.R. and Salisbury, J.W. (1970). Visible and near-infrared spectra of minerals and rocks: I. Silicate minerals. Mod. Geol. 1, 283-300.

Hunt, G.R. and Salisbury, J.W. (1972). Visible and near-infrared spectra of minerals and rocks: II. Carbonates. Mod. Geol. 2, 23-30.

Hunt, G.R. Salisbury, J.W. and Lenhoff, C.J. (1971a). Visible and near-infrared spectra of minerals and rocks: III. Oxides and hydroxides. Mod. Geol. 2, 195-205.

Hunt, G.R., Salisbury, J.W. and Lenhoff, C.J. (1971b). Visible and near-infrared spectra of minerals and rocks: IV. Sulphides and sulphates. Mod. Geol. 3, 1-14.

Hunt, G.R., Salisbury, J.W. and Lenhoff, C.J. (1972). Visible and near-infrared spectra of minerals and rocks: V. Halides, phosphates, arsenates, vanadates and borates. Mod. Geol. 3, 121-132.

Hunt, G.R., Salisbury, J.W. and Lenhoff, C.J. (1973). Visible and near-infrared spectra of minerals and rocks: VII. Acidic igneous rocks. Mod. Geol. 4, 217-224.

Irvine, W.M. and Lane, A.P. (1973). Photometric properties of Saturn's rings. Icarus 18, 171-176.

Kuiper, G.P., Cruikshank, D.P. and Fink, U. (1970). As reported in Sky and Telescope 39, 14.

Lebofsky, L.A. and Fegley, M. Jr. (1976). Laboratory reflection spectra for the determination of chemical composition of icy bodies. Icarus 28, 379-387.

Lebofsky, L.A., Johnson, T.V. and McCord, T.B. (1970). Saturn's rings: Spectral reflectivity and compositional implications. Icarus 13, 226-230.

McCord, T.B., Charette, M.P., Johnson, T.V. Lebofsky, L.A. and Pieters, C. (1972). Lunar spectral types. J. Geophys. Res. 77, 1349-1359.

McCord, T.B. and Clark, R.N. (1979). Atmospheric extinction 0.65-2.50μm above Mauna Kea. Pub. A.S.P. 91, 571-576. Thesis App B

McCord, T.B., Clark, R.N. and Huguenin, R.L. (1978). Mars: Near-infrared spectral reflectance and compositonal implication. J. Geophys. Res. 83, 5433-5441.

McCord, T. B., Clark, R. N., McFadden, L.A., Pieters, C. M., Owensby, P.D., and Adams, J.B. (1980)a. Moon: Near-infrared spectral reflectance, A first good look. J. Geophys. Res. to be submitted.

McCord, T.B., Clark, R.N., Singer, R.B. and Huguenin, R.L. (1980b). Mars: Near-infrared reflectance spectra of surface regions and compositional implications. To be submitted to J. Geophys. Res. Thesis I Ch 3

Nygard, S. (1975). Alpha Lyrae/Sun flux ratios for use in standard star calibration: Results of three techniques. Masters Thesis, Massachusetts Institute of Technology, Cambridge, Masschusetts.

Pilcher, C.B., Chapman, C.R., Lebofsky, L.A. and Kieffer, H.H. (1970). Saturn's rings: Identification of water frost. Science 167, 1372-1373.

Pollack, J.B., Summers, A. and Baldwin, B. (1973). Estimates of the size of particles in the rings of Saturn and their cosmogenic implications. Icarus 20, 263-278.

Pollack, J.B., Whitteborn, F.C., Edwin, F.E., Strecker, D.W., Baldwin, J.B., and Bunch, B.E. (1978). Near-infrared spectra of the Galilean satellites: Observation and compositional implications. Icarus 36, 271-303.

Puetter, R.C. and Russel, R.W. (1977). The 2-4μm Spectrum of Saturn's rings. Icarus 32, 37-40.

Singer, R.B. (1977). Visible and near-infrared spectral photometry of the rings of Saturn from silicon diode vidicon images. Bull. Amer. Astron. Soc., 9, 523 (Abstract).

FIGURE CAPTIONS

Figure 1 The reflectance spectrum of Saturn's rings from 0.65 - 2.5μm. The error bars are slightly larger at 1.4 and 1.9μm due to the effect of telluric water absorption (the error bars are larger at 1.4 than 1.9μm since the transmission of CVF is several times less at 1.4μm).

Figure 2 Comparison of the spectrum in Figure 1 with a theoretical ice spectrum with a characteristic mean particle radius of 24 micrometers.

Figure 3 The spectral reflectance of water frost is shown here for different grain sizes (from Clark, 1980b). Halon is a white reflectance standard. These data were acquired with the same CVF spectrometer as for the ring spectrum shown in Figure 1. The phase angle is 10° with normal incidence. The fine grains frost had a particle size of approximately 30 micrometers; the coarse, several millimeters.

Figure 4 Comparison of the visible and near infrared spectra from other studies with those from this work.

Figure 5 Comparison of the ring spectrum from this paper (solid line) with that from Puetter and Russell (1977).

Figure 6 A composite reflectance spectrum of the rings of Saturn from 0.325 - 4.08μm and scaled to unity at 1.02μm is shown.

TABLE CAPTION

The ring geometry and observational parameters are shown. The tilt angle of the ring plane as seen from the earth and sun is given by B and B', respectively. Negative numbers indicate that the south face is visible. The inner edge of the aperture was located at the ansae of the inner edge of the B ring.

Table I

Parameters of Saturn's Rings Observations

UT Date of observation	Phase angle (degrees)	B (degrees)	B' (degrees)	Integration time (sec)	Number of scans averaged	Aperture diameter (arcsec)
4/21/76	6.33	-22.3	-20.2	1000	100	14.4
4/22/76	6.32	-22.3	-20.2	1000	100	14.4
4/23/76	6.31	-22.3	-20.2	500	50	14.4
2/02/77	0.10	-16.8	-16.7	1400	140	9.5
2/03/77	0.17	-16.9	-16.7	900	90	9.5
2/05/77	0.38	-16.9	-16.7	1000	100	9.5
2/16/78	0.17	-11.6	-11.4	1000	100	9.5
2/19/78	0.41	-11.7	-11.4	2900	290	9.5
2/20/78	0.51	-11.7	-11.4	120	120	9.5
2/21/78	0.63	-11.8	-11.3	1000	100	9.5
			Totals:	11,900	1,190	

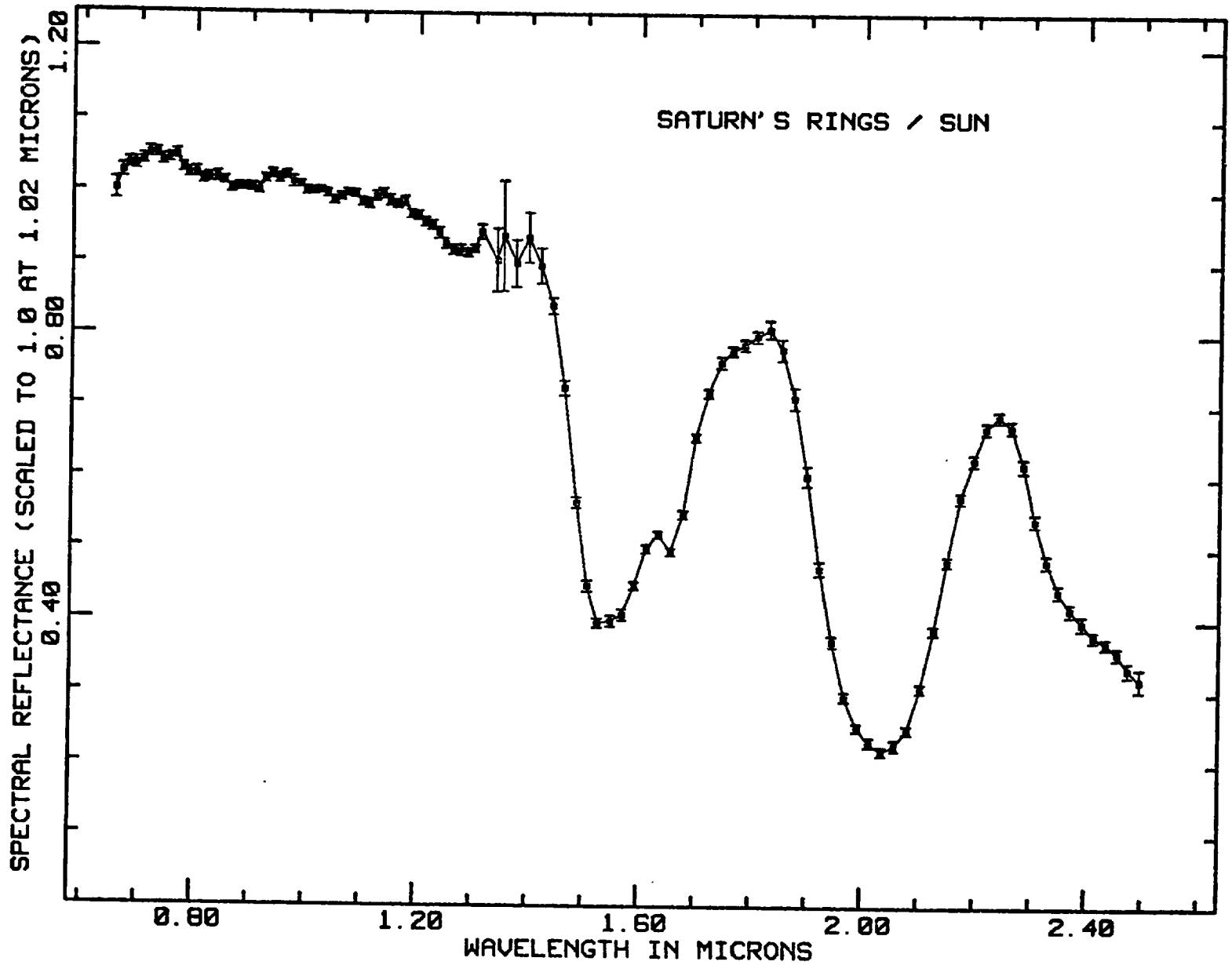

SATURN'S RINGS / SUN
SPECTRAL REFLECTANCE (SCALED TO 1.0 AT 1.02 MICRONS)
1.20
0.80
0.40
0.80
1.20
1.60
2.00
2.40
WAVELENGTH IN MICRONS

Figure 1

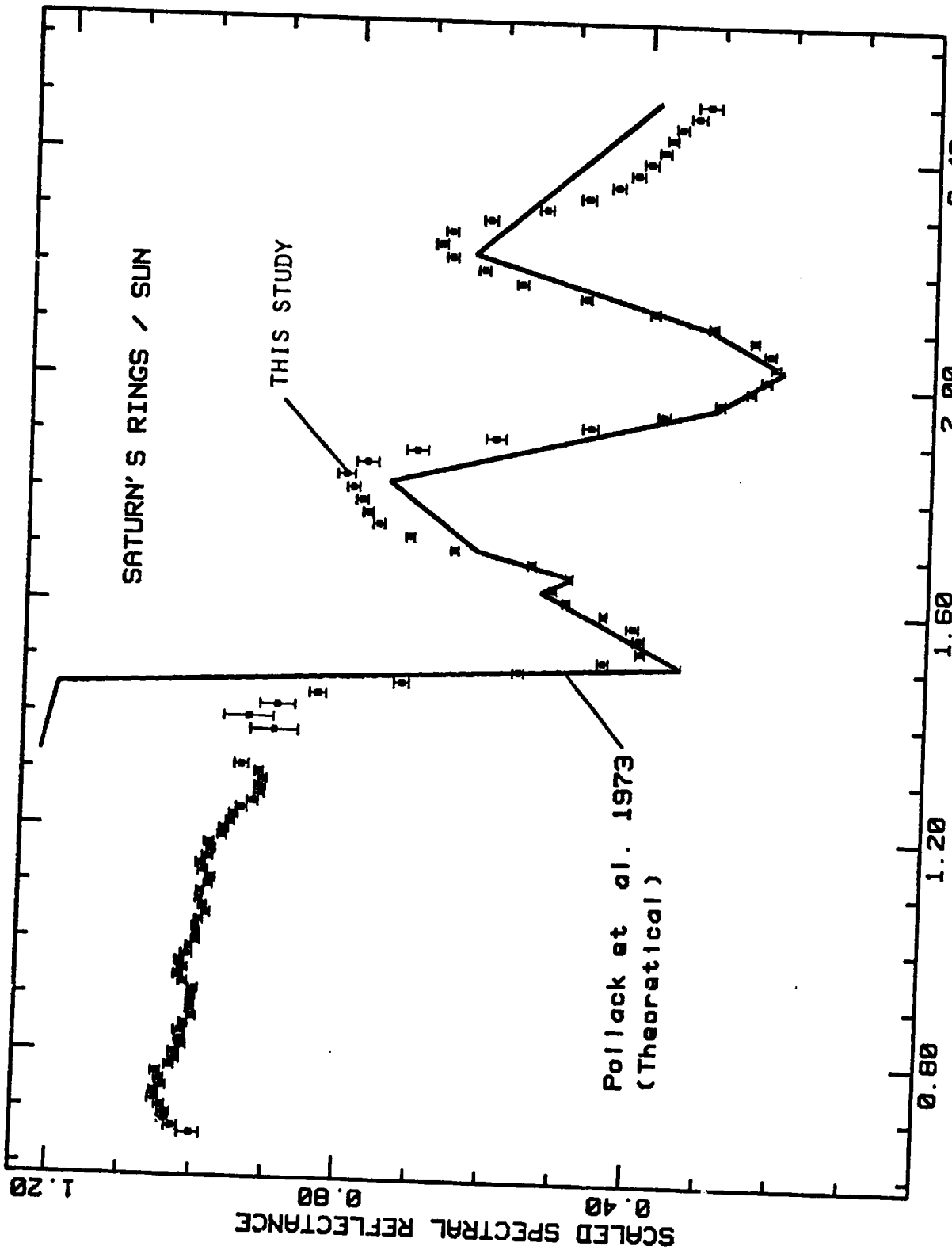

SATURN'S RINGS / SUN
THIS STUDY
Pollack et al. 1973
(Theoratical)
SCALED SPECTRAL REFLECTANCE
0.40
0.80
1.20
0.80
1.20
1.60
2.00
2.40
WAVELENGTH IN MICRONS

Figure 2

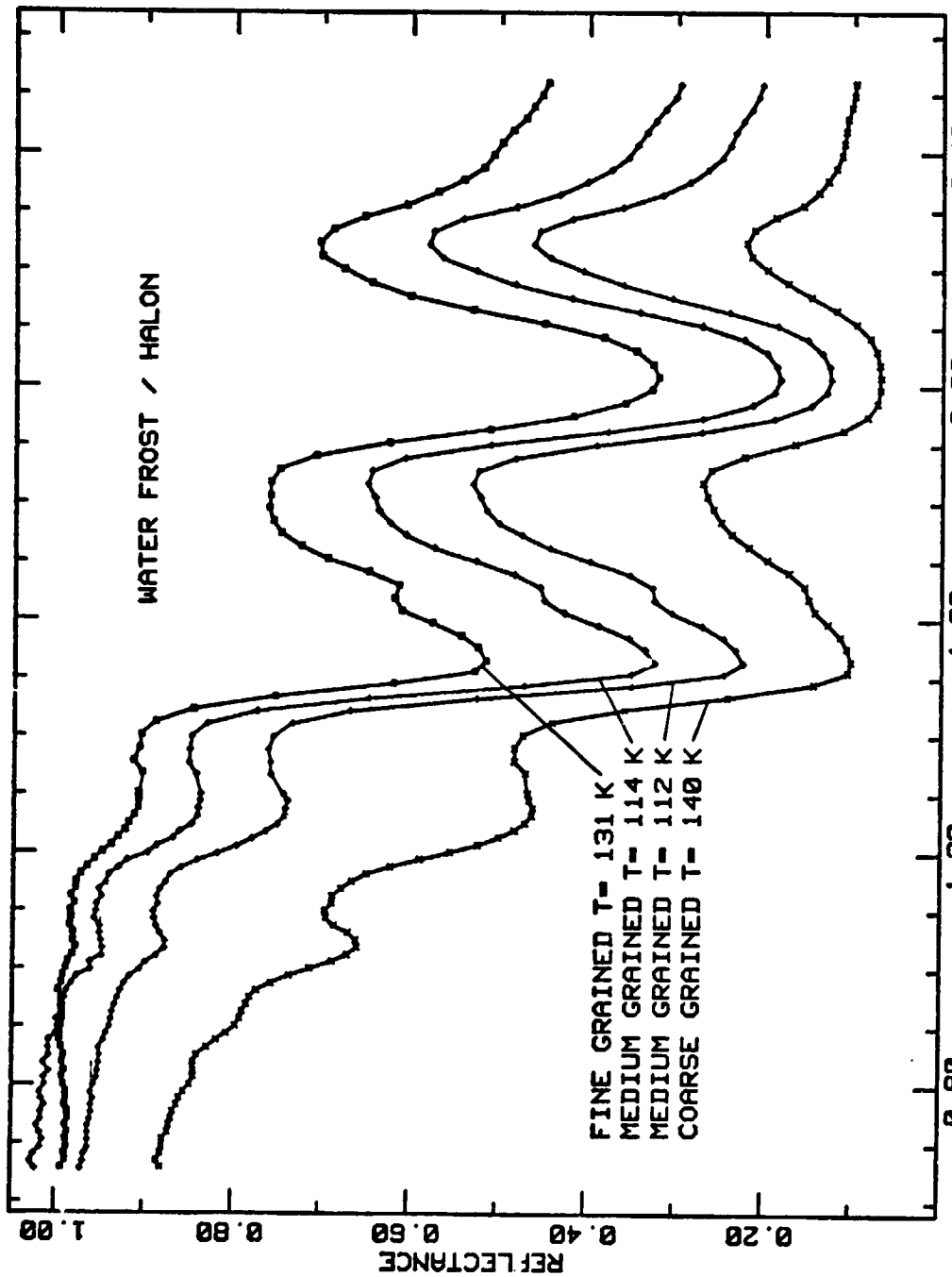

WATER FROST / HALON
FINE GRAINED T= 131 K
MEDIUM GRAINED T= 114 K
MEDIUM GRAINED T= 112 K
COARSE GRAINED T= 140 K
REFLECTANCE
0.20
0.40
0.60
0.80
1.00
0.80
1.20
1.60
2.00
2.40
WAVELENGTH IN MICRONS

Figure 3

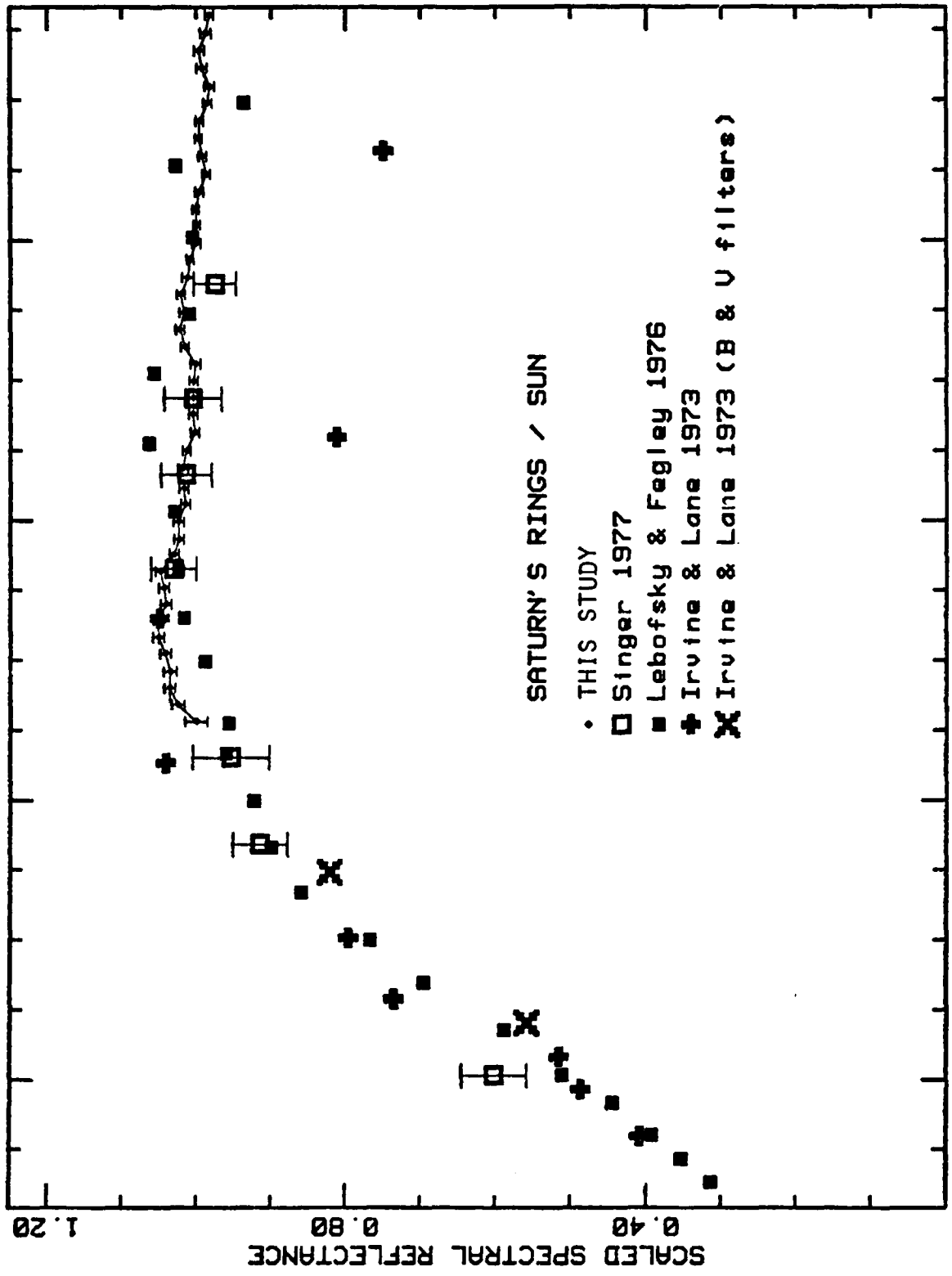

SATURN'S RINGS / SUN
• THIS STUDY
□ Singer 1977
■ Lebofsky & Fegley 1976
✚ Irvine & Lane 1973
✖ Irvine & Lane 1973 (B & V filters)
SCALED SPECTRAL REFLECTANCE
0.40
0.80
1.20
0.40
0.60
0.80
1.00
WAVELENGTH IN MICRONS

Figure 4

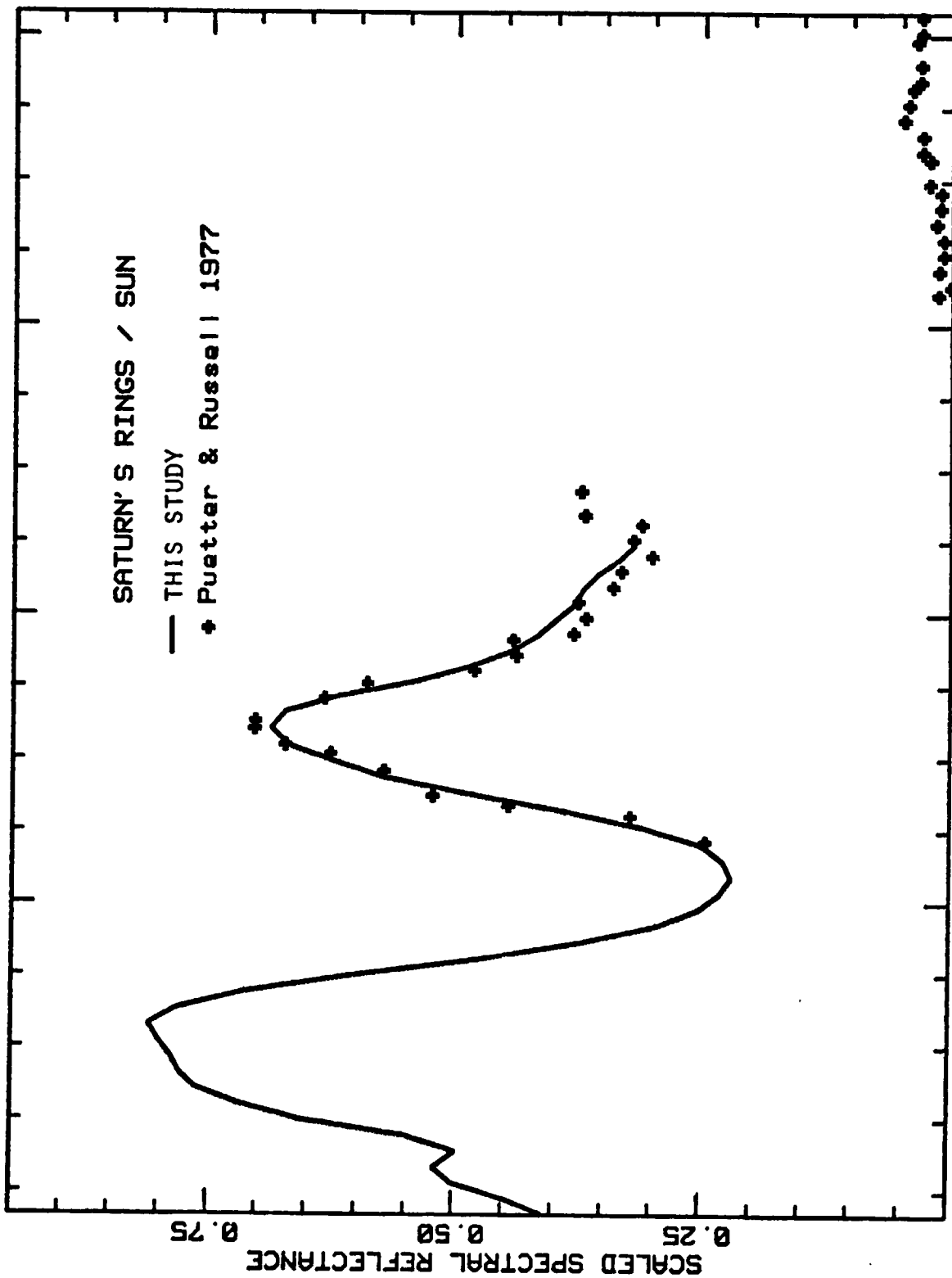

SATURN'S RINGS / SUN
THIS STUDY
Puatter & Russell 1977
SCALED SPECTRAL REFLECTANCE
0.25
0.50
0.75
2.00
2.40
2.80
3.20
WAVELENGTH IN MICRONS

Figure 5

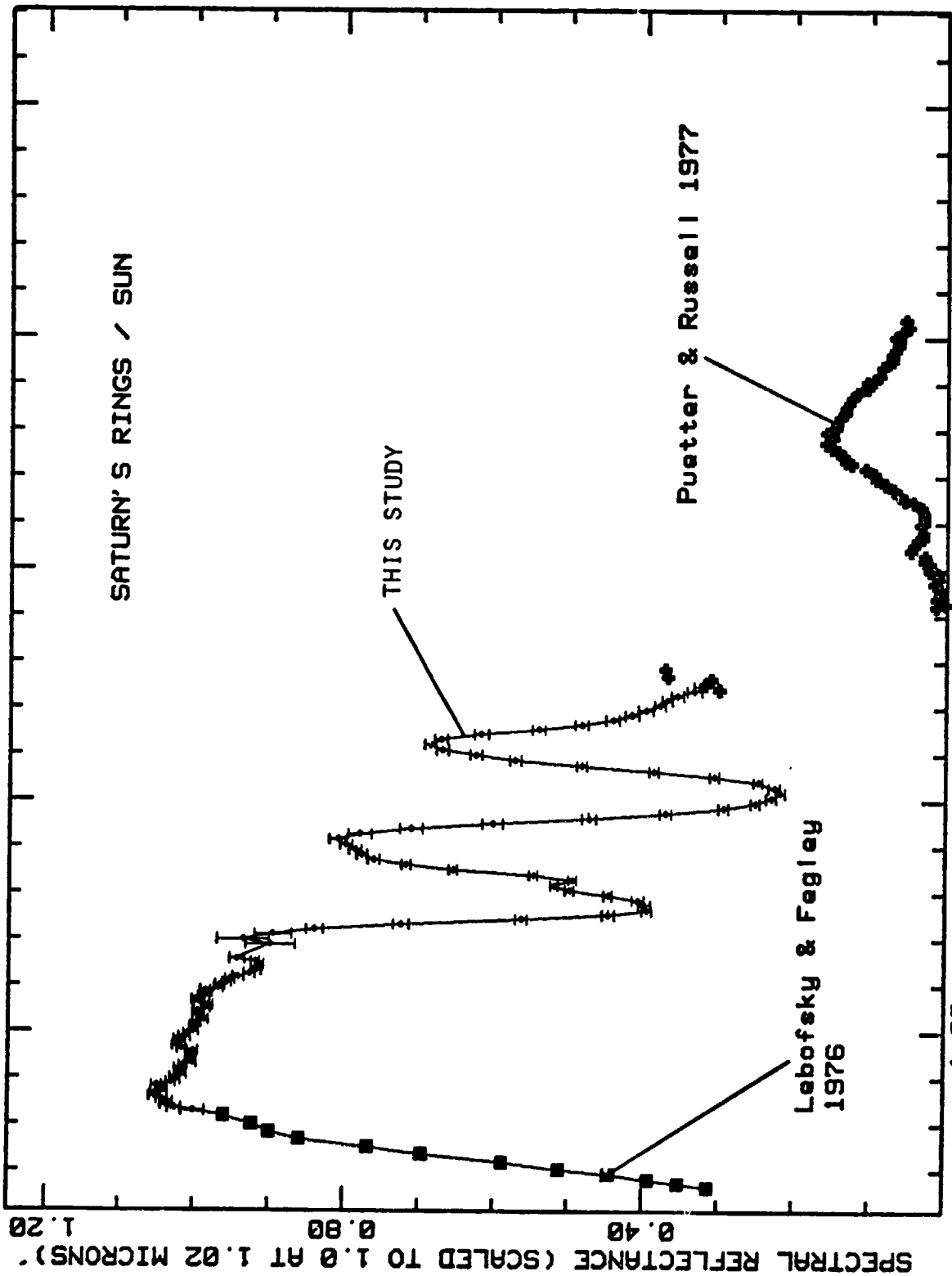

SATURN'S RINGS / SUN
THIS STUDY
Puetter & Russell 1977
Lebofsky & Fegley 1976
SPECTRAL REFLECTANCE (SCALED TO 1.0 AT 1.02 MICRONS)
0.40
0.80
1.20
1.00
2.00
3.00
4.00
5.00
WAVELENGTH IN MICRONS

Figure 6

SECTION I

CHAPTER 3

Mars: Near-Infrared Reflectance Spectra of Surface Regions and Compositional Implications

This chapter constitutes a portion of a paper which is to be submitted for publication to the Journal of Geophysical Research. Authors of the complete paper: T.B. McCord, R.N. Clark, R.B. Singer, and R.L. Huguenin.

Abstract

Reflectance spectra (0.65 - 2.50 μm) are presented for 11 martian areas. The spectral resolution is ∿1½% and the spatial resolution is 1000 - 2000 km. These are the first high quality spectrophotometric data at these wavelengths for regions on the surface. Spectral features previously observed are confirmed and better defined, and a number of important spectral properties are characterized for the first time. The spectra show water ice absorptions in the 1.5 and 2 μm regions, which if due to surface frost, would imply the presence of 1 to 2 mg/cm^2 H_2O. However, other studies have shown that the presence of a frost on the surface is unlikely. Water ice may exist in the pore structure of clay minerals if the clay structure is saturated. The dark region spectra indicate about four times less water ice than seen in bright regions. Since some bright material is present in dark regions there may be no water ice associated with the dark materials themselves. The presence of weak 2.3-μm absorption bands in many of the spectra imply the presence of hydroxylated magnesium-rich minerals such as amphiboles (anthophyllite) and sheet silicates (serpentine, talc, and magnesian smectites). The apparent absence of a 2.2-μm absorption implies that montmorillonite may not be a major component of the martian regolith. Many of the spectra also show

apparent absorptions at 1.9 μm, in the wing of the 2.0-μm martian atmospheric CO_2 absorption, which are due to bound water, strengthening the previous conclusions. Observed dark regions have previously not well determined near-infrared spectral shapes characteristic of thin semi-transparent alteration coatings overlying dark unaltered rock. Previously observed ferrous- and ferric-iron absorptions in the 1-μm region are better defined by these new data. Clinopyroxene (augite) is definitely present but olivine is not spectrally apparent.

INTRODUCTION

In order to define and characterize surface geologic units on Mars, one needs both morphological and compositional information. Although the recent spacecraft missions to Mars have provided a wealth of data on the type of surface features present, limited compositional and mineralogical information was returned, and most of that information was obtained only in the immediate vicinities of the two Viking landers. The reflectance spectrum of minerals, rocks and soils often contain electronic and molecular absorptions which are diagnostic of surface mineralogy. A review of this technique for geochemical remote sensing as applied to Mars is provided by Singer, et al. (1979). The Viking orbiters provided 3-color images, some of which have been processed into multispectral maps showing the extent of compositionally different surface color units (Soderblom, et al., 1978; Strickland, 1979; McCord et al., 1980b). The visible spectral region is dominated by ferric-oxide charge-transfer absorptions and most other mineralogic information is masked. Reflectance spectra covering a broader spectral region, particularly at near-infrared wavelengths, are required to further investigate the mineralogy and petrology of the martian surface.

The ideal source for this type of data would be a visible and near-infrared spectral mapper in orbit

around Mars; this experiment is unfortunately not likely to be flown for a number of years to come. The Galileo mission to Jupiter provides an excellent opportunity to obtain this type of data on its swingby of Mars, but the passage will be rapid and data will not be available until 1982 at the earliest. It is clear that earthbased telescopic reflectance spectroscopy will be an important source of compositional information for many years to come.

We report here on new, near-infrared reflectance spectra (0.65 to 2.50 μm) for regions on the martian surface observed in 1978. The high photometric quality of these data combined with increased near-infrared spectral coverage compared to previous regional observations provide new information about the spectral behavior and therefore the composition and physical nature of martian surface materials.

OBSERV' IONS AND DATA REDUCTION

The spectral reflectance (0.65 to 2.50 μm) of 11 regions on Mars, 1000-2000 km in diameter, were obtained during the 1978 apparition using the University of Hawaii 2.2m telescope located on Mauna Kea, Hawaii. A cooled (to 77 K) CVF (circular variable filter) spectrometer with an InSb detector was used to measure alternatively Mars and the standard star Beta Geminorum. The instrument and the method are described in detail by McCord et al. (1978, 1980a).

The CVF scans the spectrum from 0.65 μm to 2.50 μm every 10 seconds with 1½% spectral resolution. Successive scans were co-added and then written onto magnetic tape after 10 scans (100 seconds) which we call a run. The spectrum is divided into 120 data points (separate spectral channels). A mirrored chopper rotating at 24 Hz was used to chop between the object and sky. The sky signal was subtracted from the object signal by the digital data system. Two chop cycles make up one data channel. The aperture consists of a cooled mirror (at 77 K) mounted 45° to the optical axis at the cassegrain focus with the aperture hole in the center. Thus the location of the aperture appears as a black spot in the field of view. A beam splitter in the viewing optics allows photographs of the aperture location and the field of view to be taken while data is being obtained.

The aperture location during each observation was determined from the photographs using an orthographic-to mercator-projection computer program; areas of multiple observations of a region were combined to obtain the composite locations displayed in Figure 1.

The reflectance of each Martian area was determined using the star Beta Geminorum as a standard flux source and performing an extinction analysis as described by McCord and Clark (1979). The Beta Geminorum/Sun spectrum was measured on previous observing runs using the Apollo 16 lunar landing site and returned samples as intermediate standards (McCord et al., 1978,, 1980a).

RESULTS

The reflectance spectra of 11 regions on Mars are shown in Figures 2 and 3. The spectra have been scaled to unity at a wavelength of 1.02 μm. The error bars represent ±1 standard deviation of the mean of several independent measurements of the same region. Bright region results are shown in Figure 2, arranged with spectra most characteristic of bright regions at the top grading into spectra showing some intermediate characteristics at the bottom. Figure 3 shows spectral results for five dark regions and for the north polar region.

The locations of the bright and dark areas observed during the 1978 apparition, as well as those previously observed by this group (McCord and Westphal, 1971; McCord et al., 1977) are shown in Figure 1. The larger size of the 1978 regions is due to poor observing conditions and the relatively small angular size of Mars (12.6 arcsec.) at the time of these observations. Nevertheless these new near-infrared data substantially increase our knowledge of the martian surface. The dates, times, earth air mass range, integration time, and martian central meridian for each observation are given in Table 1.

A comparison of representative martian spectral types is given in Figure 4. Included is an average of

the highest quality bright region spectra, the spectrum for area 78-5, which has predominantly bright region characteristics but with some indication of intermediate to dark material, and the spectrum for area 78-10, which is the highest quality dark region spectrum.

These observations were made during a period (L_S=48-50°) of nearly maximum transparency of the martian atmosphere as measured directly by the Viking landers (afternoon visible optical depth ≈0.4, Pollack et al., 1979). Observational problems caused by the Earth's atmosphere are responsible for much of the variation in data quality. Bright region spectra 78-1B and 78-2 show rather sharp but repeatable features near 0.75 μm, 0.93 μm, and from 2.2 to 2.5 μm. A careful study of these and other data obtained on the same nights has shown that these features are probably instrumental in origin and do not represent martian phenomena.

ANALYSIS AND INTERPRETATION

General Spectral Characteristics

Bright region spectra are characterized from the visible to 0.75 μm by the wing of intense Fe^{3+} charge-transfer absorptions centered in the U.V., and by a weaker, asymmetric Fe^{3+} crystal-field absorption near 0.87 μm. These features have been attributed to a ferric oxide content of about 6 to 8 wt. % (Huguenin et al., 1977). From the band minimum near 0.87 μm to about 1.3 μm the spectrum slopes upwards. Between 1.4 and 1.7 μm there is a broad absorption which has been interpreted as H_2O ice from previous integral disc observations (McCord et al., 1978). Superimposed on this are narrower Mars atmospheric CO_2 absorptions, at 1.34, 1.45, and 1.62 μm. From 1.8 to 2.2 μm the spectrum is dominated by a deep, partially resolved triplet absorption also caused by martian atmospheric CO_2.

In contrast to bright region spectra, dark region spectra have a more distinctive peak near 0.75 μm and slope fairly uniformly downwards to 2.5 μm. This infrared spectral shape was not previously well defined and has important implications for compositional analysis, as discussed below. The martian CO_2 absorptions are of course the same as those discussed for bright regions. Dark region spectra show Fe^{2+} crystal-field

absorptions near 1 μm as well as the Fe^{3+} band near 0.87 μm described for bright regions.

Dark regions observed in 1978 had approximately one-half the reflectance at 1 μm as bright regions. This value is consistent with previous observations of regional reflectance differences made by McCord and Westphal (1971) and Binder and Jones (1972). Typical bright and dark region spectra from 0.3 to 2.5 μm are shown scaled to approximate normal reflectance in Figure 5. The spectra are composites of infrared data presented here and visible data from McCord and Westphal (1971) and McCord et al. (1977). Spectral effects of a model martian CO_2 atmosphere have been removed (Kieffer, 1968; McCord et al., 1978). This CO_2 correction is approximate, neglecting variations in surface topography.

Spectrum 78-5 is for Arabia, which although considered a classic bright region shows characteristics in some ways intermediate between bright and dark regions. The near-infrared absorption minimum occurs at longer wavelengths than for other bright regions and the slope is much flatter from 1.0 to 1.3 μm, although not negative as it is for dark region spectra. The implication here is that Arabia has a moderate amount of exposed dark material, or at least an excess ferrosilicate soil component compared to some other bright regions. Similar properties were noted by

Huguenin et al. (1977) in 1969 observations of this area (McCord and Westphal, 1971). If these characteristics have in fact survived through nearly ten years of global dust cyclying, a surface composed of dark boulders scattered on a background of bright soil seems plausible. Such a situation is observed at both Viking lander sites, for which no detailed spectra have yet been obtained.

The spectrum of the martian north polar cap region is shown in Figure 3. The spectrum appears similar to the dark region spectrum 78-10 shortward of 1.3 μm. Longward of 1.3 μm is a relatively strong water ice absorption extending from 1.4 to 1.8 μm. Centered at 2.0 μm is the strong CO_2 (atmospheric) absorption and the 2-μm ice band. Beyond 2.2 μm the reflectance decreases as seen in spectra of water frost. This spectrum is analyzed in detail in Clark and McCord (1980a).

Dark Region Composition

The earliest positive determination that dark regions on Mars consist largely of mafic igneous rocks was provided by Adams and McCord (1969) who successfully modeled a dark region spectrum from 0.3 to 1.1 μm using basalt grains with artificially induced surface oxidation. Huguenin (1973a, b, 1974) proposed that UV photostimulated oxidation on Mars would produce

surface alteration layers about 1 micrometer thick on basaltic rocks. He interpreted previously obtained spectrophotometry from 0.3 to 1.1 μm (McCord and Westphal, 1971; McCord et al., 1977) to indicate such a thin oxidized layer (Huguenin, 1976).

The near-infrared dark region spectra presented here provide new information about dark region spectral shape. The negative slope from about 1.1 μm to 2.5 μm had not been previously determined, and is atypical of unweathered or homogeneously oxidized rocks and minerals. Singer (1980a) has shown that this distinctive shape is in fact indicative of a brighter, oxidized layer overlying a dark unoxidized iron-bearing substrate, such as basaltic or ultramafic rock, in agreement with the earlier work described above. Analogy to naturally occurring alteration layers on terrestrial basalts indicates that the coatings on martian rocks (or rock fragments) are thicker than originally suggested by Huguenin (1973a, 1976), being somewhere between a few mircometers to over 10 micrometers thick (Singer, 1980a).

Absorptions near 1 μm, observed in nearly all previous dark region spectra, are defined significantly better in the new data, particularly for region 78-10. Adams (1968) was the first to suggest that these might be caused by Fe^{2+} in ferromagnesian minerals such as pyroxenes and olivines. Huguenin et al. (1977, 1978)

have provided detailed interpretations of the dark region spectra obtained in 1969 (McCord and Westphal, 1971) and 1973 (McCord et al., 1977). Spectrum 78-10 shows a compound structure near 1 μm, with a band centered near 0.88 μm and one near 0.99 μm. Detailed analysis by Singer (1980b) has shown that the 0.88-μm band is most likely caused by Fe^{3+} crystal-field transitions in the oxidized coating, with the possibility of some contribution from Fe^{2+} crystal-field absorptions in orthopyroxene or low-calcium pigeonite in the underlying rocks. The 0.99-μm band is firmly interpreted as indicating an augite clinopyroxene as a major component of these dark region rocks. Olivine, interpreted by Huguenin et al. (1977, 1978) to be abundant in most previously observed dark regions, was found to not be a major constituent in dark regions observed in 1978. A detailed discussion about olivine determination and the petrologic significance of olivine on Mars is given by Singer (1980b).

Spectral Evidence for Water

The spectra in Figures 2 and 3 all show a drop in reflectance from 1.3 to 1.4 μm. McCord et al. (1978) interpreted integral disc spectra with features similar to those seen here to be due to water ice plus a highly desiccated mineral hydrate. In order to investigate this possibility further the martian

spectra were modeled using an ice spectrum and spectra typical of oxidized basalt. Figure 6 show the spectra used in the simulation. The simulated spectrum for the bright area is typical of alteration products of mafic igneous rocks. The simulated spectrum for the dark area is typical of spectra of a thin (a few to over 10 micrometers thick) layer of alteration product overlying unweathered basalt (c.f. Adams and McCord, 1969; Singer, 1980a).

The ice spectrum is typical of a medium grained frost with grain sizes around 200 micrometers (see Clark, 1980a) and is scaled to a value of 0.18 at 1.02 μm. This scaling gave the best fit in the simulation below. The reflectance of an optically thick, medium grained frost is above 0.9 at 1.02 μm. If the simulated bright spectrum and the ice spectrum are added, then rescaled to 1.0 at 1.02 μm, the result can be compared to the Mars average bright area spectrum as seen in Figure 7a (top). The resultant simulation shows a reasonable match to the Mars spectrum. Dividing the bright area spectrum by the simulated spectrum gives the residual spectrum shown in Figure 7a (bottom). This residual spectrum agrees very well with the martian atmospheric CO_2 transmittance spectrum (described previously).

A similar analysis for the dark area spectrum 78-10 is shown in Figure 7b (top). The fit is not as

good as that obtained for the bright area although some of the apparent drop beyond 1.4 μm may still be explained by water ice. If the water ice absorption features were only about half as deep as those in Figure 7b, the fit would be better. Also, since the dark areas have a reflectance about half that of bright areas, the amount of water contributing to the dark area 78-10 spectrum is less. Thus the amount of water ice present is at least four times less in the dark areas.

The water ice spectrum fit to the bright area in Figure 7a indicates that an optically thick patch of medium grained frost covers approximately 5% of the area measured if the ice and bright material are in large scale patches. If the frost were evenly distributed on the surface, approximately 1 to 2 mg/cm^2 would be present based on laboratory studies by Clark (1980b). If the water ice is mixed with the other minerals in the surface, the amount of water in the top few millimeters would be about 5-10 wt. % (see Clark, 1980b). This amount of ice is difficult to explain based on current models (e.g. Clark, 1978; Farmer and Doms, 1979) unless the amount of bound water in the regolith is saturated.

The residual spectrum in Figure 7a shows apparent absorptions around 2.3 μm and at 1.9 μm in the wing of the 2.0-μm martian atmospheric CO_2 band. These

absorptions are indicative of bound water, the 1.9-μm absorption due to the $\nu_1 + \nu_2$ and $\nu_3 + \nu_2$ overtones and that at 2.3 μm due to an overtone of an Mg-OH bending mode and the OH stretch (e.g. Hunt and Salisbury, 1970; Hunt et al., 1971). Clark (1980b) has shown that bound water absorptions do not shift in wavelength appreciably ($\lesssim$100 Å) in the temperature range 290K to 150K. Clark (1980a, b) also showed that the bound water absorptions are distinguishable from pure water frost or ice. Anderson et al. (1967) showed the amount of water bound to montmorillonite decreases as the temperature is decreased below 273K. As the temperature decreases, bound water is forced out of clay structures and forms micro-crystals of ice in the pore structure. This would tend to occur during the martian night. As the temperature rises the next day, the ice will sublime if the H_2O vapor pressure in the atmosphere is too low. However, the ice crystals are within the clay mineral grains and as the temperature rises the clay minerals will tend to reabsorb the water. Thus an increase in vapor pressure may never be seen above the surface. Further study is needed to test this hypothesis.

The dark area simulation shows that there is about four times less water ice apparent than in the bright area simulation. The dark area observed was over 1000 km in diameter and some bright area material

is almost certainly present in patches. Singer and McCord (1979) investigated the affects of streaks and splotches of spectrally isolated bright material on the spectral reflectance of dark regions. Their results show that the drop in reflectance from 1.3 to 1.4 μm and the other signatures of water ice are decreased when the contribution of bright material to the spectrum is removed. Although a unique solution cannot be obtained, the water ice signature appears to be absent in spectra of "pure" dark materials.

The 2.3 μm Absorption

Nearly every spectrum in Figures 2 and 3 shows the presence of a 2.3-μm absorption feature. Because of the subtlety of these features a detailed examination was conducted of observations of Saturn's rings, the Gallilean satellites, and the Moon taken with the same instrument and two different calibration routes (Clark and McCord, 1980b, c; McCord et al., 1980a). No similar bands were found in other data, even those taken the same nights; therefore it is quite certain that these absorptions are characterisitic of Mars. The presence and center wavelengths of these features can be determined well from these data, but the band depths, or even the relative depths, are much less certain.

A single absorption at this location (∿2.3 μm) indicates an Mg-OH bond; often a weaker band of similar origin appears near 2.4 μm (Hunt and Salisbury, 1970). An absorption near 2.4 μm is possibly also present in some of these spectra, but the depth is approaching the noise limit of the data. Absorptions near 2.2 μm, characteristic of Al-OH bonds, may also be weakly present but are much less certain than the bands near 2.3 μm. One reason for this might be masking of any 2.2-μm features by the wing of the strong atmospheric CO_2 absorption. Weak absorptions just longward of 2.3 and 2.4 μm, and perhaps a very weak absorption just longward of 2.2 μm, are apparent in a spectrum of the integral martian disk obtained in 1976 by McCord et al. (1978). Carbonates are apparently not detected in any of the near-infrared data since a stronger 2.55 μm absorption would be expected to accompany one near 2.35 μm (Hunt and Salisbury, 1971).

In addition to providing evidence for hydroxylated minerals on Mars, a 2.3-μm band has interesting petrologic implications. Mg content greater than Al content in an unweathered igneous rock is characteristic of a mafic to ultramafic composition, generally with abundant olivine. Relative enrichments of Mg are also seen in certain pyroxenites, relatively uncommon terrestrial ultramafic rocks consisting primarily of pyroxenes (Nockolds et al., 1978). These observations correlate

with the Viking XRF analysis team conclusions that the measured soil chemistry is most consistent with the weathering products of mafic igneous rock (Toulmin et al., 1977); more recently a pyroxenite parent composition has been considered (B.C. Clark, personal communication, 1979). Very mafic to ultramafic average compositions for martian lavas have also been suggested by Maderazzo and Huguenin (1977) and McGetchin and Smyth (1978).

Mg-OH features would most probably be characteristic of alteration products of mafic igneous rocks rather than the rocks themselves. Possible Mg-rich minerals which might form by such alteration are anthophyllite (ferromagnesian amphibole) and a variety of trioctohedral sheet silicates such as serpentine, talc, and magnesian smectites (saponite, hectorite). The apparent absence (or at least extreme weakness) of any 2.2-μm Al-OH absorptions would seem to argue against montmorillonite as a major component of martian soils.

ACKNOWLEDGEMENTS

Much of this work was carried out at the University of Hawaii's Mauna Kea Observatory and Institute for Astronomy. This research was supported by the NASA grants NSG 7323 and 7590.

REFERENCES

Adams, J.B., Lunar and martian surfaces: Petrologic significance of absorption bands in the near-infrared, Science 159, 1453-1455, 1968.

Adams, J.B., and T.B. McCord, Mars: Interpretation of spectral reflectivity of light and dark regions, J. Geophys. Res. 74, 4851-4856, 1969.

Anderson, D.M., Gaffney, E.S., and Low, P.F., Frost phenomena on Mars, Science 155, 319-322, 1967.

Binder, A.B., and J.C. Jones, Spectrophotometric studies of the photometric function, composition, and distribution of the surface materials of Mars, J. Geophys. Res. 77, 3005-3019, 1972.

Clark, B.C., Implications of abundant hygroscopic minerals in the Martian regolith, Icarus 34, 645-655, 1978.

Clark, R.N., Water frost and ice: The near-infrared spectral reflectance 0.65-2.5 μm, J. Geophys. Res., submitted, 1980a. Thesis II Ch1

Clark, R.N., The spectral reflectance of water-mineral mixtures at low temperatures, J. Geophys. Res., submitted 1980b. Thesis II Ch2

Clark, R.N., and T.B. McCord, Mars residual north polar cap: Earth-based spectroscopic confirmation of water ice as a major constituent and evidence for hydrated minerals, J. Geophys. Res., submitted 1980a. Thesis III Ch1

Clark, R.N., and T.B. McCord, The Galilean satellites: Near-infrared spectral reflectance measurements (0.65-2.5μm) and a 0.325-5 μm summary, Icarus, in press 1980b. Thesis I Ch 1

Clark, R.N., and T.b. McCord, The rings of Saturn: New near-infrared reflectance measurements and a 0.326-4.08 μm summary, Icarus, submitted 1980c. Thesis I Ch 2

Farmer, C.B., and P.E. Doms, Global seasonal variation of water vapor on Mars and the implications for permafrost, J. Geophys. Res. 84, 2881-2888, 1979.

Huguenin, R.L., Photostimulated oxidation of magnetite. 1. Kinetics and alteration phase identification, J. Geophys. Res. 78, 8481-8493, 1973a.

Huguenin, R.L., Photostimulated oxidation of magnetite. 2. Mechanism, J. Geophys. Res. 78, 8495-8506, 1973b.

Huguenin, R.L., The formation of goethite and hydrated clay minerals on Mars, J. Geophys. Res. 79, 3895-3905, 1974.

Huguenin, R.L., Mars: Chemical weathering as a massive volatile sink, Icarus 28, 203-212, 1976.

Huguenin, R.L., J.B. Adams, and T.B. McCord, Mars: Surface mineralogy from reflectance spectra, in Lunar Science VIII, 478-480, Lunar Science Institute, Houston, 1977.

Huguenin, R.L., J.W. Head, and T.R. McGetchin, Mars: Petrologic units in the Margaritifer Sinus and Coprates

Quadrangle, Reports of Planetary Geology Program, 1977-1978, NASA Tech. Memo 79729, 1978.

Hunt, G.R., Spectral signatures of particulate minerals in the visible and near infrared, Geophys. 74, 501-513, 1977.

Hunt, G.R., and J.W. Salisbury, Visible and near-infrared spectra of minerals and rocks: I. Silicate minerals, Mod. Geol. 1, 283-300, 1970.

Hunt, G.R., and J. W. Salisbury, Visible and near-infrared spectra of minerals and rocks: II. Carbonates, Mod. Geol. 2, 23-30, 1971.

Hunt, G.R., J.W. Salisbury, and C.J. Lenhoff, Visible and near-infrared spectra of minerals and rocks: III. Oxides and Hydroxides, Mod. Geol. 2, 195-205, 1971.

Kieffer, H.H., Near infrared spectral reflectance of simulated Martian frosts, Ph.D. Dissertation, Calif. Inst. of Technol., Pasadena, 1968.

Madarazzo, M., and R.L. Huguenin, Petrologic implications of Viking XRF analysis based on reflection spectra and the photochemical weathering model, (abstract) Bull. Am. Astron. Soc. 9, 527-528, 1977.

McCord, T.B., and J.A. Westphal, Mars: Narrow-band photometry, from 0.3 to 2.5 microns of surface regions during the 1969 apparition, Astrophys. J. 168, 141-153, 1971.

McCord, T.B., R.L. Huguenin, D. Mink, and C. Pieters, Spectral reflectance of Martian areas during the 1973 opposition: Photolectric filter photometry 0.33-1.10 μm, Icarus 31, 25-39, 1977.

McCord, T.B., R.N. Clark, and R.L. Huguenin, Mars: Near-infrared spectral reflectance and compositional implication, J. Geophys. Res. 83, 5433-5441, 1978.

McCord, T.B., and R.N. Clark, Atmospheric extinction 0.65-2.50 μm above Mauna Kea, Pub. Astron. Soc. Pac. 91, 571-576, 1979. Thesis App B

McCord, T.B., R.N. Clark, L.A. McFadden, C.M. Pieters, P.D. Owensby, and J.B. Adams, Moon: Near-infrared spectral reflectance, A first good look, J. Geophys. Res. to be submitted, 1980a.

McCord, T.B., R.B. Singer, J.B. Adams, B.R. Hawke, J.W. Head III, R.L. Huguenin, C.M. Pieters, S. Zisk, and P. Mouginis-Mark, Definition and characterization of Mars surface units, J. Geophys. Res. to be submitted, 1980b.

McGetchin, T.R., and J.R. Smyth, The mantle of Mars: Some possible geological implications of its high density, Icarus 34, 512-536, 1978.

Nockolds, S.R., R.W.O'B Knox, and G.A. Chinner, Petrology for Students, Cambridge University Press, 1978.

Pollack, J.B., D.S. Colburn, F.M. Flaser, R. Kahn, C.E. Carlston, and D. Pidek, Properties and effects

of dust particles suspended in the Martian atmosphere J. Geophys. Res. 84, 2929-2946, 1979.

Singer, R.B., The composition of the Martian dark regions: I, Visible and near-infrared spectral reflectance of analog materials and interpretation of telescopically observed spectral shape, to be submitted to J. Geophys. Res., 1980a.

Singer, R.B., The composition of the Martian dark regions: II, Analysis of telescopically observed absorptions in near-infrared spectrophotometry, to be submitted to J. Geophys. Res., 1980b.

Singer, R.B., T.B. McCord, R.N. Clark, J.B. Adams, and R.L. Huguenin, Mars surface composition from reflectance spectroscopy: A summary, J. Geophys. Res., in press, December 1979.

Soderblom, L.A., K. Edwards, E.M. Eliason, E.M. Sanchez, and M.P Charette, Global color variations on the Martian surface, Icarus 34, 446-464, 1978.

Strickland, E.L. III, Martian albedo/color units: Viking lander 1 stratigraphy vs. Orbiter color observations, (abstract) Bull. Am. Astron. Soc. 11, 574, 1979.

Toulmin, P. III, A.K. Baird, B.C. Clark, K. Keil, H.J. Rose, Jr., R.P. Christian, P.H. Evans, and W.C. Kelliher, Geochemical and mineralogical interpretation of the Viking inorganic chemical results, J. Geophys. Res. 82, 4625-4634, 1977.

FIGURE CAPTIONS

Figure 1: Locations on Mars for spectrophotometric observations by McCord and others. The first two digits represent the year of observation (e.g. 69-1 was observed in 1969). The 1969 observations (0.3 to 1.1 μm) are described by McCord and Westphal (1971); the 1973 observations (0.3 to 1.1 μm) are described by McCord et al. (1977); the 1978 observations (0.65 to 2.50 μm) are presented in this paper. The locations of observations for which the surface was partially or wholly obscured by atmospheric dust are not shown. (Base map: USGS Topographic Map of Mars I-961, 1976).

Figure 2: The reflectance spectra of bright regions obtained in this study are plotted here scaled to a value of 1.0 at 1.02 μm. The error bars represent ±1 standard deviation of the mean of several independent observations.

Figure 3: The reflectance spectra of the dark regions and the north polar region obtained in this study are plotted here scaled to 1.0 at 1.02 μm. The error bars represent ±1 standard deviation of the mean of several independent observations.

Figure 4: The reflectance spectra of three characteristic martian surface types are compared: (top) the average of three bright region spectra (78-1A, 3, and 4) from Figure 2, (middle) an intermediate type spectrum (78-5), and (bottom) a dark region spectrum (78-10).

Figure 5: Composite reflectance spectra from 0.33 to 2.50 μm are shown for typical bright and dark region spectra scaled approximately to normal reflectance. A model atmospheric CO_2 spectrum has been removed so that these spectra are more representative of surface material. The visible data are from McCord and Westphal (1971) and McCord et al. (1977).

Figure 6: The reflectance spectrum representing the continuum for the bright (top) and dark (middle) regions are shown. These spectra were chosen as described in the text. The top spectrum is approximately that of a heavily oxidized basalt and the middle spectrum that of a thin layer of oxidation layer on a basalt. The bottom spectrum is that of H_2O ice (Clark, 1980a). These spectra are used in producing those shown in Figure 7.

Figure 7: The reflectance spectrum of the average bright area shown in Figure 4 (top) is shown

here (a) with an over-plot of a combination of the bright area continuum and the H_2O ice spectrum shown in Figure 6. Beneath is shown the residual spectrum created by dividing the two spectra shown at top. Plotted on the residual spectrum is the transmission spectrum of CO_2 for the path length of the Mars atmosphere as described in the text. Most of all of the features in the residual spectrum are accounted for by the CO_2 absorptions. In part (b) of this figure a similar sequence to part (a) is shown, but for the dark area spectrum 78-10. The simulation, which represents about half the water ice in the part (a) simulation does not fit as well as for bright area spectra and indicates even less water ice is present in the dark region.

TABLE CAPTIONS

The martian observational parameters for the spectra in Figures 2 and 3 are tabulated. The times are the beginning times of the first and last runs (100 seconds per run). The air mass values are also the values at the beginning of the first and last run. The last column, CM_0, is the central meridian longitude in degrees of the martian sub-earth point at the mid-point of the observation. The spectrum 78-10 in Figure 3 is the average of data from two nights (February 14 and 16). The martian north pole was tilted toward the earth 9°.25 and toward the sun 18°.70. The planetocentric longitude of the sun, L_s, was 49° (spring in the northern hemisphere).

TABLE I

Mars Observational Parameters

UT Date Feb. 1978	Area	Time (UT)	Earth Air Mass Range	Runs	Total Integrating Time Sec.	CM_0
20	78 - 1A	05:55 - 06:05	1.17 - 1.14	6	600	205
21	78 - 1B	06:41 - 07:00	1.07 - 1.04	11	1100	208
21	78 - 2	08:01 - 08:18	1.00 - 1.01	9	900	227
20	78 - 3	07:20 - 07:31	1.02 - 1.02	6	600	226
16	78 - 4	08:57 - 09:04	1.01 - 1.02	4	400	285
14	78 - 5	07:19 - 07:24	1.05 - 1.05	2	200	278
20	78 - 6	10:52 - 11:06	1.27 - 1.33	6	600	278
20	78 - 7	10:05 - 10:23	1.12 - 1.17	8	800	267
21	78 - 8	08:21 - 08:33	1.01 - 1.01	7	700	232
20	78 - 9	07:47 - 08:00	1.01 - 1.00	7	700	233
14	78 - 10	07:26 - 07:28	1.05 - 1.04	2	200	280
16	78 - 10	10:09 - 10:14	1.09 - 1.10	4	400	302
20	78 - 11	06:11 - 06:22	1.13 - 1.10	6	600	209

ORIGINAL PAGE IS
OF POOR QUALITY

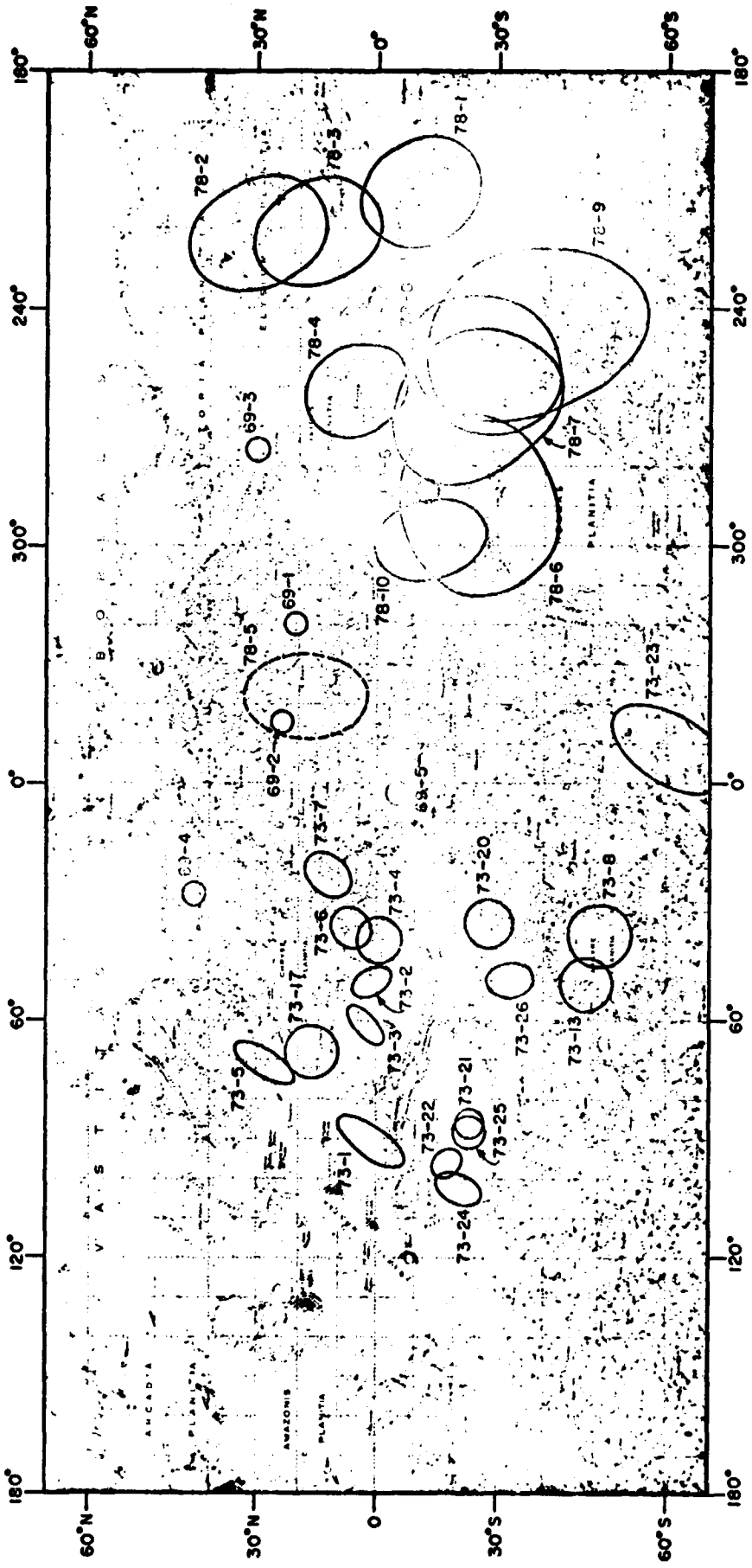


Figure 1

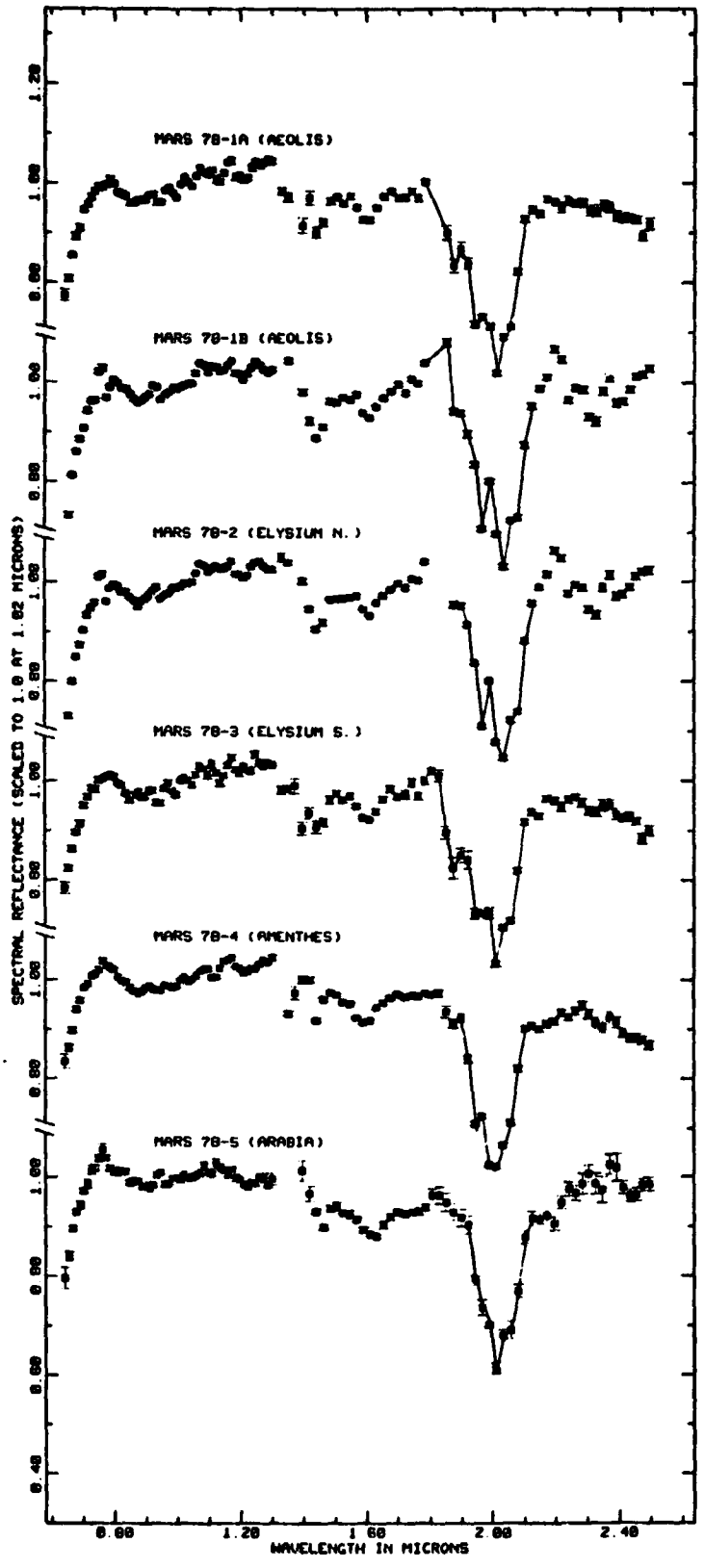

MARS 78-1A (AEOLIS)
MARS 78-1B (AEOLIS)
MARS 78-2 (ELYSIUM N.)
MARS 78-3 (ELYSIUM S.)
MARS 78-4 (AMENTHES)
MARS 78-5 (ARABIA)
SPECTRAL REFLECTANCE (SCALED TO 1.0 AT 1.02 MICRONS)
WAVELENGTH IN MICRONS
0.80
1.20
1.60
2.00
2.40

Figure 2

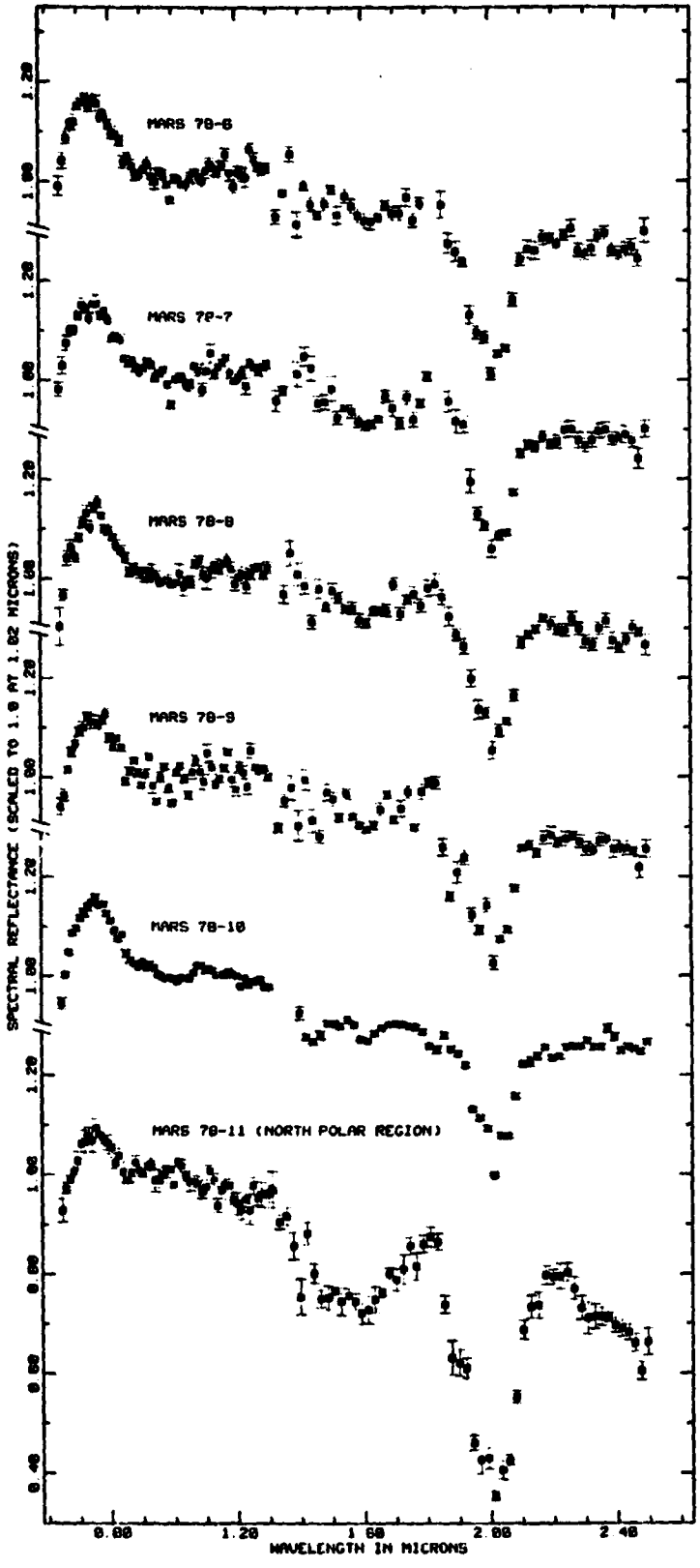

MARS 78-6
MARS 78-7
MARS 78-8
MARS 78-9
MARS 78-10
MARS 78-11 (NORTH POLAR REGION)
SPECTRAL REFLECTANCE (SCALED TO 1.0 AT 1.82 MICRONS)
WAVELENGTH IN MICRONS
0.80
1.20
1.60
2.00
2.40

Figure 3

ORIGINAL PAGE IS
OF POOR QUALITY

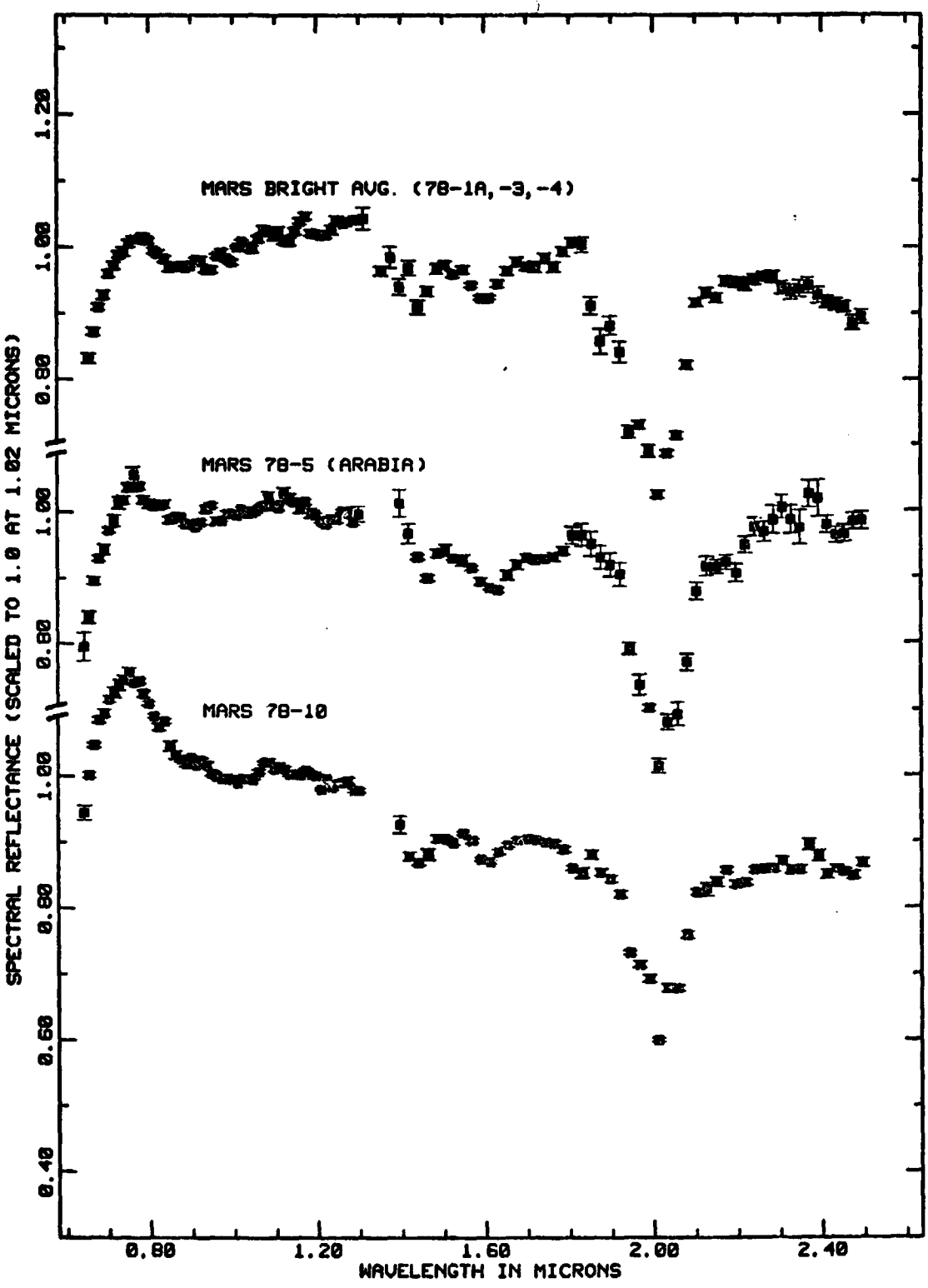


Figure 4

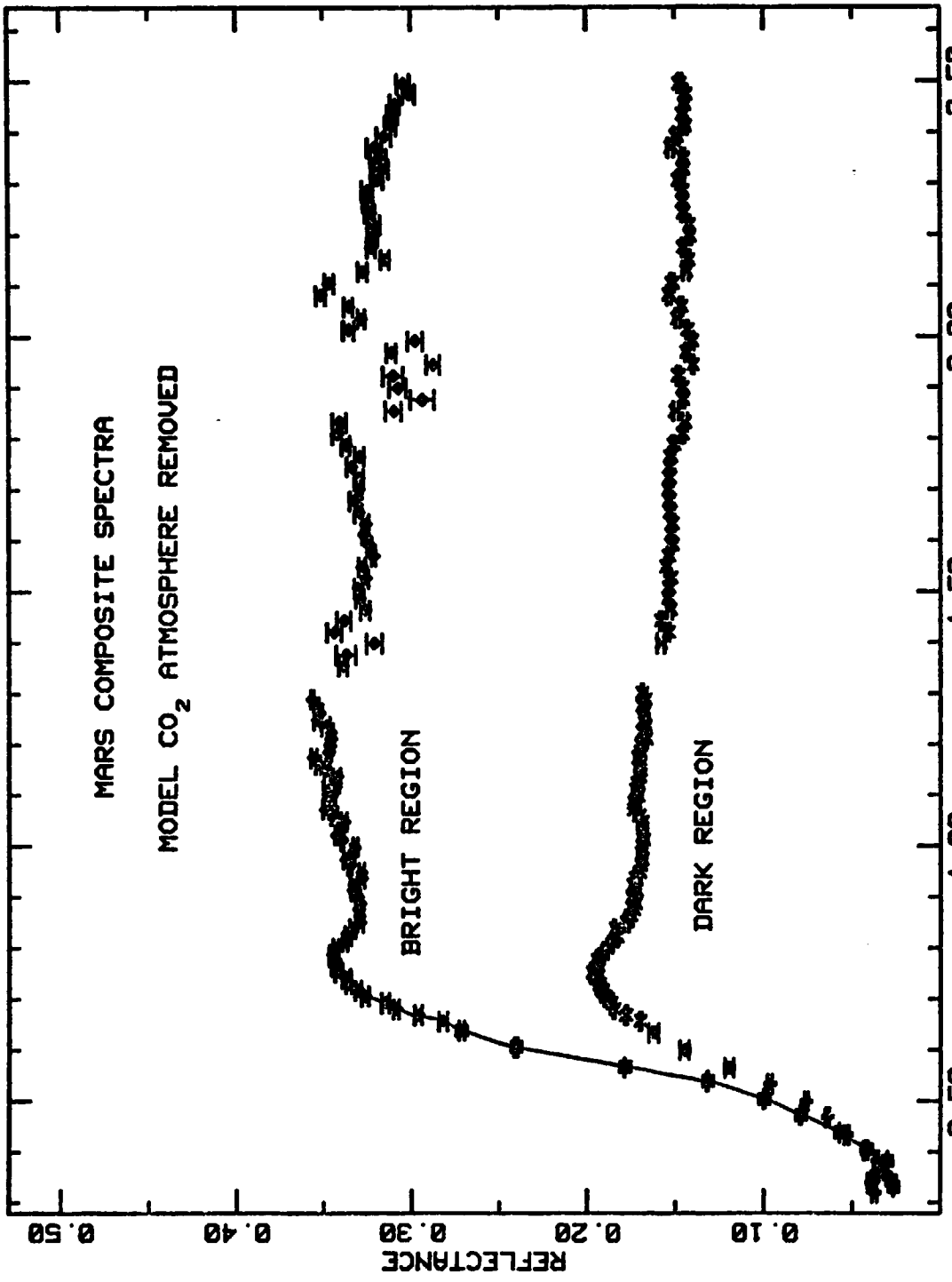

MARS COMPOSITE SPECTRA
MODEL CO_2 ATMOSPHERE REMOVED
BRIGHT REGION
DARK REGION
REFLECTANCE
0.10
0.20
0.30
0.40
0.50
0.50
1.00
1.50
2.00
2.50
WAVELENGTH IN MICRONS

Figure 5

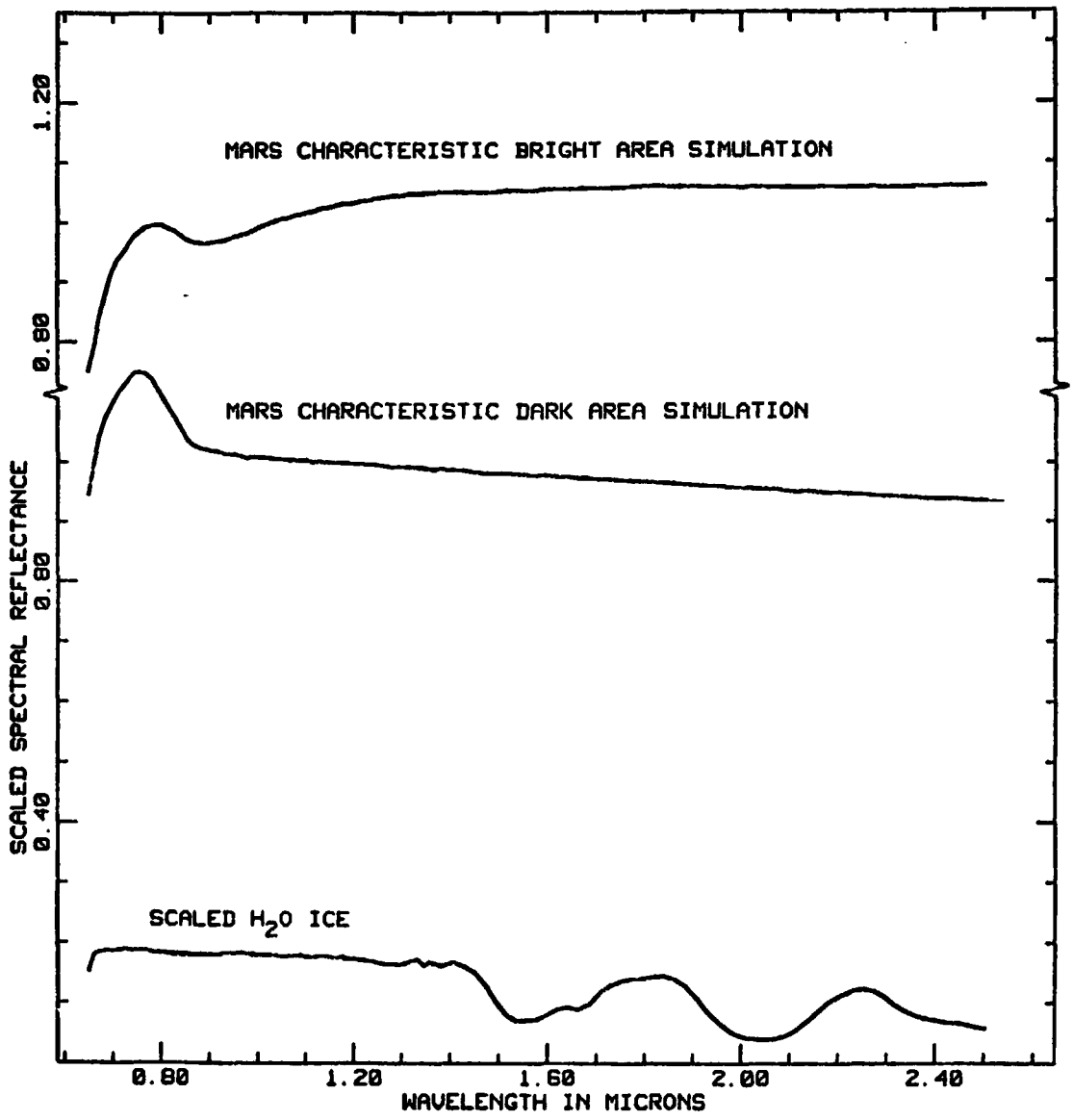

MARS CHARACTERISTIC BRIGHT AREA SIMULATION
MARS CHARACTERISTIC DARK AREA SIMULATION
SCALED H_2O ICE
SCALED SPECTRAL REFLECTANCE
1.20
0.80
0.80
0.40
0.80
1.20
1.60
2.00
2.40
WAVELENGTH IN MICRONS

Figure 6

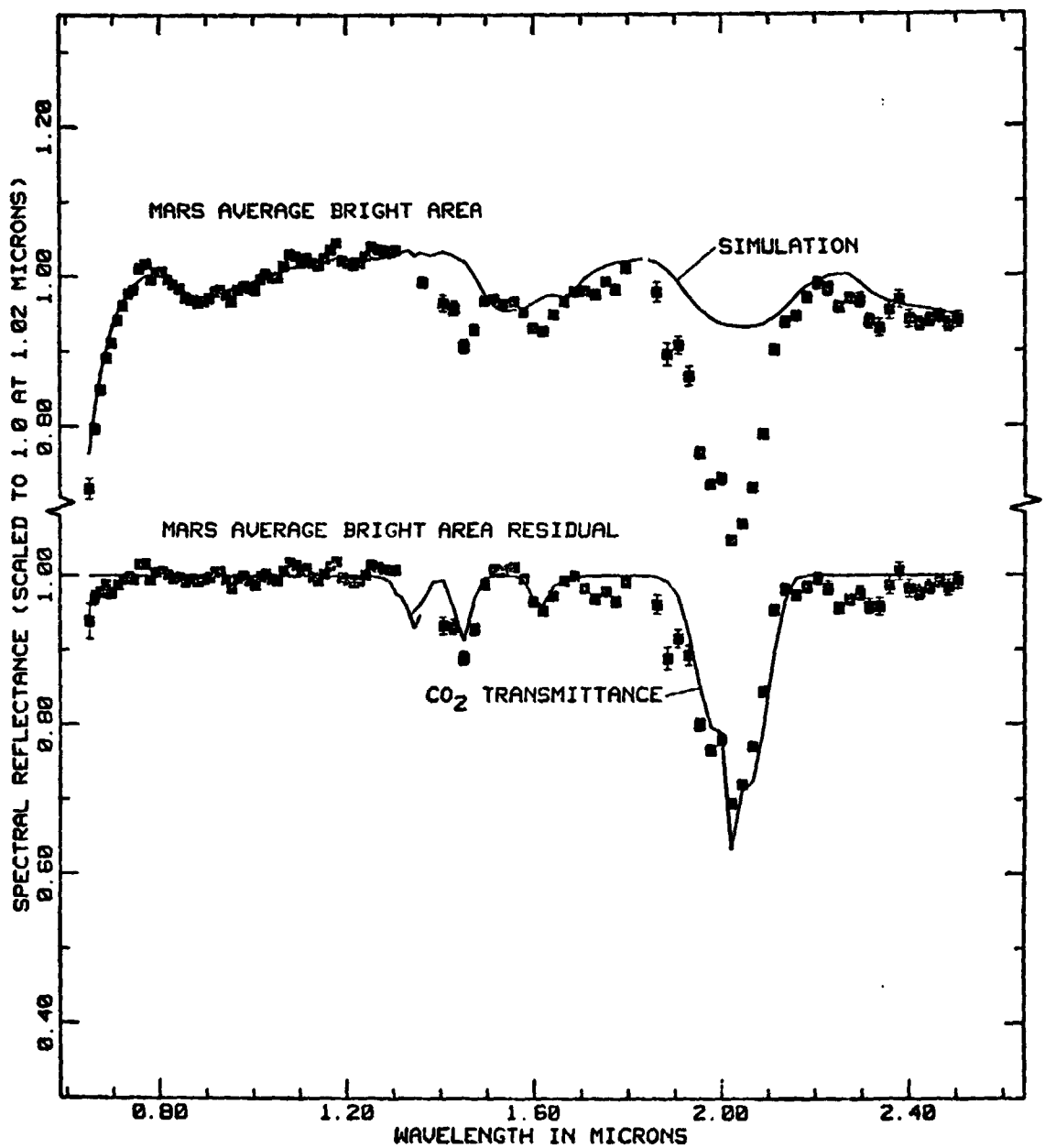

MARS AVERAGE BRIGHT AREA
SIMULATION
MARS AVERAGE BRIGHT AREA RESIDUAL
CO_2 TRANSMITTANCE
SPECTRAL REFLECTANCE (SCALED TO 1.0 AT 1.02 MICRONS)
1.20
1.00
0.80
1.00
0.80
0.60
0.40
0.80
1.20
1.60
2.00
2.40
WAVELENGTH IN MICRONS

Figure 7A

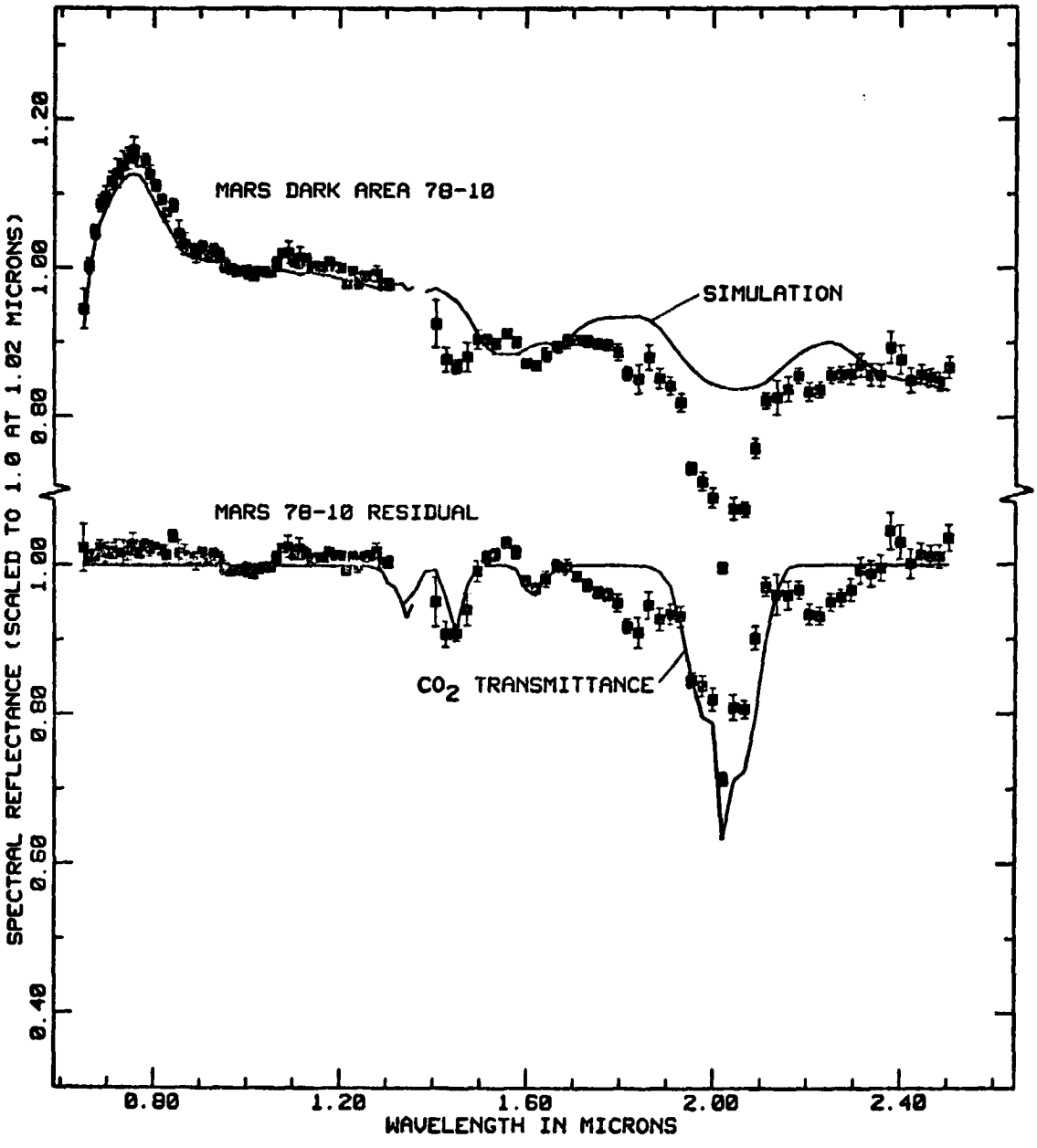

MARS DARK AREA 78-10
SIMULATION
MARS 78-10 RESIDUAL
CO_2 TRANSMITTANCE
SPECTRAL REFLECTANCE (SCALED TO 1.0 AT 1.02 MICRONS)
1.20
1.00
0.80
1.00
0.80
0.60
0.40
0.80
1.20
1.60
2.00
2.40
WAVELENGTH IN MICRONS

Figure 7B

SECTION II

LABORATORY STUDIES

SECTION II

CHAPTER 1

Water Frost and Ice: The Near-Infrared Spectral Reflectance 0.65-2.5 μm

This chapter has been submitted for publication to the Journal of Geophysical Research. Author: R.N. Clark.

ABSTRACT

The spectral reflectance of water frost and frost on ice as a function of temperature and grain size is presented with 1½% spectral resolution in the 0.65 to 2.5-μm region. The well known 2.0- 1.65- and 1.5-μm solid water absorption bands are precisely defined along with the little studied 1.25-μm band, and the previously unidentified (in reflectance) 1.04- 0.90- and 0.81-μm absorption bands. The spectral contrast of the 1.5-μm band complex is quantitatively analyzed using a non-linear least squares algorithm to resolve the band into four gaussian components as a function of grain size and temperature. It is found that the 1.65-μm component, which was thought to be a good temperature sensor, is highly grain size dependent and poorly suited to temperature sensing. Another gaussian component appears to show an excellent dependence of width with grain-size while being independent of temperature. The relative apparent band depths are different for frost layers on ice than for thick layers of frost and may explain the apparent band depths seen in many planetary reflectance spectra.

INTRODUCTION

Water ice has been identified on several solar system objects using reflectance spectroscopy: the Galilean satellites Europa, Ganymede and Callisto (Pilcher et al., 1972), Saturn's rings (Pilcher et al., 1970) and several of the satellites of Saturn (Fink et al., 1976; Morrison et al., 1976). New reflectance spectra of the Galilean satellites and Saturn's rings are now comparable in quality to that achievable in the laboratory in the 0.35- to 2.5-μm region (Clark and McCord 1979a, b). Thus an understanding of the reflectance spectra of water ice is important for planetary remote sensing studies.

Most studies of the spectra of water ice have been of the transmittance in the infrared beyond about 2.5 μm. This method is used in order to help determine the structure of the ice. Wavelengths shortward of 2.5 μm have been largely ignored due to the great complexity of the overtone bands present in this spectral region. Ockman (1958) reviewed the reflectance and transmittance spectra of ice and the possible assignments of the observed bands. Kieffer (1968, 1970) presented reflectance spectra of water frost which showed some variations with temperature and grain size. Fink and Larson (1975) presented

evidence for the temperature dependence of the 1.65-μm band and attempted to remove effects due to grain size in order to provide a calibration curve of the relationship.

Reflectance spectra of water frost and water frost on ice are presented here in order to show the large range of spectral contrasts and features which may be encountered in remote sensing of planetary surfaces.

EXPERIMENTAL EQUIPMENT

The spectrometer used in this study is the same as that used in obtaining reflectance spectra of planetary surfaces (e.g. Clark and McCord 1979a, b; McCord et al. 1978) except that it is used on a laboratory goniometer rather than a telescope. The spectrometer uses an indium antimonide solid state detector, a circular variable filter, and apertures (to select the area being measured), all cooled to liquid nitrogen temperature. The optics to view the sample include a cassegrain telescope operating in an inverted mode with the sample located at the cassegrain focus. The light source is mounted on a movable arm and is collimated by an f/8 off-axis parabolic mirror. The viewing path is reflected by four mirrors on a movable arm to allow for varying the angle of emission of the light. The mirrors are mounted so as to cancel mirror-induced polarization. The sample is illuminated by a 250 watt quartz halogen bulb in an integrating sphere operated from a constant voltage power supply. The collimation of the light source was 1°7 and 1°1 for the viewing beam. The angle of incidence was 0° and the angle of emission 10° for the data presented here. The light source is uniform in intensity to better than 2% over a 30mm diameter area, and the area viewed by

the spectrometer was 6mm in diameter. The intensity of the light source at the sample was 1.25 milliwatts per square centimeter as measured by a Tektronix J16 digital photometer with a J6502 probe. The sensitivity of the spectrometer is excellent, being at the state of the art in present indium antimonide detector systems. The signal to noise of the data is better than 0.3% on samples with high reflectance ($\gtrsim$ 90%) from one 100-second integration, and the light source is stable to better than 0.5% over many (5-10) hours (after an initial warm-up of about 1 hour).

The environmental chamber for frost growth consists of quartz optical dome 24 centimeters in diameter with radiation shielding covering most of the dome but allowing a narrow viewing slit (for phase angle work). The chamber was operated with one sample chamber directly attached to the copper cold finger. The standard is on a movable arm which was warmer than the sample. This mode allows cooling of samples to $\sim$100 K with LN_2 as the coolant. Frost growth was performed by opening a flask of distilled water to the chamber when under vacuum. The water then boiled and condensed on the cold surface in the chamber. The chamber may be operated at pressures ranging from a vacuum ($\lesssim$ millitorr) to

a little above atmospheric pressure and can be cooled or warmed slowly enough to obtain 1 to 2 K temperature resolution. The samples can be monitored visually with a 10x to 40x viewer and photographed with a 3x, f/110 camera system giving a resolution at the sample of 20 - 30 micrometers and a very good depth of field.

CALIBRATION

The data presented in this study were obtained using Halon (NBS test number 232.04/213908, 1975) as the reflectance standard. The reflectance of halon is ∿ 99% or greater at all wavelengths in this spectral region and is generally quite smooth except for a small (∿ 1½%) absorption centered at 2.15 μm. Halon is an excellent standard because of its high reflectance, long term stability, and the fact that it does not absorb water and standards prepared by different people agree excellently. The sample and standard are each measured by the spectrometer in 100-second integration periods (called runs). A run is made up of 10 scans of the spectrum with the signal coadded in the digital data system on each scan (1 revolution of the circular variable filter takes 10 seconds). Several runs are taken of each sample or standard to be measured, and the results (of each run) are written onto magnetic tape for later processing by computer. A dark measurement (no light on the sample) is taken several times an hour. The dark signal is typically less than 0.1% of the data and is subtracted from the signal of the sample and standard. The signal ratio of the

sample to the Halon then gives the reflectance. The reproducibility of the Halon signal is better than 0.5% over many hours. This is due to the stability of the light source and the solid state detector system (operating at 77 Kelvin). The analysis was performed with the interactive processing routines described by Clark (1979).

SPECTRA OF WATER FROST

The spectral reflectance of water frost over a range of grain sizes are shown in Figure 1. The fine grained frost has a characteristic grain size of approximately 50 micrometers, while the coarse grained frost has a typical grain size of .4 to 2 millimeters as determined from photographs and visual inspection. The grain sizes were crudely controlled by the rate of frost growth - the coarsest frost taking over 24 hours to form, the finest, about 3 hours. The frost depth was 4 - 5mm except for the coarsest, which was ∿ 20mm deep.

The major well known features are the 2.02-2.02-μm, 1.55-μm, and the 1.65-μm bands. The 1.26-μm feature has been seen in several published reflectance spectra (e.g. Kieffer, 1970; Fink and Larson, 1975) but has received little or no attention. The 1.04-, 0.90-, and 0.81-μm absorptions have not been reported before (in reflectance). Ockman (1958) summarized the observed features in water ice (mostly from absorption studies), with the band assignments shown in Table 1.

Fink and Larson (1975) observed the temperature dependence of the 1.65-μm absorption. This feature becomes more prominent with decreasing temperature.

Fink and Larson attempted to derive a calibration curve by computing the equivalent width of the 1.65-μm feature divided by the equivalent width of the large 1.5-μm complex (including the 1.65-μm band).

GAUSSIAN COMPONENT ANALYSIS

In order to analyze quantitatively the frost spectra, gaussian components were fit to the absorption features using a non-linear least squares analysis routine. This routine was adapted from the work of Kaper et al. (1966) and Bevington (1969). The routine is currently limited to fitting five gaussian components and a 6th order continuum. The gaussian analysis was performed by taking the logarithm of the reflectance and performing the fit in energy space. This type of analysis is for the purpose of quantitatively describing the absorption features - each gaussian component does not necessarily describe an actual overtone absorption.

Five gaussian components are not enough to describe the water ice spectra in Figure 1. Thus, only portions of the spectrum were analyzed at one time. A continuum was first removed from each spectrum before the gaussian analysis. This consisted of a cubic spline fit to the data points

at the wavelengths 0.668-, 0.752-, 0.850-, 0.948, 1.123-, 1.398-, 1.831-, and 2.242-μm. The cubic spline routine is described in Clark (1979), and a sample continuum is shown in Figure 2 fit to the coarse grained frost from Figure 1. The ratio of the frost to the continuum is shown in Figure 3. The relative band depths as a function of grain size are easily seen. Note that the 2.0-μm band becomes saturated before any of the other features. The absorption features were then analyzed with the gaussian analysis program. The 1.5-μm and 2.0-μm features were analyzed separately. The 0.81-, 0.90-, 1.04-, and 1.25-μm bands were analyzed simultaneously for the coarse grained frost and the 1.04- and 1.25-μm features were analyzed simultaneously for the medium and fine grained frosts. There were no absorption features apparent at 0.81 or 0.90 μm greater than the noise level (∿ 0.2%) in the medium and fine grained frosts. Each gaussian analysis was performed by fitting a two term continuum and the gaussian features simultaneously. The additional straight line continuum adjustment was needed since the sum of the fitted gaussians would be forced toward zero (in natural logarithm space) at the points where the cubic spline was fitted. This additional continuum allows a better fit in the

wings of the gaussians. In practice, the continuum adjustment was only a few percent in the region of the feature fitted. The continuum used is not necessarily the true continuum since the wings of the absorptions overlap. However, for the purposes of the quantitive analysis in this paper, the continua used do not affect the trends observed since the continua are chosen consistently.

GAUSSIAN ANALYSIS RESULTS

Tables 2 and 3 show the gaussian parameters derived from Figure 3 as described above. The gaussian centers have an additional ∿0.2% uncertainty in wavelength above the errors given in the tables due to the wavelength calibration of the circular variable filter. The relative uncertainties in wavelength due to the CVF calibration in any one spectrum (e.g. the fine grained frost positions) are less than 0.1%. Table 4 shows the gaussian components of the 1.5-μm feature. Four gaussians were required to describe adequately the feature. The continuum for this feature was treated slightly differently. The feature was first analyzed with the variable continuum as described above for about 30 frosts. The continuum terms were seen to vary slightly due to the scatter in the data. Thus

an average of the continuum terms was used to adjust the continuum of the 1.5-μm feature before the gaussian analysis. The average continuum used is:

$$y = 0.1484 - 0.1276\ (\tfrac{1}{\lambda}), \qquad (1)$$

where y is the relative reflectance continuum value at wavelength λ (in μm).

Inspection of Tables 2 and 3 show that there is no apparent change in band position as a function of grain size or temperature for any of the gaussian components, although the (0.79 μm^{-1}) band apparently split into two components for the coarse grained frost. The amplitudes generally increase in band depth with increasing grain size. The gaussian width's in Table 2 apparently decrease with increasing grain size, just the opposite of gaussian 2 in Table 3. However, gaussian 1 does not show any apparent trend with grain size but the width appears to decrease with decreasing temperature.

ANALYSIS OF THE 1.5-μm FEATURE

Table 4 shows the results of the gaussian analysis for the 1.5-μm feature. In general, the center positions do not change with grain size or temperature. The amplitudes and widths appear to be

more complex. Figures 4 and 5 show the relationships of the gaussians and the general quality of the fits. The gaussian amplitudes generally increase in intensity with increasing grain size, except for the 1.65-μm band which appears more complicated. The widths of gaussians 1, 2 and 3 appear relatively constant with grain size (there may be a very slight temperature dependence of gaussian 3). Gaussian 4 seems to decrease in width with increasing grain size.

In order to define these relationships better, the 1.5-μm feature was analyzed for the coarse grained frost as a function of temperature and for a series of medium grained frosts at essentially a constant temperature.

The 1.65-μm absorption was previously identified as being temperature dependent by Fink and Larson (1975). They measured the equivalent width of the 1.65-μm band and the entire 1.5-μm feature and plotted the ratio in an attempt to calibrate the temperature dependence. This was performed over a variety of temperatures for two different grain sized frosts. They drew a mean line with a bend located around 100 K. The two frosts covered the temperature ranges 55 to 150 and 90 to 230 K. No explanation was given for the apparent bend in the

calibration curve.

In an attempt to reproduce the calibration curve, the ratio of the gaussian integrated intensities (the gaussian integrated intensity = the gaussian amplitude times the width) of gaussian 3 divided by sum of the integrated intensities of all four gaussians was plotted as a function of temperature for all the frosts analyzed. The result is shown in Figure 6. The temperature dependence of the coarse grained frost is clearly seen. However, the medium grained frosts which were all within 2 K of each other in the range 112 to 114 K clearly show a grain size dependence (since that is the only parameter varied). Other methods of displaying the data (e.g. plotting gaussian amplitude vs temperature) indicate the same relationship.

Inspection of Fink and Larson's calibration curve shows that two lines could be drawn, one for each grain size. Thus the slope of the calibration curve is apparently grain size dependent, making it difficult to determine temperature accurately in remote sensing applications.

The width of gaussian 4 seems to be grain size dependent while being independent of temperature. Figure 7 shows the width of gaussian 4 as a function of temperature. The width of gaussian 4 for the

coarse grained frost from 140 to 240 K is almost constant, decreasing from about 0.87 μm^{-1} at 140 to 0.84 μm^{-1} at 240 K. This decrease is probably due to the change in grain size of the frost which increased slightly as the temperature rose. A frost will tend to metamorphose with time since the larger grain sizes have a lower energy state. The medium grained frost at 112 to 114 K in Figure 7 metamorphosed and displays the change in width of gaussian 4 with grain size. The width of gaussian 4 of the fine grained frost from Figure 1 is 0.165 μm^{-1}, being above the top limit of the graph. This gaussian component could be very useful in determining the grain size of frosts for remote sensing planetary surfaces. Further work is needed to determine more precisely the relationship involved.

SPECTRAL REFLECTANCE OF WATER FROST ON ICE

In an attempt to make an ice sample with absorptions stronger than the coarse frost in Figure 1, a sample holder (25mm inside diameter, and 18mm deep) was packed with a 1mm layer of Halon on the bottom and filled with 17mm of water. As the sample cooled, the pressure in the chamber was lowered, but not enough to boil the water when above freezing. As the sample froze, a small amount of frost grew on the sample surface, probably from the water in the vapor phase. As the sample cooled, the frost continued to grow as seen in Figure 8. It is curious that the 1.5- and 2-μm bands are not saturated. In fact, the albedo at the bottom of these absorptions is greater than that for the coarse grained frost. The frost on the sample in Figure 8 contained a range of particle sizes from less than about 50 micrometers to a few tenths of a millimeter and a thickness varying from ∿0.5mm (bottom curve) to about 1mm (top).

When the sample reached about 120 K, a small amount of air was let into the chamber through a copper tube that was aimed at the sample surface. The short burst of air blew the frost off the ice surface. The bottom spectrum in Figure 9 is the ice surface with very little frost. Some of the frost which was blown off the sample surface fell on

warmer parts of the chamber (warmer than the cold finger). The H_2O vapor pressure then increased and water began to condense back onto the cold finger (and some on the sample surface). This frost regrowth is shown in Figure 9. The frost had a grain size of less than about 30 micrometers. As the fine grained frost layer increases, the albedo increases with only a small effect on the apparent relative band depths. The higher overtone bands (e.g. at 1.04 μm) tend to decrease in depth while the longer wavelength bands (e.g. at 1.6 and 2.0 μm) increase in depth with increasing frost thickness. After the thin layers of frost were blown off the sample surface two more times, the spectrum in Figure 10 (bottom) was obtained of essentially the ice surface. The ice surface was not perfectly smooth, but contained a microstructure about 30 micrometers or less in size. The 1.6- and 2.0-μm absorptions appear relatively less intense than in Figure 9.

The very thin scattering layer at the surface of the ice (whether from microstructure or a fine grained frost) causes some light to be scattered out of the sample. The long wavelength light in the 1.6- and 2.0-μm absorptions which is scattered into the ice is totally absorbed and does not effect the

appearance of the reflectance spectrum. The shorter wavelengths ($\lesssim$ 1.4 μm) can penetrate the thin scattering layer (since they may be scattered many times without being absorbed) deep into the ice layer before being scattered back out of the sample. This accounts for the relatively deep 1.25-, 1.04-, 0.90-, and 0.81-μm bands when the 1.6- and 2.0-μm bands are apparently weak (relative to the peaks at 1.4-, 1.83-, and 2.24-μm seen in Figure 1). The relative band depths can be easily illustrated by removing a continuum as seen in Figures 2 and 3. The curves in Figure 11 show the result of removing a cubic spline continuum from the bottom spectra in Figures 9 and 10.

The enhancement of higher overtone water ice bands relative to the 1.6- and 2.0-μm bands is seen on many solar system objects: The Galilean satellites Europa, Ganymede, and Callisto (Clark and McCord, 1979a), Saturn's Rings (Clark and McCord 1979b), and possibly Mars (McCord et al. 1979). Europa even has a highly asymetric 1.6-μm ice band very similar to the spectra in Figure 9 which has been a puzzle for several years. Analysis of these spectra is currently under way.

CONCLUSIONS

Reflectance spectra of water frost show a large range of spectral contrast. Three new (in reflectance) absorptions are identified shortward of 1.1 μm. The absorption features were analyzed with a non-linear least squares algorithm in order to compare quantitatively differences between spectra as a function of temperature and grain size. The 1.65 μm absorption which was previously thought to be a good temperature sensor is shown to be highly grain size dependent.

Thin layers of water frost on ice radically change the appearance of the reflectance spectrum, enhancing higher overtone bands relative to longer wavelength bands, very similar to that seen on several objects in the solar system. Hence, thin layers of water frost may cover ice on the surfaces of these objects.

ACKNOWLEDGEMENTS

I would like to especially thank Tom McCord for help, encouragement, and for providing the computer and necessary laboratory facilities to carry out this work.

This work was supported under NASA grants NSG 7590 and 7312.

REFERENCES

Bevington, P. R., Data Reduction and Error Analysis for the Physical Sciences. New York: McGraw-Hill, 1969.

Clark, R. N., A large scale interactive one dimensional array processing system, Pub. Astron. Soc. Pac. submitted, 1979. Thesis App A

Clark, R. N., and McCord, T. B., The Galilean satellites: New near-infrared spectral reflectance measurements (0.65 - 2.5 μm) and a 0.325 - 5 μm summary, Icarus submitted, 1979a. Thesis I Ch 1

Clark, R. N., and McCord, T. B., The rings of Saturn: New near-infrared reflectance measurements and a 0.326 - 4.08 μm summary, Icarus submitted, 1979b. Thesis I Ch 2

Fink, U., and Larson, H. P., Temperature dependence of the water-ice spectrum between 1 and 4 microns: Application to Europa, Ganymede and Saturn's rings, Icarus 24, 411-420, 1975.

Fink, U., Larson, H. P., Gautier, T. N. III, and Treffers, R. R., Infrared spectra of the satellites of Saturn: Identification of water ice on Iapetus, Rhea, Dione and Tethys, Astrophys. J. Lett., 207, 63-67, 1976.

Kaper, H. G., Smith, D. W., Schwartz, U., Takakubo, K., and Van Woerden, H., Computer analysis of observed

distributions into gaussian components, Bull. Astron. Inst. Neth., 18, 465-487, 1966.

Kieffer, H. H., Near infrared spectral reflectance of simulated Martian frosts. Ph.D. thesis. California Inst. Tech. 1968.

Kieffer, H. H., Spectral reflectance of CO_2 - H_2O frosts, J. Geophys. Res., 75, 501-509, 1970.

McCord, T. B., Clark, R. N., and Huguenin, R. L., Mars: Near-infrared spectral reflectance and compositional implication, J. Geophys. Res., 83, 5433-5441, 1978.

McCord, T. B., Clark, R. N., Singer, R. B., and Huguenin, R. L., Mars: Near-infrared spectra of surface regions and compositional implication, J. Geophys. Res., to be submitted, 1980. Thesis I Ch 3

Morrison, D., Cruikshank, D. P., Pilcher, C. B., and Rieke, G. H., Surface compositions of the satellites of Saturn from infrared photometry, Astrophys. J. Lett., 207, 213-216, 1976.

Ockman, N., The infrared and raman spectra of ice, Advanc. Phys., 7, 199-220, 1958.

Pilcher, C. B., Chapman, C. R., Lebofsky, L. A., and Kieffer, H. H., Saturn's Rings: Identification of water frost, Science 167, 1372-1373, 1970.

Pilcher, C. B., Ridgway, S. T., and McCord, T. B. Galilean satellites: Identification of water frost, Science 178, 1087-1089, 1972.

FIGURE CAPTIONS

Figure 1. The spectral reflectance of water frost relative to the reflectance standard Halon is shown for several different grain sizes. The characteristic grain sizes for the frosts (top to bottom) are: 50, 100, 200, and 400 - 2000 micrometers.

Figure 2. A cubic spline continuum is fit to the coarse grained frost from Figure 1.

Figure 3. a) The reflectance spectra from Figure 1 with a cubic spline continuum removed as shown in Figure 2. b) An expanded view of (a) in the 0.65- to 1.40-μm region.

Figure 4. Gaussian component analysis of the 1.5-μm band for the fine (top) and medium (middle and bottom) grained frosts in Figure 3. The analysis included data only in the 1.40- to 1.84-μm interval (the data points seen outside of this region are in the 1.25- and 2.0-μm bands and were not included in this analysis). The four gaussian components are shown as light lines and the multiplication of the four components and the continuum is shown as the heavy line. The fit is excellent in all cases.

Figure 5. The gaussian analysis for the coarse grained frost as in Figure 4. The 140 K frost (top) is from Figure 3 and the 243 K frost (bottom) after the frost had warmed up.

Figure 6. The ratio of the integrated gaussians from many frost analyses is shown as a function of temperature. The numbers refer to the gaussians 1, 2, 3 and 4 in Table 4.

Figure 7. The width of gaussian 4 in the 1.5-μm band analysis is shown as a function of temperature. The only variation appears to be with grain size. The data points at 112 to 114 K are the analysis of the medium grained frost in Figure 3 as the frost metamorphosed.

Figure 8. Growth of water frost on ice is shown. The abledo rises as the frost depth increases, the 1.5-and 2-μm bands increase in apparent depth and the higher overtones decrease in apparent depth.

Figure 9. Same as Figure 8 but a much finer grain size. The frost depth has a greater effect on albedo than on the apparent band depths than coarser grained frost growth in Figure 8.

Figure 10. The reflectance of ice with some microstructure on the surface (bottom) and a thin (< .1mm) layer of frost (top curves).

Figure 11. The bottom spectra from figures (a) 9 and (b) 10 with a cubic spline continuum removed as seen in Figure 2 to illustrate the apparent band depths.

TABLE CAPTION

Table 1. Assignments of the hexagonal ice bands from Ockman (1958). The assignments were determined from Raman spectroscopy (R) or infrared transmittance spectroscopy (IR). The subscripts on the band assignments are translational (T, T', T", ...) and rotational (R, R', R").

TABLE 1

Wavelength (μm)	Frequency (cm^{-1})	Source	Assignment
189	53	R	(ν_T)?
103	97	R	(ν_T)?
82	122	R	(ν_T)?
62	160	IR	ν_T
56	177	R	(ν_T)?
52	193	R	(ν_T)?
47	212	R	ν_T
43	232	R	ν_T
40	252	R	ν_T
37	272	R	ν_T
34	294	R	ν_T
22	457	R	(ν_T)??
19.4	516	R	?
18.5	540	IR	$(\nu_{R'})$??
16.7	600	R	?
15.2	660	IR	$(\nu_{R''})$??
12.5	800	IR	ν_R
8.93	1120	R	$\nu_R + \nu_T$
6.90	1450	R	$2\nu_R$
6.098	1640	IR	ν_2

TABLE 1 (continued)

Wavelength (μm)	Frequency (cm^{-1})	Source	Assignment
4.494	2225	IR	ν_2+ $\nu_{R'}$
			$\nu_2+\nu_{R''}$
3.311	3020	IR	?
3.182	3143	R	ν_1
3.145	3180	IR	$2\nu_2$
3.075	3252	IR	ν_3
3.024	3307	R	$\nu_1+\nu_{T'}$, $\nu_3+\nu_{T''}$
2.983	3252	R	$\nu_3+\nu_{T''''}$
2.939	3402	R	$\nu_3+\nu_{T'}$
2.528	3955	IR	$\nu_1+\nu_R$, $\nu_3+\nu_R$
2.410	4150	IR	$\nu_1+\nu_R+\nu_T$, $\nu_3+\nu_R+\nu_T$, $^3\nu_2$
2.208	4530	IR	$\nu_1+\nu_R+\nu_{R'}$, $\nu_3+\nu_R+\nu_{R'}$,
			$\nu_1+2\nu_R$, $\nu_1+\nu_R+\nu_{R''}$,
			$\nu_1+\nu_2$, $^3\nu_2$
1.998	5005	IR	$\nu_2 + \nu_3$
1.786	5600	IR	$\nu_1+\nu_2+\nu_{R'}$, $\nu_2+\nu_3+\nu_R$
1.639	6100	IR	$\nu_2+\nu_3+\nu_R+\nu_T$,
			$\nu_2+\nu_3+2\nu_{R'}$, $\nu_2+\nu_3+2\nu_{R''}$
			$2\nu_1$, $\nu_1+2\nu_2$, $^2\nu_2+\nu_3$, $^2\nu_3$
1.538	6500	IR	$\nu_2+\nu_3+2\nu_R$, $\nu_1+2\nu_2+\nu_T$,
			$2\nu_2+\nu_3+\nu_T$, $^2\nu_2+\nu_3$, $^2\nu_3$,
			$2\nu_1$, $\nu_1+2\nu_2$

TABLE 1 (Continued)

Wavelength (μm)	Frequency (cm^{-1})	Source	Assignment
1.495	6690	IR	$\nu_1+\nu_3$
1.287	7775	IR	$\nu_1+\nu_3+2\nu_R$, $\nu_1+\nu_3+\nu_R+\nu_{R'}$, $\nu_1+\nu_3+\nu_R+\nu_{R''}$, $\nu_1+\nu_3+2\nu_{R''}$, $3\nu_2+\nu_3$, $\nu_2+2\nu_3$, $2\nu_1+\nu_2$, $3\nu_2$
1.259	7940	IR	$\nu_1+\nu_2+\nu_3$
1.108	9025	IR	$\nu_1+\nu_2+\nu_3+\nu_R$, $3\nu_2+\nu_3+\nu_R$, $\nu_1+3\nu_2+\nu_R$, $\nu_2+2\nu_3+\nu_R$,
1.034	9667	IR	$2\nu_1+\nu_3$
0.9009	11100	IR	$2\nu_1+\nu_2+\nu_3$
0.8000	12500	IR	$3\nu_1+\nu_3$

TABLE 2

Gaussian Components of the "0.81 to 1.25 μm" Absorption Features

Frost	Temp (°K)	Gauss #	Gaussian Center Position (μm^{-1})	Gaussian Amplitude Ln (1-depth)	Gaussian Width (μm^{-1})
Fine	131	1		<- 0.002	
		2		<- 0.002	
		3	0.9580±.0037	-0.015±.003	0.0896±.0135
		4	0.7907±.0013	-0.049±.002	0.0942±.0065
Medium Fine	114	1		<- 0.002	
		2		<- 0.002	
		3	0.9704±.0027	-0.030±.003	0.0833±.0100
		4	0.7884±.0010	-0.082±.003	0.0845±.0041
Medium Coarse	112	1		<- 0.002	
		2		<- 0.002	
		3	0.9632±.0015	-0.038±.002	0.0711±.0050
		4	0.7923±.0005	-0.117±.002	0.0761±.0020
Coarse	140	1	1.2391±.0055	-0.013±.003	0.0656±.0171
		2	1.1123±.0029	-0.022±.002	0.0688±.0084
		3	0.9688±.0005	-0.113±.002	0.0687±.0016
		4A	0.7574±.0016	-0.075±.009	0.0432±.0030
		4B	0.8038±.0011	-0.242±.004	0.0683±.0019

TABLE 3

Gaussian Components of the "2 μm" Absorption Feature

Frost	Temp (°K)	Gauss #	Gaussian Center Position (μm^{-1})	Gaussian Amplitude Ln (1-depth)	Gaussian Width (μm^{-1})
Fine	131	1	.5096±.0009	- .511±.047	.0269±.0009
		2	.4874±.0010	- .687±.030	.0322±.0012
Medium Fine	114	1	.5099±.0005	-0.638±.060	.0247±.0008
		2	.4876±.0008	-1.092±.027	.0361±.0011
Medium Coarse	112	1	0.5106±.0005	-0.726±.071	0.0250±.0009
		2	0.4872±.0008	-1.263±.031	0.0375±.0013
Coarse	140	1	0.5136±.0005	-0.769±.061	0.0257±.0009
		2	0.4876±.0008	-1.186±.024	0.0402±.0015

TABLE 4

Gaussian Components of the "1.5 μm" Absorption Feature

Frost	Temp (°K)	Gauss #	Gaussian Center Position (μm^{-1})	Gaussian Amplitude Ln (1-depth)	Gaussian Width (μm^{-1})
Fine	131	1	.6609±.0012	-.434±.026	.0331±.0017
		2	.6354±.0010	-.260±.031	.0269±.0029
		3	.6057±.0014	-.208±.018	.0323±.0026
		4	.6212±.0026	-.136±.015	.1649±.0149
Medium Fine	114	1	.6597±.0010	-.710±.048	.0324±.0015
		2	.6347±.0009	-.383±.050	.0269±.0024
		3	.6056±.0018	-.292±.045	.0371±.0039
		4	.6226±.0016	-.245±.045	.1217±.0100
Medium Coarse	112	1	.6600±.0010	-.856±.069	.0332±.0016
		2	.6345±.0008	-.431±.049	.0266±.0023
		3	.6050±.0021	-.350±.081	.0385±.0049
		4	.6231±.0015	-.344±.093	.1071±.0092
Coarse	140	1	.6646±.0006	-.886±.036	.0337±.0010
		2	.6376±.0011	-.342±.041	.0280±.0019
		3	.6041±.0010	-.151±.032	.0269±.0031
		4	.6261±.0007	-.776±.050	.0881±.0014

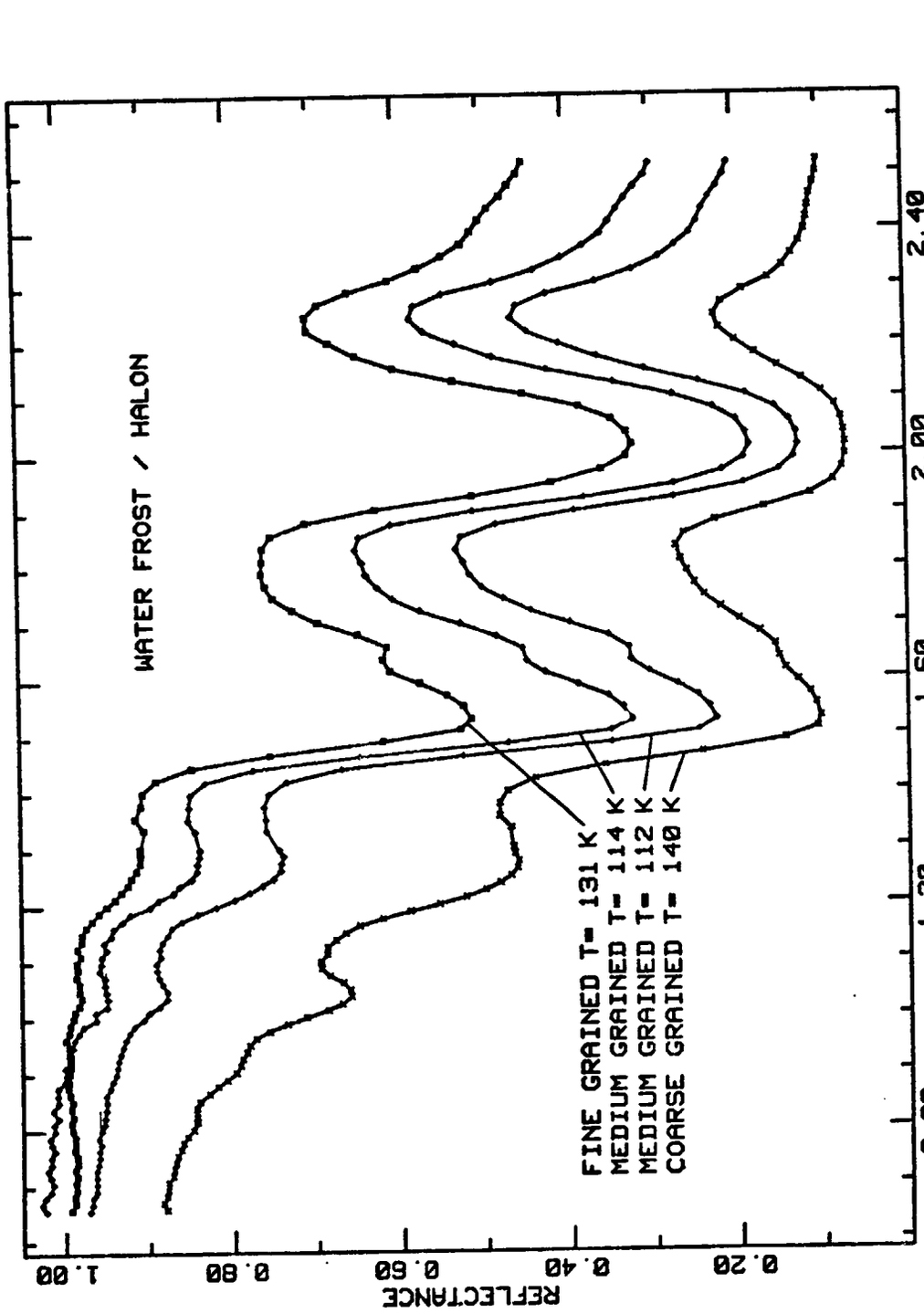

WATER FROST / HALON
FINE GRAINED T= 131 K
MEDIUM GRAINED T= 114 K
MEDIUM GRAINED T= 112 K
COARSE GRAINED T= 140 K
REFLECTANCE
0.20
0.40
0.60
0.80
1.00
WAVELENGTH IN MICRONS
0.80
1.20
1.60
2.00
2.40

Figure 1

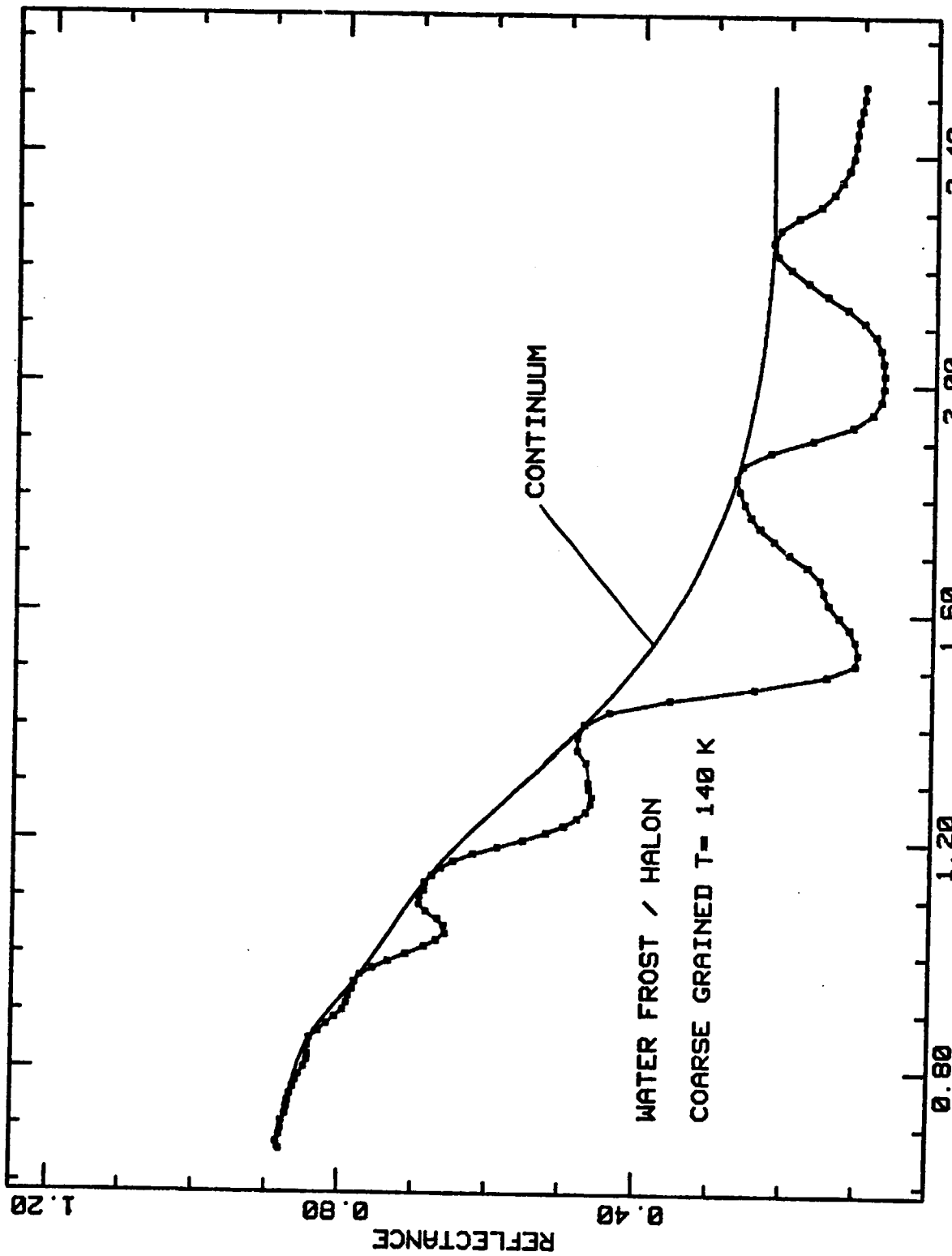

CONTINUUM
WATER FROST / HALON
COARSE GRAINED T= 140 K
REFLECTANCE
0.40
0.80
1.20
0.80
1.20
1.60
2.00
2.40
WAVELENGTH IN MICRONS

Figure 2

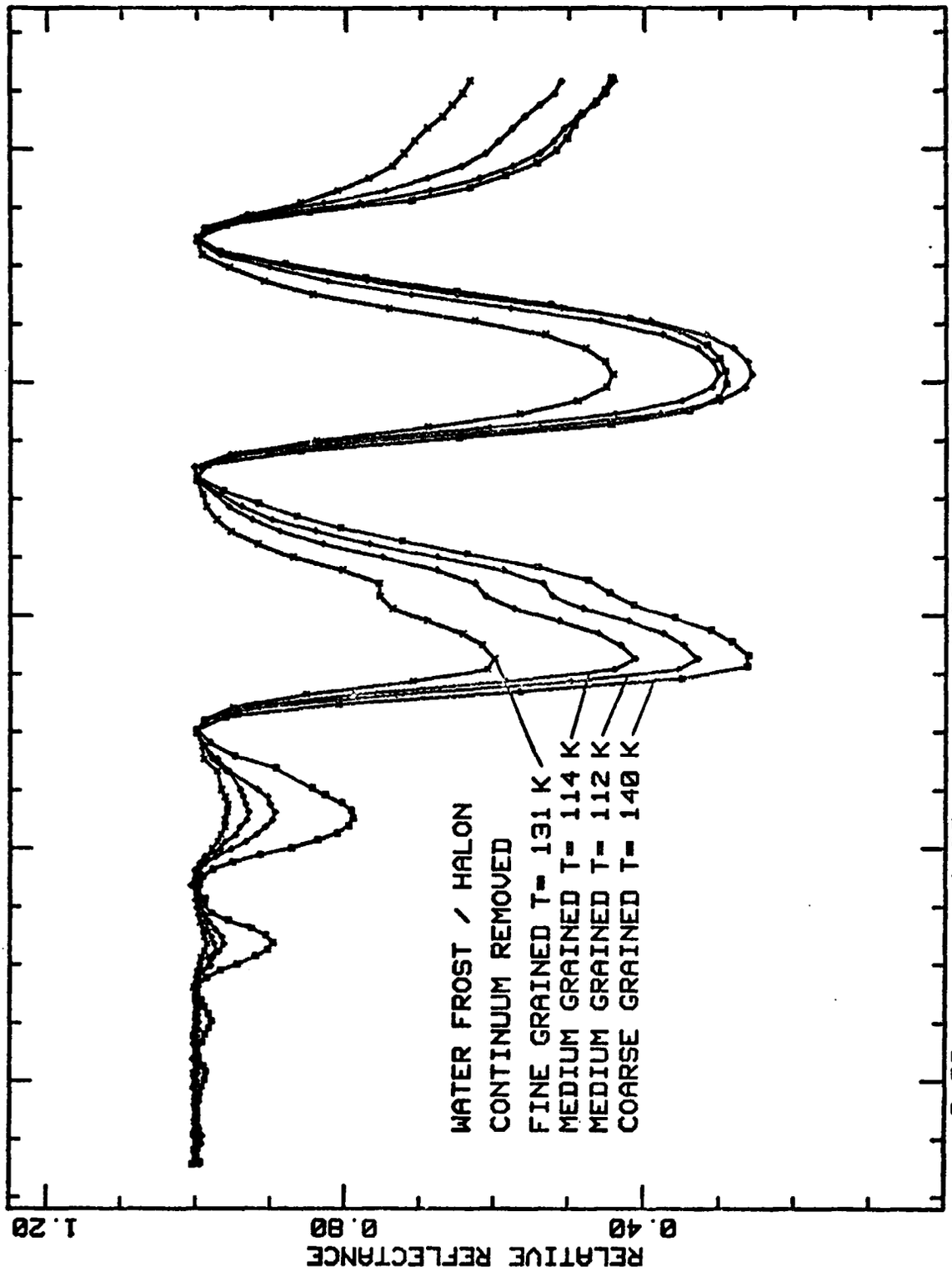

WATER FROST / HALON
CONTINUUM REMOVED
FINE GRAINED T= 131 K
MEDIUM GRAINED T= 114 K
MEDIUM GRAINED T= 112 K
COARSE GRAINED T= 140 K
RELATIVE REFLECTANCE
0.40
0.80
1.20
0.80
1.60
2.00
2.40
WAVELENGTH IN MICRONS

Figure 3A

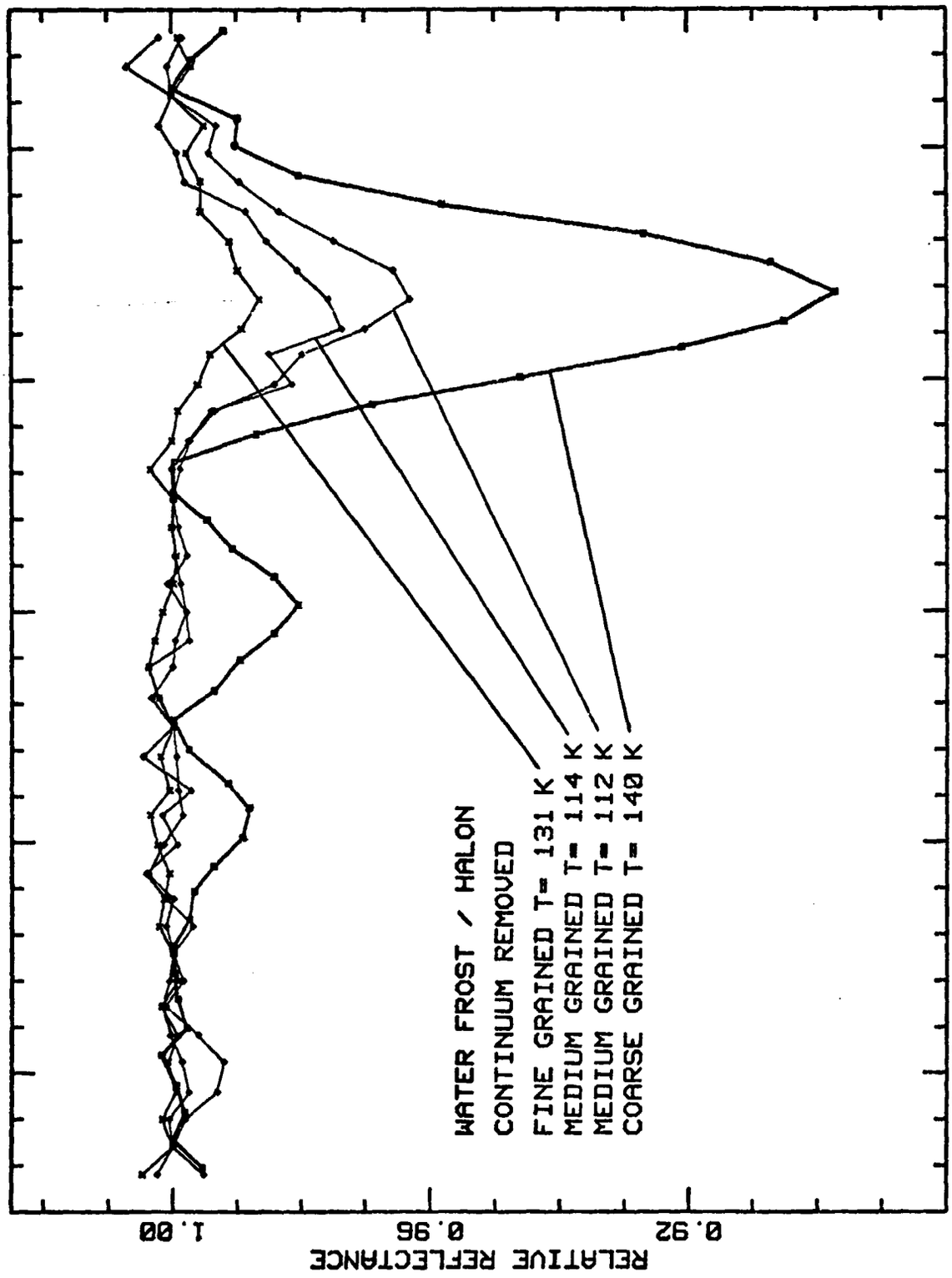

WATER FROST / HALON
CONTINUUM REMOVED
FINE GRAINED T= 131 K
MEDIUM GRAINED T= 114 K
MEDIUM GRAINED T= 112 K
COARSE GRAINED T= 140 K
RELATIVE REFLECTANCE
1.00
0.96
0.92
0.70
0.80
0.90
1.00
1.10
WAVELENGTH IN MICRONS

Figure 3B

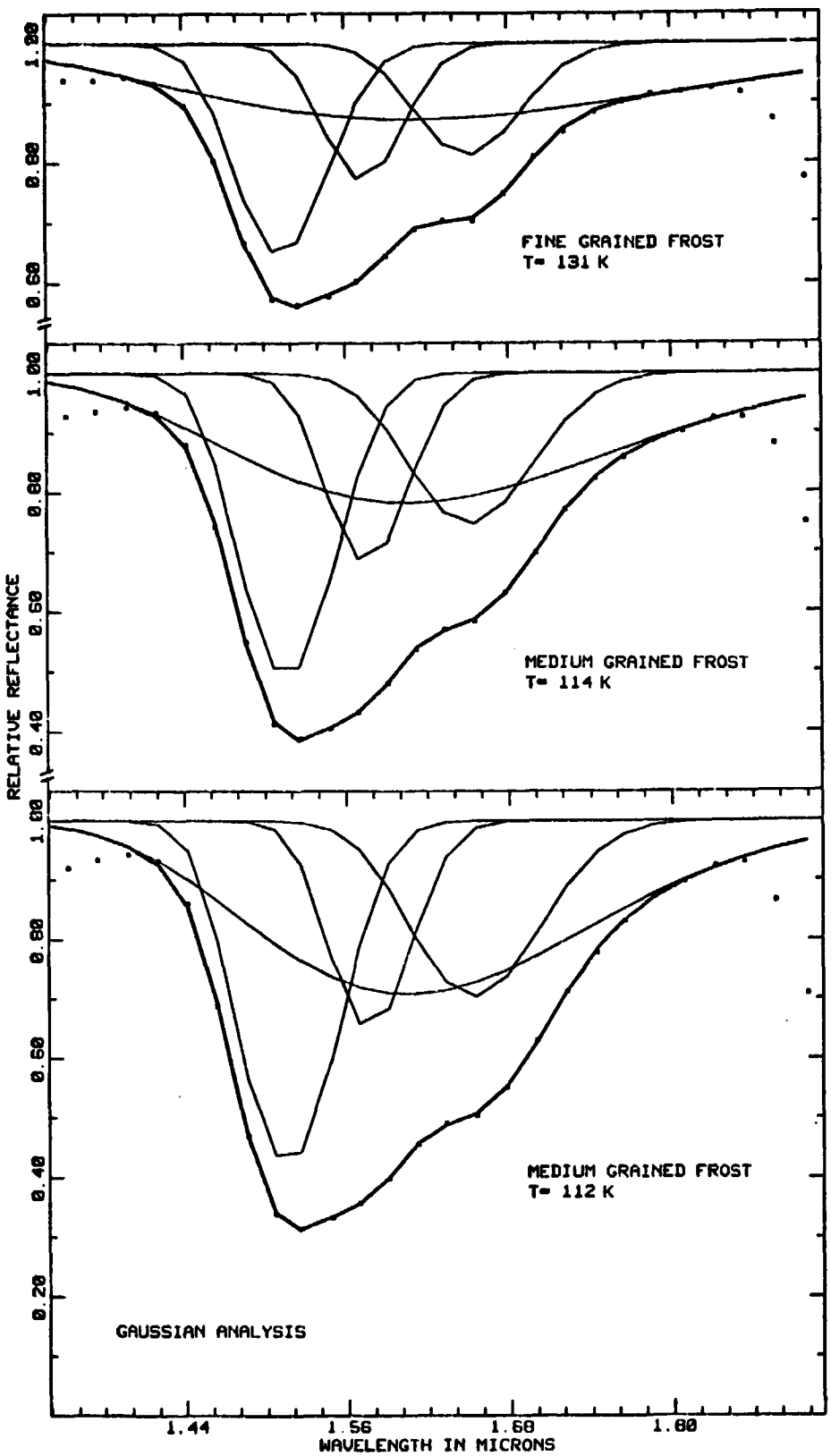

FINE GRAINED FROST
T= 131 K
MEDIUM GRAINED FROST
T= 114 K
MEDIUM GRAINED FROST
T= 112 K
GAUSSIAN ANALYSIS
RELATIVE REFLECTANCE
WAVELENGTH IN MICRONS
1.44
1.56
1.68
1.80

Figure 4

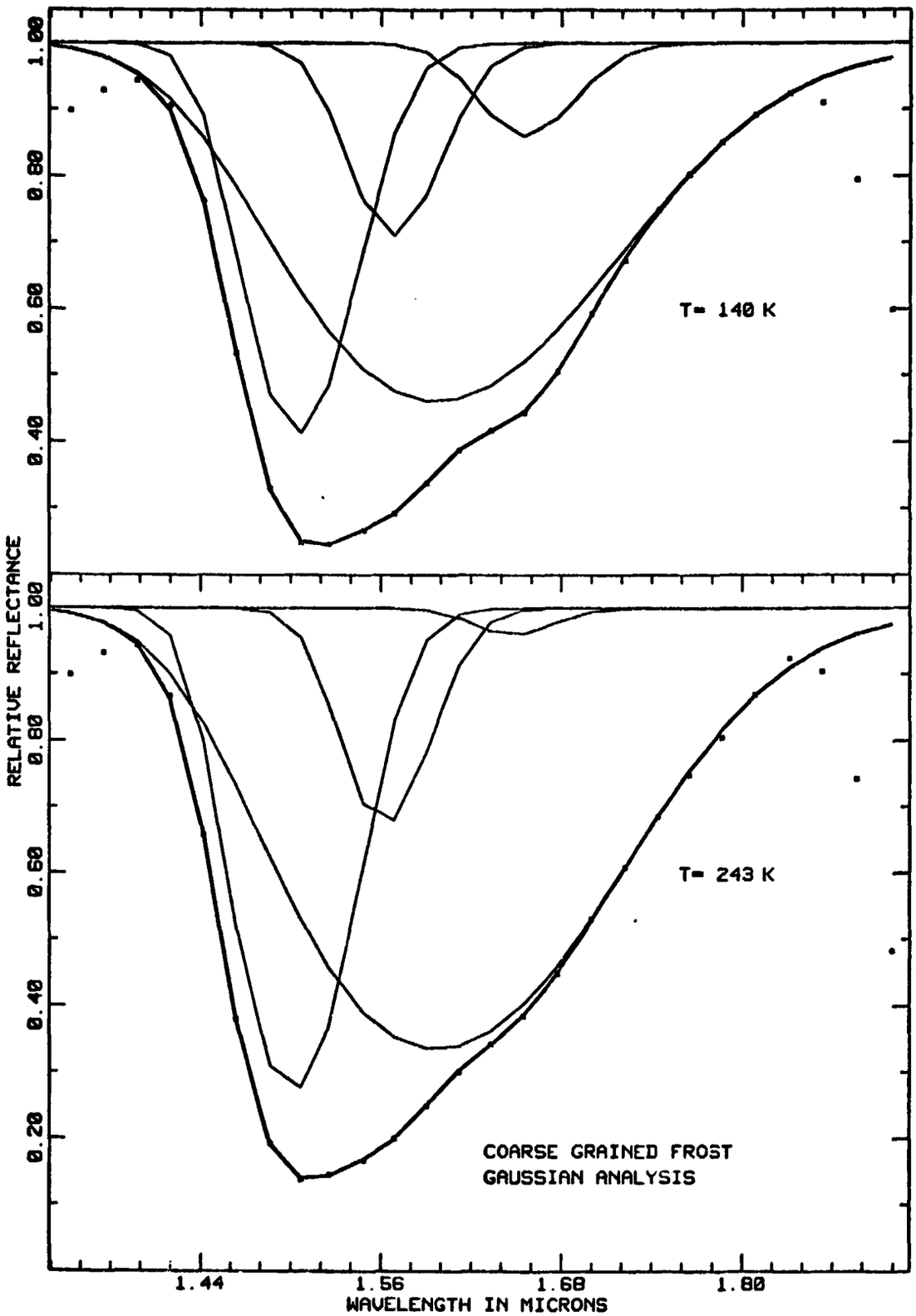

1.00
0.80
0.60
0.40
T= 140 K
RELATIVE REFLECTANCE
1.00
0.80
0.60
0.40
0.20
T= 243 K
COARSE GRAINED FROST
GAUSSIAN ANALYSIS
1.44
1.56
1.68
1.80
WAVELENGTH IN MICRONS

Figure 5

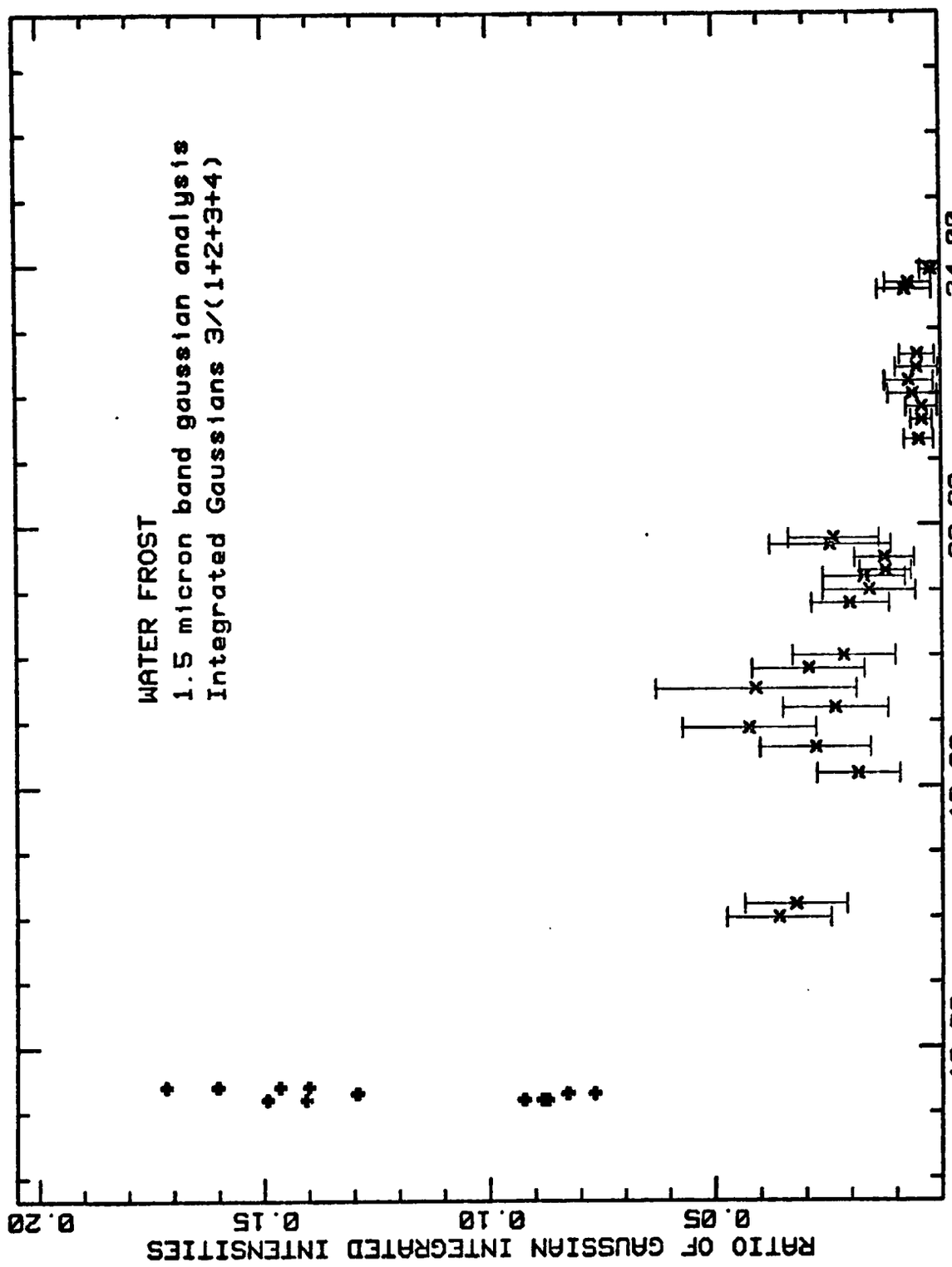

WATER FROST
1.5 micron band gaussian analysis
Integrated Gaussians 3/(1+2+3+4)
RATIO OF GAUSSIAN INTEGRATED INTENSITIES
0.05
0.10
0.15
0.20
12.00
16.00
20.00
24.00
TEMPERATURE (°K) (10¹)

Figure 6

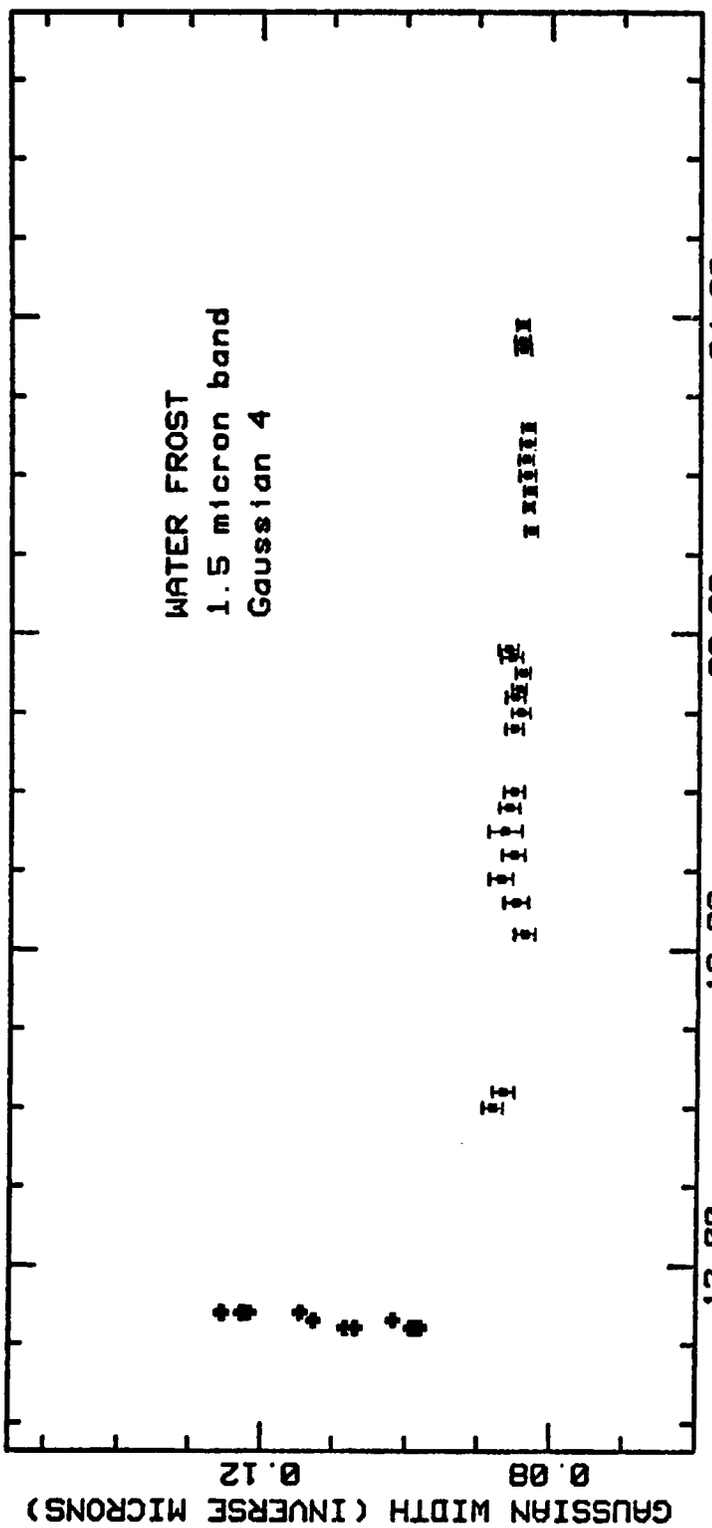

WATER FROST
1.5 micron band
Gaussian 4
0.12
0.08
GAUSSIAN WIDTH (INVERSE MICRONS)
12.00
16.00
20.00
24.00
TEMPERATURE (°K) (10¹)

Figure 7

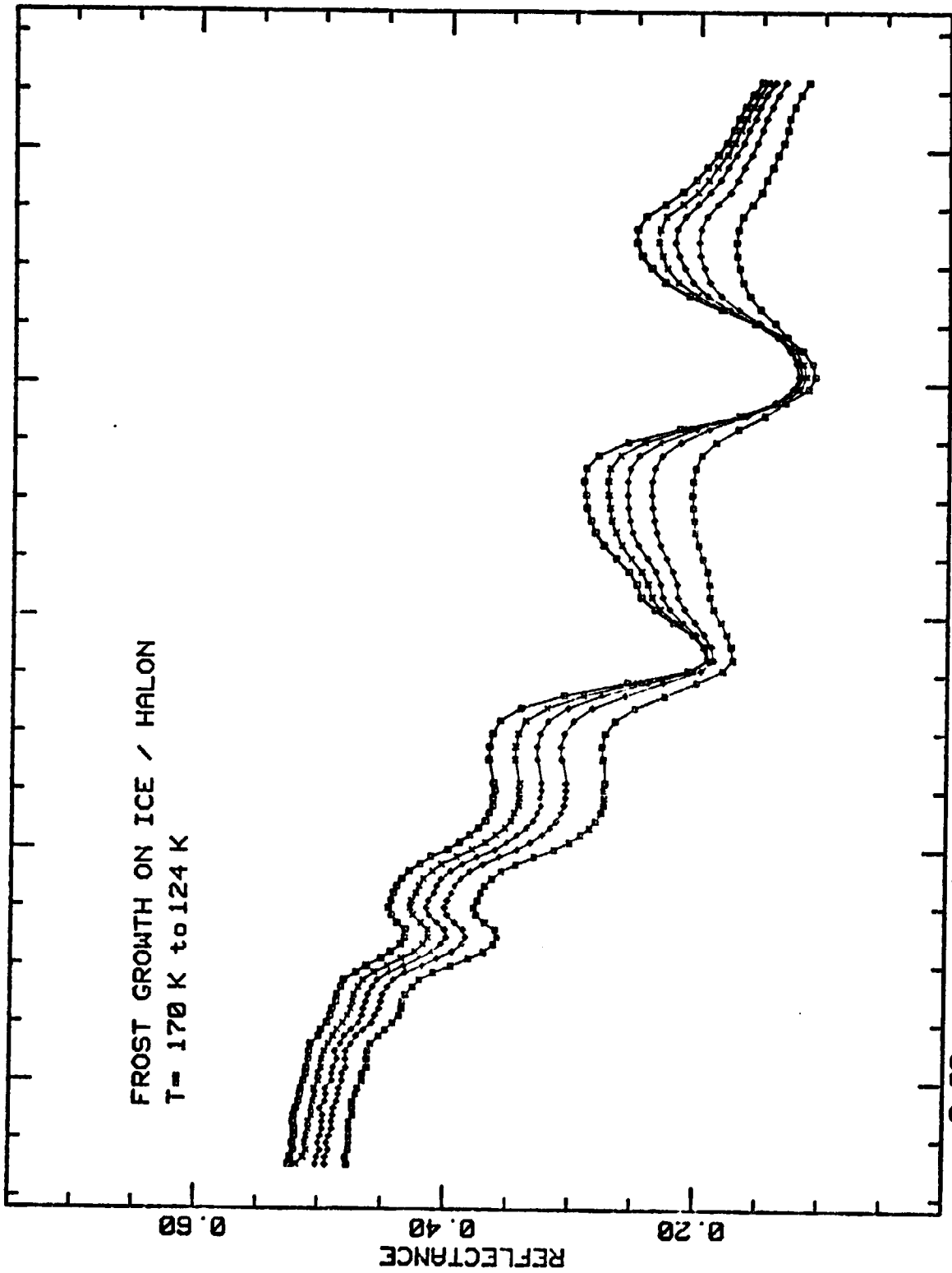

FROST GROWTH ON ICE / HALON
T= 170 K to 124 K
REFLECTANCE
0.20
0.40
0.60
WAVELENGTH IN MICRONS
0.80
1.20
1.60
2.00
2.40

Figure 8

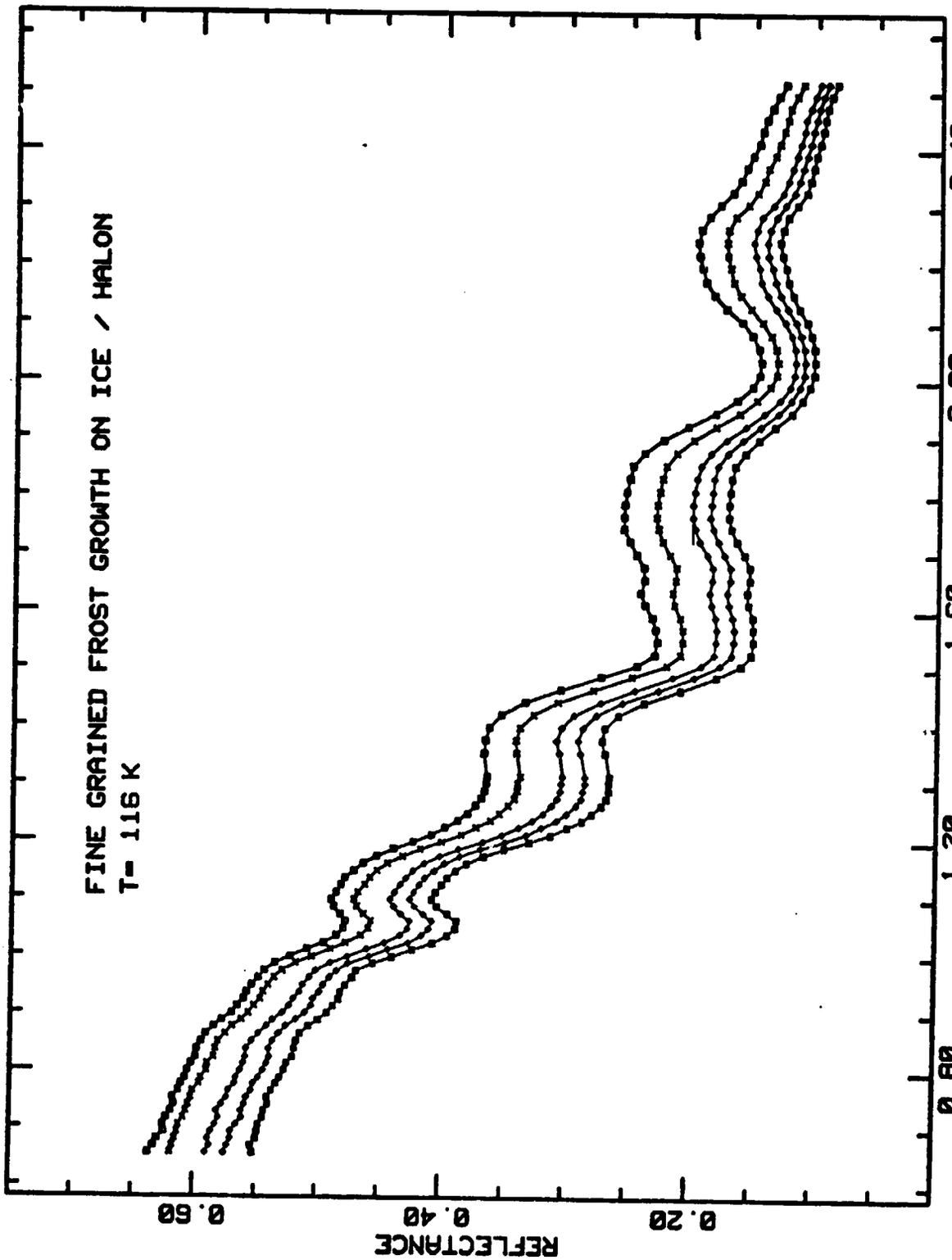

FINE GRAINED FROST GROWTH ON ICE / HALON
T= 116 K
REFLECTANCE
0.20
0.40
0.60
0.80
1.20
1.60
2.00
2.40
WAVELENGTH IN MICRONS

Figure 9

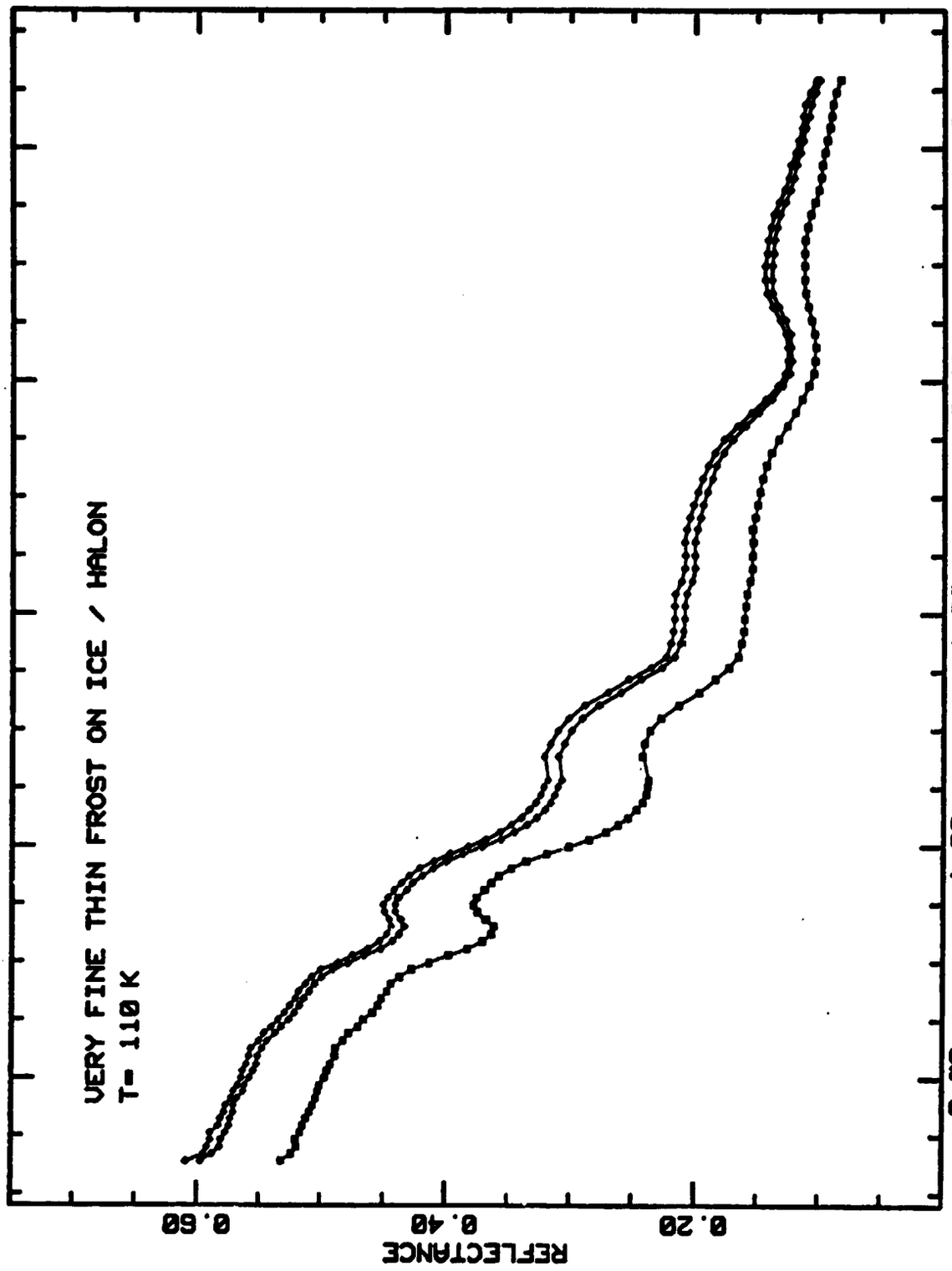

VERY FINE THIN FROST ON ICE / HALON
T= 110 K
REFLECTANCE
0.20
0.40
0.60
WAVELENGTH IN MICRONS
0.80
1.20
1.60
2.00
2.40

Figure 10

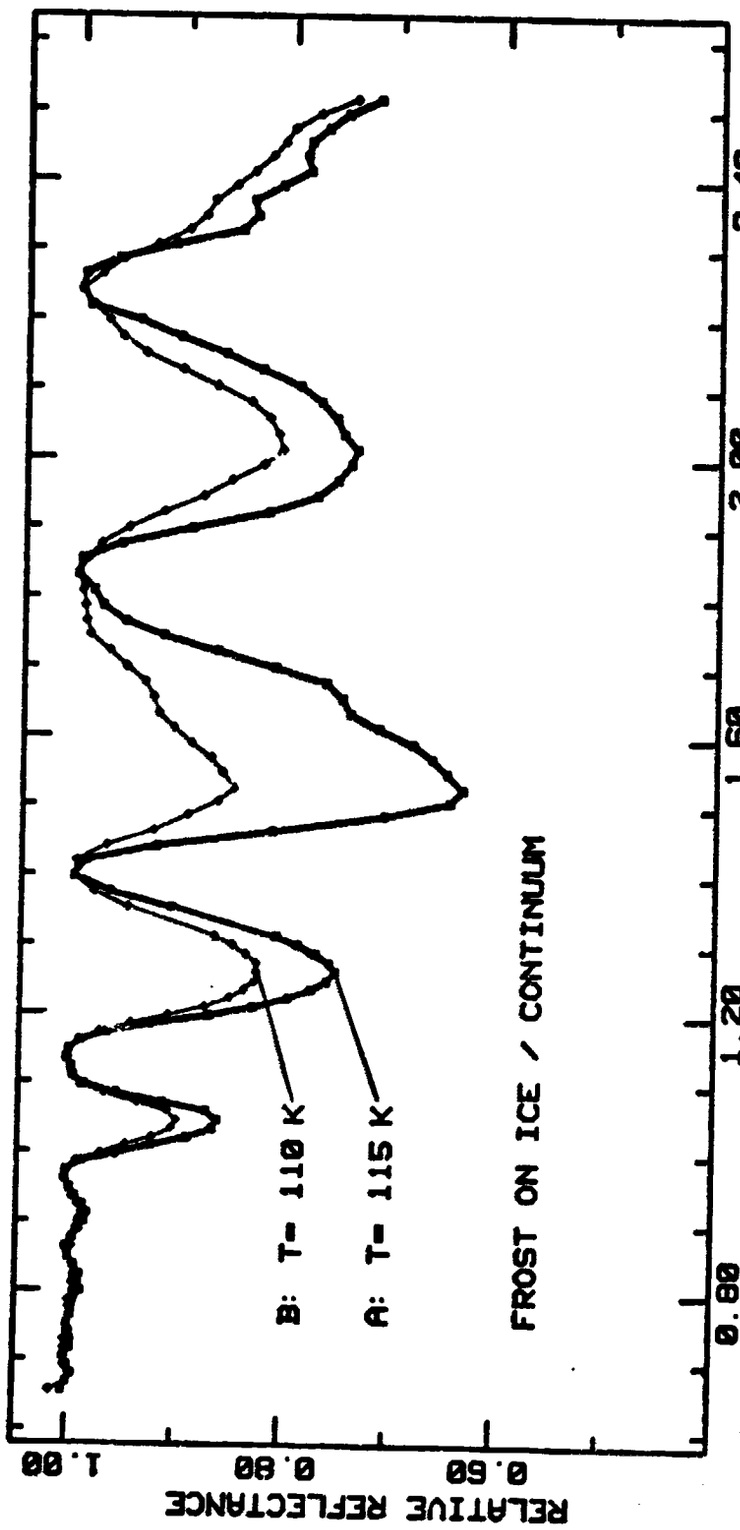

RELATIVE REFLECTANCE
0.60
0.80
1.00
0.80
1.20
1.60
2.00
2.40
WAVELENGTH IN MICRONS
FROST ON ICE / CONTINUUM
A: T= 115 K
B: T= 110 K

Figure 11

SECTION II

CHAPTER 2

The Spectral Reflectance of Water-Mineral Mixtures of Low Temperatures

This chapter has been submitted for publication to the Journal of Geophysical Research. Author: R.N. Clark.

ABSTRACT

Laboratory reflectance spectra in the 0.325 - 2.5 μm region of bound water, water-mineral mixtures, mineral grains on frost, and frost on minerals are presented. It is found that the wavelengths of bound water absorptions do not shift appreciably with temperature and can be detected when large amounts of free water ice are present. The decrease in the visible reflectance seen in many planetary reflectance spectra containing strong water ice absorptions can be explained by water-mineral mixtures, mineral grains on frost, or frost on mineral grains. Mineral grains on frost are detectable in very small quantities (fractional areal coverage $\lesssim$ 0.005) depending on the mineral reflectance features, while it takes a thick layer of frost ($\gtrsim$ 1 mm) to mask a mineral below 1.4 μm, again depending on the mineral reflectance. Frost on a very dark surface (albedo $\sim$ 6%) is easily seen, however a dark mineral mixed with water could completely mask the water absorptions (shortward of 2.5 μm).

INTRODUCTION

Water frost has been identified as being present on the surfaces of many solar system objects: Mars (McCord et al. 1978, 1979; Clark and McCord, 1979a), the Galilean satellites Europa, Ganymede, and Callisto (e.g. Pilcher et al., 1972; Clark and McCord, 1979b), Saturn's rings (Pilcher et al., 1970; Clark and McCord 1979c) and Saturn's satellites (Fink et al., 1976; Morrison et al., 1976). However, portions of the spectra for these objects indicate that something other than pure water frost is influencing the spectra. A "dirty" frost has been suggested as a possible cause by numerous authors but no laboratory studies are known to have been performed. This paper presents the first results of laboratory studies of the spectral reflectance of bound water, water-mineral mixtures, frost on minerals, and mineral grains on frost at the low temperatures typical of those found on the Galilean satellites, Mars, and Saturn's rings and satellites.

EXPERIMENTAL EQUIPMENT

The spectrometers used in this study are the same as those used in obtaining reflectance spectra of planetary surfaces (e.g. Clark and McCord 1979a, b; McCord et al. 1978) except that they are used on a laboratory goniometer rather than a telescope. The 0.65- to 2.5-μm spectrometer uses an indium antimonide solid state detector, a circular variable filter, and apertures (to select the area being measured), all cooled to liquid nitrogen temperature. The second instrument is a filter photometer which uses 25 interference filters covering the range 0.325 - 1.0 μm with an S1 photomultiplier tube as the detector. The optics to view the sample include a cassegrain telescope operating in an inverted mode such that the sample is located at the cassegrain focus. The light source is mounted on a movable arm and is collimated by an f/8 off-axis parabolic mirror. The viewing path is reflected by four mirrors on a movable arm to allow for varying the angle of emission of the light. The mirrors are mounted in a way to cancel mirror induced polarization. The sample is illuminated by a 250 watt quartz halogen bulb in an integrating sphere using a constant voltage power supply. The collimation of the light source was 1°7 and 1°1 for the viewing

beam. The angle of incidence was 0° and the angle of emission 10° for the data presented here. The light source is uniform in intensity to better than 2% over a 30mm diameter area, and the area viewed by the spectrometer was 6mm in diameter. The intensity of the light source at the sample was 1.25 milliwatts per square centimeter as measured by a Tektronix J16 digital photometer with a J6502 probe. The sensitivity of the IR spectrometer is excellent, being at the state of the art in present indium antimonide detector systems. The signal to noise of the data is better than 0.3% on samples with high reflectance ($\gtrsim$ 90%) from one 100-second integration, and the light source is stable to better than 0.5% over many (5-10) hours (after an initial warm-up of about 1 hour). The sensitivity of the filter photometer is greater than that of the IR instrument, and the reproducibility is better than 1% from run to run. Typically, several runs are then taken on each sample to increase the signal to noise to below $\sim$ 0.1% unless the sample is changing with time (e.g. temperature).

The environmental chamber for frost growth consists of a quartz optical dome 24 centimeters in diameter with radiation shielding covering most of the dome (inside and out) but allowing a narrow

viewing slit (for phase angle work). The reflectance standard and samples are located in the environmental chamber in one of two modes. In one mode, a six-position turntable is employed allowing five samples and the standard to be cooled via a one inch diameter copper bar extending into a liquid nitrogen bath (or other cool substance) and flexible metal fingers touching the turntable. The samples and standard are alternately rotated into view and thus are measured along exactly the same optical path. The standard may be covered during frost growth or particle sprinkling, avoiding possible contamination. This mode enables cooling of fine grain (low thermal conductivity) samples to about 140 K with LN_2 as the coolant. The data in Figures 1 through 5, 7 through 11 and 17 were obtained using this mode. The other data were obtained in a second mode which has one sample chamber directly attached to the copper cold finger. The standard is on a movable arm and is warmer than the sample. This mode allows cooling to $\sim$100 K with LN_2 as the coolant. Frost growth and small particle distribution on samples are possible in both modes. The chamber may be operated at pressures ranging from a vacuum ($\lesssim$ millitorr) to a little above atmospheric pressure and can be cooled or warmed slowly enough to obtain

1 to 2 K temperature resolution. The samples can be monitored visually with a 10x to 40x viewer and photographed with a 3x, f/110 camera system giving a resolution at the sample of 20 - 30 micrometers and a very good depth of field. A more complete description of the goniometer and environment chamber is in preparation.

CALIBRATION

The data presented in this study used Halon (NBS test no. 232.04/213908, 1975) as the reflectance standard. The reflectance of Halon is ∿ 99% or greater at all wavelengths in this spectral region and is generally quite smooth except for a small (∿ 1½%) absorption centered at 2.15 μm. Halon is an excellent standard because of its high reflectance, long term stability, and the fact that it does not absorb water and standards prepared by different people agree excellently. The sample and standard are each measured by the IR spectrometer in 100-second integration periods (called runs). A run is made up of 10 scans of the spectrum with the signal coadded in the digital data system on each scan (1 revolution of the circular variable filter takes 10 seconds). The filter photometer measured the spectrum in approximately 5-minute integration periods. Several runs are taken of each sample or standard to be measured and the results (of each run) are written onto magnetic tape for later processing by computer. A dark measurement (no light on the sample) is taken several times an hour. The dark signal is typically less than 0.1% of the Halon signal and is substracted from the data of the sample and standard. The signal ratio of the sample

intensity to the Halon intensity then gives the reflectance. The repoducibility of the Halon signal is better than 0.5% over many hours. This is due to the good stability of the light source and the IR solid state detector system (operating at 77 K) and the cold phototube (196 K). The analysis was performed with the interactive processing routines described by Clark (1979).

BOUND WATER

The reflectance spectra of minerals with bound water are fairly well known (e.g. Hunt and Salisbury 1970) at room temperature, but few reflectance spectra have been obtained at low temperature ($\lesssim$ 270 K). The term bound water is used here to mean water molecules in the crystal of the mineral or absorbed onto the surfaces of the mineral grains. It has been thought that bound water bands may shift in wavelength with temperature and look like water ice at low temperatures. The spectra of three minerals containing bound water or hydroxyl ions were measured as a function of temperature to determine what changes occur.

Montmorillonite. The montmorillonite measured here was a Wyoming bentonite obtained from Wards Scientific Co., and is similar to that used in several other research studies (e.g. Anderson et al., 1967). The absorption characterisitcs of water onto montmorillonite grains are fairly representative of silicate surfaces in general (Anderson et al., 1967). The general formula can be expressed as $(Al,Mg,Fe)_4(OH)_n(Si,Al,Fe)_8O_{20-n}(OH)_n \cdot mH_2O$. The amount of water bound to the surface is always less than one monolayer at low temperatures and is around 0.5 monolayer average at 100 K (Anderson et al.,

1967). Figure 1 shows the reflectance spectrum of montmorillonite as a function of temperature. The positions of the 1.4- and 2.2-μm OH bands shift less than about 50 Å (the limit to which the relative band positions can be determined) with a range of temperature of 293 to 177 K. The 1.9-μm band appears to have shifted longward about 100 Å with the change of temperature from 293 to 239 K, but does not appear to shift with lower temperatures. A complication exists because the absorption bands are decreasing in strength since the amount of bound water decreases with temperature and forms ice. Thus water ice absorption bands should become apparent at lower temperatures. This is not clearly seen since the pressure in the environment chamber was kept low in order to prevent frost from forming on the sample, tending to dehydrate the sample. Also, the cold finger was generally colder than the sample, causing water to continually migrate to the coldest surface and thus dehydrating the sample. The small shift of the 1.9-μm band might be due to the formation of some ice in the sample. In any case, the bound water bands do not shift appreciable and are in significantly different positions than the ice bands at 1.5 and 2.0 μm. This will become more apparent in the water-mineral mixtures section.

Kaolinite. Figure 2 shows kaolinite at 2 temperatures. There are no apparent shifts in the band positions ($\gtrsim$ 50 Å). The general formula is $Al_2Si_2O_5(OH)_4$ and contains very little bound water as seen by the weak 1.9-μm band. The hydroxyl bands are quite distinctive and should be easily recognizable in the presence of water ice (as will be seen in the water-mineral mixture section).

Beryl. Beryl ($Be_3Al_2Si_6O_{18}$) contains two types water which Wood and Nassau (1968) called type I and II according to the orientation of the water being either parallel or perpendicular to the channel sites. Wood and Nassau (1968) attributed the side lobes of the 1.4- and 1.9-μm absorptions as seen in Figure 3 to sum and difference bands involving rotational frequencies. There is no apparent shift in these band positions with temperature. The large absorption at 0.82 μm is caused by ferrous iron in the octahedral Al^{+3} site and decreases in width with decreasing temperture. The low temperature spectrum also contains a weak feature at 0.[illegible] μm which may be some fine structure in the 0.82-μm band. The absorption at 1.15 μm is due to type I water (Wood and Nassau, 1968) and does not shift with wavelength. The absorptions below 0.6 μm have apparently shifted in wavelength, and 3 bands appear at low temperature where only 2 were apparent at 293 K.

WATER-MINERAL MIXTURES

Remote sensing of the outer solar system solid surfaces has led to the identification water ice or frost as noted previously. It would be truly remarkable if these objects were made of pure water, but the reflectance spectra do not indicate pure water at all wavelengths (e.g. see McCord and Clark 1979b, c for summary spectra of the Galilean satellites and Saturn's rings). It has been suggested that these objects have a "dirty" ice on the surface (e.g. comets are often referred to as "dirty snowballs", and Callisto has a low albedo, ∿17%, indicating some dark material is on the surface along with the water). Other investigators have tried to explain why silicate - water ice mixtures could not account for the reflectance of Saturn's rings and possibly Europa and Ganymede (Lebofsky et al., 1970, Lebofsky and Fegley, 1976). However, the reflectance spectra of minerals mixed with water have not been studied in the laboratory.

Mixtures of water and several minerals were prepared and the reflectance spectra measured at room and low temperatures. The samples were accurately weighed on an analytical balance and the appropriate amount of water was also weighed and added to the sample. The samples were about 12 cubic centimeters

in volume in the sample holders, ensuring that they were optically thick. Five samples were measured at a time in the environment chamber, with the Halon standard in the sixth position in the sample turntable. The weight percentages of added water are accurate to better than 0.5% for the samples measured at room temperature, but the surfaces of the samples tended to dehydrate at low temperatures since they were under a vacuum in order to keep frost from growing on the surfaces. Thus the equivalent amount of water seen in the low temperature spectra was estimated from the water band intensities. As more samples were run, the experience in controlling the chamber pressure resulted in less dehydration, and a higher accuracy in the estimated equivalent water content. The low temperature spectra of the montmorillonite have the greatest error in water content ($\sim$ 5% in the $<$ 30 weight % range, and $\sim$ 10% in $>$ 30 weight % range), the Kaolinite is next with errors of $\sim$ 5% ($>$ 30 weight % water) and $\sim$ 2% for water contents of $\sim$10%. The errors of the water content in the low temperature spectra of the Mauna Kea red cinder and the charcoal are about 1%.

Figure 4 shows the room temperature spectra of montmorillonite. The albedo has decreased dramatically from the dryer sample in Figure 1. Figure 5

shows montmorillonite-water mixture spectra at low temperatures. The major ice bands occur at 1.5 and 2.0 μm, and weaker overtones occur at 1.25 and 1.04 μm. The 2.2-μm OH band is readily apparent, even in the sample with 60 weight % water ice. The bound water at 1.4 and 1.9 μm is also apparent at the short wavelength side of the 1.5- and 2.0-μm ice bands. Figure 6 from Clark (1979b), shows the reflectance of pure water frost for comparison.

The spectra of Kaolinite and water mixtures are shown in Figures 7 and 8. The OH absorptions at 2.2 and 1.4 μm are easily visible. The decrease in reflectance in the visible is typical of many reflectance spectra of planetary surfaces. In fact, qualitatively, the Kaolinite and water ice spectra closely resemble spectra of Saturn's rings, Ganymede and Europa, all of which have prominent water ice bands and a decrease in reflectance in the visible. This result contradicts the explanation by Lebofsky et al. (1970) and Lebofsky (1973) of why water-silicate mixtures are difficult to match to spectra of Saturn's rings.

Figures 9 and 10 show the spectra of mixtures of water and Mauna Kea red cinder. The iron oxide absorption at 0.87 μm is quite prominent and does not change with different amounts of water present in

sample. Thus diagnostic mineral bands in the 1-μm region and shorter can be easily detected in water-mineral mixtures. The 0.87-μm iron oxide band decreases in width with decreasing temperature, indicating that mineral spectra should be obtained at the same temperature as the surface under study when detailed comparisons are being made.

As an illustration of an opaque material suppressing the water absorption bands, Figure 11 shows the spectra of charcoal and water mixtures at room and low temperatures. The water absorptions are below any level of certain detection although the 2-μm absorption may be weakly present in the 296 K, 30 weight % H_2O spectrum. The 30 weight %, low temperature spectrum had a very small amount of frost structure on the surface (a few micrometers thick) and weakly shows the 2μm ice band. In general, the addition of water lowered the abledo and changed the slope slightly. The albedo appears to be a sensitive test for water content. However, this is material dependent as seen by the albedo changes of the montmorillonite and kaolinite, the montmorillonite decreasing much more in albedo with added water than the kaolinite.

There exists an additional absorption at 1.8 μm in mixture spectra when both bound water and free

water are presen The montmorillonite spectra in Figure 1 do not show a 1.8-μm band, whereas it appears in the spectra of water and montmorillonite in Figures 4 and 5. It also appears in the kaolinite-water, in the red cinder-water spectra and in spectra of pure liquid water indicating it is a combination overtone of water. This band is less apparent or absent in frost on mineral spectral, mineral grains on frost spectra or pure frost spectra. Since it is not apparent in pure ice spectra, this band may be an indicator of mineral and water mixtures. Further study is needed to determine the origin and nature of this absorption.

MINERAL GRAINS ON FROST

Another possible condition that is likely to be encountered on planetary surfaces is mineral grains which have been deposited on a frost layer. This condition could arise from meteor impacts throwing up particles or from wind blown dust (e.g. on Mars). Mineral grains were deposited on frosts and the reflectance spectrum was measured to show how the spectrum changed. The montmorillonite particles were propelled onto the frost surface through a copper tube by opening a chamber filled with the particles to room air when the environment chamber was under vacuum. The amount of air used was enough to propell the grains but not enough to blow the frost grains off the surface. The frost grains were slighly disturbed, however. The red cinder and charcoal grains were deposited on frost surfaces using a "salt shaker" system which was in the environment chamber under vacuum. The grains fell gently about 4 centimeters to the frost surface.

Figure 12 shows the results of the montmorillonite grains on the frost. The fractional areal coverage was determined from photographs taken during the measurements of the reflectance spectra. A fractional areal coverage of only 0.002 ± 0.001 is

discernible by a slight drop in abledo and a very slight indication of the 2.2-μm OH band in the side of the 2-μm frost band. The relative depths of the frost bands decrease with increasing montmorillonite coverage.

The effect of Mauna Kea red cinder grains on frost is shown in Figure 13. An areal coverage of only 5% has a large influence on the reflectance spectrum, decreasing the abledo at shorter wavelengths with the 0.9-μm absorption readily apparent.

Figure 14 and 15 show the results of sprinkling charcoal particles on frost. An areal coverage of 0.4 drastically reduces the abledo. Since the frost surface is not flat, and has a "fairy castle" structure, the charcoal particles fall into the structure and greatly reduce the number of scatterings between frost particles and lowering the albedo more than is indicated by the fractional coverage. Even with this low albedo, the frost bands are still apparent, being reduced in depth an amount approximately equivalent to the fractional areal coverage. As soon as the particles are deposited on the frost, the frost begins to grow on the particles, raising the albedo and increasing the frost band depth as shown in Figure 15. Whether or not this is likely to happen on a planetary surface, such as on

Ganymede, needs further investigation.

FROST GROWTH ON MINERALS

A likely occurence on planetary surfaces is a frost growth on a regolith surface. Figures 16 and 17 show frost growth on Mauna Kea red cinder (grain size $\leq$ 125 micrometers). The frost grain size is less than 30 micrometers. As the frost thickness increases, the abledo increases and the frost bands increase in depth. The spectra of frost on Mauna Kea red cinder shows the 0.9-μm band even when the frost thickness is 0.6 mm. A coarser grained frost would be more transparent below 1.4 μm than the fine grained frost, requiring a much thicker frost layer to mask the 0.9 μm band in the cinder. The very thin frost layers on the charcoal indicate that a small amount of frost will rapidly increase the albedo and that even though the abledo is low, the water absorption bands are still prominent. This is quite different than what is seen with water-charcoal mixtures. Very thin frost layers on any surface would then show diagnostic water absorptions. The linear decrease in reflectance with increasing wavelength occurs in scattering cases with a natural distribution in grain sizes (Hansen and Travis, 1974).

CONCLUSIONS

Laboratory spectra of minerals with bound water and hydroxyl show that the wavelengths of the absorption bands do not shift appreciably with temperature indicating that bound water and OH should be detectable when large amounts of ice are present. Spectra of water and mineral mixtures verify the above conclusion and show that the decrease in reflectance in the visible wavelengths seen in many planetary reflectance spectra can be explained by ice mixed with minerals which have a decrease in reflectance in the visible. Mixtures of a low albedo material (in the 1.4 - 2.5-μm region) with water tend to suppress the water absorptions. In general, the overall albedo of a material decreases when mixed with water although the magnitude is material dependent.

Depositing mineral grains on a frost layer decreases the albedo more than would be indicated by the fractional areal coverage of the grains, presumably due to a large decrease in scattering. Very small amounts of particles on the frost (a fractional areal coverage $\sim$ 0.005) may be detectable depending on the absorptions in the mineral grains. Deposition of mineral grains on a frost may also cause the decrease in reflectance at shorter wavelengths if the

reflectance of the mineral also exhibits the decrease. The frost absorption bands are decreased in depth approximately equal to the fractional areal coverage of the mineral grains.

Frost growth on a mineral produces spectra similar to those from deposition of mineral grains on a frost. Below 1.4 μm, the frost is relatively transparent, thus the mineral absorptions are difficult to mask.

Work is currently under way in further analyzing these and other spectra to see if it is possible to distinguish between water-mineral mixtures, mineral grains on frost, and frost on a mineral surface.

ACKNOWLEDGEMENTS

I would like to thank Mike Gaffey and Bob Singer for several useful discussions. I would like to give my deepest thanks to Tom McCord for his help, encouragement, and for providing the computer and necessary laboratory facilities to carry out this work. This work was supported under NASA grants NSG 7590 and 7312.

REFERENCES

Anderson, D. M., Gaffey, E. S., and Low, P. F., Frost phenomena on Mars. Science 155, 31-322, 1967.

Clark, R. N., A large scale interactive one dimensional array processing system. Pub. Astron. Soc. Pac. submitted, 1979a. Thesis App A

Clark, R. N., Water frost and ice: The near infrared spectral reflectance 0.65 - 2.5 μm. J. Geophys. Res. submitted, 1979b. Thesis II Ch1

Clark, R. N., and McCord, T. B., Mars residual north polar cap: Earth-based spectroscopic confirmation of water ice as a major constituant and evidence for hydrated minerals, J. Geophsy. Res., submitted 1980a. Thesis III Ch1

Clark, R. N., and McCord, T. B., The Galilean satellites: New near-infrared reflectance measurements (0.65 - 2.5 μm) and a 0.325 - 5 μm summary. Icarus submitted, 1979b. Thesis I Ch 1

Clark, R. N., and McCord, T. B., The rings of Saturn: New near-infrared reflectance measurements and a 0.325 - 4.08 μm summary. Icarus submitted, 1979c. Thesis I Ch 2

Fink, U., Larson, H. P., Gautier, T. N. III, and Treffers, R. R., Infared spectra of the satellites of Saturn: Identification of water ice on Iapetus, Rhea, Dione and Tethys. Astrophys. J. Lett., 207, 63-67, 1976.

Hand, G. R., and Salisbury, J. W., Visible and near-infrared spectra of minerals and rocks: I silicate

minerals. Mod. Geol., 1, 283-300, 1970.

Hansen, J. E., and Travis, L. D., Light scattering in planetary atmospheres. Space Sci. Res., 16, 527-610, 1974.

Lebofsky, L. A., and Fegley, M. B., Jr., Laboratory reflection spectra for the determination of chemical composition of icy bodies. Icarus 28, 379-387, 1976.

Lebofsky, L. A., Johnson, T. V., and McCord, T. B. Saturn's rings: Spectral reflectivity and compositional implications. Icarus 13, 226-230, 1970.

McCord, T. B., Clark, R. N., and Huguenin, R. L. Near-infrared spectral reflectance and compositional implication. J. Geophys. Res., 83, 5433-5441, 1978.

McCord, T. B., Clark, R. N., Singer, R. B., and Hugenin, R. L., Mars: Near-infrared reflectance spectra of surface regions and compositional implication. J. Geophys. Res., to be submitted, 1979. Thesis I Ch 3

Morrison, D., Cruikshank, D. P., Pilcher, C. B. and Rieke, G. H., Surface compositions of the satellites of Saturn from infrared photometry. Astrophys. J. Lett., 207, 213-216, 1976.

Pilcher, C. B., Chapman, C. R., Lebofsky, L. A. and Kieffer, H. H., Saturn's rings: Identification of water frost. Science 167, 1372-1373, 1970.

Pilcher, C. B., Ridgway, S. T., and McCord, T. B. Galilean satellites: Identification of water frost. Science 178, 1087-1089, 1972.

Wood, D. L. and Nassau, K., The characterization of beryl and emerald by visible and infrared absorption spectroscopy. American Mineralogist 53, 777-800, 1968.

FIGURE CAPTIONS

Figure 1 The reflectance spectrum of montmorillonite at several temperatures is shown. The absorption bands do not shift appreciably in wavelength with temperture. The light source intensity was about ten times lower for these spectra than the others in this study resulting in the decreased signal to noise below 0.9 μm.

Figure 2 The reflectance spectrum of kaolinite at two temperatures show there is no apparent shift of the 1.4- and 2.2-μm OH bands, but two weak absorptions are seen at 0.6 and 0.5 μm at low tempearature which are not seen at 293 K.

Figure 3 The reflectance spectrum of beryl at two temperatures shows no apparent shift in the 1.15-, 1.4-, and 1.9-μm bound water bands. The ferrous iron (0.82 μm) becomes narrower at lower temperature with some fine structure (at 0.95 μm). Three absorptions in the visible at 0.7, 0.5 and 0.35 μm are seen at 164 K which are not seen or are shifted in wavelength at 293 K.

Figure 4 Spectra of montmorillonite with A) 50 weight percent water and B) 90 weight percent water mixed in the sample.

Figure 5 The spectral reflectance of montmorillonite mixed with water is shown at low temperatures. The water ice and bound water components are: A) 15%, 15%; B) 20%, 15%; and C) 60%, and 8% by weight.

Figure 6 The spectral reflectance of pure water frost from Clark (1979b) is shown for several different grain sizes. The characteristic grain sizes are (top to bottom) are: 50, 100, 200, and 400 - 2000 micrometers.

Figure 7 The spectra of Kaolinite at room temperature is shown mixed with A) 25 weight percent water, and B) 60 weight percent water. The 1.4- and 2.2-μm OH absorptions are easily seen in both spectra, the 1.4-μm band being a depression in short wavelength wing of the 1.5-μm water band.

Figure 8 The spectra of Kaolinite mixed with water at low temperature. The weight percentage of water in each sample is: A) 10, B) 25, and C) 40. The 1.4- and 2.2-μm OH absorptions are easily seen in the wings of the water ice bands. The temperature of each

sample was: A) 152 K, B) 150 K, and C) 218 K.

Figure 9 Spectra of Mauna Kea red cinder (grain size $\leq$ 125 micrometers) mixed with water. The weight percentage of water in each sample was: A) 1, B) 5, C) 12, and D) 30. Some settling occurred in sample D, resulting in about 0.5 μm of water on the red cinder surface, causing the very strong water absorptions.

Figure 10 The same samples is in Figure 9 except at low temperature. The temperature and weight percentage of water in each sample was: A) 189 K, 1; B) 191 K, 5; C) 186 K, 12; and D) 186 K, $\sim$ 30. The water surface layer of (d) crystallized near the edge of the sample, leaving the cinder-water mixture exposed.

Figure 11 The spectra of charcoal (grain size $\leq$ 125 micrometers) and water mixtures are shown at both high and low temperatures. The weight percentage of water in each sample was: A and D) 0, B and E) 5, and C and F) 30. Some frost condensed on the surface of sample F, changing the slope of the spectrum and slightly raising the abledo

(frost thickness: a few micrometers). The grains were very porous and did not stick together as compared to the red cinder in Figure 9 and 10, which was saturated with 30 weight % water. The water bands are completely suppressed.

Figure 12 The spectra of montmorillonite grains on medium grained frost is shown. The frost with no montmorillonite grains (bottom) is the same as the 112 K frost in Figure 6. The fractional areal coverage of the montmorillonite grains on the frost was, from bottom to top: 0, 0.002 $\pm$ 0.001, 0.1 $\pm$ 0.05, and 0.7 $\pm$ 0.1. The 0.002 fractional coverage is detectable by a drop in reflectance in the 0.65 μm region from 0.98 to 0.90 and a very slight hint of the 2.2-μm OH band in the wing of the 2μm water band.

Figure 13 The spectral reflectance of Mauna Kea red cinder grains ($\leq$ 125 micrometers) on frost is shown with fractional areal coverage of A) 0.0, B) 0.05 $\pm$ 0.01, C) 0.10 $\pm$ 0.03, D) 0.30 $\pm$ 0.07, E) 0.5 $\pm$ 0.1, and F) 0.8, $\pm$ 0.1. The spectrum (G)is that of Figure 10A (189 K).

Figure 14 The effects of sprinkling charcoal grains ($\leq$ 125 micrometers) on frost is shown. A) The fractional areal coverage (top to bottom) is: 0.0, 0.4 $\pm$ 0.1, and 0.7 $\pm$ 0.1. B) The bottom two spectra from (A) is shown on an expanded scale.

Figure 15 As soon as particles are sprinkled on the frost, the frost begins to grow, covering the newly deposited grains. The spectra from Figure 14 (areal coverage A: 0.4, and B: 0.7) are at the bottom with frost growth raising the albedo.

Figure 16 The spectra of frost growth on Mauna Kea red cinder shows a decrease at shorter wavelengths even when the 1.5- and 2-μm frost bands are very prominent. The frost depths are A) 0.0, B) 0.05, C) 0.1, D) 0.2, E) 0.3, and F) 0.6 mm. The frost grain size is less than 30 micrometers.

Figure 17 The spectra of frost on charcoal shows prominent water absorptions, even at low albedoes. The frost grain size was <30 micrometers and the depths were (bottom to top): 0.0, 0.05 $\pm$ 0.02, 0.15 $\pm$ 0.05, 0.3 $\pm$ 0.1 mm.

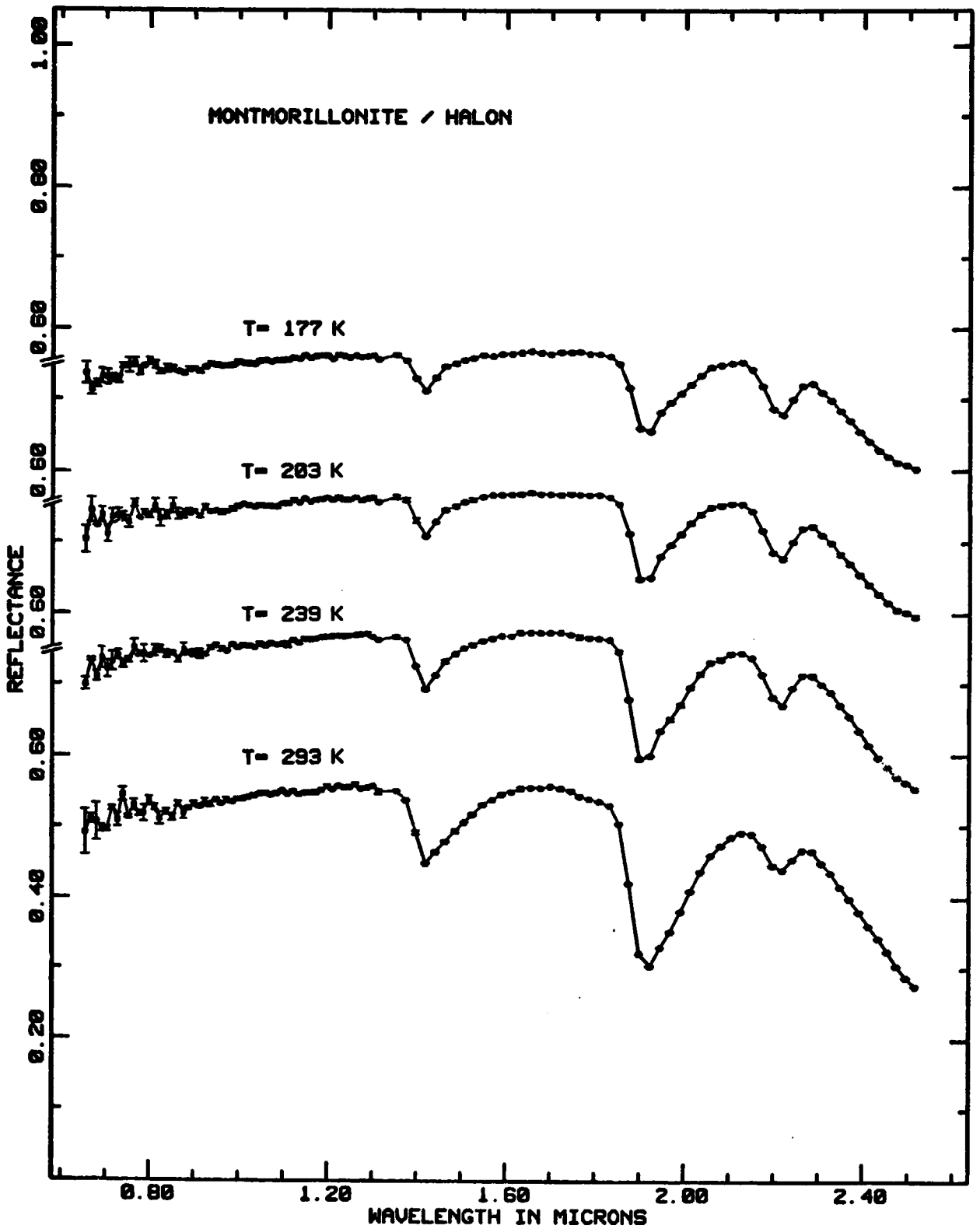

MONTMORILLONITE / HALON
T= 177 K
T= 203 K
T= 239 K
T= 293 K
REFLECTANCE
1.00
0.80
0.60
0.60
0.60
0.60
0.40
0.20
0.80
1.20
1.60
2.00
2.40
WAVELENGTH IN MICRONS

Figure 1

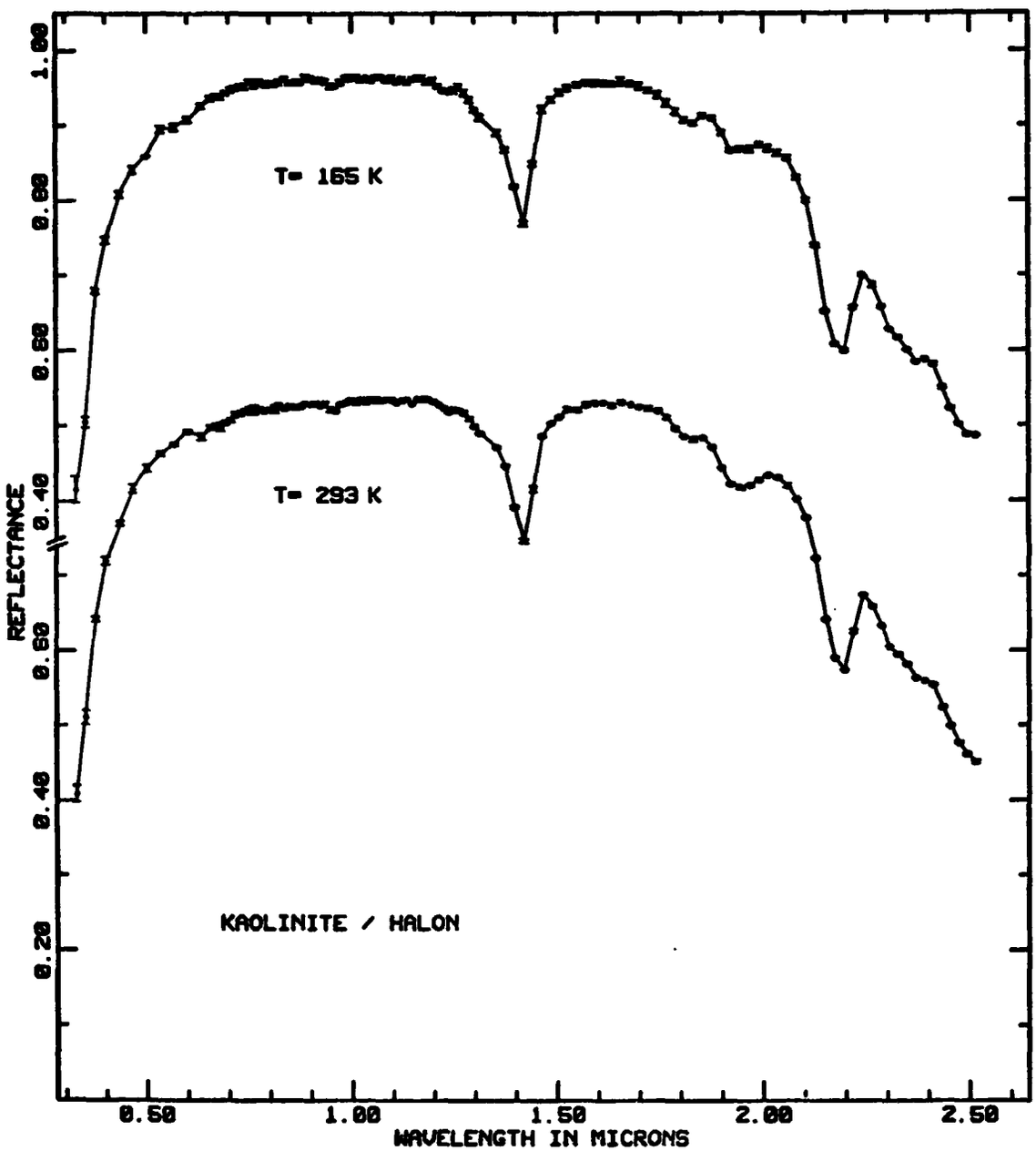

T= 165 K
T= 293 K
KAOLINITE / HALON
REFLECTANCE
1.00
0.80
0.60
0.40
0.20
0.50
1.00
1.50
2.00
2.50
WAVELENGTH IN MICRONS

Figure 2

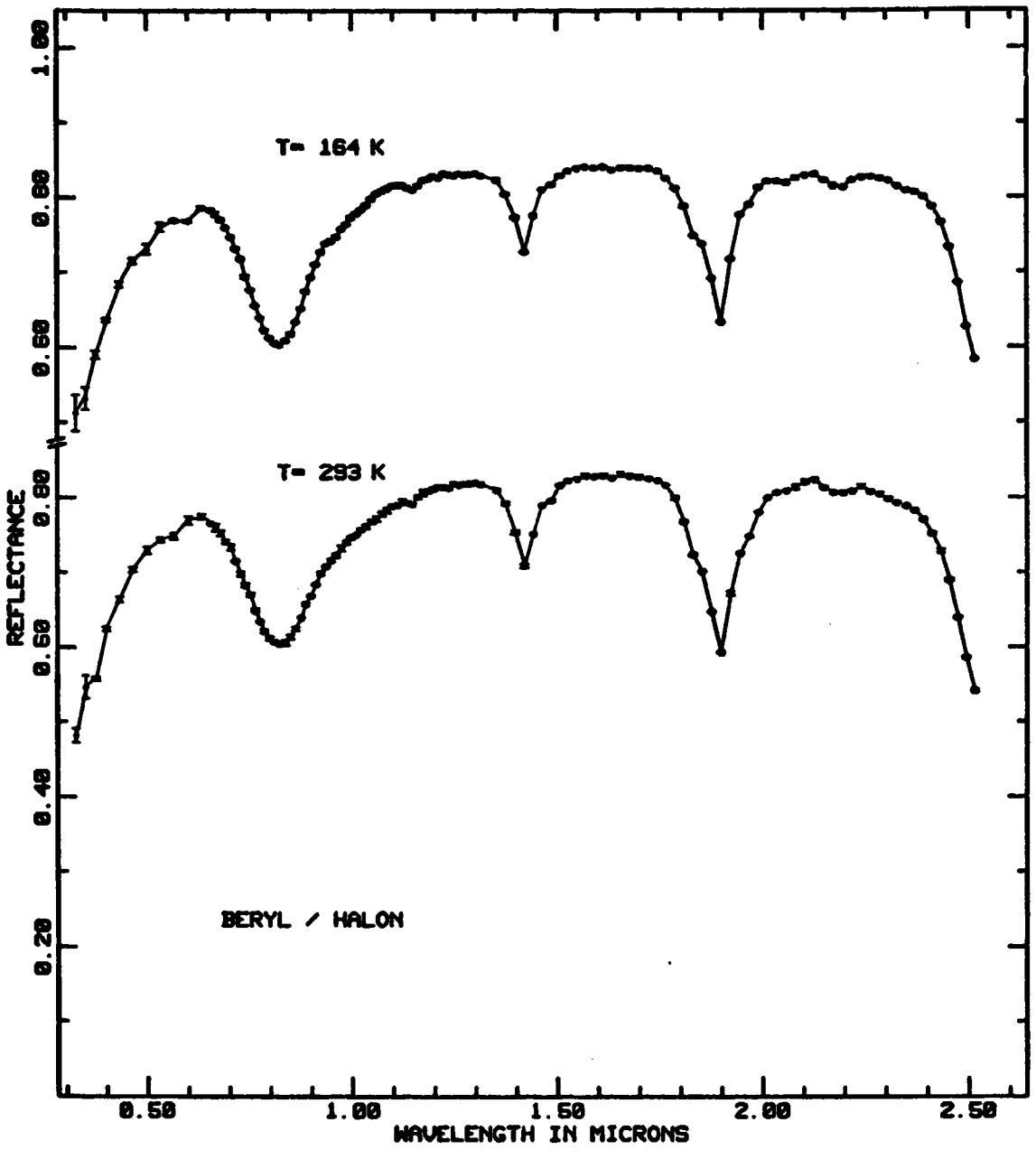

T= 164 K
T= 293 K
BERYL / HALON
REFLECTANCE
1.00
0.80
0.60
0.40
0.20
0.50
1.00
1.50
2.00
2.50
WAVELENGTH IN MICRONS

Figure 3

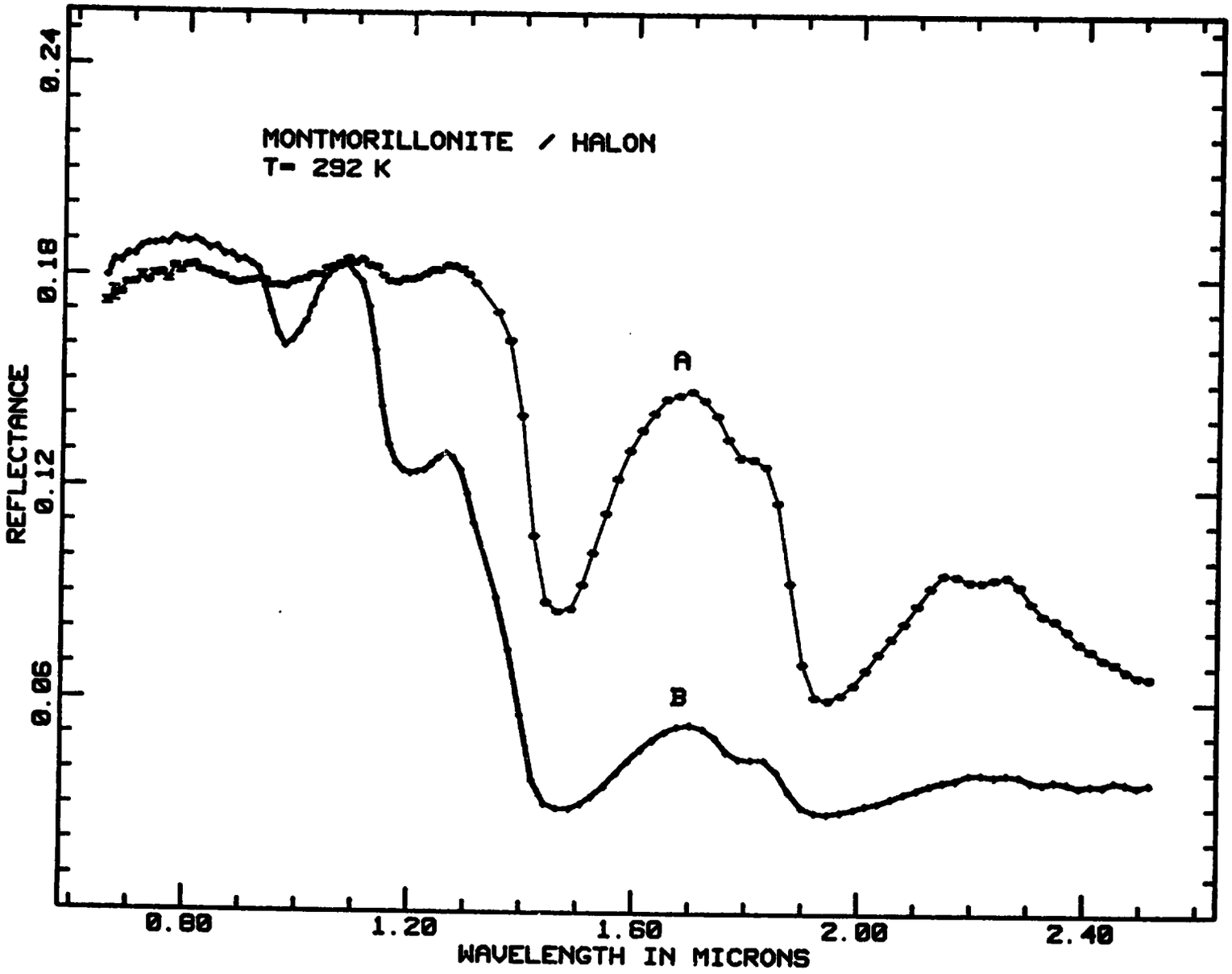

MONTMORILLONITE / HALON
T= 292 K
REFLECTANCE
0.24
0.18
0.12
0.06
A
B
0.80
1.20
1.60
2.00
2.40
WAVELENGTH IN MICRONS

Figure 4

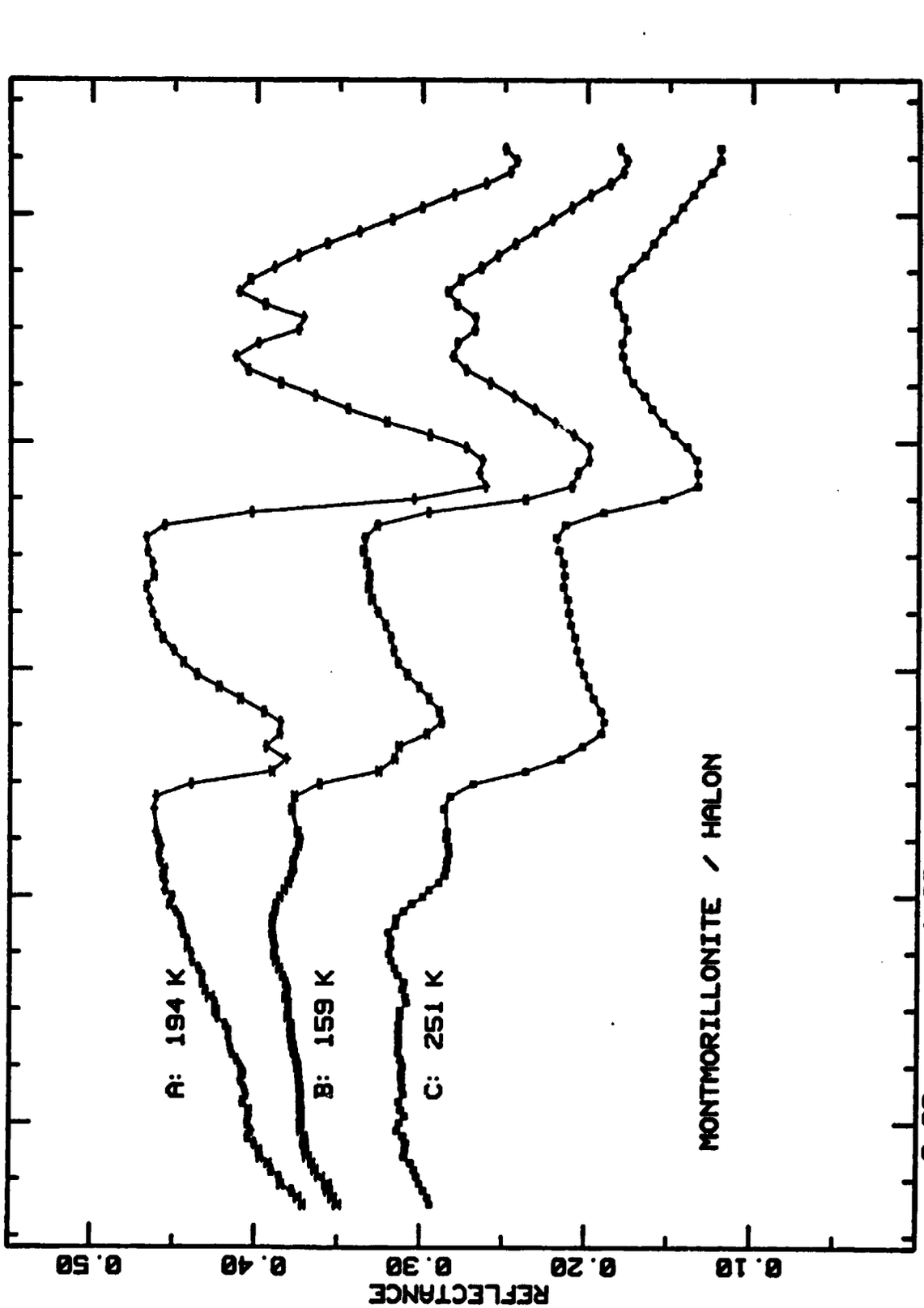

A: 194 K
B: 159 K
C: 251 K
MONTMORILLONITE / HALON
REFLECTANCE
0.10
0.20
0.30
0.40
0.50
0.80
1.20
1.60
2.00
2.40
WAVELENGTH IN MICRONS

Figure 5

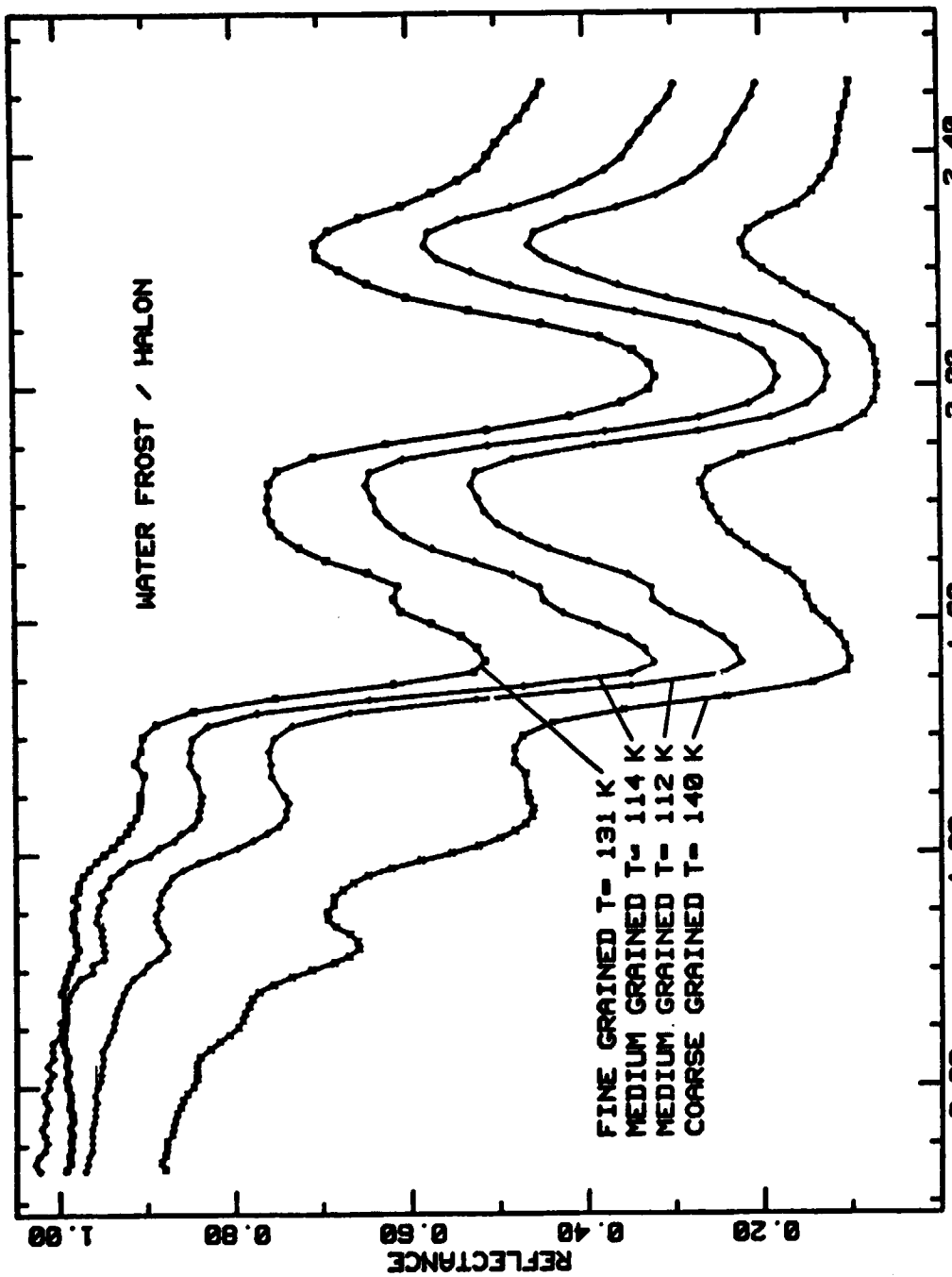

WATER FROST / HALON
FINE GRAINED T= 131 K
MEDIUM GRAINED T= 114 K
MEDIUM GRAINED T= 112 K
COARSE GRAINED T= 140 K
REFLECTANCE
0.20
0.40
0.60
0.80
1.00
0.80
1.20
1.60
2.00
2.40
WAVELENGTH IN MICRONS

Figure 6

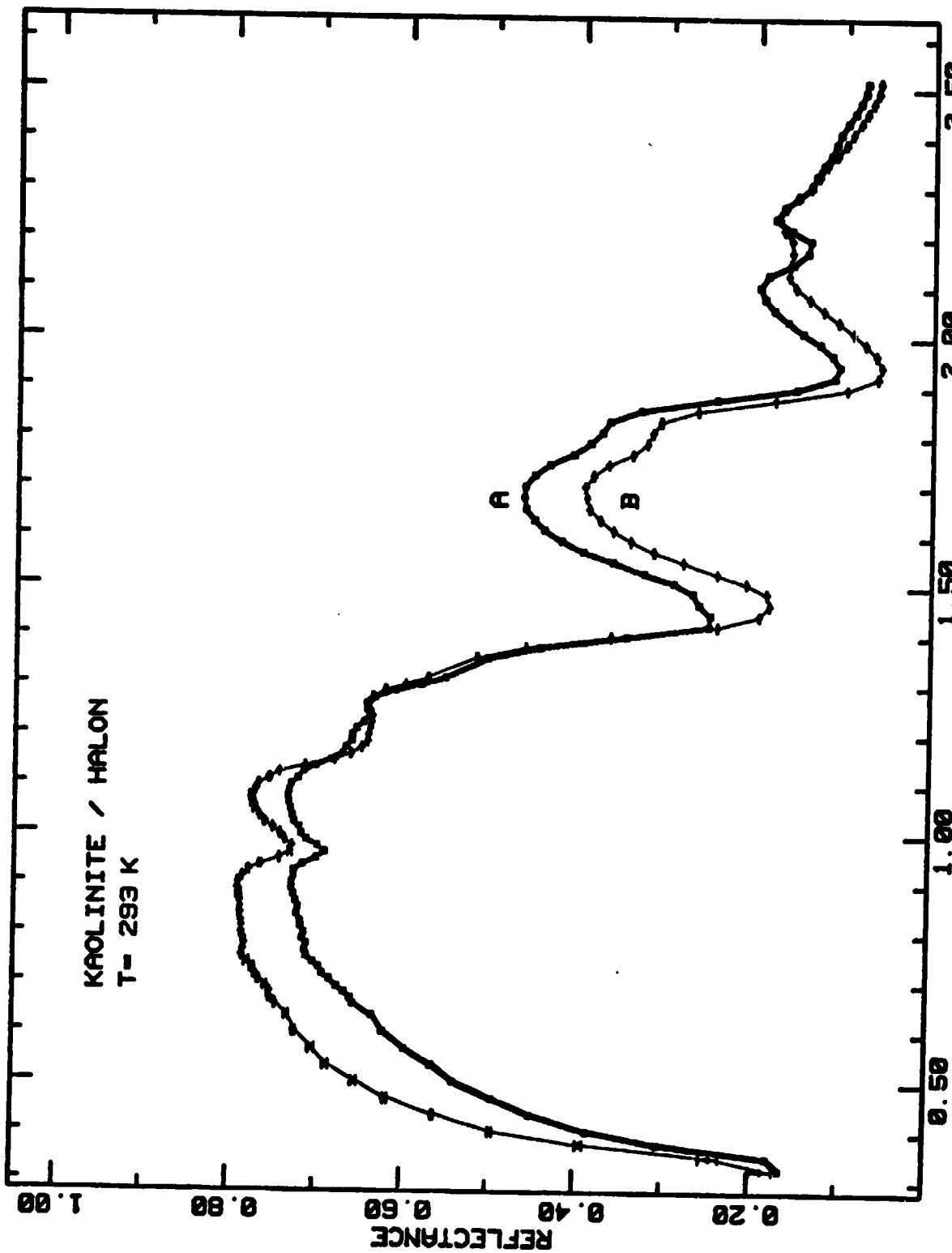

KAOLINITE / HALON
T= 293 K
A
B
REFLECTANCE
0.20
0.40
0.60
0.80
1.00
0.50
1.00
1.50
2.00
2.50
WAVELENGTH IN MICRONS

Figure 7

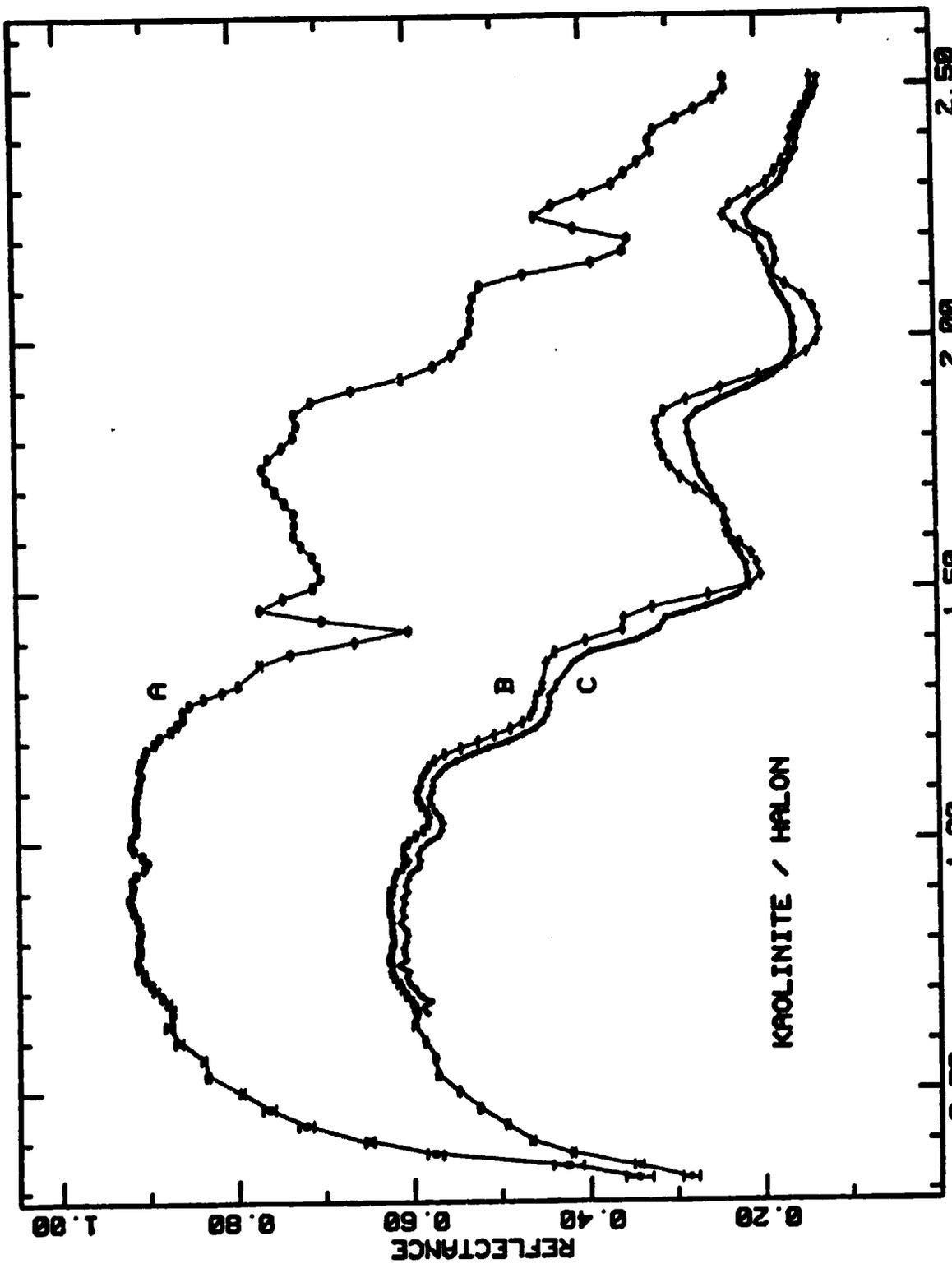

KAOLINITE / HALON
A
B
C
REFLECTANCE
0.20
0.40
0.60
0.80
1.00
0.50
1.00
1.50
2.00
2.50
WAVELENGTH IN MICRONS

Figure 8

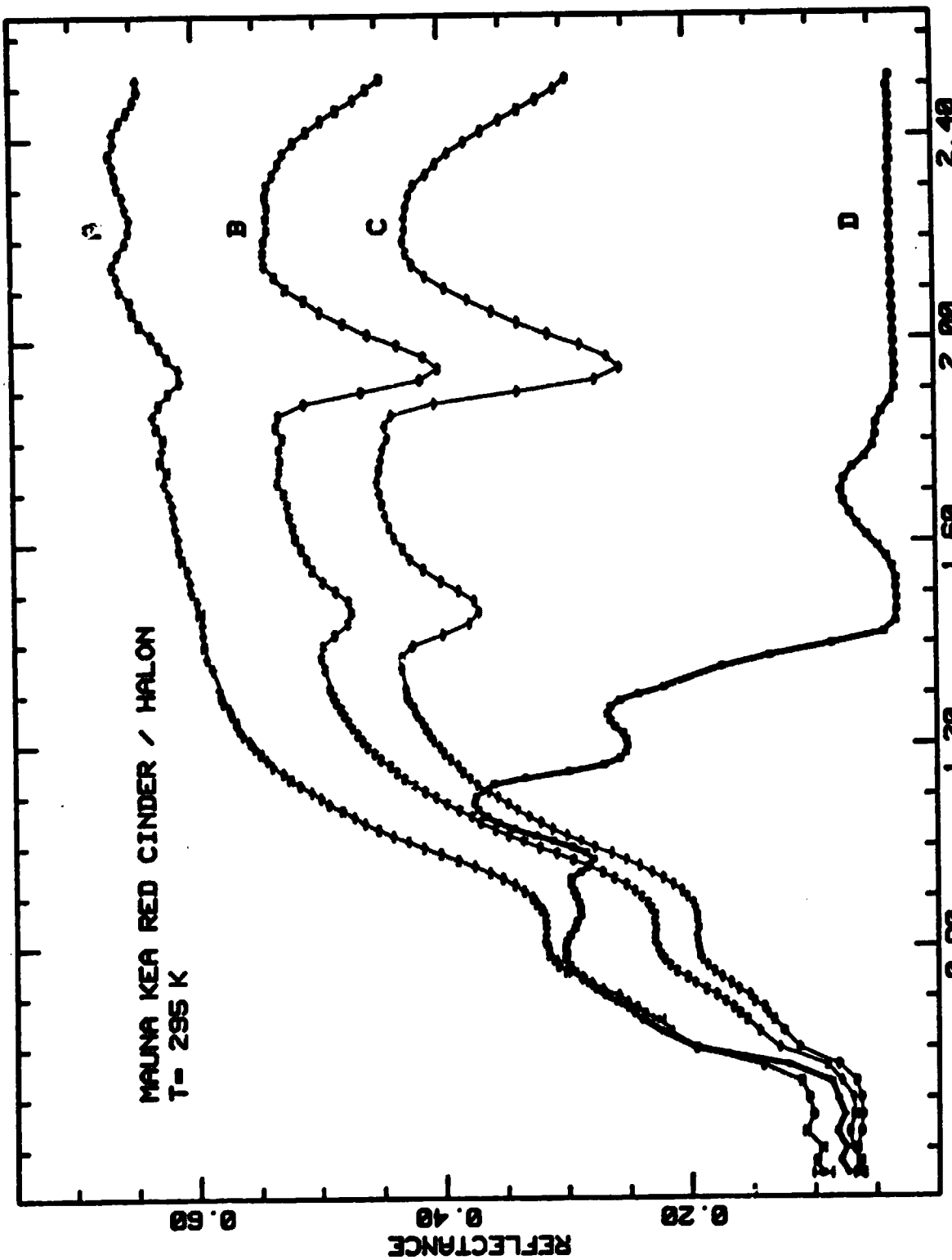

MAUNA KEA RED CINDER / HALON
T= 295 K
A
B
C
D
REFLECTANCE
0.20
0.40
0.60
0.80
1.20
1.60
2.00
2.40
WAVELENGTH IN MICRONS

Figure 9.

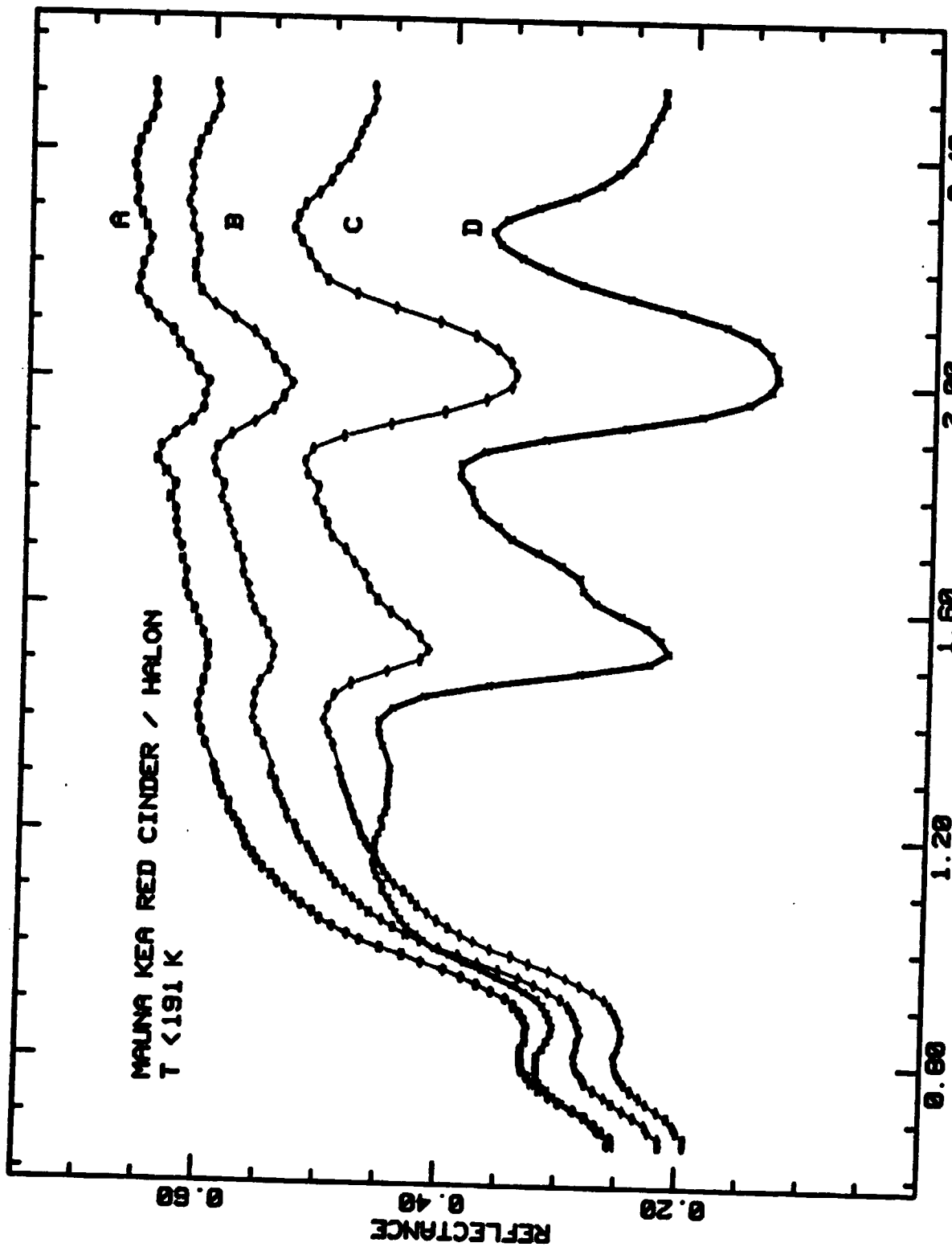

MAUNA KEA RED CINDER / HALON
T <191 K
A
B
C
D
REFLECTANCE
0.20
0.40
0.60
WAVELENGTH IN MICRONS
0.80
1.20
1.60
2.00
2.40

Figure 10

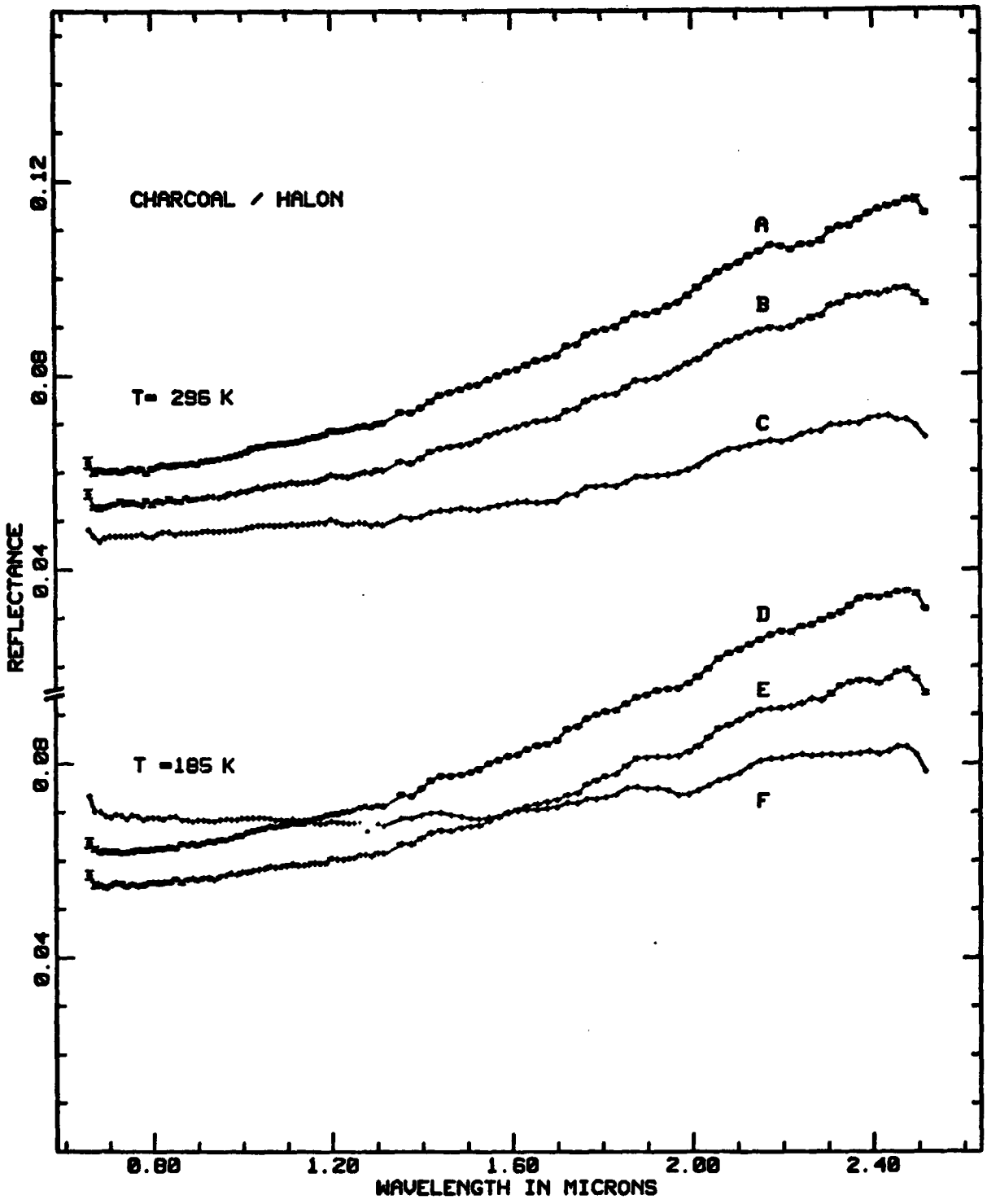

CHARCOAL / HALON
T= 296 K
T =185 K
A
B
C
D
E
F
REFLECTANCE
0.12
0.08
0.04
0.08
0.04
0.80
1.20
1.60
2.00
2.40
WAVELENGTH IN MICRONS

Figure 11

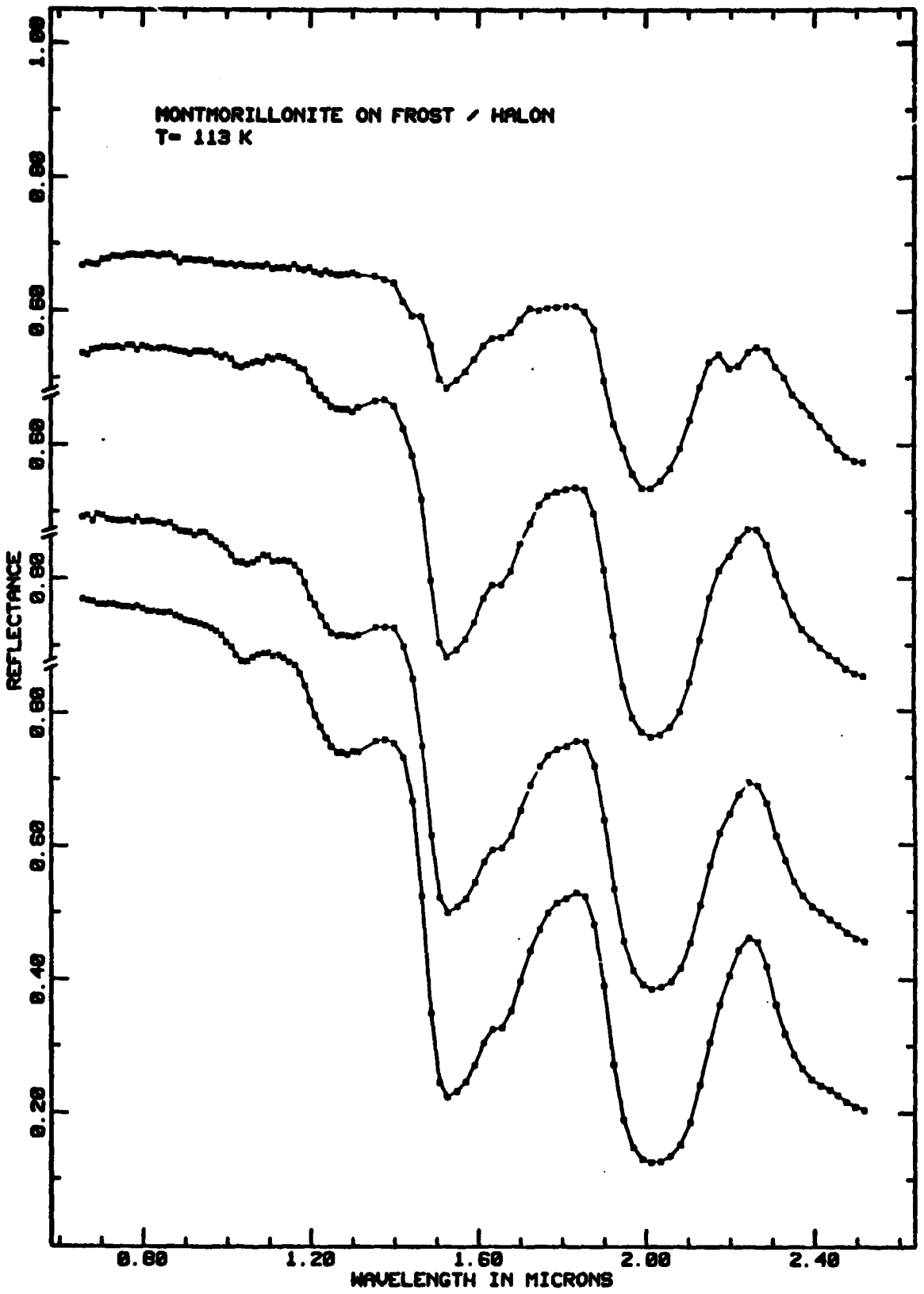

MONTMORILLONITE ON FROST / HALON
T= 113 K
REFLECTANCE
1.00
0.80
0.60
0.40
0.20
0.00
1.20
1.60
2.00
2.40
WAVELENGTH IN MICRONS

Figure 12

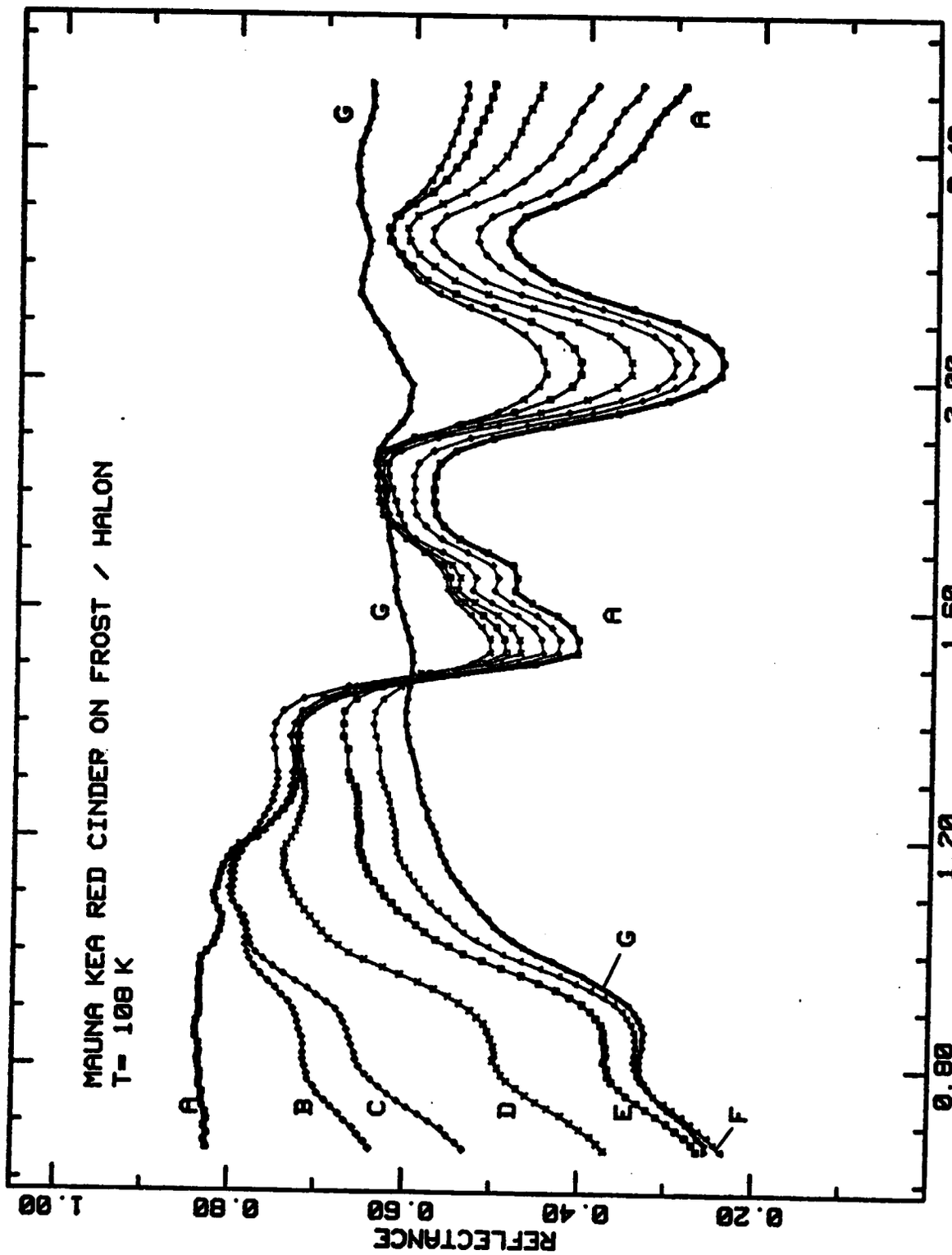

MAUNA KEA RED CINDER ON FROST / HALON
T= 108 K
REFLECTANCE
0.20
0.40
0.60
0.80
1.00
WAVELENGTH IN MICRONS
0.80
1.20
1.60
2.00
2.40
A
B
C
D
E
F
G

Figure 13

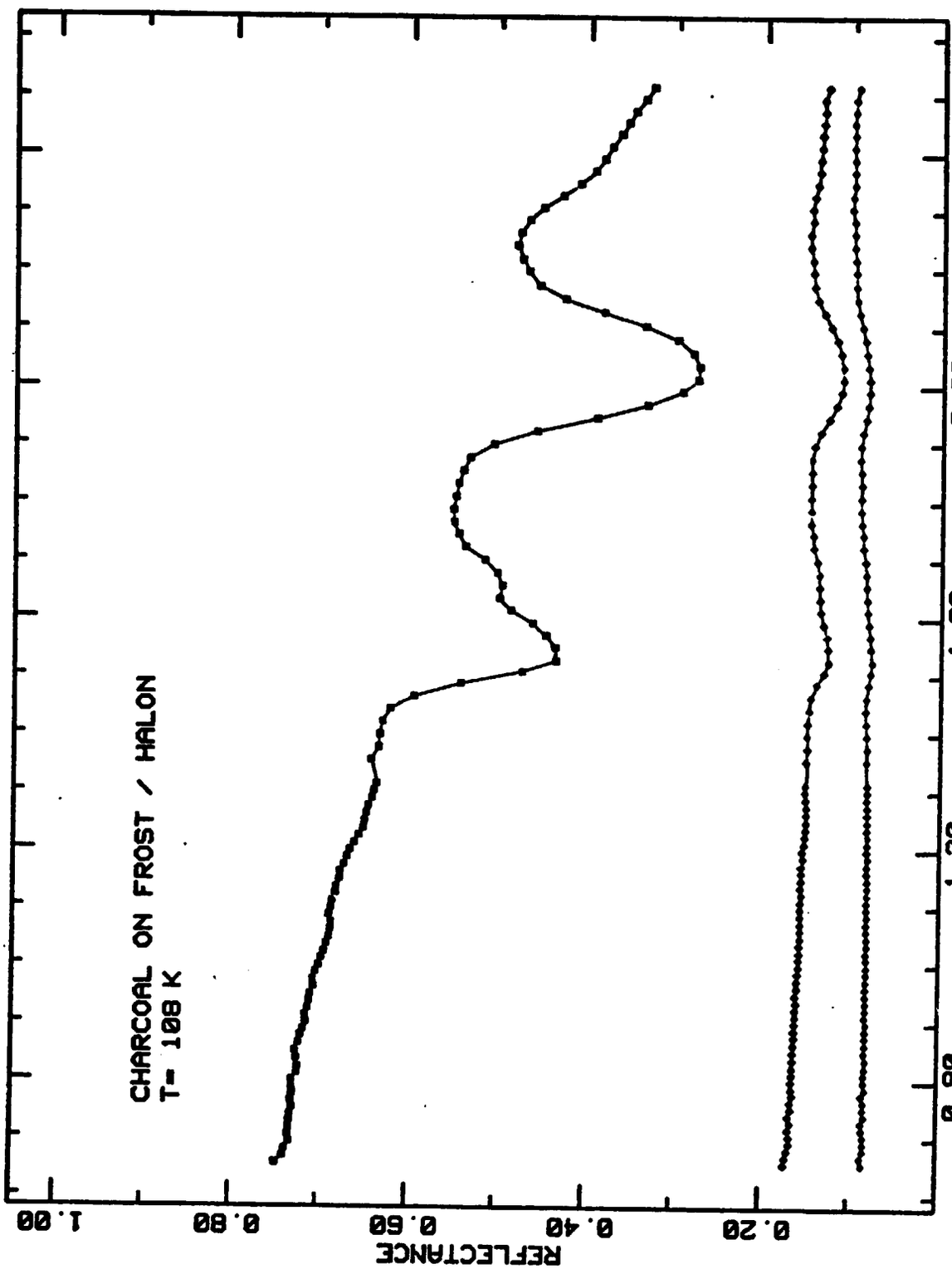

CHARCOAL ON FROST / HALON
T= 108 K
REFLECTANCE
0.20
0.40
0.60
0.80
1.00
0.80
1.20
1.60
2.00
2.40
WAVELENGTH IN MICRONS

Figure 14A

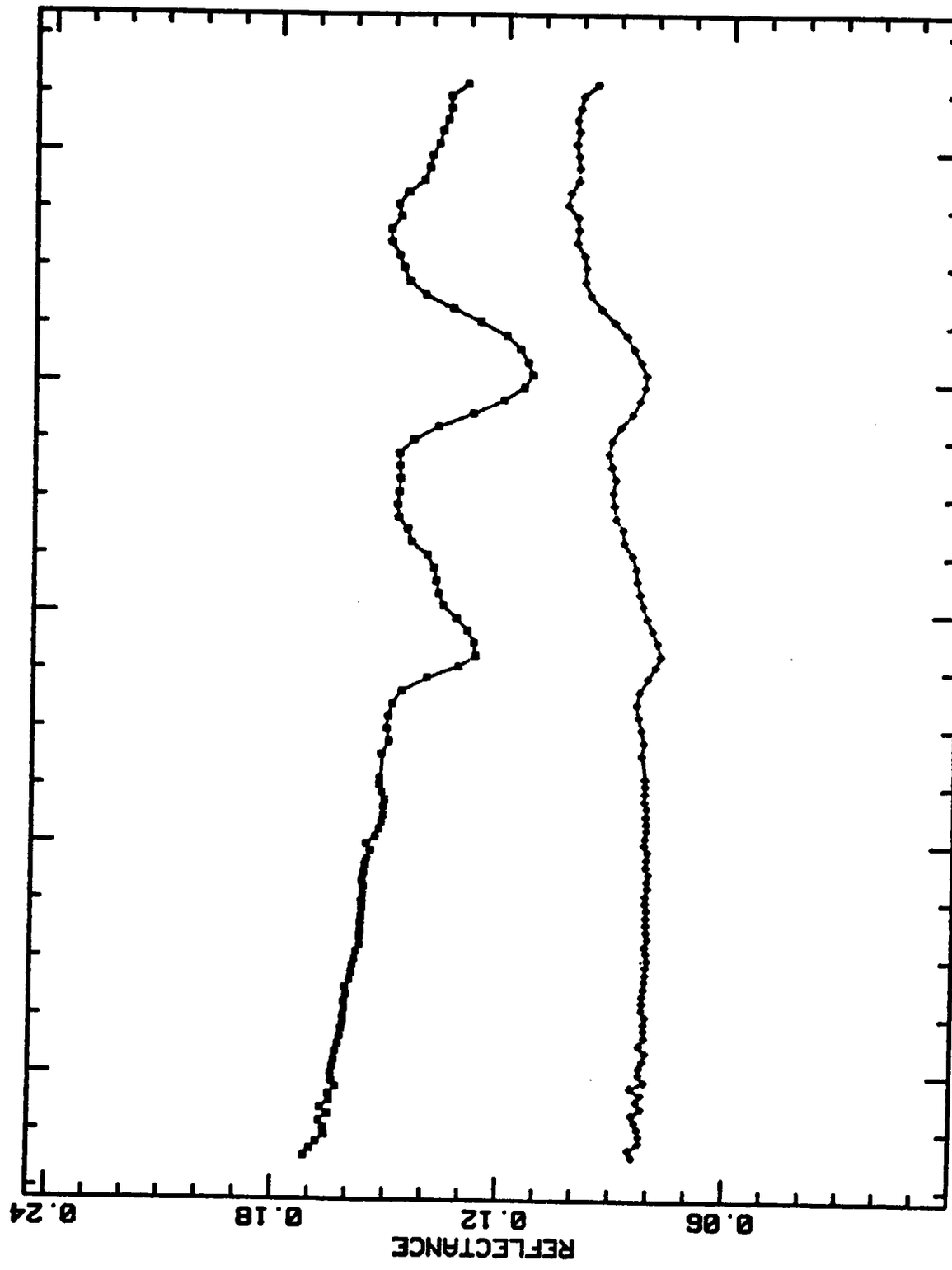

REFLECTANCE
0.06
0.12
0.18
0.24
0.80
1.20
1.60
2.00
2.40
WAVELENGTH IN MICRONS

Figure 14B

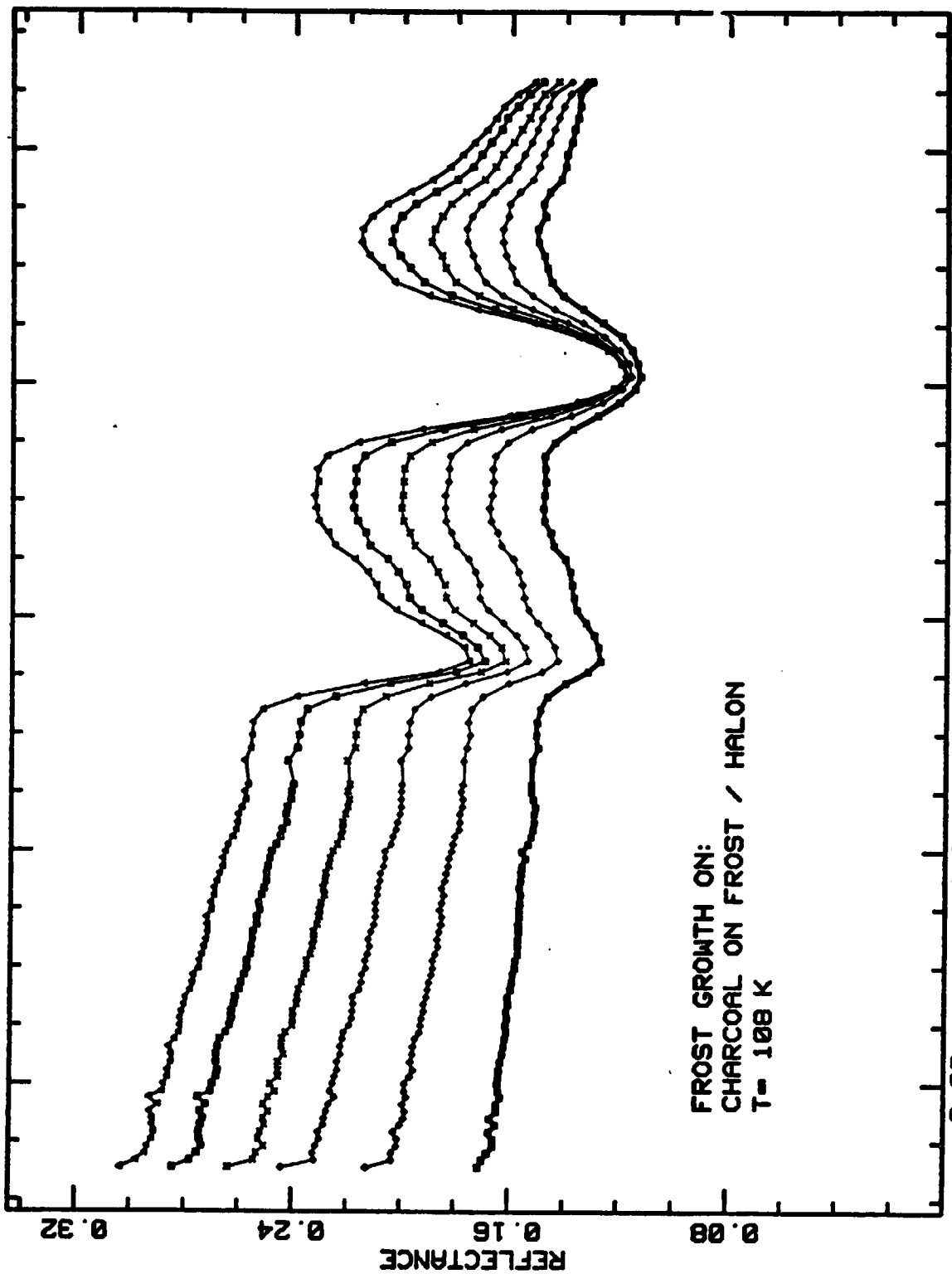

FROST GROWTH ON:
CHARCOAL ON FROST / HALON
T= 108 K
REFLECTANCE
0.08
0.16
0.24
0.32
WAVELENGTH IN MICRONS
0.80
1.20
1.60
2.00
2.40

Figure 15A

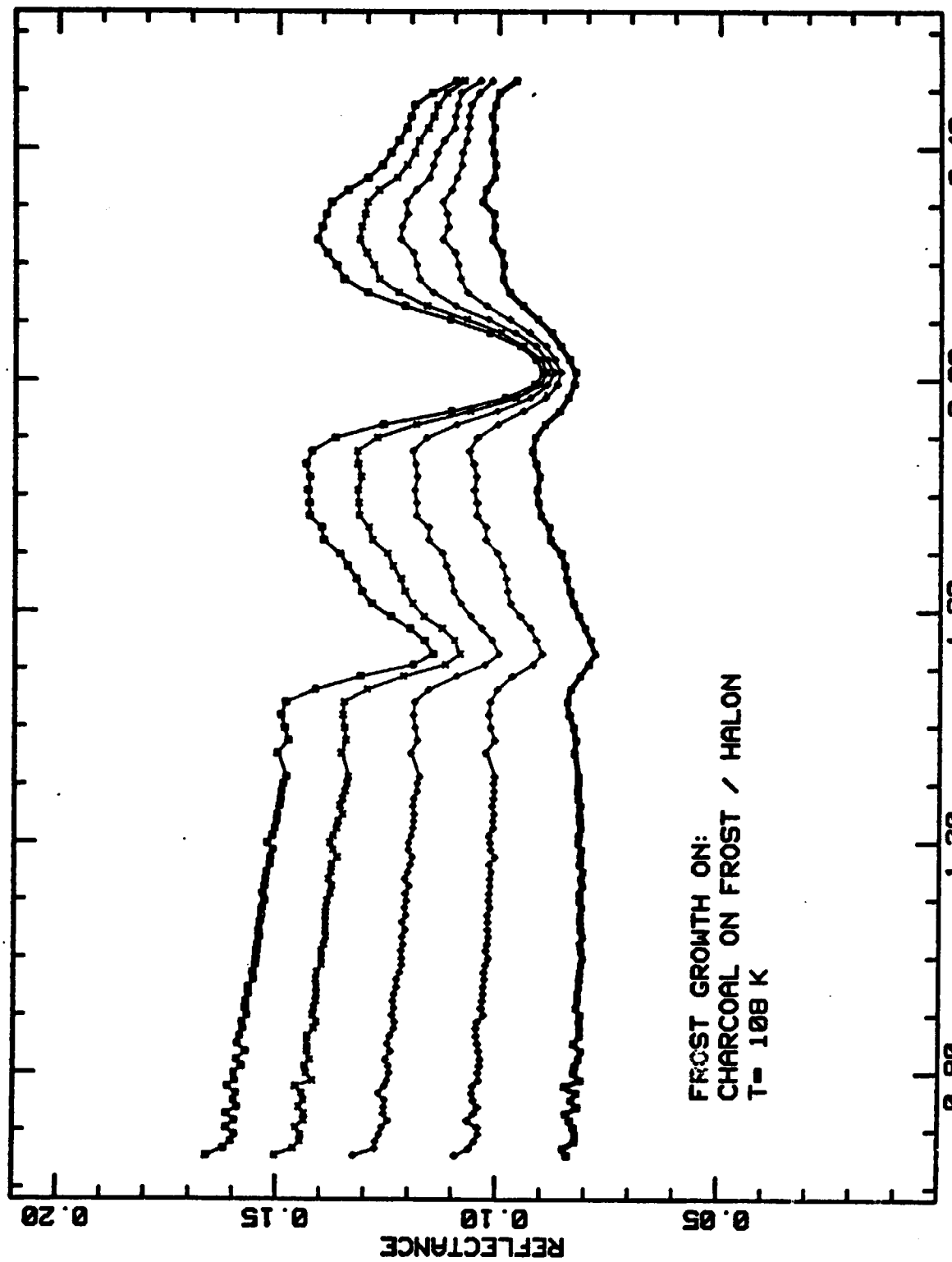

FROST GROWTH ON:
CHARCOAL ON FROST / HALON
T= 108 K
REFLECTANCE
0.05
0.10
0.15
0.20
WAVELENGTH IN MICRONS
0.80
1.20
1.60
2.00
2.40

Figure 15B

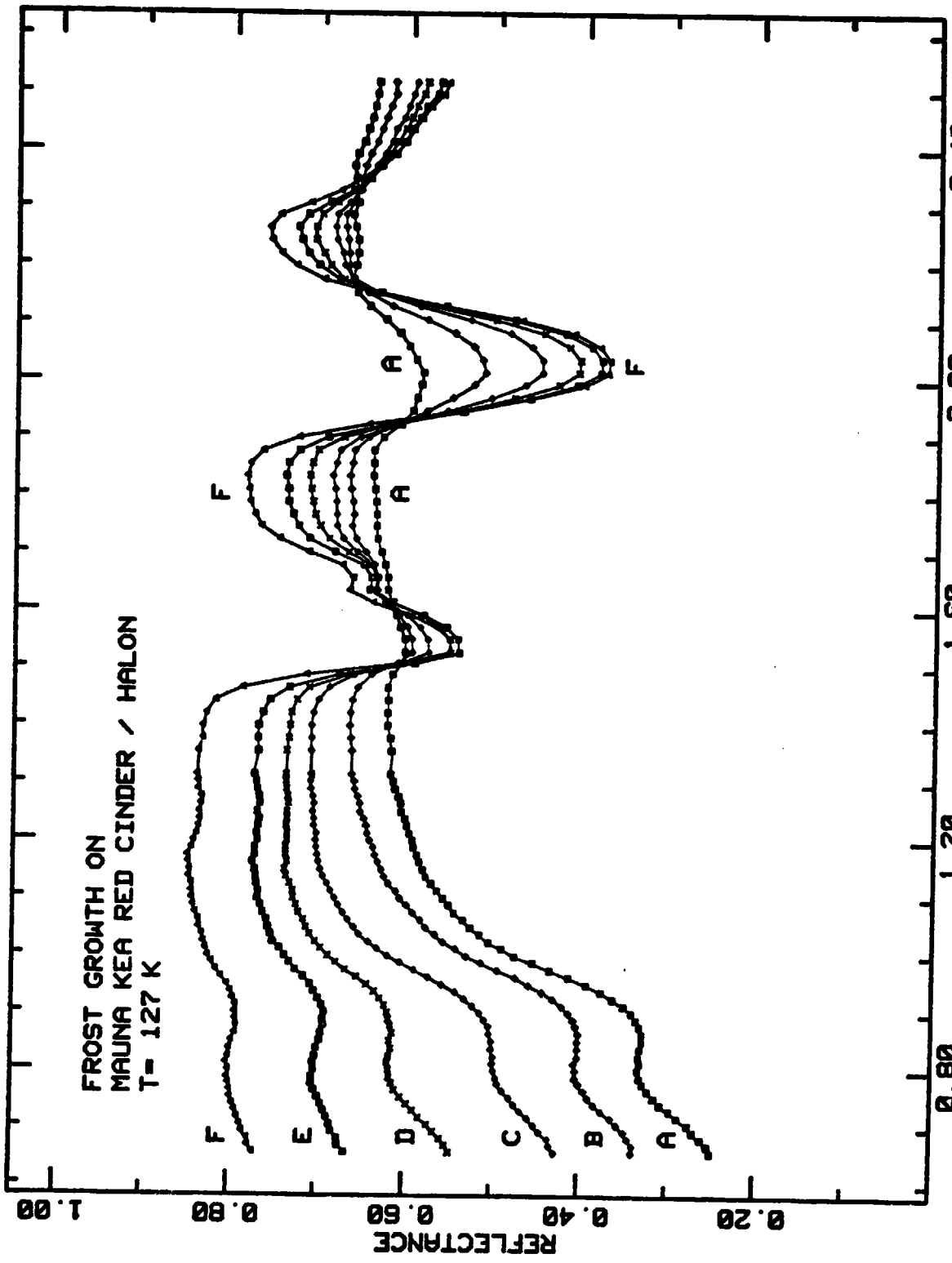

FROST GROWTH ON
MAUNA KEA RED CINDER / HALON
T= 127 K
F
E
D
C
B
A
F
A
F
A
REFLECTANCE
0.20
0.40
0.60
0.80
1.00
0.80
1.20
1.60
2.00
2.40
WAVELENGTH IN MICRONS

Figure 16

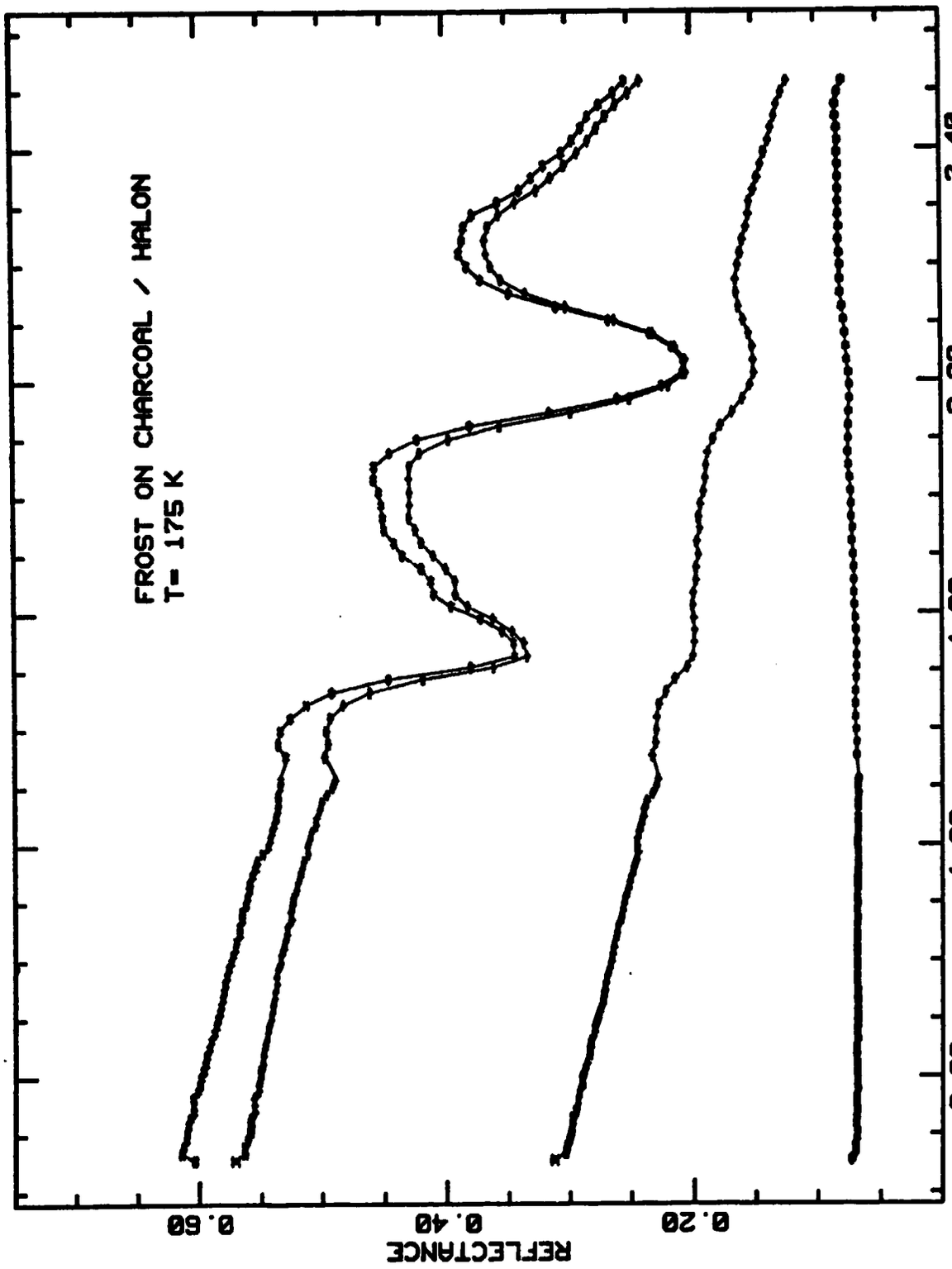

FROST ON CHARCOAL / HALON
T= 175 K
REFLECTANCE
0.20
0.40
0.60
0.80
1.20
1.60
2.00
2.40
WAVELENGTH IN MICRONS

Figure 17

SECTION III

INTERPRETATION OF PRESENT DATA

SECTION III

CHAPTER 1

Mars Residual North Polar Cap:
Earth-Based Spectroscopic Confirmation of Water Ice
As a Major Constituent and Evidence for
Hydrated Minerals

This chapter has been submitted for publication to the Journal of Geophysical Research. Authors: R.N. Clark, and T.B. McCord.

ABSTRACT

A new reflectance spectrum of the martian north polar cap is analyzed and it shows water ice absorption features. This evidence confirms the result of the Viking IRTM and MAWD experiments which indicate that the north residual polar cap of Mars is composed of water ice during the season observed (northern hemisphere spring, $L_s = 50°$). The spectra presented here show that other materials are probably present as well. These other materials may be hydrated minerals as indicated by weak absorptions in the spectrum at 1.9, 2.3 and possibly 1.4μm, but the materials seem to be otherwise spectrally bland.

INTRODUCTION

The composition of the Martian polar caps has been the subject of intenstive study and controversy for many years. The composition of the caps was speculated in the first half of this century to be either H_2O or CO_2 ice. Spectroscopic or other quantitative compositional evidence has proven elusive until recent times. This was due to the small apparent size of the caps, which makes them intrinsically difficult to observe from Earth, and to the lack of instrumentation.

Early, low spectral resolution ($\sim$10%) observations were said to indicate that the caps are composed of water ice (Kuiper, 1952; Moroz, 1964). More recently, Herr and Pimentel (1969) tentatively identified CO_2 in the south polar cap from the Mariner 7 infrared spectrometer experiment. Larson and Fink (1972) positively identified CO_2 in the south cap from 11 narrow absorption features using earthbased Fourier spectroscopy. The temperature measurements of the Viking Infrared Thermal Mapper (IRTM), as discussed by Kieffer et al. (1976) indicate that the composition of the north residual polar cap is water and not CO_2.

This result is strengthened by the Viking MAWD (Mars Atmospheric Water Detector) experiment which detected large amounts of water in the atmosphere over the polar cap (Farmer et al., 1976; Farmer and Doms, 1979). The albedo of the polar cap is lower than expected for pure water frost and indicates some other matieral is present (Kieffer et al., 1976). This raises the question of what the composition of the material is and could it make up substantial part of the bright cap material (e.g. hydrated salts or clays rather than pure water ice)?

We present here new earthbased reflectance spectra of the north polar cap which indicate the composition is at least mostly water ice plus another component with a "gray" reflectance. The other minerals in the ice cap appear to be hydrated.

OBSERVATIONS

The Mars north polar cap reflectance spectrum analyzed here was first presented in McCord et al. (1980a), where the reader is referred for details on the data acquisition and reduction. Briefly, the data were obtained with a cooled circular variable filter (CVF) spectrometer on February 20, 1978 from 0611 to 0622 UT using the University of Hawaii 2.2-m telescope on Mauna Kea. The CVF scans spectrum from 0.65 to 2.5μm every 10 seconds with 1½% spectral resolution, yielding 120 separate spectral channels. Successive scans were coadded and then written onto magnetic tape after 10 scans (100 seconds), which we call a run. Background radiation from the sky and instrument was subtracted using a mirrored chopper rotating at 24 Hz. The circular aperture was located in a cooled mirror mounted at 45° to the optical axis at the telescope cassegrain focus. The location of the aperture appeared as a black spot when the observer viewed the field reflected by the mirrored aperture plate. A beam splitter in the viewing optics allowed photographs of the field and the aperture position to be made while the observer was positioning and guiding the aperture on the planet. The aperture location

during each of the observation runs was determined from the photographs.

The spectral reflectance calculated from the measurements of the standard star Beta Gemini and Mars according to the equation

$$R_m \propto \frac{I_{Mars}}{I_{\beta\ Gem}} \times \frac{I_{\beta\ Gem}}{I_{Apollo\ 16\ site}} \times R_{Apollo\ 16}$$

$$\propto \frac{I_{Mars}}{I_{\beta\ Gem}} \times \frac{I_{\beta\ Gem}}{I_{Sun}}$$

$$\propto \frac{I_{Mars}}{I_{Sun}} ,$$

where R_m is the reflectance of Mars, $R_{Apollo\ 16}$ samples the reflectance of returned lunar soil samples, and I_{Mars}, $I_{\beta\ Gem}$, $I_{Apollo\ 16}$, and I_{Sun} are the intensities of the respective object measured at the same air mass using an extinction analysis (McCord and Clark, 1979). The Beta Gemini/Sun ratio was measured on previous observing runs using the Apollo 16 lunar landing site and returned lunar samples as intermediate standards (McCord et al., 1978, 1980a, b).

ANALYSIS

The aperture often contained both the north polar cap and adjacent regions during the measurement because of telescope positioning errors. Therefore, it was necessary to remove the contribution from the adjacent regions. The extent and location of the contaminating adjacent region was determined from photographs made during observations. The mean aperture location as drived from six photographs using an inverse orthographic projection program is shown in Figure 1. From these photographs and those obtained from the Lowell Observatory Planetary Patrol Program (using the 61-cm telescope on Mauna Kea) at nearly the same time as the spectra, the southern limit of the north polar cap was determined to be approximately 60° N latitude and the subpolar region was seen to be a dark or low albedo area. Further, from these photographs, no polar hood or noticeable clouds or haze were evident in the polar or subpolar regions, nor were any expected (James et al., 1979; James, 1979; James, personal communication) since the season was spring in the northern hemisphere (the planetocentric longitude of the sun, L_s = 49°93). Using the photographs,

the relative flux contributions of the subpolar region and cap spectra were computed. It was assumed that the spectrum of the dark subpolar contaminating region was like that of other dark regions of Mars; such a spectrum was obtained from McCord et al. (1980a) (their area 78-10). The contribution of martian atmospheric CO_2 to the subpolar region spectrum was different than that of the area 78-10 spectrum (due to the difference in equivalent air mass). Following McCord et al. (1980a), the atmospheric pathlength difference was calculated and the extra CO_2 absorption was added to the area 78-10 spectrum. The area 78-10 spectrum was then scaled according to the relative flux contribution and plotted in Figure 2 below the polar region spectrum. After subtracting the subpolar region contribution, the north polar cap reflectance spectrum is obtained (Figure 3, top).

Shown superimposed on the polar cap spectrum (Figure 3) is a laboratory spectrum of a medium grain-sized H_2O frost from Clark (1980a) to which a gray spectral component has been added (60% frost, 40% gray). The gray component (a spectrum of constant reflectance with wavelength) represents

a material with a lower albedo than H_2O frost and with no evident absorption bands. The fraction of gray component added to the H_2O frost spectrum was determined by the best fit obtainable with the polar cap spectrum.

H_2O-frost-plus-gray-component spectrum matches the polar cap spectrum rather well, but some deviations, especially near 2.0μm, are evident. The contribution of the martian atmospheric CO_2 to the polar cap spectrum was next calculated using an effective Martian air mass of 3.5, after the method of McCord et al. (1980a). This Mars atmospheric CO_2 spectrum was compared in Figure 3 (bottom) to the residual spectrum made by dividing the polar cap spectrum by the H_2O-frost-plus-gray-component spectrum. Here it is seen that many of the residual absorption features are indeed due to martian atmospheric CO_2, and that the H_2O-frost-plus-gray-component spectrum matches the polar cap spectrum very well.

DISCUSSION

This identification of water ice in the north polar cap does not alone indicate that water makes up all or even most of the bulk of the cap. Kieffer (1970) has shown that a small amount of water will mask the spectral features of CO_2. Kieffer's studies indicate that the 2.0 and 2.7μm regions are the most diagnostic for determining the presence of CO_2 in the presence of H_2O. The 2.7μm region is not covered by our spectrum and in any case it is masked by the strong martian CO_2 atmospheric fundamental band. The 2-μm region must be used but even here there is a moderately strong gaseous CO_2 absorption. Examination of Kieffer's (1970) spectra of CO_2 and H_2O frost indicate that the ratio of the H_2O frost band depths (2.0/1.5μm) is increased if CO_2 is present. However, even when the fractional weight of H_2O is $\sim$0.2 or greater, this band depth ratio is essentially that of pure water frost. The analysis in Figure 3 indicates that the H_2O ice band depth ratio for the cap is essentially the same as for the medium grained H_2O frost. Thus we see no spectral evidence in the north polar cap spectrum for CO_2 ice.

The Viking IRTM experiment showed that the north polar cap temperatures reach 200 to 210K during the summer (Kieffer et al., 1976) indicating that CO_2 ice could not have been present at that time. This temperature constraint, combined with the spectroscopic evidence for H_2O ice indicates that the north polar cap of Mars is dirty water ice, at least at the surface during northern hemisphere spring and summer.

The simulation in Figure 3 indicates that the light from the north polar cap is 60% from a medium grained H_2O frost and 40% from other components. This does not mean that the weight percent of the frost content is 60%. The actual fractional weight of H_2O in the cap surface is difficult to determine at this time since it is not known how the gray component is mixed in the cap material. However, Clark (1980b) has shown that a very small amount of mineral grains mixed with a frost can greatly reduce the reflectance of the mixture, depending on the reflectance of the mineral grains. If the contaminate mineral grains are similar to the martian dust, with reflectance values at 1μm ∿35%, the polar cap could contain 10-40 wt % of these

grains. This is a rough estimate, however, and depends on the distribution of the grains in the ice.

The residual spectrum (Figure 3, bottom) seems to show additional weak absorption features which may be due to other minerals in the cap. There are possible absorption bands at 2.3 and 1.9μm, which are typical of hydrated minerals (e.g. Hunt and Salisbury, 1979). Clark (1980b) has shown that bound water absorptions do not shift in wavelength appreciably ($\lesssim$ 100 Å) and are spectroscopically distinguishable from pure water ice. The 1.9-μm region is a difficult region in which to observe due to the strong telluric water band and the martian CO_2 band. However, this depression is seen in the wing of the CO_2 band in the spectra of all Martian areas observed (McCord et al., 1978, 1980a), even when the effect of telluric water has been over-removed. A similar absorption would be expected at 1.4μm if the 1.9-μm band exists and is due to water of hydration. Some of the bound water absorption could be due to minerals in the subpolar region. However, the absorptions could not be due entirely to subpolar region minerals because the light contributing

from that area is much smaller that the cap (Figure 2), and the observed absorptions are too deep. If the subpolar region is made of dark material similar to other dark regions on Mars, little or no bound water would be present (McCord et al. 1980a). Unfortunately, the data are not of sufficient quality in this region to precisely define the 1.4-μm band because of the combined effect of the 1.4-μm telluric water band and the low transmittance of the CVF at 1.4μm.

With the higher sensitivity instrumentation in operation now, and the more favorable oppositions in the coming years, these features can be better defined and the composition of the mineral phases present can be more accurately determined.

ACKNOWLEDGEMENTS

Some of this work was performed while the authors were in residence at the Institute for Astronomy, University of Hawaii.

This work was supported under NASA grants NSG 7323 and 7590.

REFERENCES

Clark, R.N., Water frost and ice: The near-infrared reflectance 0.65-2.5μm, J. Geophys. Res. submitted, 1980a. Thesis II Ch1

Clark, R. N., The spectral reflectance of water-mineral mixtures at low temperature, J. Geophys. Res. submitted, 1980b. Thesis II Ch2

Farmer, B. C., Davies, D.W., and La Porte, D.D., Mars: Northern summer ice cap-Water vapor observations from Viking 2, Science 194, 1339-1341, 1976.

Farmer, C.B., and Doms, P.E., Global seasonal variation of water vapor on Mars and the implications for permafrost, J. Geophys. Res. 84, 2881-2888, 1979.

Herr, K.C. and Pimentel, G.C., Infrared absorptions near three microns recorded over the polar cap of Mars, Science 166, 496-499, 1969.

Hunt, G.R., and Salisbury, J.W., Visible and near-infrared spectra of minerals and rocks. I: Silicate minerals, Mod. Geol. 1, 283-300, 1970.

James, P.B., Briggs, G., Barnes, J., and Spruck, A., Seasonal recession of Mars' south polar cap as seen by Viking, J. Geophys. Res. 84, 2889-2992, 1979.

James, P.B., Seasonal behavior of Martian polar caps, Second International Colloquium on Mars, 44, 1979.

Kieffer, H., Spectral reflectance of CO_2-H_2O frosts, J. Geophys. Res. 75, 501-509, 1970.

Kieffer, H.H., Chase, S.C. Jr., Martin, T. Z., Miner, E.D., and Palluconi, F.D., Martian north polar summer temperatures: Dirty water ice. Science 194, 1341-1344, 1976.

Kuiper, G. P., Planetary atmospheres and their origin, The atmospheres of the earth and planets, ed. G. P. Kuiper, Univ. of Chicago, pp. 306-405, 1952.

Larson, H.P. and Fink, U., Identification of carbon dioxide frost on the martian polar caps, Astrophys. J. Lett. 171, 91-95, 1972.

McCord, T.B., and Clark, R.N., Atmospheric extinction 0.65-2.50μm above Mauna Kea, Pub. Astron. Soc. Pac. 91, 571-576, 1979. Thesis App B

McCord, T. B., Clark, R. N., and Huguenin, R.L., Mars: Near-infrared spectral reflectance and compositional implication. J. Geophys. Res. 83, 5433-5441, 1978.

McCord, T.B., Clark, R.N., McFadden,L.A., Pieters, C.M., Owensby, P.D., and Adams, J.B., Moon: Near infrared spectral reflectance, a first

good look, J. Geophys. Res. to be submitted, 1980b.

McCord, T.B., Clark, R.N., Singer, R.B., and Huguenin, R.L., Mars: Near-infrared reflectance spectra of surface regions and compositional implication, J. Geophys. Res., to be submitted, 1980a.

Thesis
I Ch 3

FIGURE CAPTIONS

Figure 1 The mean aperture location is shown for the polar region spectrum shown in Figure 2. The polar cap limit was at 60° north latitude.

Figure 2 The reflectance spectrum of the north polar regions of Mars (top) from McCord et al. (1980a) shows broad absorption features due to water ice (at 1.5 and 2μm) and CO_2 gas (at 2μm). The assumed subpolar region spectrum (bottom) from Mccord et al. (1980a) is scaled relative to the polar region spectrum to indicate the fractional light received in the portion of the aperture not on the polar cap. These spectra are reduced to reflectance and thus have the earth's atmospheric absorptions and solar radiance removed. The error bars are ±1 standard deviation of the mean for 6 runs.

Figure 3 Top: The reflectance of the north polar cap (points) was derived by subtracting the subpolar region spectrum from the polar region spectrum in Figure 2. The

superimposed simulation spectrum (line) indicates the light from the polar cap is consistent with assuming 60% of the light from water frost and 40% from a gray material (using an additive model).

Bottom: The residual spectrum (points) indicates most of the residual features are consistent with the expected CO_2 atmospheric transmittance (line).

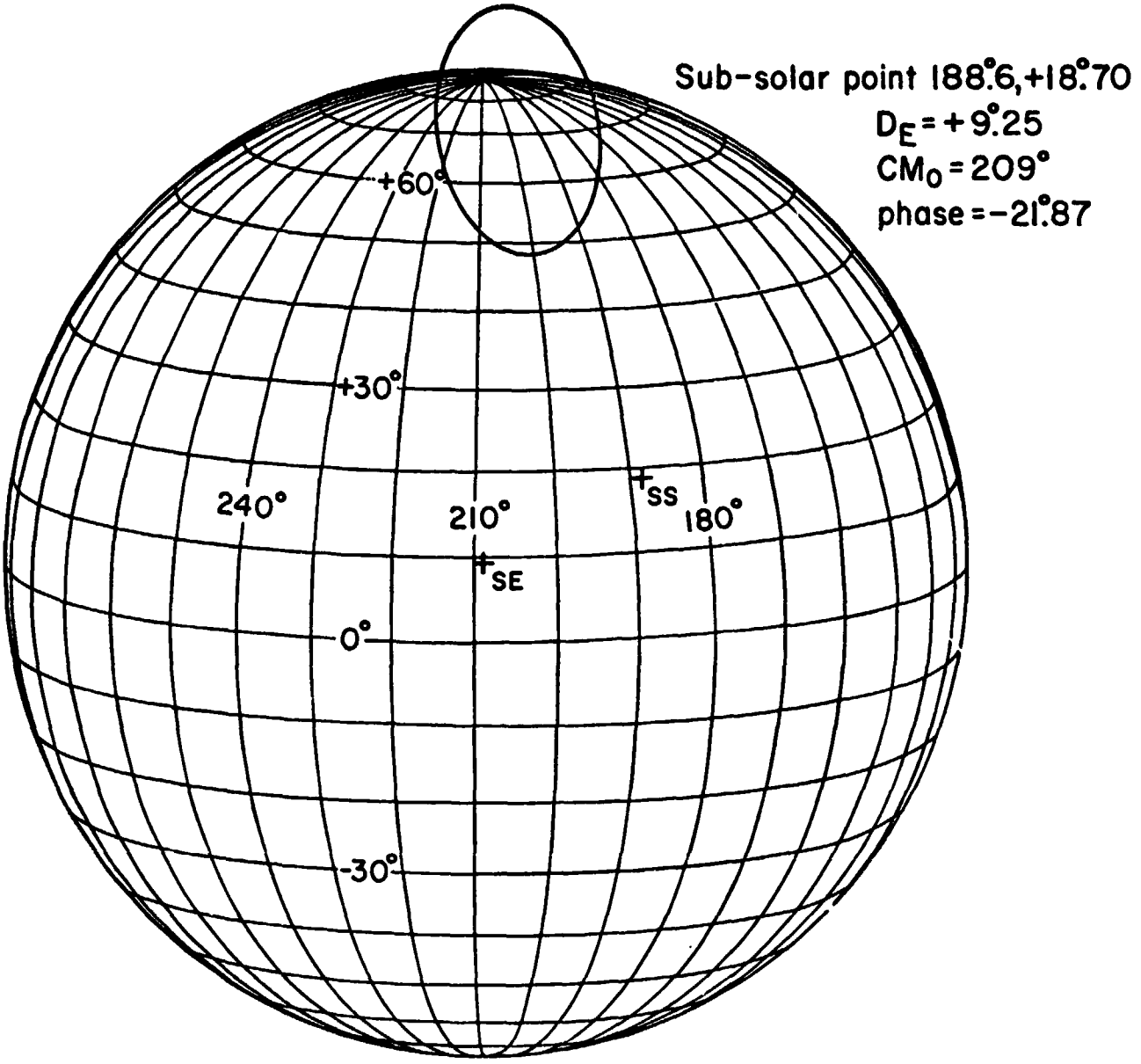

Sub-solar point 188°.6, +18°.70
D_E = +9°.25
CM_0 = 209°
phase = −21°.87
+60°
+30°
240°
210°
+SS
180°
+SE
0°
-30°
Mars Feb 20, 1978 6:18 UT

Figure 1

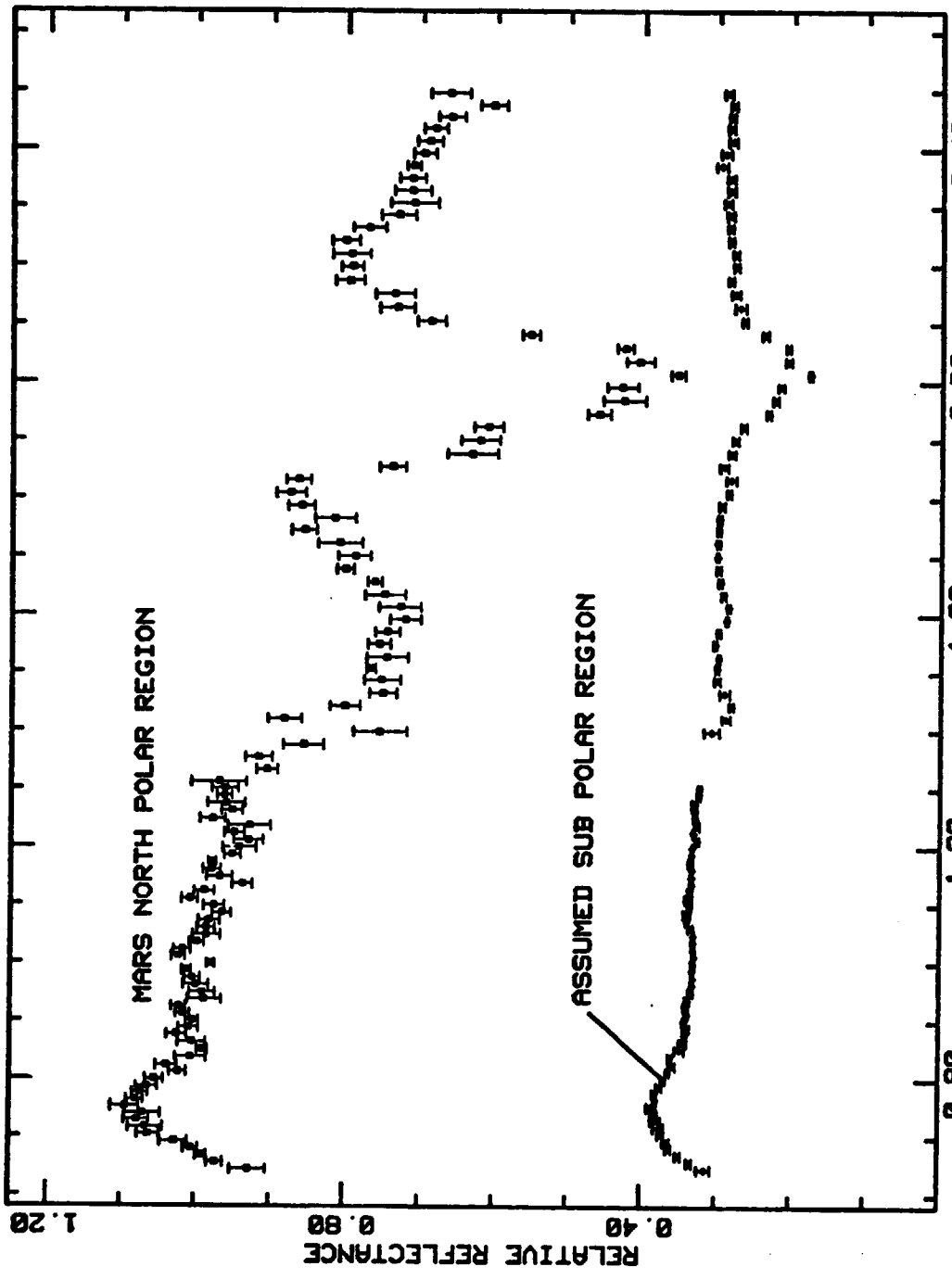

MARS NORTH POLAR REGION
ASSUMED SUB POLAR REGION
RELATIVE REFLECTANCE
0.40
0.80
1.20
0.80
1.20
1.60
2.00
2.40
WAVELENGTH IN MICRONS

Figure 2

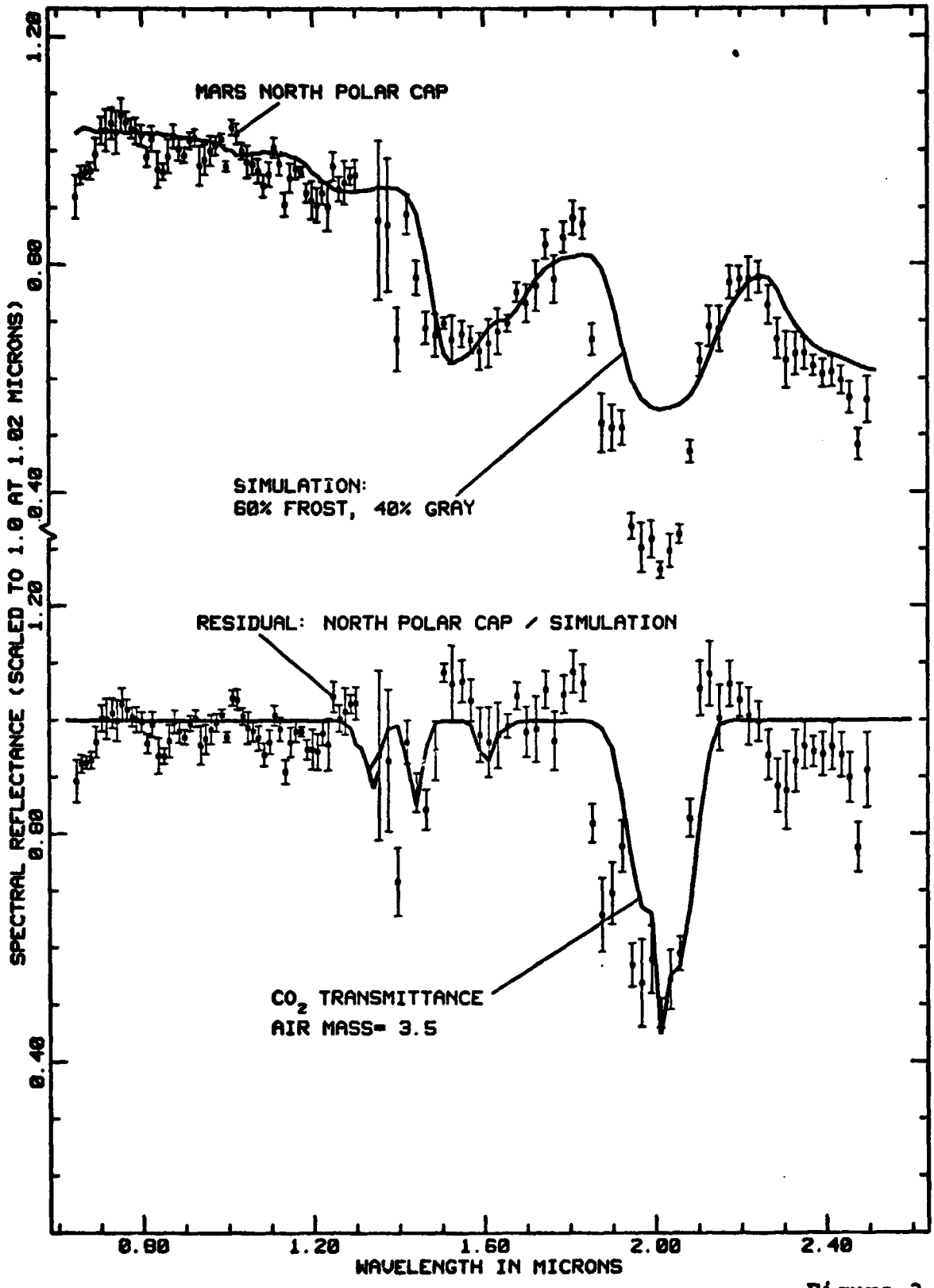

MARS NORTH POLAR CAP
SIMULATION:
60% FROST, 40% GRAY
RESIDUAL: NORTH POLAR CAP / SIMULATION
CO_2 TRANSMITTANCE
AIR MASS= 3.5
SPECTRAL REFLECTANCE (SCALED TO 1.0 AT 1.02 MICRONS)
1.20
0.80
0.40
1.20
0.80
0.40
0.80
1.20
1.60
2.00
2.40
WAVELENGTH IN MICRONS

Figure 3

SECTION III

CHAPTER 2

Ganymede, Europa, Callisto and Saturn's Rings: Compositional Analysis from Reflectance Spectroscopy

This chapter has been submitted for publication to the journal Icarus. Author: R.N. Clark.

ABSTRACT

The reflectance spectra of Ganymede, Europa, Callisto and Saturn's rings are analyzed using recent laboratory reflectance studies of water frost, water ice, and water and mineral mixtures. It is found that the spectra of the icy Galilean satellites are characteristic of water ice (e.g. blocks) or frost on ice rather than pure water frost, and that the decrease in reflectance at visible wavelengths is caused by other mineral grains in the surface. The spectra of Saturn's rings are more characteristic of water frost with some other mineral grains mixed in the frost but not on the surface. The impurities on all these objects are not in spectrally isolated patches but intimately mixed with the water. The impurity grains appear to have reflectance spectra typical of minerals containing Fe^{3+}. Some carbonaceous chondrite meteorite spectra show the necessary spectral shape. Ganymede is found to have more water ice on the surface than previously thought (~90%), as is Callisto (30 - 60%). The surface of Europa has a vast frozen water surface with only a few percent impurities. Saturn's rings also have only a few percent impurities. A new absorption

feature is identified in Ganymede, Callisto, and probably Europa at 1.15μm which is also seen in the spectra of Io but not in Saturn's rings. This feature has not been seen in laboratory studies and its cause is unknown.

INTRODUCTION

Water ice has been identified on the surfaces of Ganymede, Europa, Callisto and in Saturn's rings (e.g. Pilcher et al., 1970, 1972; Fink et al., 1976; Pollack et al., 1978). However, the decrease in reflectivity from the visible to the ultraviolet indicates something other than pure water ice is present (e.g. Lebofsky et al., 1970; Irvine and Lane, 1973; Johnson and McCord, 1971; Nelson and Hapke, 1978).

Clark and McCord (1980a, b) recently obtained high precision reflectance measurements of the Galilean satellites and Saturn's rings that are of a quality approaching that attainable in the laboratory. These papers identified several new absorption features on Europa, Ganymede, Callisto and Saturn's rings which were mostly due to water ice, however weak absorptions appear in the 0.8 to 0.9-μm region which may be due to silicates.

Lebofsky (1973) and Lebofsky and Fegley (1976) found that contaminated water frosts (e.g. NH_3+10H_2O, H_2S+10H_2O, NH_4SH+H_2O) which have been irradiated with ultraviolet light also show a decrease in reflectivity in the visible and ultraviolet. Most of these frosts have a strong

absorption around 0.6μm which is not seen in spectra of Ganymede, Europa or Callisto and may be present only weakly in spectra of Saturn's rings in the wing of a much stronger absorption at visible wavelengths. Their irradiated H_2S+10H_2O frost spectrum matches reasonably well in the visible with Saturn's rings and Ganymede. However, their H_2S+10H_2O and NH_4HS+H_2O spectra show a very sharp decrease in reflectance beyond about 0.9μm, which is inconsistent with spectra of Saturn's rings or the Galilean satellites. The irraded frost spectra also show a reflectance near unity at 0.7μm which is too high for Ganymede and Callisto.

The bulk densities of Europa, Ganymede and Callisto are 3.03, 1.93, and 1.79 g/cm^3 respectively (Smith et al., 1979) which indicate some "rocky" material is present. It is reasonable to assume that some of this material is present on the surfaces especially considering the low visual albedoes of Callisto and Ganymede. The low albedo surface material could also be due to particles falling on the surfaces after the bodies were formed.

Clark (1980a, b) has performed laboratory spectral reflectance measurements of water and

water-mineral mixtures at the low temperatures typical of those found on the Galilean satellites and Saturn's rings. These papers and the spectra of the Galilean satellites and Saturn's rings (Clark and McCord 1980a, b) form most of the background for the more detailed analysis presented here.

BACKGROUND

This section summarizes some of the important results of the laboratory studies of Clark (1980a, b) and addresses some of the questions relevant to the interpretation of the reflectance spectra of Ganymede, Europa, Callisto, Saturn's rings, and other icy objects.

The reflectance of water frost at several grain sizes is shown in Figure 1. When a detailed comparison is made between a telescopic spectrum and a typical frost spectrum measured in the laboratory, it soon becomes apparent that the relative absorption band depths do not agree. For example, if the 1.5-μm absorption feature in the laboratory spectrum fits that in the telescopic spectrum, the depths of the features at 2.0 and 1.25μm are usually different and do not match well. The difference in the relative band depths varies from object to object. For example, the ratio of the 1.25 to the 1.5-μm absorption features is greater for typical frost spectra than for spectra of Ganymede, Europa and Callisto, while it is less for spectra of Saturn's rings. This will be analyzed in the next section. Clark (1980a) showed that a thin layer of frost on a thick ice

block can greatly change relative band depths seen in the reflectance spectra. This scattering condition tends to increase the depths of the higher overtone absorptions relative to those at longer wavelengths.

Laboratory reflection spectra of frozen water- mineral mixtures, mineral grains on frost and frost on minerals tend to show a decrease in the higher overtone ice absorptions relative to low overtone absorptions which occur at longer wavelengths (Clark, 1980b). Clark (1980b) showed that bound water bands which typically occur at 1.4 and 1.9μm do not shift appreciably with temperature and can be distinguished from the free water ice bands at 1.5 and 2.0μm even when large amounts of ice are present. These laboratory studies also show that a decrease in reflectivity in the visible can be explained by water ice-mineral mixtures, mineral grains on frost, or frost grains on a mineral if the mineral also shows a decrease in reflectivity in the visible. This is due to the relative transparency of water ice at visible wavelengths. The shape of the decrease is not completely understood (e.g. slope) when water is present in the sample. The apparent decrease is dependent on the amount and

location of the water in the sample and the frost on or around the mineral grains. The shape of the decrease is a nonlinear combination of the individual component spectra since the scattering conditions are usually wavelength dependent. The wavelengths at which there is a relatively abrupt change in the reflectance slope (e.g. a charge transfer edge) will also show in water-mineral mixture spectra, as will any mineral absorptions where the ice is relatively transparent (e.g. shortward of 1.4μm). This is well seen in Figure 2 which the 0.9-μm absorption and the beginning of the visible downturn at 0.8μm even when the red cinder grains are covered by a fine grained frost about 0.6mm thick.

ANALYSIS

The reflectance spectra of the Galilean satellites and Saturn's rings from Clark and McCord (1980a, b) are shown in Figures 3 and 4. The first step of the analysis is to remove a continuum from each spectrum by a method similar to that used by Clark (1980a). The continuum removed spectra provide a clearer display of the relative band depths of the water ice overtone absorptions. The continuum used is a cubic spline as described by Clark (1980c) and fitted to the relative peaks in the reflectance spectra between the absorption features. An example of such a fit is displayed in Figure 5. The results of the cubic spline continuum removal from the telescopic spectra are shown in Figures 6 and 7 compared with laboratory spectra with their continua removed. First, the continuum removed spectra will be discussed then the object-by-object analysis will be presented.

The medium grained frost, as compared with Saturn's rings in Figure 6, shows a very good match to the 1.5- and 2.0-μm absorptions. The 1.65-μm absorption feature is different due partially to a difference in temperature between

the rings and the laboratory sample (∿ 90K versus 112 K). The band depths of the 1.25- and 1.03-μm absorptions are smaller in Saturn's rings than in the medium grained frost spectrum.

The frost on ice spectrum as compared with Ganymede in Figure 6 shows more variation in the relative band depths. The ratios of the band depths of the higher overtone to the lower overtone absorptions are greater for the frost on ice spectrum than for the medium grained frost. The 2.0-μm band depth is less in the Ganymede spectrum as compared to the frost on ice spectrum, while the 1.5-μm and 1.25-μm absorptions are greater. The 1.03-μm absorption is the same in both spectra.

The comparison of the Europa trailing side spectrum with those of medium and fine grained frosts is shown in Figure 7. The 1.5-μm band in Europa appears to be intermediate between the medium and fine grained frosts. The 2.0-μm absorption in Europa is quite asymmetric, while frost and frost on ice spectra show symmetric bands. The higher overtones at 1.25 and 1.03μm are stronger in Europa than the frost spectra indicating a different grain size distribution, such as a frost on ice.

The spectrum of Callisto in Figure 7 shows a very strong absorption at 1.2μm relative to the water ice absorption at 1.5μm. The ratio of the band depths of the 1.5- and 2.0-μm absorptions is greater than unity which is something not seen in laboratory spectra of pure water frost but is seen in frost on ice spectra (Figure 7). The 1.2-μm absorption in Callisto is different than that seen in frost or frost on ice spectra because it is broader and occurs at a shorter wavelength. The peak between the 1.03- and 1.25-μm pure water ice and frost absorptions occurs at 1.13μm where there is significant absorption in the spectrum of Callisto. This is also seen in spectra of Europa and Ganymede but not Saturn's rings. This may indicate an absorption due to some other component in the surfaces of these objects.

The continuum in a reflectance spectrum is also very important since the presence of other minerals with water ice can change the apparent continuum shape (see Clark, 1980b, and Figure 2). In an effort to determine what other components might be contributing to the spectra, more detailed comparisons with the laboratory spectra are made below. Previous investigators have typically

measured the approximate band depths of the 1.5- or 2.0-μm water frost features and computed the fractional areal coverage of water frost based on a typical laboratory spectrum. However, it has been shown that this is not accurate since the band depths vary depending on the grain sizes and distribution of the water. Comparing the depths of many overtones gives a greater constraint on the grain size distribution and shape of the continuum of uncontaminated water. This then helps to determine the possible shape of the spectrum of any contaminates.

GANYMEDE

We first compare the spectrum of Ganymede with a frost on ice spectrum as seen in Figure 8. Except for small differences in the relative band depths in the frost on ice spectrum, the match to Ganymede is excellent. It is important to note that the short wavelength side of the 1.5-μm water absorption matches that for Ganymede. This indicates that there is no detectable bound water on Ganymede since bound water and hydroxyl bands typically occur at 1.4μm and would cause a noticeable deviation from the pure water spectrum. A

slightly more sensitive spectral region for hydroxyl bands occurs near 2.2μm where there is a slight depression in the Ganymede spectrum in the wing of the 2.0-μm water ice band. However, this small depression is well within the uncertainty in the data and the only conclusion that can be drawn is to place an upper limit of ∿5% areal coverage of a mineral similar to montmorillonite. This is based on the laboratory studies of Clark (1980b). The absolute reflectance levels are not very diagnostic in that a few particles scattered in a frost layer can drastically lower the reflectance with only a small effect on the relative water ice band depths (Clark 1980b). The frost on ice spectrum which is scaled to Ganymede has a reflectance of slightly greater than 80% at 0.8μm. If the surface had a few percent areal coverage of other mineral grains, the overall reflectance could be decreased to that seen on Ganymede. However, the water ice band depth would decrease an amount equal to the fractional areal coverage (Clark 1980b). In addition, the absorption seen in Ganymede near 0.8 - 0.85μm is similar to Fe^{3+} absorption in minerals (e.g. Hunt and Salisbury, 1970; Hunt et al., 1971). The reflectance of Ganymede in the 3-μm region is very low (≤3%)

but not zero, (Pollack et al., 1978) confirmining the conclusion above that some non-H_2O mineral grains are exposed on the surface. However, most of the mineral grains are probably covered by the ice and frost.

If we divide the Ganymede spectrum by the frost on ice spectrum, and include the visible wavelengths (the frost on ice spectrum is white in the visible), we obtain the spectrum in Figure 9. The peak at 2 μm is caused by the slightly different band depths in the spectra in Figure 8. The important features are the downturn in the visible, the 0.8-μm absorption and the 1.2-μm absorption. The 0.8-μm absorption may be slightly accentuated from the slightly concave nature of the frost on ice spectrum. The long wavelength side of the 1.15-μm feature may be affected due to a difference in the band depth of the 1.25-μm frost on ice absorption. There appears to be an absorption in Ganymede at 1.15 μm. All the Galilean satellites seem to have an absorption here but not Saturn's rings. When a near-infrared spectrum of Io is compared to the Ganymede spectrum from Figure 9, the result is a striking match as seen in Figure 10. Thus, Ganymede and

Io may have similar compositions of some surface components. Sulfur dioxide frost has been identified on the surface of Io (e.g. Fanale et al., 1979) and elemental sulfur is almost as certain (e.g. Nash and Fanale, 1977). No spectra were found which show an absorption similar to this feature at 1.15μm. The published reflectance spectra of SO_2 frost are of such a small grain size (Fanale et al., 1979; Smythe et al., 1979) that the presence of a 1.5-μm absorption is uncertain. Ganymede does not have a 4.08-μm absorption as does Io (which is due to SO_2 frost-e.g. Fanale et al., 1979) (D. Cruikshank-1979, private communication). This still does not rule out SO_2 frost since water ice absorption is very strong in the 4-μm region and may suppress absorptions from other minerals.

Saturn's Rings

We next compare the spectrum of Saturn's rings with that of a medium grained frost in Figure 11. The 1.5- and 2.0-μm absorptions agree reasonably well but the frost has a reflectance which is too high shortward of 1.4μm. This is not a problem because the addition of a mineral to the

frost could easily decrease the reflectance in this region. The short wavelength sides of the 1.5 and 2.0-μm frost bands agree with those of Saturn's rings indicating there is no detectable bound water in the rings. The shape of the 2.0-μm absorption in Saturn's rings is slightly different than for the frost. No explanation can be given for this discrepancy yet as it has not been seen in the laboratory.

If we divide Saturn's rings spectrum by the frost spectrum, and include the visible wavelengths (the frost is white in the visible) we obtain an estimate of the non-frost component spectral shape as seen in Figure 12. However, we must be careful in interpreting the features in the ratio spectrum. The variations beyond 1.4μm are due to differences in the band shapes. There appears to be a shallow absorption just beyond 1.1μm. However, from Figure 6 we saw that the 1.25-μm frost band was stronger than the corresponding absorption in Saturn's rings. Thus the ratio spectrum shows a rise at 1.25μm. This rise, along with the similar affects of the 1.03-μm frost band cause the apparent 1.12-μm absorption. The important features to note are the visible

downturn, the absorption at 0.85μm and at 0.6μm. The 0.6-μm weak absorption appears to be real, however, the shape may be affected slightly in the way the visible and infrared data are matched (see Clark and McCord, 1980b). The ratio spectrum appears very much like spectra of materials containing ferric oxide. All of the above features are seen to varying degrees in some mineral spectra and are attributed to Fe^{3+}. The shape of the visible downturn cannot be compared directly to other spectra without taking into account the modifying effects of the water. Since the higher overtone absorptions are weaker than those at longer wavelengths on Saturn's rings as compared to the water frost, the impurity grains must be distributed within the "fairycastle" structure of the frost or be completely covered by the frost. (see Clark 1980a, b). The latter could be a frost layer on the impurity grains or the impurity could be embedded in the frost grains.

The reflectance of the rings is near zero around 3μm (Puetter and Russell, 1977) indicating that any impurity grains must be covered by water as noted above. Beyond 3.4μm, the reflectance rises to a peak at 3.6μm which may be higher than expected for a pure frost-indicating further that

some impurities exist. There are some small differences in the water absorption band shapes between the laboratory spectra and the spectra of Ganymede and Saturn's rings. The laboratory spectra were obtained at normal incidence with a phase angle of 10° (Clark 1980a, b). The telescopic spectra are of the integral disc (of the satellites or ring particles) and at phase angles less than 10°. Glasser (1979) has shown that the absorption band depths are different for the frost Geometric albedo spectrum than the reflectance spectrum. The effects are smaller than that seen for frost on ice as compared to frost spectra but could explain some of the observed differences in band shape. A more detailed study of frost spectral albedoes needs to be performed and included in future analyses.

Europa

The spectrum of Europa (trailing side, Figure 3) is the most unusual of the four objects described here. The 1.5- and 2.0-μm absorptions are very asymmetric compared to those for water frost. The higher overtones at 1.03 and 1.25μm

appear similar in shape and depth to those on Ganymede. Figure 13 shows the Europa spectrum compared with a water ice spectrum. The ice spectrum is from Clark (1980a) and has almost no frost on the surface of an ice block. The 1.5-μm absorption appears very asymmetric and similar to Eruopa. The short wavelength edge of the absorption (1.4 - 1.5μm) matches very well and indicates there is no detectable bound water. The 2.0-μm absorption of the Europa spectrum is also very asymmetric whereas the absorption in the water ice spectrum is more symmetric. None of the water ice, frost, and frost on ice spectra measured by Clark (1980a) show a 2.0-μm absorption that is as asymmetric as that seen on Europa. There are indications that a mixture of water ice and other minerals might cause such an asymmetry (Clark, 1980b) however, to fully understand this, more laboratory work needs to be performed. Although the water ice spectrum matches Europa in the 1.6-μm region, the relative reflectance is too high shortward of 1.2μm. The addition of other minerals could easily lower the reflectance and account for the visible downturn, however, the reflectance of Europa and the water ice spectrum

are similar at 1.0μm. Thus, what is needed to obtain a good match to the Europa spectrum is to raise the reflectance of the water ice spectrum at wavelengths beyond 1μm relative to that at 1μm. This is also readily done with the addition of another mineral component if the mineral reflectance is greater than that of the water beyond about 1.2μm (see Clark, 1980b Figure 13).

The spectrum of Europa has a weak absorption at about 0.87μm which may be due to an iron oxide. Europa has the weakest absorption in this spectral region of the four objects discussed here. This is to be expected, however, since Europa has the strongest water absorptions and thus the water can be the most effective in masking absorptions in this region as compared to the other objects discussed. Europa also has the smallest downturn in the visible, consistent with the weakest 0.8-μm absorption.

A concern with telescopic spectra is the residual calibration errors which may be present. Since the moon was used as a calibration standard (e.g. the Apollo 16 landing site and returned lunar samples; see McCord et al. 1980), there is the possibility of residual absorptions from the

moon contaminating the spectra. Lunar absorptions occur at longer wavelengths (0.9 - 1.0μm) and investigations of possible calibration errors revealed that any residual absorptions would be broader than the features seen here and not more than about 1.5% in depth (R. Clark and P. Owensby-unpublished). This indicates that at least some of the 0.87-μm absorption in Europa is real, and that the 0.8 to 0.9-μm absorptions in Ganymede, Saturn's rings, and Callisto are even more certain.

Europa may have an absorption at 1.15μm similar to that for Ganymede. The 1.25μm absorption on Europa is similar to that on Ganymede. The absorption in this region starts at about 1.1μm but the peak between the water ice absorptions is at a longer wavelength. Also the water ice spectrum is convex at 1.15μm whereas the Europa spectrum is much flatter. None of the spectra of Clark (1980a, b) show such an absorption shape indicating an impurity is probably absorbing in this region. The spectral features in Europa are so unusual however, that we cannot be certain of a 1.15-μm absorption.

Although we do not have an overall good match of a laboratory spectrum to the Europa spectrum,

from the discussion above we conclude that the material on Europa that is not water ice has similar spectral characteristics to that on Ganymede. There is more water on the surface of Europa than on Ganymede and the contaminating minerals are probably embedded in the ice since Europa reflects almost no light in the 3- to 5-μm region (Pollack et al. 1978).

Callisto

Callisto displays much weaker water ice absorption features than the other three objects discussed so far. Figure 14 shows the Callisto spectrum compared with two simulations. Simulation A is the medium grained frost spectrum (T = 114 K) from Figure 1 with a constant of 2.0 added to each data point and rescaled to Callisto at 1.7μm. Simulation B is the spectrum of Europa also with a constant of 2.0 added and then rescaled to match at 1.7μm. If the water ice absorptions are due to patches of ice largely separate from the other darker materials, the simulations would represent a 30% areal coverage of water ice.

Based on separate patches of 30% ice and 70% other material, one would expect the 3μm water

absorption to be only 1.5 times as deep as the 1.5- and 2.0-μm ice band depths (e.g. see Clark and McCord, 1980a; Pollack et al., 1978). However, the 3-μm absorption is more than 4 times deeper than the 1.5- and 2.0-μm absorptions. This indicates that some water is present with the dark material on Callisto. Pollack et. al. (1978) concluded from this that the water must be bound to the dark material. However, Pimentel et. al. (1974) showed that a water ice layer less than 1 micrometer thick, which is transparent in the visible will completely saturate the 3-μm region. This is what makes the 3-μm region so sensitive for remote sensing for water - the ν_1 and ν_3 fundamentals occur here. Since the 3-μm region is so easily saturated, it is difficult to use it for determining the details of the H_2O occurrence. For instance, a regolith could contain 15 weight % bound water with a 1 micrometer ice sheet at the surface. A spectrum of the surface would show the ice absorption and totally mask the bound water underneath at 3μm. In contrast, the 1.5- and 2.0-μm ice absorptions are not as absorbing and the bound water bands would be easily seen (see Clark 1979b). However, the 1.5- and 2.0-μm regions

have limitations also since a small amount of opaque material mixed with the mineral containing water will tend to suppress the water bands (see Gaffey, 1976; Johnson and Fanale, 1973; Clark 1980b). Since the bound water bands tend to occur at shorter wavelengths than ice, the 3-μm region might be used much like the 1.5- and 2.0-μm regions as shown by Clark (1980b). However, if much free water ice exists in or on the sample, the 3-μm region may become very saturated with the apparent wing of the absorption moving shortward and again masking any bound water bands.

The simulations in Figure 14 show that the water ice absorptions at 1.5 and 2.0μm are intermediate in shape between a medium grained frost and that of Europa. In addition, Callisto's higher overtone water ice absorptions are deeper than those at longer wavelengths relative to water frost (see Figure 7). This indicates that a frost on ice spectrum is representative of the water component on the surface of Callisto. However, the strong downturn in the visible and the asymmetric ice bands indicate that some of the dark material is mixed with the water ice. The frost on ice spectrum which would account for the water ice band depths decreases too steeply toward

longer wavelengths. Thus an additional material is necessary in the frost on ice to flatten the spectrum (as was discussed with Europa). Many of the mineral grains are probably completely surrounded by water, at least partially, if not fully, accounting for the strong 3μm band. There is no indication of bound water in the Callisto spectrum. There is one data point which is low at 2.2μm where OH absorptions occur but they are usually wider than this. The one low data point may only be noise in the data.

The absorption at 1.15μm shows easily when compared to simulation B. This has the same position, shape, and depth as the absorption in Io and Ganymede (see Figure 10). The 0.9-μm absorption in Callisto is very similar to that on Io and Europa, but it is longward of that seen in the spectrum of Ganymede and Saturn's rings. Thus the dark material on Callisto looks similar to that on Ganymede except the 0.9-μm absorption is at a slightly longer wavelength.

DISCUSSION

The spectral reflectance of the non-water component on Ganymede, Europa, Callisto, and Saturn's rings are similar but there are some differences in composition. All show a decrease in reflectivity in the visible and an absorption in the 0.8- to 0.9-μm region. Many mineral reflectance spectra show such characteristics. The details of visible near-infrared spectral reflectance vary with Fe^{3+} content, crystal structure, and hydration state. An example is the palagonite spectrum shown in Figure 15. Many carbonaceous chondritic meteorites show reflectance spectra similar to the non-water component spectra on the icy Galilean satellites and Saturn's rings (see Gaffy, 1976). There is very little bound water detected in the other solar system objects discussed here. The surface of Ganymede is probably about 90% free water ice and frost, Europa even greater (95 to almost 100%), Callisto a minimum of 30% and probably closer to 60%, and Saturn's rings are probably greater than 90% water ice. The telescopic data puts limits of bound water at around $5 \pm 5\%$ for these objects. This was derived using the studies of Clark (1980b).

The uncertainty is due mostly in calibrating the earth's atmospheric water absorptions which occur in the same wavelength region. With so much water present on these objects, one might expect some to be bound to the minerals. The above limit is consistent with some of the non-water component being carbonaceous chondritic in composition. Consolmagno and Lewis (1976) explained the observed densities and apparent water on the surfaces of Europa, Ganymede, and Callisto by primordial accretion of material and differentiation of Europa and Ganymede but not Callisto. In addition, they note that some dust such as carbonaceous chondritic material could coat the surfaces of the satellites as described by Johnson and Fanale (1973). Their model employed the Poynting Robertson effect to cause small dark particles to spiral inward toward Jupiter where they would first encounter Callisto, then Ganymede and Europa. Pollack et. al. (1978) proposed a similar mechanism with the particles originating from the outer satellites of Jupiter. Although it appears that water ice in conjunction with other minerals can explain the observed features in the icy Galilean satellites and Saturn's rings, radiation

damage may still play a role considering the radiation environments within which these objects lie. However, little is known on the spectral effects of radiation on water-silicate mixtures. The UV-irradiation work of Lebofsky (1973) and Lebofsky and Fegley (1976) did not extend beyond 1.1μm. The proton irradiation work of Nash and Fanale (1977) show that changes occur to some materials but the materials they studied are not applicable to the icy satellites.

The recent images from the Voyager spacecraft tend to indicate that meteorite debris is slowly covering the surfaces of at least Ganymede and Callisto (Smith et. al. 1979). Both satellies show bright rayed craters and darker craters which are apparently slowly being covered by debris. The UV radition studies of Lebofsky and Fegley showed that darkening of their impure ices occurred on time scales of days to months. Radiation damage is unlikely to cause all the darkening since the bright multi-ring structures are ∿4 billion years old (Smith et. al., 1979). The bright rayed craters are probably at least hundreds of millions of years old if they occurred around the same time as the lunar craters Tycho and Copernicus.

The bright rayed craters on Ganymede show that water ice exists even in the dark ancient

terrain (assuming the bright rays are due to water ice). Some rayed craters have formed on the boundaries of the grooved terrain and ancient cratered terrain (see Smith et al., 1979, Figure 19). Some of these show bright rays extending into the grooved terrain whereas no bright rays are seen extending into the dark, ancient terrain. One crater itself is half bright and half dark. This does not necessarily indicate that the dark, ancient terrian does not contain significant amounts of water. The water could be well mixed with the dark material as would be expected to occur due to gardening during the heavy bombardment stage. In addition, particles which land gently on a bright ice surface will tend to be warmer than the ice from absorbed sunlight and tend to migrate into the ice surface. Small grains which fall to the surfaces will impact at several kilometers per second, clearly penetrating into the ice. An ice-dark material surface can appear as dark or darker than the dark material alone (see Clark 1980b). Thus the dark ancient terrain on Ganymede may contain as much water near the surface as Callisto (∿60 wt %), while greater amounts of water exist below the mixed

surface. The younger grooved terrain probably contains much more water ($\gtrsim$90%) as indicated by the water ice relative band depths in the integral disc reflectance spectra. The bright rayed craters on Ganymede have visual albedoes around 0.5 (Squyers and Veverka, 1979) and indicate that if the contaminating material is dark, as on Callisto, that only trace amounts are present ($\lesssim$2%). Ganymede also shows thin polar caps (see Smith et al., 1979 Figure 12) through which surface features are visible. This is typical of a thin frost layer probably about 0.1mm thick or less (see Clark 1980b). Some frost and fine scale structure probably exists in the ice elsewhere on Ganymede, giving the overall characteristic frost on ice spectrum.

Thus the surface of Ganymede is a vast frozen ocean with more water at the surface than previously thought. Callisto also contains more water than Ganymede at the surface but has more impurities mixed with the ice than Ganymede. The surface of Europa is also a vast frozen ocean and contains less than a few percent impurities. Saturn's rings are more like frost balls, which are several centimeters in size (see Pollack, 1975; Ostro et al. 1979) with a few percent

impurities.

ACKNOWLEDGEMENTS

I would like to give a special thanks to Tom McCord for help and encouragement and for providing the computer and necessary resources to carry out this work. A portion of this work was carried out while the author was at the Institute for Astronomy, University of Hawaii. This work was supported by NASA grant NSG 7312

REFERENCES

Clark, R. N. (1980a). Water frost and ice: The near-infrared spectral reflectance 0.65-2.5μm J. Geophys. Res. submitted. Thesis II Ch1

Clark, R. N. (1980b). The spectral reflectance of water-mineral mixtures at low temperatures. J. Geophys. Res. submitted. Thesis II Ch2

Clark, R. N. (1980c). A large scale one-dimensional array processing system. Pub. Astron. Soc. Pac. submitted. Thesis App A

Clark, R. N., and McCord, T. B. (1980a). The Galilean satellites: New near-infrared spectral reflectance measurements (0.65-2.5μm) and a 0.325-5μm summary. Icarus submitted. Thesis I Ch 1

Clark, R. N., and McCord, T. B. (1980b). The rings of Saturn: New near-infrared reflectance measurements and a 0.326-4.08μm summary. Icarus submitted. Thesis I Ch 2

Consolmagno, G. J., and Lewis, J. S. (1976). Structural and thermal models of icy Galilean satellites. In Jupiter(T. Gehrels, Ed.), pp. 1035-1051. Univ. of Arizona Press, Tucson.

Fanale, F. P., Brown, R. H., Cruikshank, D. P., and Clark, R. N. (1979). Significance of absorption features in Io's infrared reflectance spectrum. Nature 30, 761-763.

Fink, U., Larson, H. P. Gautier, T. N. III, and Treffers, R. R. (1976). Infrared spectra of the satellites of Saturn: Identification of water ice on Iapetus, Rhea, Dione, and Tethys. Astrophys. J. Lett. 207, 63-67.

Gaffey, M. J. (1976). Spectral reflectance characteristics of the Meteorite Classes. J. Geophys. Res. 81, 905-920.

Glasser, F. M. (1979). A laboratory determination of the geometric albedo of water frost, 0.2μm to 2.0μm. Bull. Am. Astron. Soc. 11, 598.

Hunt, G. R., and Salisbury, J. W. (1970). Visible and near-infrared spectra of minerals and rocks: I. Silicate minerals. Mod. Geol. 1, 283-300.

Hunt, G. R., Salisbury, J. W., and Lenhoff, C. J. (1971). Visible and near-infrared spectra of minerals and rocks: III. Oxides and hydroxides. Mod. Geol. 2, 195-205.

Irvine, W. M. and Lane, A. P. (1973). Photometric properties of Saturn's rings. Icarus 18, 171-176.

Johnson, T. V., and Fanale, F. P. (1973). Optical properties of carbonaceous chondrites and their relationship to asteroids. J. Geophys. Res. 78, 8507-8518.

Johnson, T. V., and McCord, T. B. (1971). Spectral geometric albedo of the Galilean satellites, 0.3 to 2.5 microns. Astrophys. J. 169, 539-594.

Lebofsky, L. A. (1973). Chemical composition of Saturn's rings and icy satellites. Ph.D. Thesis. M.I.T. Cambridge.

Lebofsky, L. A. and Fegley, M. Jr. (1976). Labortory reflection spectra for the determination of chemical composition of icy bodies. Icarus 28, 379-387.

Lebofsky, L. A., Johnson, T. V. and McCord, T. B. (1970). Saturn's rings: Spectral reflectivity and compositional implications. Icarus 13, 226-230.

McCord, T. B., Clark, R. N., McFadden, L. A., Pieters, C. M., Owensby, P.D. and Adams, J. T. (1980). Moon: Near-infrared spectral reflectance, A first good look. J. Geophys. Res. submitted.

McFadden, L. A., Bell, J., and McCord, T. B. (1980). Visible spectral reflectance measurements 0.3-1.1μm of the Galilean satellites at many orbital phase angles 1977-1978. Icarus to be submitted.

Nash, D. B., and Fanale, F. P. (1977). Io's surface composition based on reflectance

spectra of sulfur/salt mixtures and proton-irradiation experiments. Icarus 31, 40-80.

Nelson, R. M., and Hapke, B. W. (1978). Spectral reflectivities of the Galilean satellites and Titan, 0.32 to 0.86 micrometers. Icarus 36, 304-329.

Ostro, S. J., Pettengill, G. H., and Campbell, D. B. (1980). Radar observations of Saturn's rings at intermediate tilt angles. Icarus submitted.

Pilcher, C. B., Chapman, C. R., Lebofsky, L. A. and Kieffer, H. H. (1970). Saturn's rings: Identification of water frost. Science 167, 1372-1373.

Pilcher, C. B., Ridgeway, S. T., and McCord, T. B. (1972). Galilean satellites: Identification of water frost. Science 178, 1087-1089.

Pimental, G. C., Forney, P. B., and Herr, K. C. (1974). Evidence about hydrate and solid water in the Martian surface from the 1969 Mariner infrared spectrometer. J. Geophys. Res. 79, 162-1634.

Pollack, J. B. (1979). The rings of Saturn. Space Sci. Res. 18, 3-93.

Pollack, J. B., Witteborn, F. C., Edwin, F. E., Strecker, D. W., Baldwin, B. J., and Bunch, B. E. (1978). Near-infrared spectra of the

Galilean satellites: Observation and compositional implications. Icarus 36, 271-303.

Puetter, R. C., and Russell, R. W. (1977). The 2-4μm spectrum of Saturn's rings. Icarus 32, 37-40.

Singer, R. B. (1977). Visible and near-infrared spectral photometry of the rings of Saturn from silicon diode vidicon images. Bull. Amer. Astron. Soc. 9, 523 (abstract).

Smith, B. A., Soderblom, L. A., Johnson, T. V., Ingersoll, A. P., Collins, S. A., Shoemaker, E. M., Hunt, G. E., Masursky, H., Carr, M. H., Davies, M. E., Cook II, A. F., Boyce, J., Danielson, G. E., Owen, T., Sagan, C., Beebe, R. F., Veverka, J., Strom, R. G., McCauley, J. F., Morrison, D., Briggs, G. A., Suomi, V. E. (1979). The Jupiter system through th eyes of Voyager I. Science 204, 951-971.

Smythe, W. D., Nelson, R. M., and Nash, D. B. (1979). Spectral evidence for SO_2 frost or absorbate on Io's surface. Nature 30, 766-766.

Squyres, S. W., and Veverka, J. (1979). Photometry of the surface features of Ganymede: First Voyager results. Bull. Amer. Astron. Soc. 11, 601.

FIGURE CAPTIONS

Figure 1 The spectral reflectance of water frost of different grain sizes (from Clark, 1980a). Halon is a white reflectance standard. These data were taken with the same spectrometer as the Galilean satellite and Saturn's rings spectra shown in Figure 3b and 4b. The characteristic grain sizes for the frosts (top to bottom) are: 50, 100, 200, and 400-2000 micrometers.

Figure 2 The spectra of frost growth on Mauna Kea red cinder from Clark (1980b) show a decrease in reflectance at shorter wavelengths even when the 1.5- and 2.0-μm frost bands are very prominent. The frost depths are A) 0.0, B) 0.05, C)0.1, D) 0.2, E) 0.3, and F) 0.6mm. The frost grain size is less than 30 micrometers.

Figure 3 A) The spectra of McFadden et al.(1980) are compared with the data from Clark and McCord (1980a). All the Galilean satellites show a decrease in reflectance in the visible. B) The infrared reflectance spectra of the Galilean satellites from Clark and McCord (1980a)

are shown. The geometric albedoes at 1μm are 0.90 (Io-leading), 0.85 (Io, trailing), 0.23 (Callisto-leading), 0.53 (Ganymede-leading), and 0.60 (Europa-trailing).

Figure 4 A) Spectra of Saturn's rings are compared which show the decrease in reflectance in the visible. From Clark and McCord (1980b). B) The near infrared reflectance spectra of Saturn's rings from Clark and McCord (1980b).

Figure 5 A cubic spline continuum is fit to the coarse grained frost from Figure 1. See text and Clark (1980a).

Figure 6 The infrared spectra of Ganymede and Saturn's rings with cubic spline continua removed are shown with laboratory data which have their continua removed for comparison of apparent band depths.

Figure 7 Same as for Figure 6 except for Europa and Callisto.

Figure 8 The spectrum of Ganymede is compared to a frost on ice spectrum. The agreement is excellent. The frost on the ice has

a particle size range from less than 30 to ∿200 micrometers and a depth of about 1mm. The ice block was about 17mm deep. The spectra are scaled to 1.0 at 1.02μm.

Figure 9 The Ganymede spectrum divided by the frost on ice spectrum from Figure 8 is shown here with the visible data added. The peak at 2μm is due to a difference the 2.0-μm water ice band depths.

Figure 10 The spectrum from Figure 9 is compared with the spectrum of Io, and shows the similarity in the 1.15- m absorption present in both spectra.

Figure 11 The spectrum of Saturn's rings is compared with the lower of the two medium grained frost spectra (T = 112K) from Figure 1. The frost spectrum was scaled to fit the 1.5- and 2.0-μm absorptions. The Saturn's rings spectrum is scaled to 1.0 at 1.02μm and the frost spectrum is scaled to match the 1.5- and 2.0-μm absorptions in the spectrum of the rings.

Figure 12 The spectrum of Saturn's rings divided by the frost spectrum from Figure 11 is shown. The apparent absorption at 1.1μm

is not real since the 1.25-μm frost band is deeper than in Saturn's ring causing the ratio around 1.25μm to be too high. See text.

Figure 13 The spectrum of Europa is compared to a water ice spectrum (see Clark 1980a). The water ice spectrum was scaled to match Europa around the 1.5-μm band.

Figure 14 The spectrum of Callisto is shown compared to two simulations: A) the medium grained frost (T = 114K) from Figure 1 with a constant of 2.0 added to the data and rescaled to match Callisto at 1.7μm. B) The spectrum of Europa with a constant of 2.0 added to the data and then rescaled to match Callisto at 1.7μm. The Callisto spectrum is scaled to 1.0 at 1.02μm.

Figure 15 A spectrum of a palagonite from Mauna Kea which is similar to the non-icy spectral components on Ganymede, Europa, Callisto and Saturn's rings. Absorptions at wavelengths longer than 1.4μm are due to H_2O and OH in the sample. (Spectrum from R. B. Singer, personal communication, 1979; sample courtesy of J. B. Adams.)

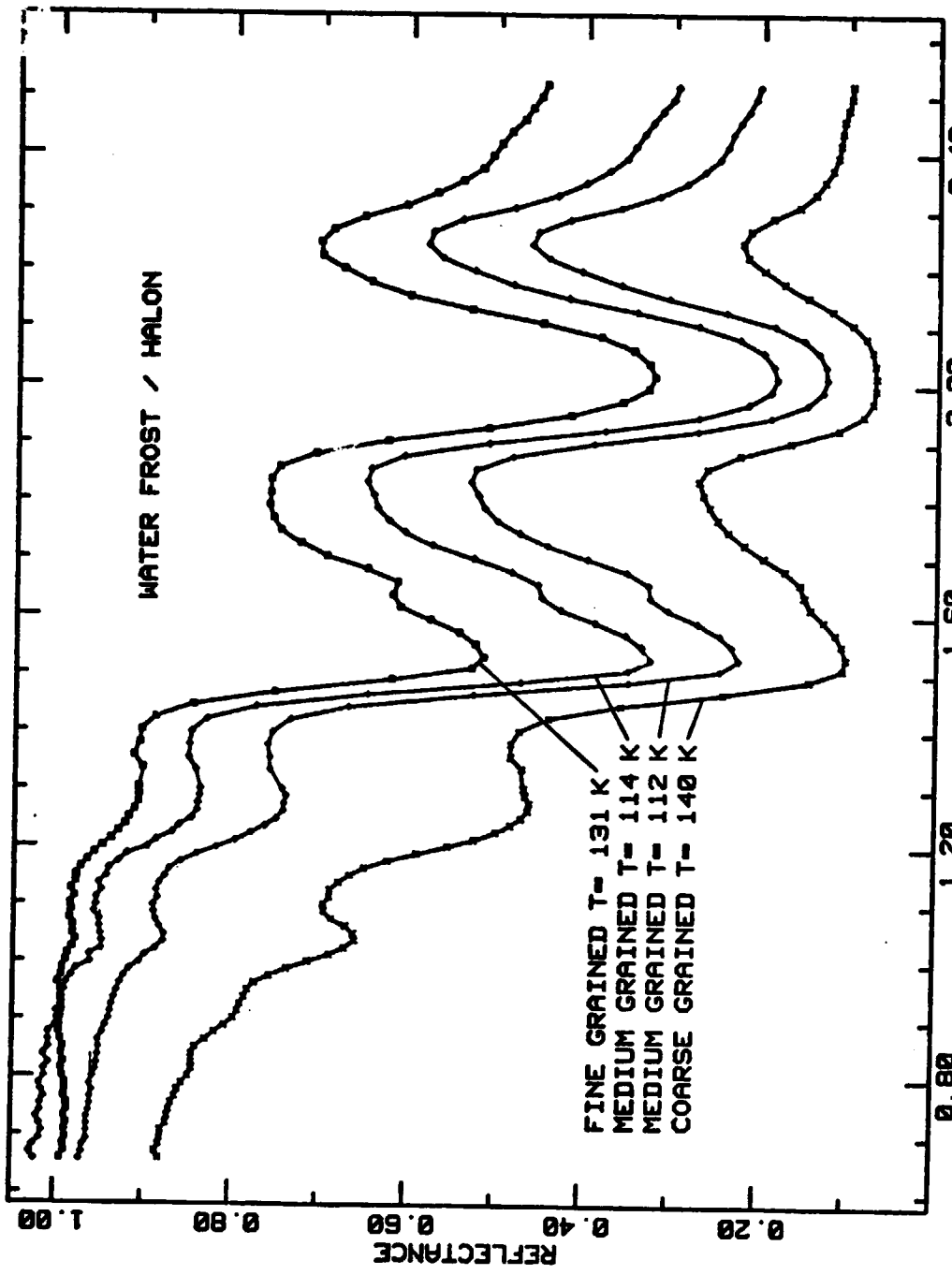

WATER FROST / HALON
FINE GRAINED T= 131 K
MEDIUM GRAINED T= 114 K
MEDIUM GRAINED T= 112 K
COARSE GRAINED T= 140 K
REFLECTANCE
0.20
0.40
0.60
0.80
1.00
WAVELENGTH IN MICRONS
0.80
1.20
1.60
2.00
2.40

Figure 1

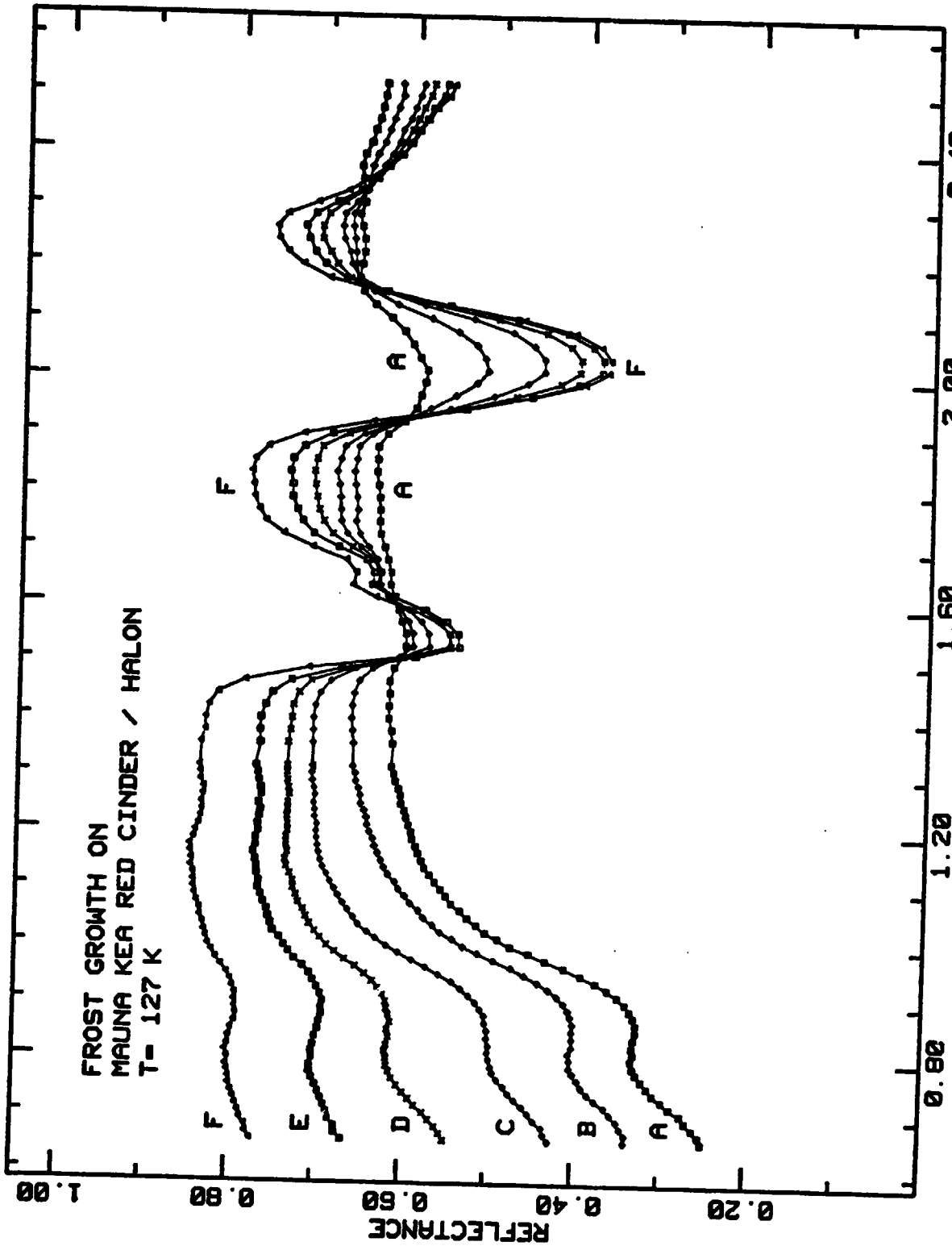

FROST GROWTH ON
MAUNA KEA RED CINDER / HALON
T= 127 K
F
E
D
C
B
A
F
A
F
A
REFLECTANCE
0.20
0.40
0.60
0.80
1.00
0.80
1.20
1.60
2.00
2.40
WAVELENGTH IN MICRONS

Figure 2

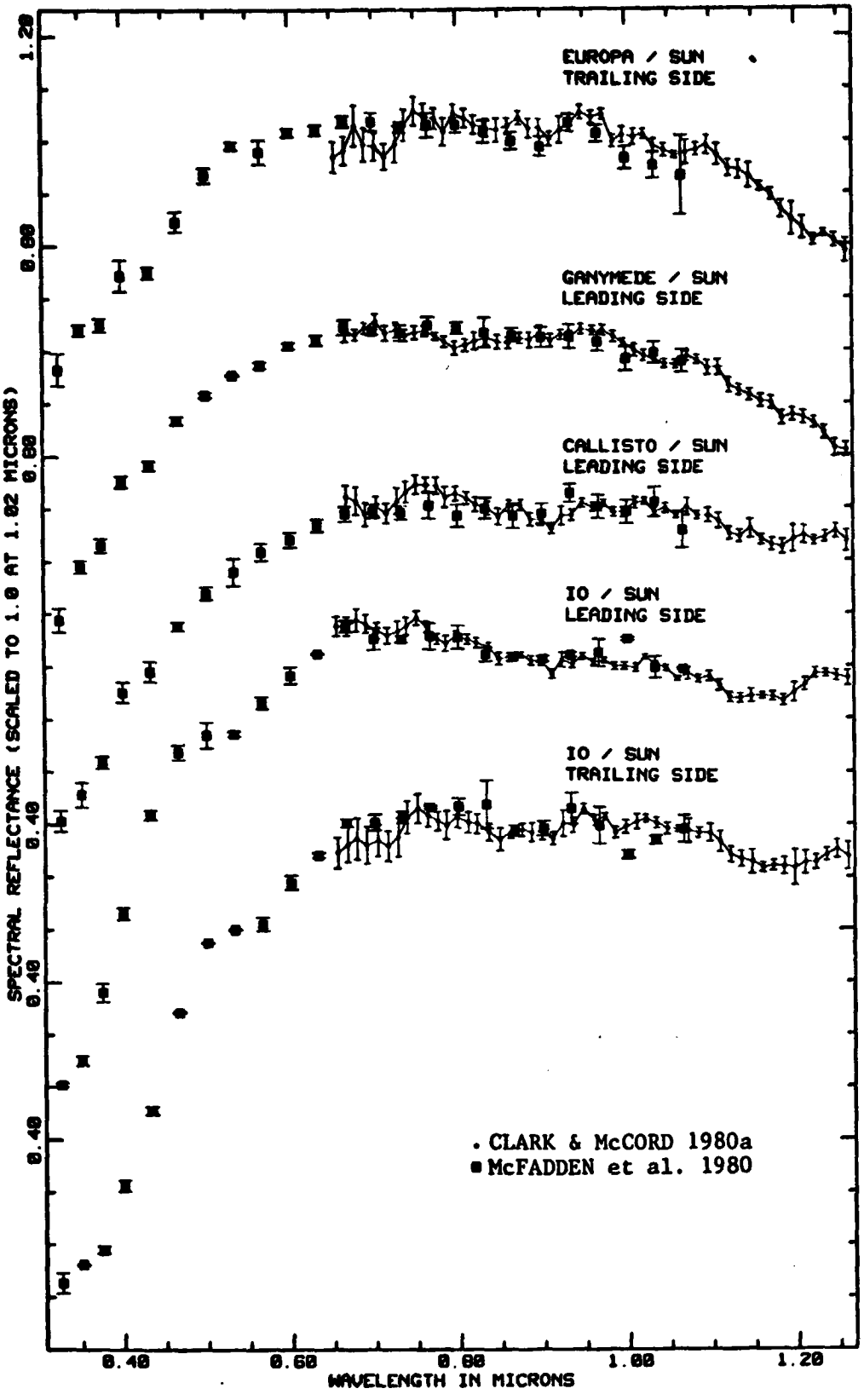

EUROPA / SUN
TRAILING SIDE
GANYMEDE / SUN
LEADING SIDE
CALLISTO / SUN
LEADING SIDE
IO / SUN
LEADING SIDE
IO / SUN
TRAILING SIDE
. CLARK & McCORD 1980a
■ McFADDEN et al. 1980
SPECTRAL REFLECTANCE (SCALED TO 1.0 AT 1.02 MICRONS)
0.40
0.60
0.80
1.00
1.20
WAVELENGTH IN MICRONS

Figure 3A

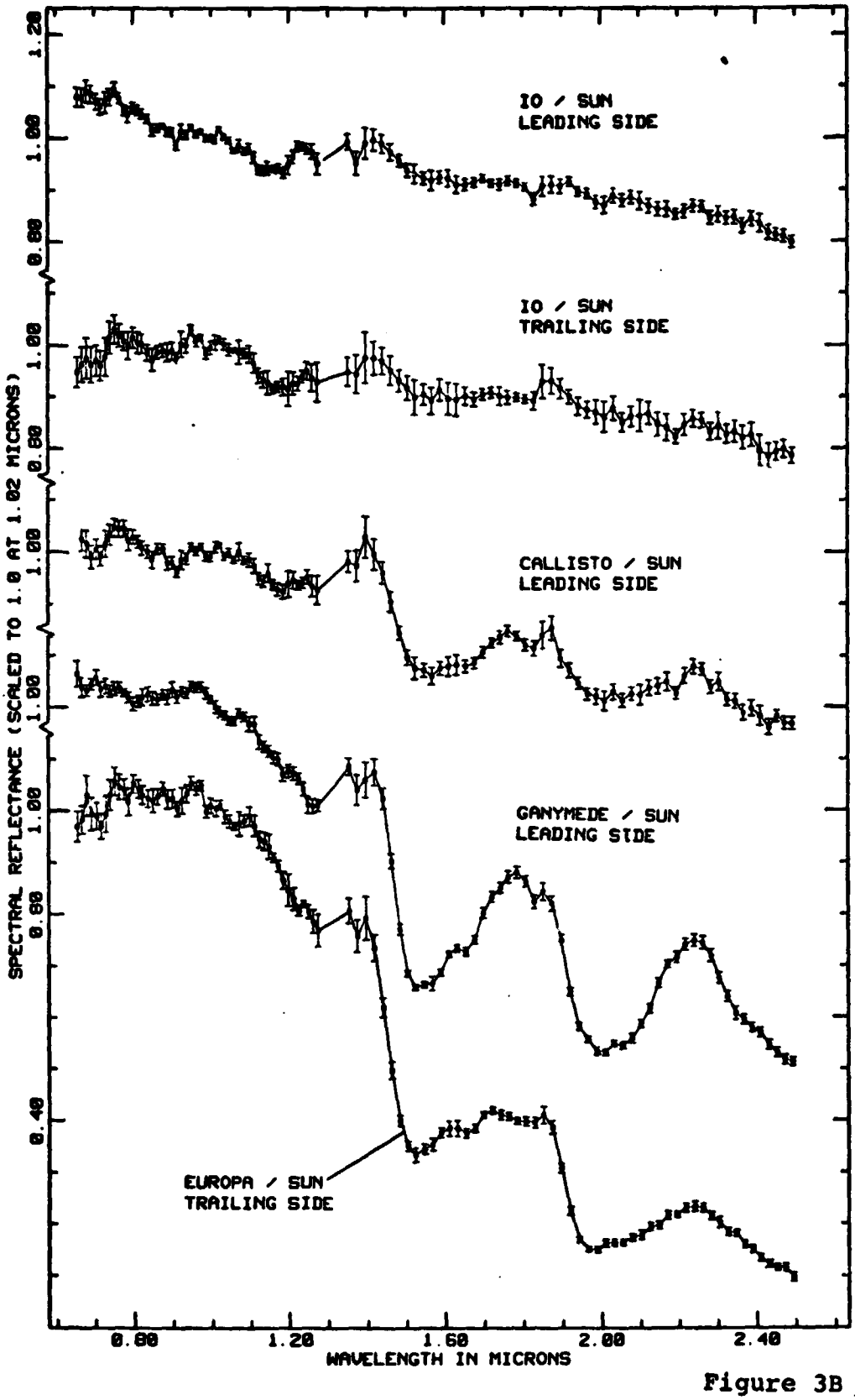

IO / SUN
LEADING SIDE
IO / SUN
TRAILING SIDE
CALLISTO / SUN
LEADING SIDE
GANYMEDE / SUN
LEADING SIDE
EUROPA / SUN
TRAILING SIDE
SPECTRAL REFLECTANCE (SCALED TO 1.0 AT 1.02 MICRONS)
1.20
1.00
0.80
1.00
0.80
1.00
1.00
0.80
0.40
0.00
1.20
1.60
2.00
2.40
WAVELENGTH IN MICRONS

Figure 3B

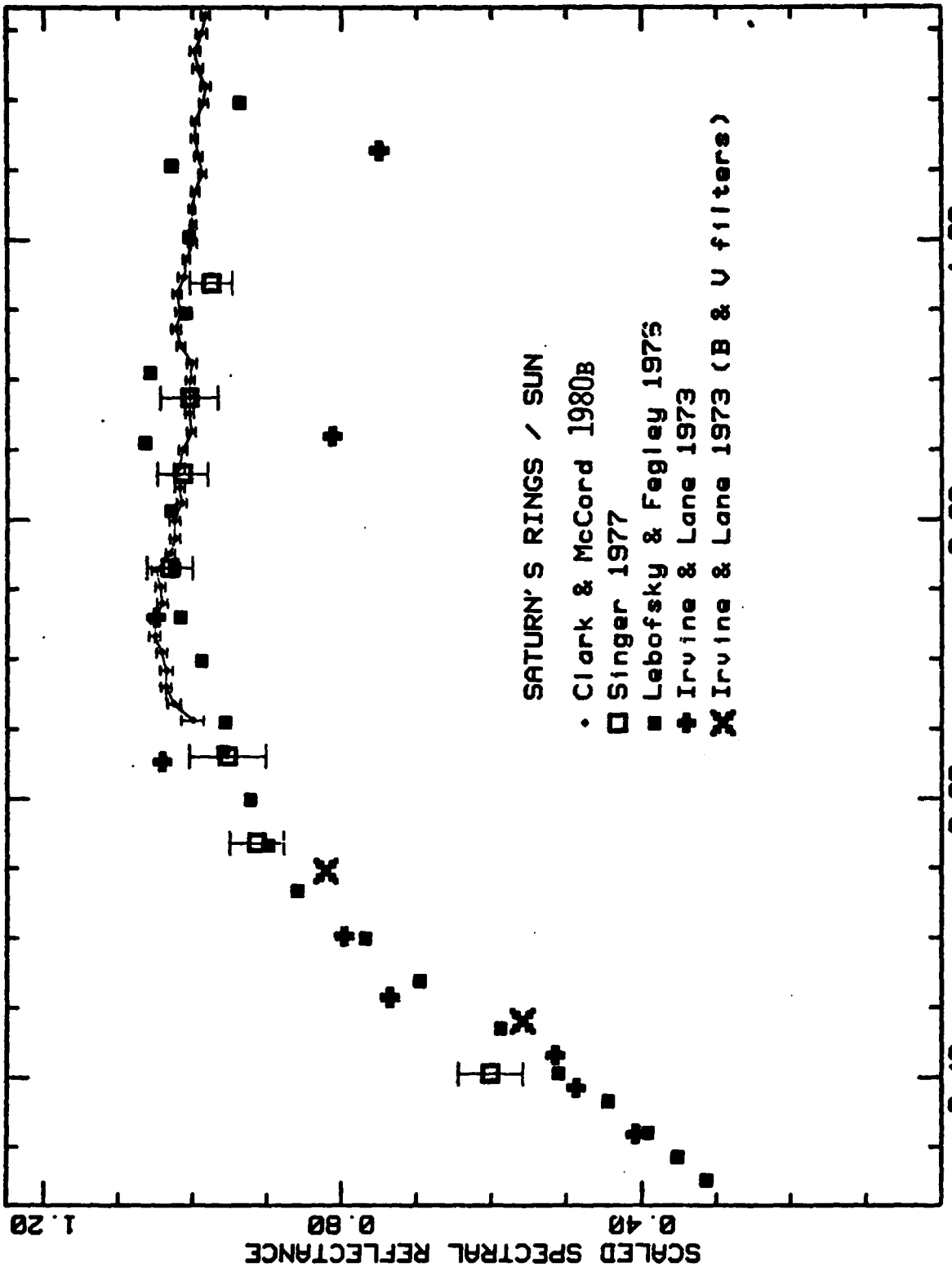

SATURN'S RINGS / SUN
• Clark & McCord 1980B
□ Singer 1977
■ Lebofsky & Fegley 1975
✚ Irvine & Lane 1973
✕ Irvine & Lane 1973 (B & V filters)
SCALED SPECTRAL REFLECTANCE
0.40
0.80
1.20
0.40
0.60
0.80
1.00
WAVELENGTH IN MICRONS

Figure 4A

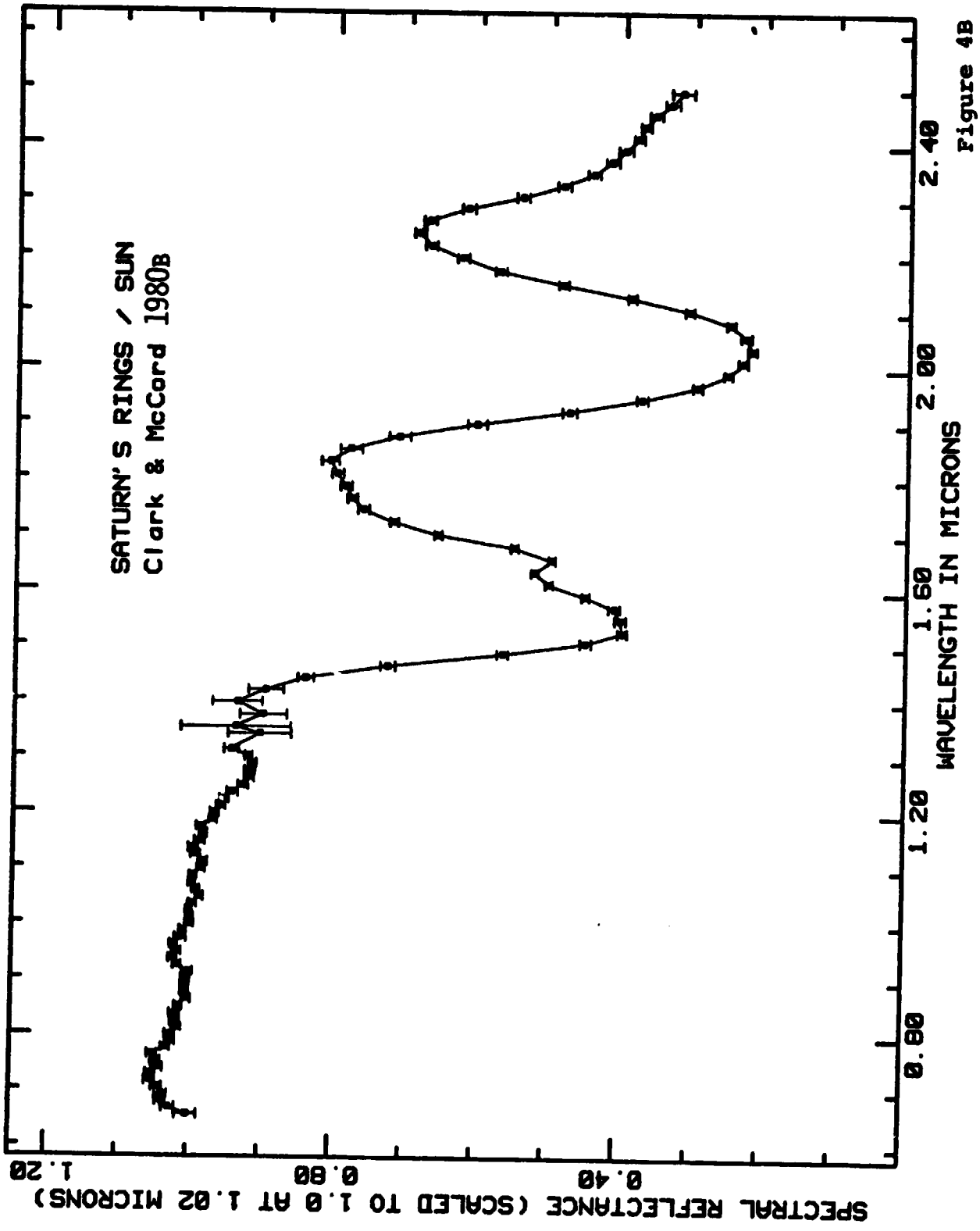

SATURN'S RINGS / SUN
Clark & McCord 1980B
SPECTRAL REFLECTANCE (SCALED TO 1.0 AT 1.02 MICRONS)
0.40
0.80
1.20
WAVELENGTH IN MICRONS
0.80
1.20
1.60
2.00
2.40

Figure 4B

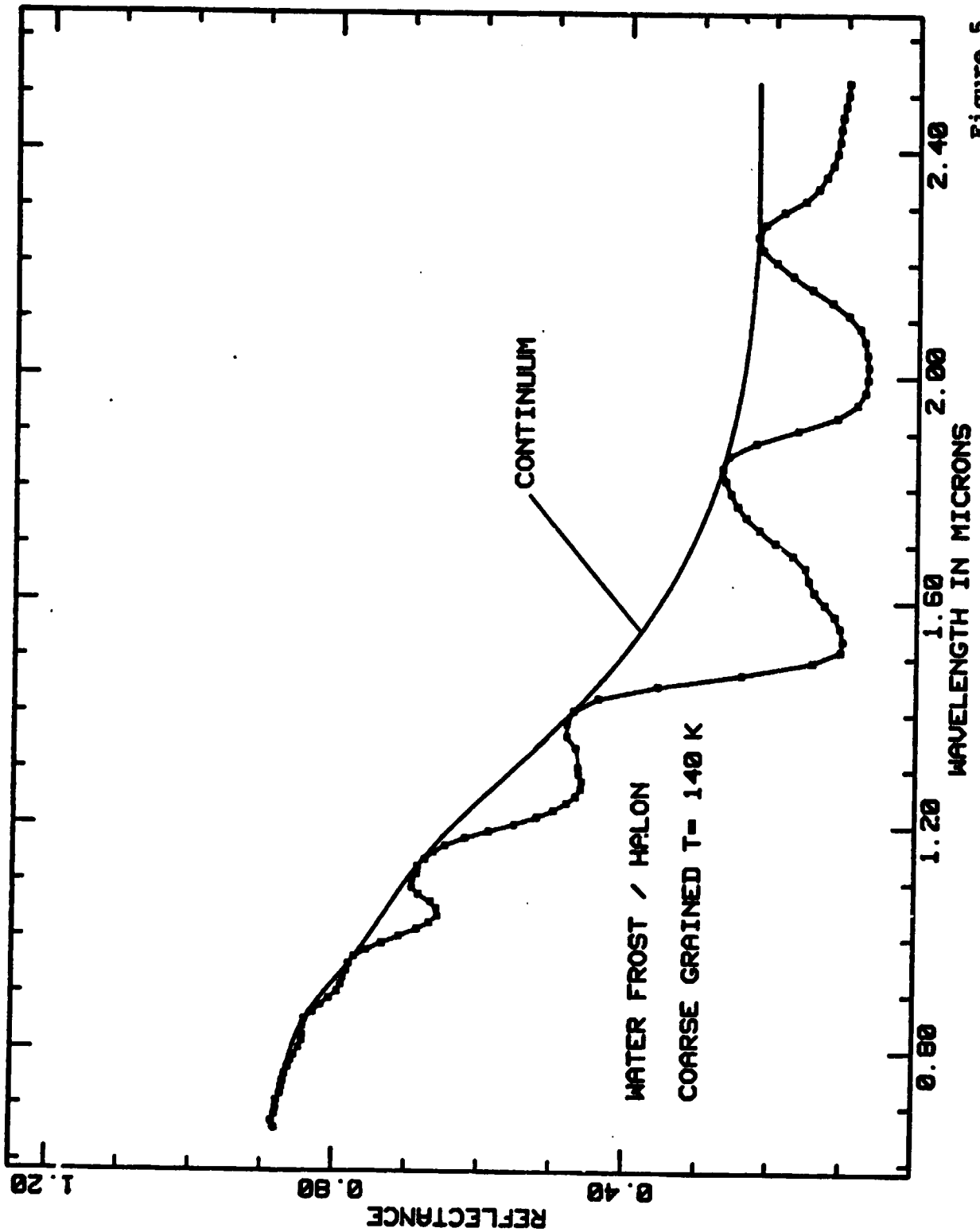

CONTINUUM
WATER FROST / HALON
COARSE GRAINED T= 140 K
REFLECTANCE
0.40
0.80
1.20
WAVELENGTH IN MICRONS
0.80
1.60
2.00
2.40

Figure 5

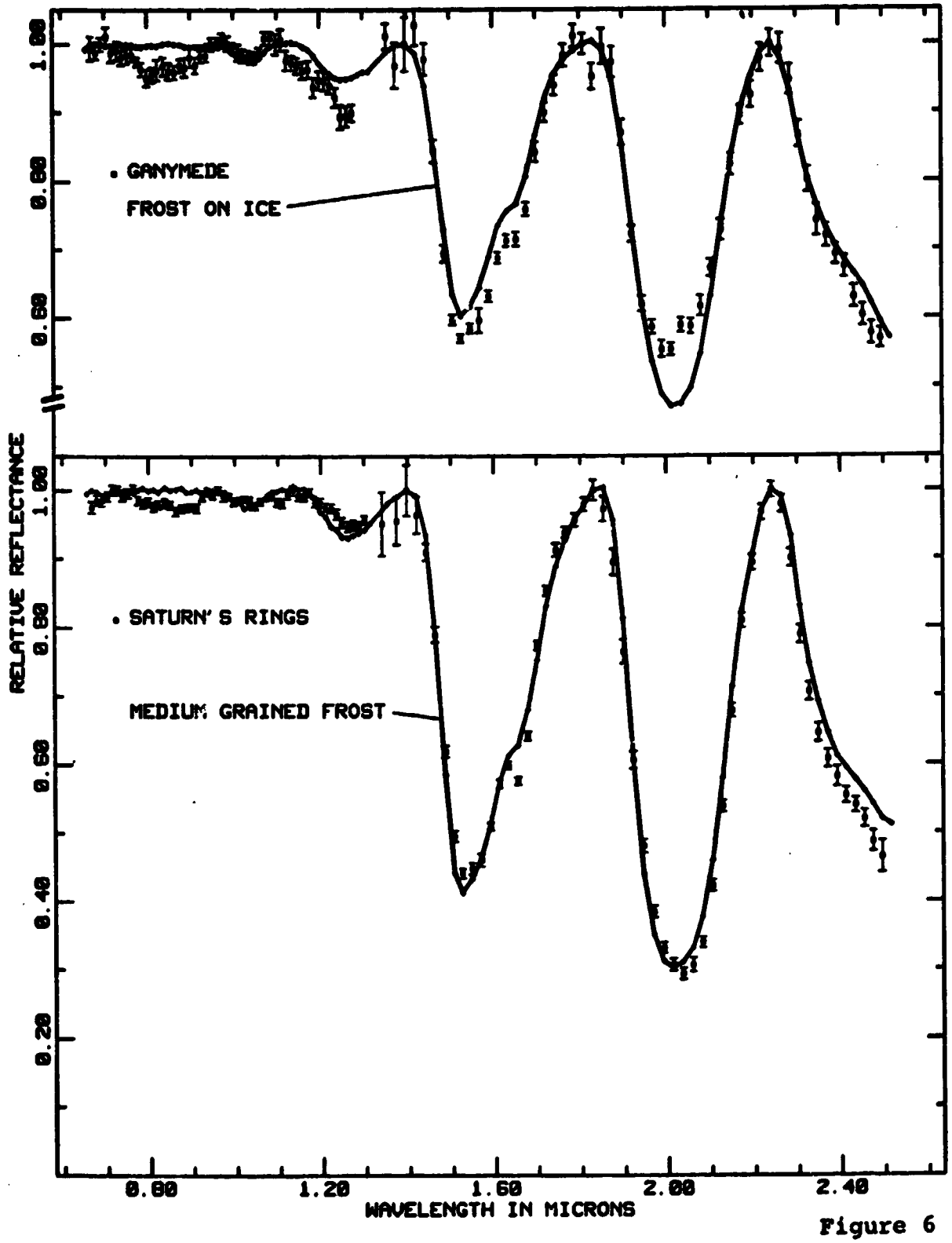

• GANYMEDE
FROST ON ICE
• SATURN'S RINGS
MEDIUM GRAINED FROST
RELATIVE REFLECTANCE
1.00
0.80
0.60
0.40
0.20
0.00
1.20
1.60
2.00
2.40
WAVELENGTH IN MICRONS

Figure 6

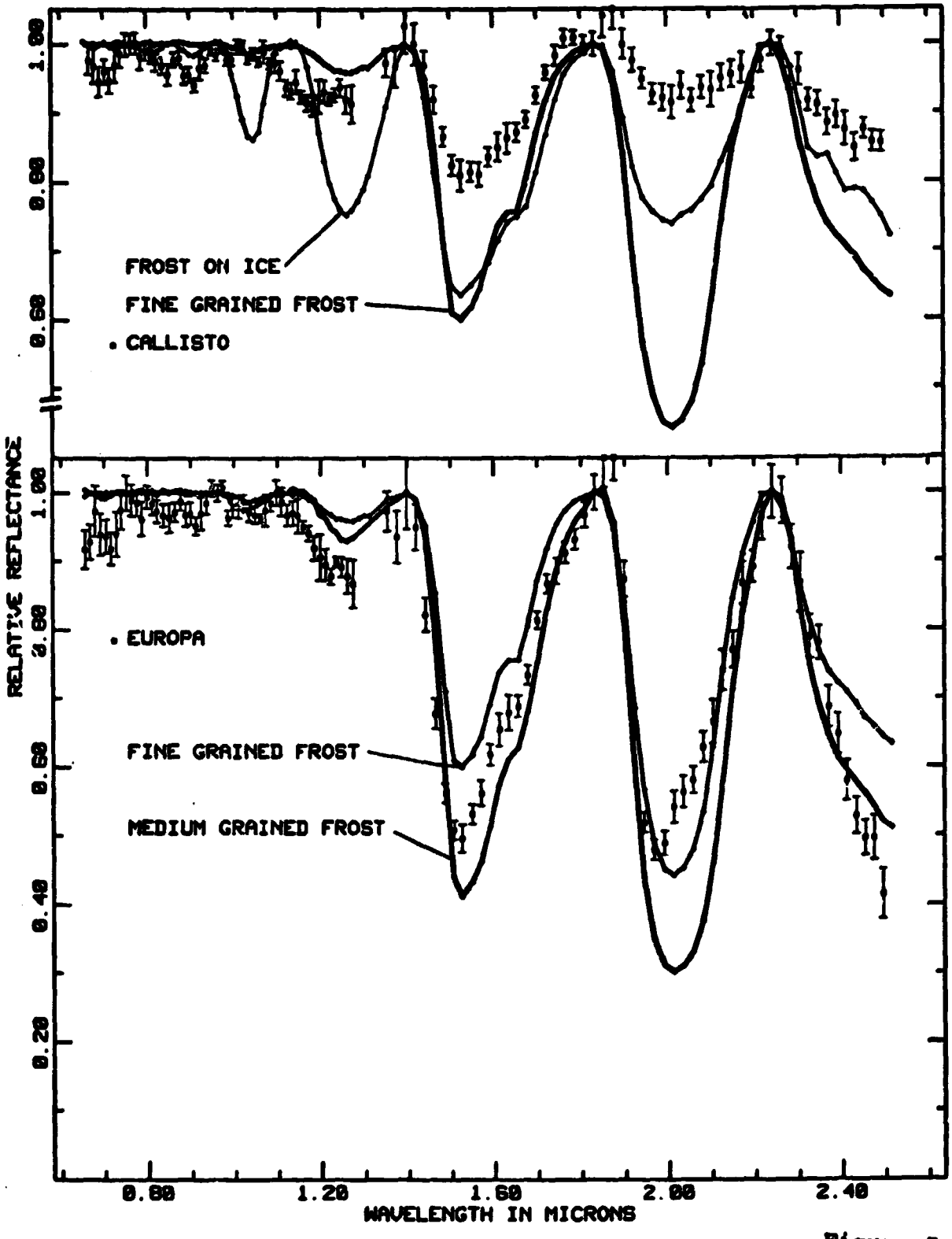

FROST ON ICE
FINE GRAINED FROST
• CALLISTO
• EUROPA
FINE GRAINED FROST
MEDIUM GRAINED FROST
RELATIVE REFLECTANCE
1.00
0.80
0.60
0.40
0.20
0.80
1.20
1.60
2.00
2.40
WAVELENGTH IN MICRONS

Figure 7

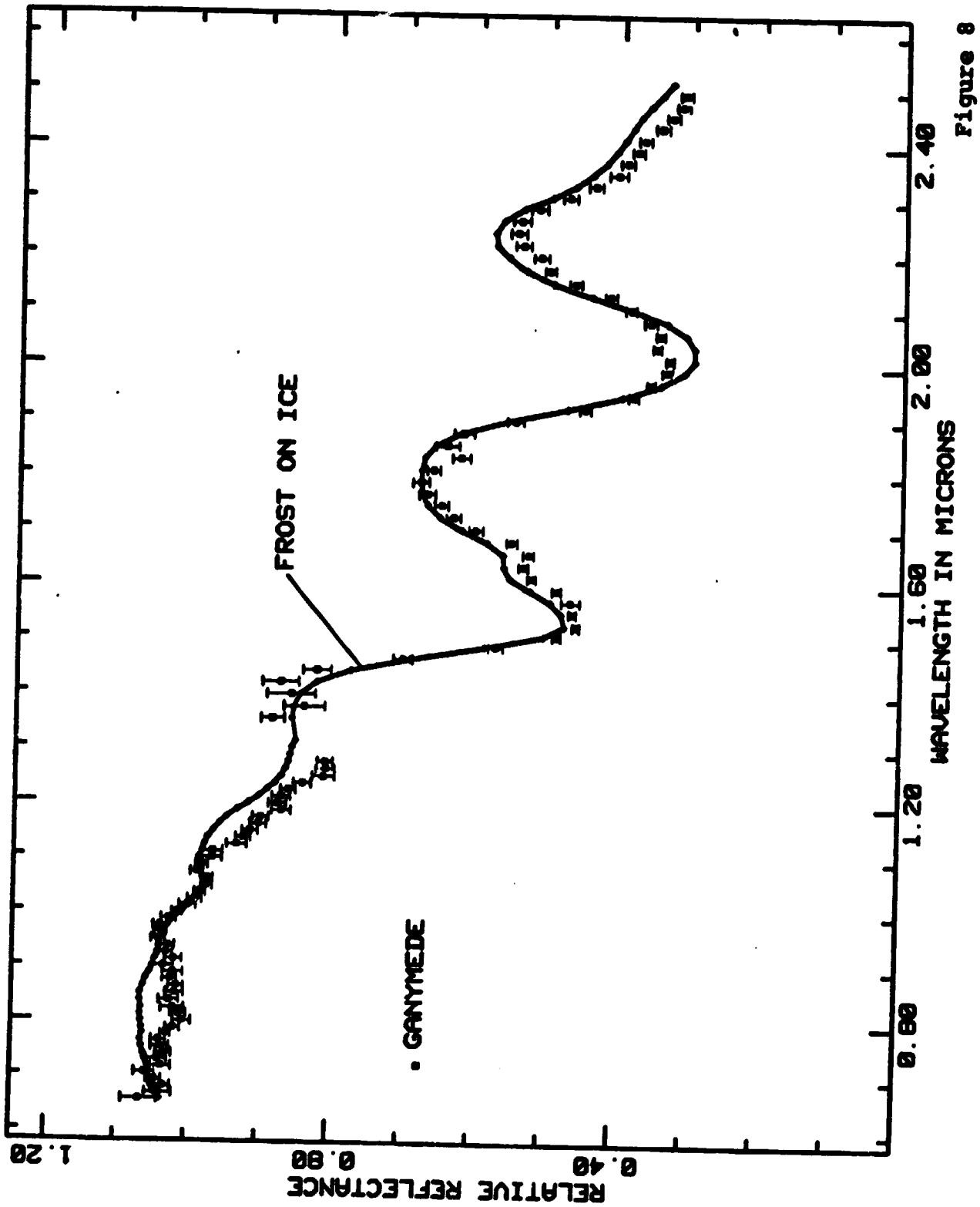

FROST ON ICE
• GANYMEDE
RELATIVE REFLECTANCE
0.40
0.80
1.20
0.80
1.20
1.60
2.00
2.40
WAVELENGTH IN MICRONS

Figure 8

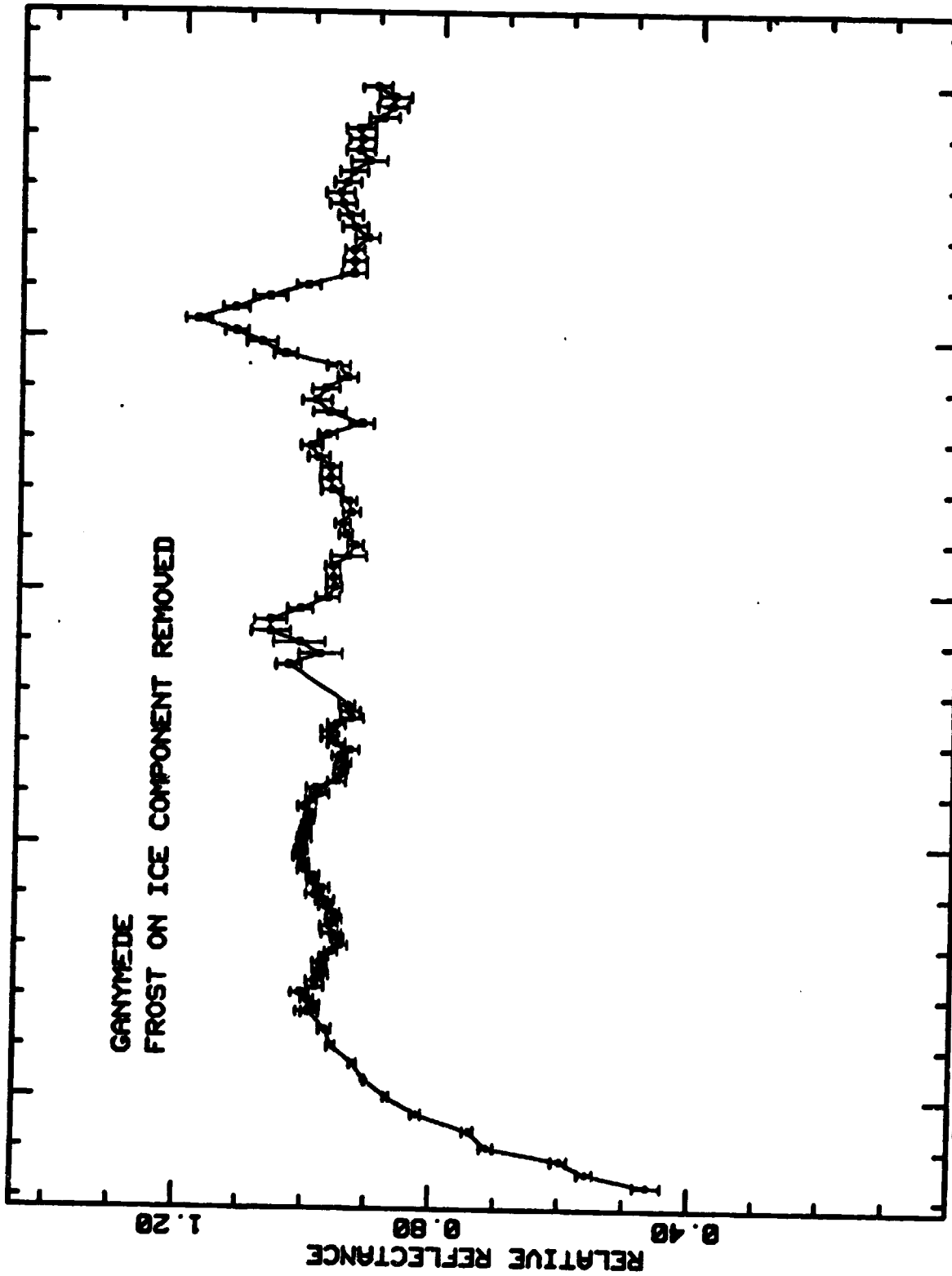

GANYMEDE
FROST ON ICE COMPONENT REMOVED
RELATIVE REFLECTANCE
0.40
0.80
1.20
0.50
1.00
1.50
2.00
2.50
WAVELENGTH IN MICRONS

Figure 9

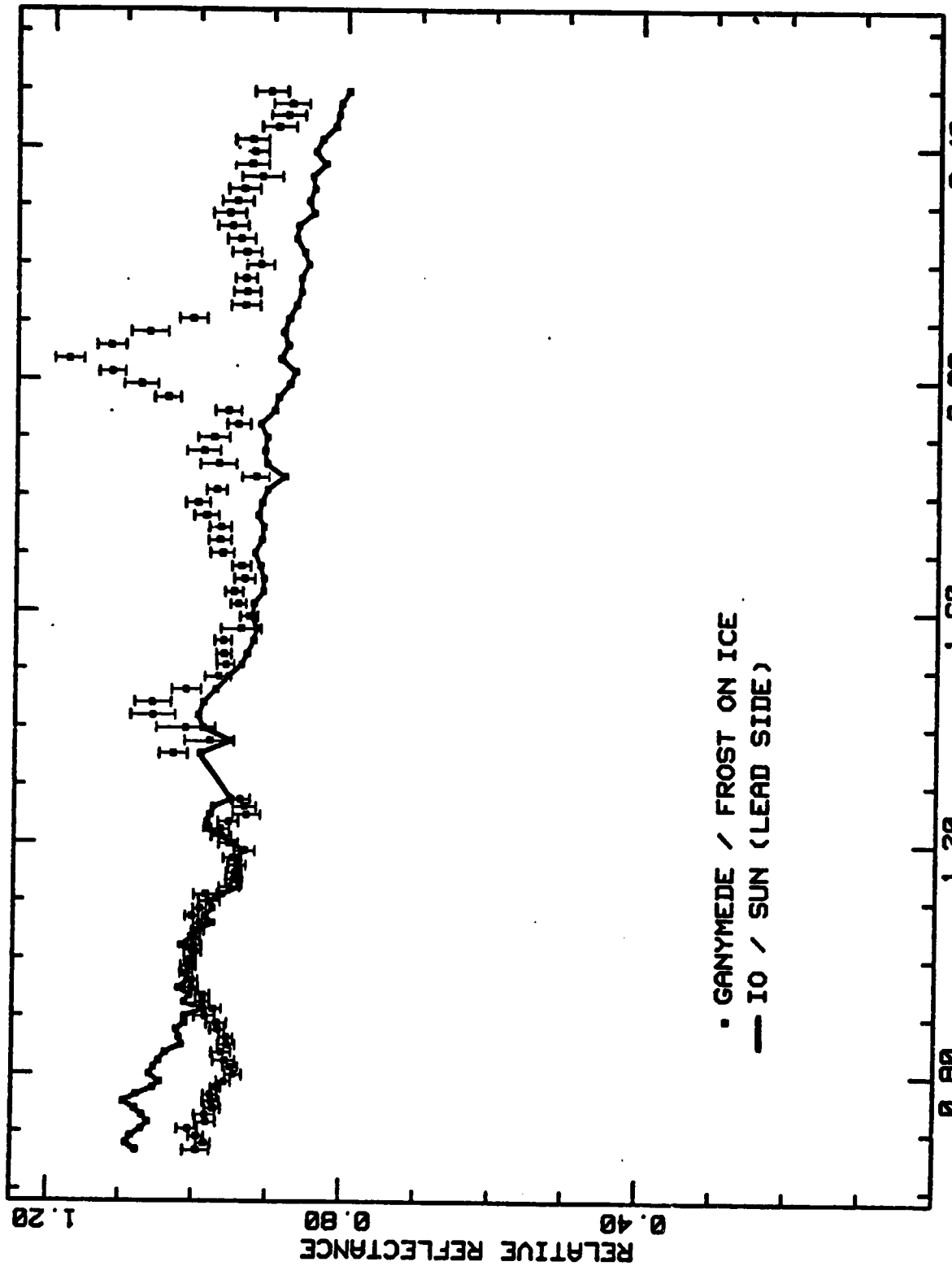

RELATIVE REFLECTANCE
0.40
0.80
1.20
0.80
1.20
1.60
2.00
2.40
WAVELENGTH IN MICRONS
▪ GANYMEDE / FROST ON ICE
— IO / SUN (LEAD SIDE)

Figure 10

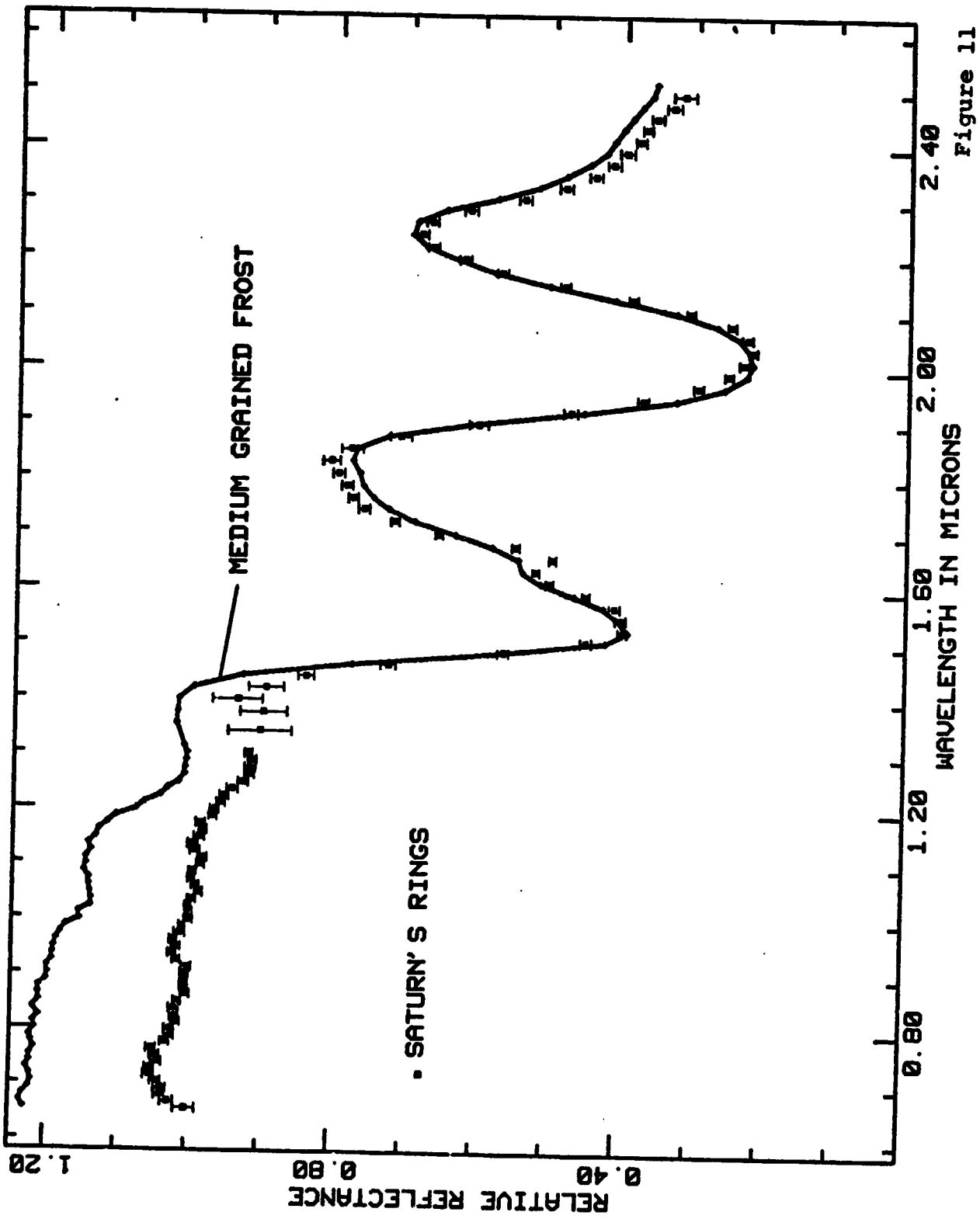

MEDIUM GRAINED FROST
• SATURN'S RINGS
RELATIVE REFLECTANCE
0.40
0.80
1.20
0.80
1.20
1.60
2.00
2.40
WAVELENGTH IN MICRONS

Figure 11

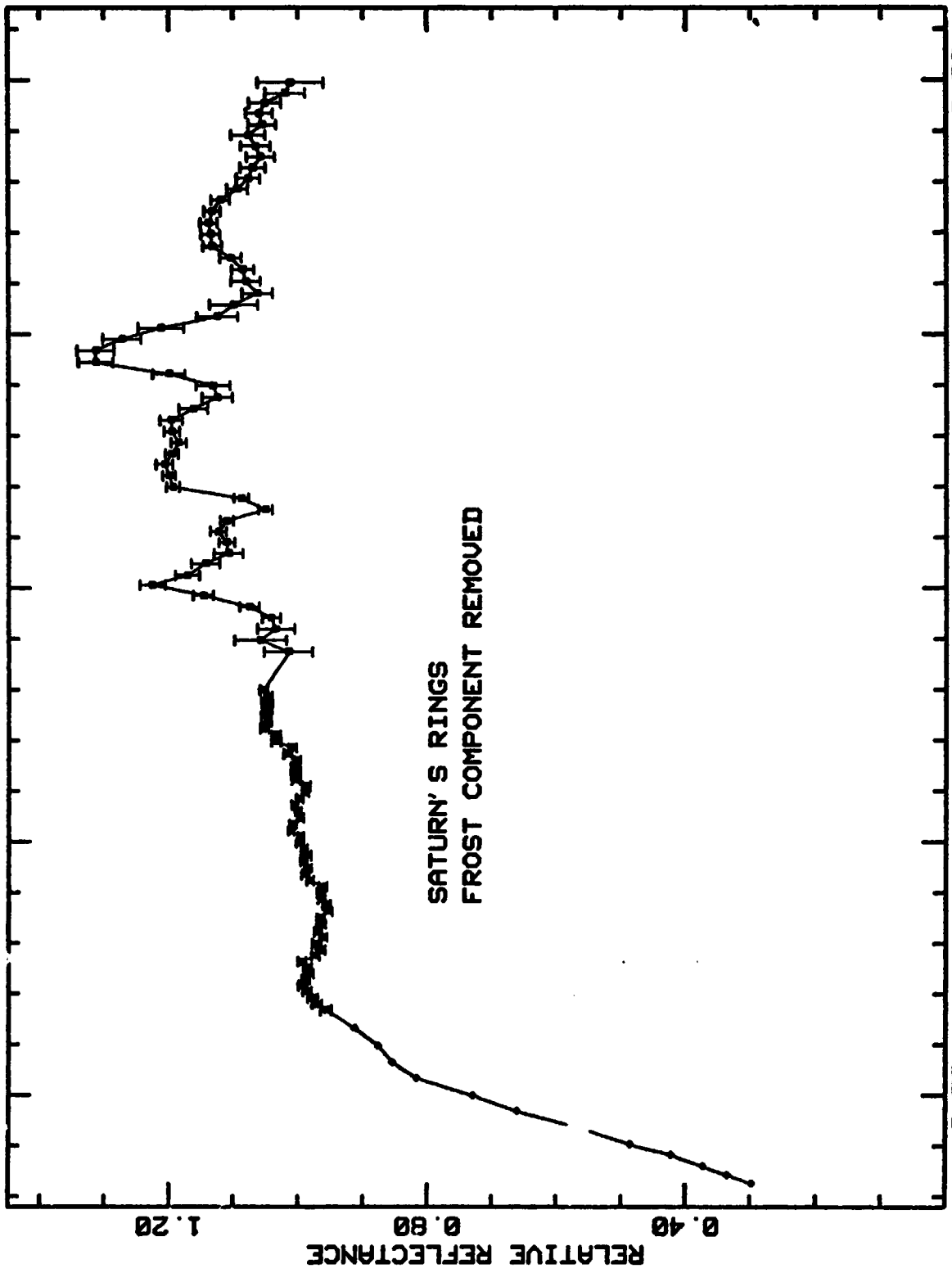

SATURN'S RINGS
FROST COMPONENT REMOVED
RELATIVE REFLECTANCE
0.40
0.80
1.20
0.50
1.00
1.50
2.00
2.50
WAVELENGTH IN MICRONS

Figure 12

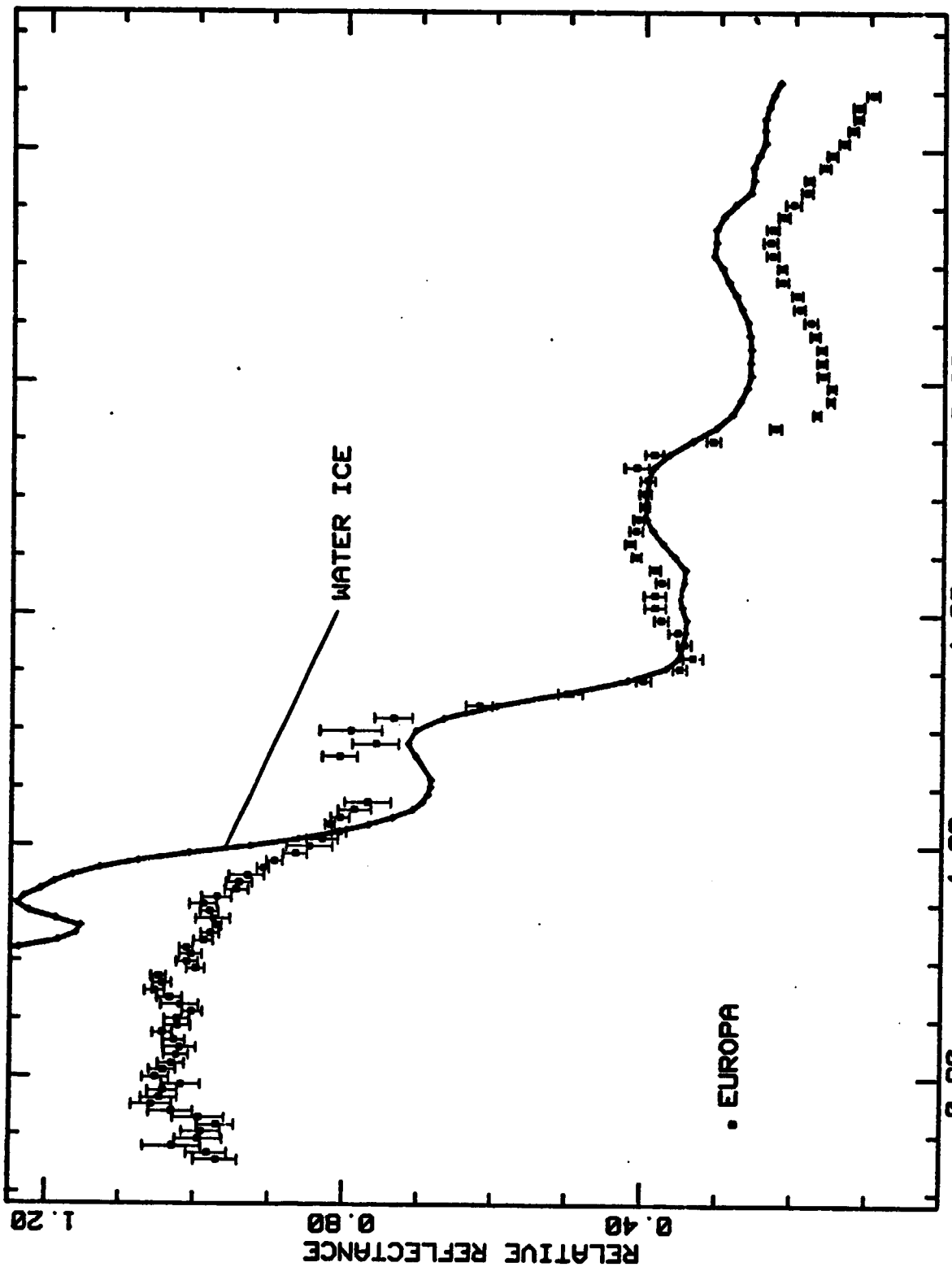

WATER ICE
EUROPA
RELATIVE REFLECTANCE
0.40
0.80
1.20
0.80
1.20
1.60
2.00
2.40
WAVELENGTH IN MICRONS

Figure 13

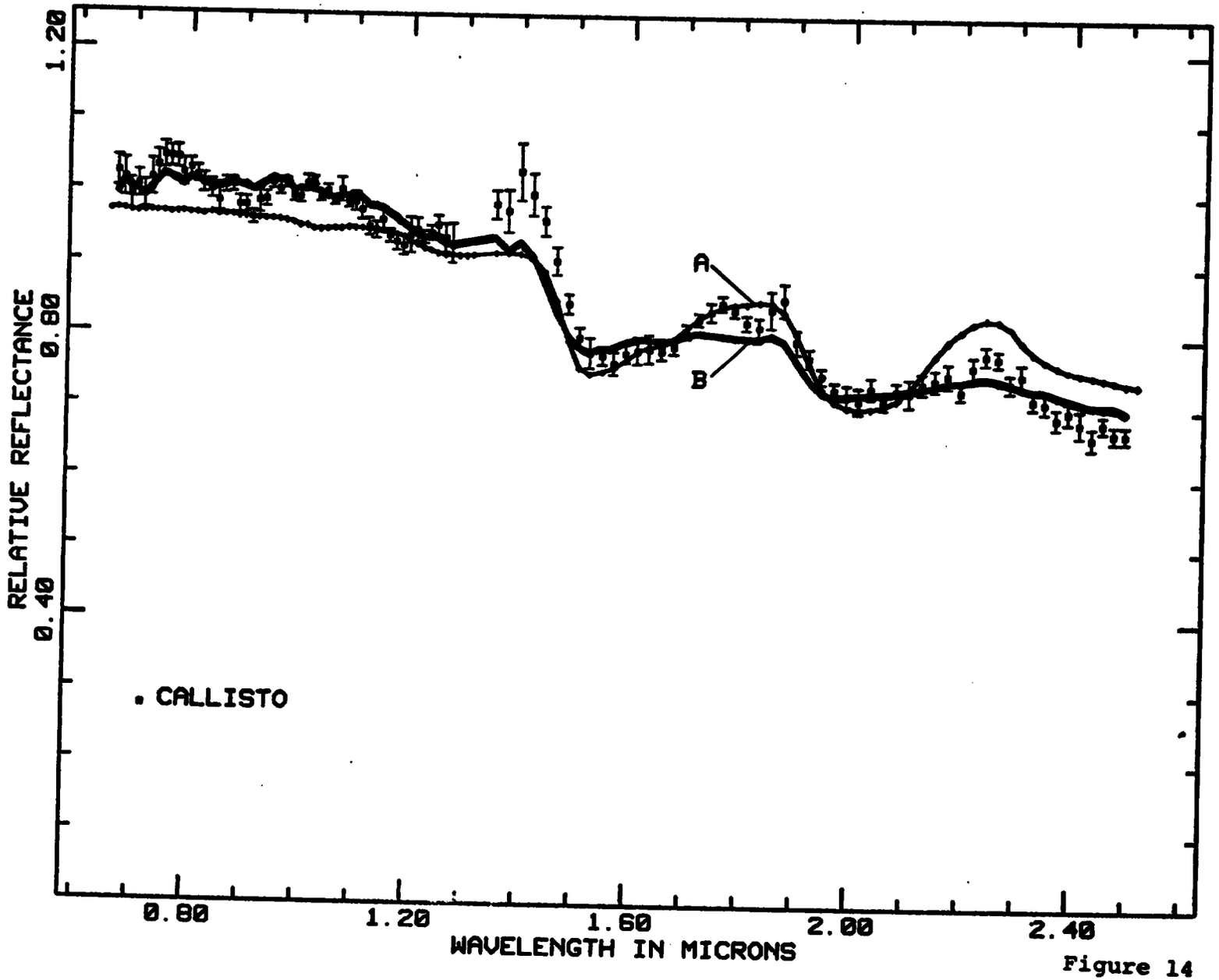

1.20
0.80
0.40
RELATIVE REFLECTANCE
A
B
• CALLISTO
0.80
1.20
1.60
2.00
2.40
WAVELENGTH IN MICRONS

Figure 14

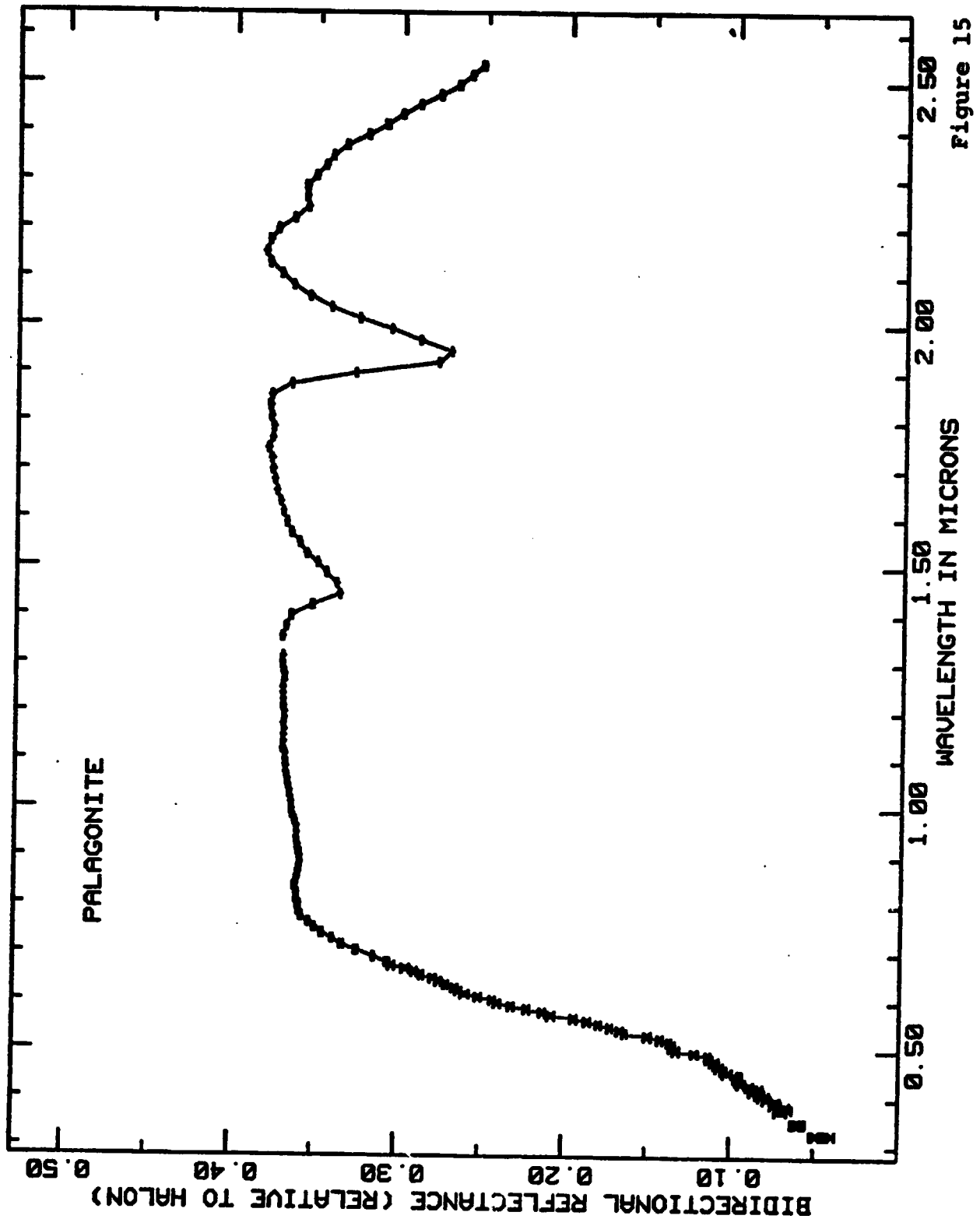

PALAGONITE
BIDIRECTIONAL REFLECTANCE (RELATIVE TO HALON)
0.10
0.20
0.30
0.40
0.50
WAVELENGTH IN MICRONS
0.50
1.00
1.50
2.00
2.50

Figure 15

APPENDIX A

A Large Scale Interactive One Dimensional Array Processing System

This chapter has been submitted for publication to the journal Publications of the Astronomical Society of the Pacific. Author: R.N. Clark.

I. PROGRAM FEATURES

A very large program has been written for processing large amounts of spectrophotometric data in an interactive mode. The program processes one-dimensional arrays up to 256 data points and the operations include addition, subtraction, multiplication, division, trigonometric functions, logarithmic and exponential functions, fractional part, integer part, and inverse. A standard deviation error analysis can also be propagated through the basic functions, (add, subtract, multiply, and divide) and some special mathematical functions to the final data for publication. Other routines include an extinction analysis for air mass computation and corrections, a plotting package for publication quality graphs, plotting data on the CRT, and a complete file management system. Specialized routines can be easily written and added to the program (such as smoothing data, interpolation to a new wavelength set, Planck black body generation).

The program is written in FORTRAN and all communication with the user is free format. All user input is thoroughly checked for possible errors so that the program cannot be inadvertently

terminated or data destroyed. A program automatic history records all operations such that anyone can trace the flow of data reduction and analysis at a later date. The file management system keeps track of device and file status control, user selected file protection, and transferring of data. Repetitous operations can be set up in a pseudo batch mode within the interactive system, minimizing user input while maintaining user control, and flexibility. The program is currently implemented on a time sharing computer system.

The program represents about three man years of work. Future plans include implementation of the program on Digital Equipment Corp. LSI-11/23 computers, also to be interfaced to our spectrometers, enabling data processing during the acquisition of spectra at the telescope.

The following sections discuss more of the details of the program. Copies of the program and a user's manual may be obtained by supplying a 2400-foot tape to the author.

II. PROGRAM MATHEMATICS

In a typical reduction process, the sky (background) is subtracted, then using the standard object observations, the extinction is computed via a linear least-squares analysis to the logarithm (base 10) of the object intensity as a function of air mass for each spectral channel. The program stores the extinction slopes (E), intercepts (I = log intensity extrapolated to zero air mass), and the correlation coefficient (for evaluating the quality of the least squares analysis). An intensity ratio for each observation of object (O) devided by standard (S) for each spectral channel is computed from the equation

$$a = {}^{O}/_{S} = {}^{O}/_{[10^{I}\ (10^{mE})]} \qquad \text{eqn 1}$$

where m is the air mass at which the object was observed. See McCord and Clark (1979) for an example of results using the extinction routines.

The error bars are computed from the addition of many object-standard ratios. The errors computed are the standard deviation of the mean for each spectral channel:

$$\sigma_a = \left(\frac{\sum_{i=1}^{n} (a_i - \bar{a})^2}{(n-1)} \right)^{\frac{1}{2}} \cdot n^{-\frac{1}{2}} \qquad \text{eqn 2}$$

where n is the number of observations, a_i is each object/standard observation, and $\bar{a}$ is the average of all the a_i's. Propagation of errors follows Bevington (1969). Given several object/standard computions (a, b, ... c) with associated errors (σ_a, σ_b, ... σ_c) the errors are computed for each spectral channel for addition, multiplication, division and subtraction as follows:

addition: $r = a + b + \ldots + c$

$$\sigma_r = \left(\sigma_a^2 + \sigma_b^2 + \ldots + \sigma_c^2\right)^{\frac{1}{2}}, \qquad \text{eqn 3}$$

multiplication and division: $r = {}^{a}/_{b}$, $r = a \cdot b$

$$\sigma_r = \left[\left(\frac{\sigma_a}{a}\right)^2 + \left(\frac{\sigma_b}{b}\right)^2\right]^{\frac{1}{2}} |r| \qquad \text{eqn 4}$$

subtraction: $r = a - b$

$$\sigma_r = \left(\sigma_a^2 + \sigma_b^2\right)^{\frac{1}{2}}. \qquad \text{eqn 5}$$

Errors analyses are not presently computed for other mathematical operations. Other mathematics include trigonometric functions (sine, cosine, tangent and inverses) in degrees or radians; logarithmic functions and inverses (natural or base 10); power functions (y^x) where y is a constant and x is each channel in the spectrum or x is the constant and y is the spectrum; integer

part, fractional part, absolute value, and inverse (1/x). These functions can be useful for analyses other than spectral, making the program a general one dimensional array processor (e.g. intensity versus time, phase angle or wavelength).

Comparison of different data sets is very important for confirming absorption (or emission) features and establishing the credibitlity of the measurements. This can be done qualitatively by plotting the different spectra on the same plot as shown in Figure 1. However, a quantitative (Fig.1) analysis requires the spectra to be sampled at the same wavelengths with the same resolution. This program uses a cubic spline function for interpolating from one wavelength set to another and a smoothing routine to degrade the spectral resolution of high a resolution spectrum to that of a low resolution spectrum.

The cubic spline function describes the physics of a flexible strip such that the strip passes through each of the data points (y_1, y_2, ... y_n) in the spectrum. The flexible strip can be represented as a series of cubic polynomials with appropriate boundary conditions. A different polynomial is calculated for each interval in the

spectrum [i.e. $S_1(x)$ on the interval (X_1, X_2), $S_2(x)$ on (X_2, X_3) ... $S_{n-1}(x)$ on (X_{n-1}, X_n)] where S_i represents a cubic ploynomial

$$S_i(x) = A_i x^3 + B_i x^2 + C_i x + D_i. \qquad \text{eqn 6}$$

The boundary conditions are that the spline must go through each function value:

$$S_n(x_i) = y_i$$

$$S_n(x_{i+1}) = y_{i+1} = S_{i+1}(x_{i+1}), \qquad \text{eqn 7}$$

and the first and second derivative of the cubic polynomials are continuous

$$S'_{m-1}(x_m) = S'_m(x_m),$$

$$S''_{m-1}(x_m) = S''_m(x_m) \qquad \text{eqn 8}$$

for m and on the interval (2, n-1). The curvature is forced to zero at the endpoints:

$$S''_1(x_1) = 0$$

$$S''_{n-1}(x_n) = 0 \qquad \text{eqn 9}$$

Once the cubic spline coefficients are computed, the spectral channels can be recomputed to any wavelength values within the limits of the function. See Carnahan and Wilkes (1973) for more detail on the cubic spline function. The error values are similarly interpolated.

The smoothing function is an exponential, and assumes equally spaced data points. Each spectral channel x_i is smoothed according to the equation

$$x_i' = \frac{\left(\frac{x_{i-k}}{2^k} + \ldots + \frac{x_{i-1}}{2} + x_i + \frac{x_{i+1}}{2} + \ldots + \frac{x_{i+k}}{2^k}\right)}{\left(1 + \frac{2}{2^1} + \ldots + \frac{2}{2^k}\right)} \qquad \text{eqn 10}$$

and

$$\sigma_i' = \frac{\left(\frac{\sigma_{i+k}^2}{2^k} + \ldots + \frac{\sigma_{i-1}^2}{2} + \sigma_i^2 + \frac{\sigma_{i+1}^2}{2} + \ldots + \frac{\sigma_{i+k}^2}{2^k}\right)^{1/2}}{\left(1 + {}^2/_{2^1} + \ldots + {}^2/_{2^k}\right)} \qquad \text{eqn 11}$$

where k is an integer selected by the user. If the data to be smoothed is not equally spaced in the independent coordinate (e.g. wavelength), the cubic spline routine can be used to interpolate. The smoothing routine can then be used to degrade the resolution of the spectrum. However, if the filter response is unusual, a special routine is needed. A more sophisticated smoothing routine convolves a high resolution spectrum to a low resolution spectrum (e.g. broadband photometry) by a numerical integration given the

(instrument + atmosphere + filter) weighted spectral response.

Many of our spectrophotometric studies use the moon as a calibration standard. Standard areas of the moon have been calibrated to the telescopic area of Appollo 16 using the reflectance of returned Apollo 16 soil samples (McCord et al., 1972, Adams and McCord, 1973, McCord et al., 1979). However, at wavelengths beyond 2μm, the thermal emission from the moon contaminates the reflectance spectra of the calibrated lunar areas. This is removed according to equation

$$R_o = \left(R'_o + \frac{R'_o(1-R_s)P_s}{R_s F} - \frac{P_o}{F}\right)\left(1 - \frac{P_o}{F}\right)^{-1} \qquad \text{eqn 12}$$

where R_o is the reflectance of the lunar (object) area with the thermal components removed, R'_o is the reflectance of the lunar area before the thermal components are removed, R_s is the reflectance of the lunar standard area (e.g. Apollo 16 with no thermal component (for Apollo 16, this would be the laboratory reflectance spectrum), P_o is the Planck function at the temperature of the lunar (object) area, P_s is the Planck function at the temperature of the lunar standard area, and F is the solar flux at the moon divided by the

quantity π. The corrections can be several percent at 2.5μm. See Clark (1979) for more details.

Other specialized routines include shifting channels left and right, sorting data into increasing wavelength order, Planck black body generation, merge two spectra into one data set, generation of a spectrum from line segments, edit a data set (for user input of data), spectrum-channel matrix transpose, (e.g. given spectra, defined as intensity versus wavelength, obtained at many air mass values, transpose the matrix to arrays of intensity versus airmass at many wavelengths) continuum fit (by curves scaling) and removal, and absorption band fit (reflection method). The last three routines were written by users and were easily added to the program since dummy subroutines have been placed in the program in anticipation of such additions.

Other programs which are interfaced to the main program are a non-linear least squares routine for analysis of 1 to 5 gaussian features (including a five term polynomial continuum) based on Kaper et al. (1966), and graph digitization using a graphics tablet. See Bevington (1969)

(Chapter 11) for a general discussion of non-linear least squares analysis.

III. PROGRAM ORGANIZATION

All user input is free format using FORTRAN read statements for each input line of 79 characters. Numbers are decoded from the character string. The command structure was designed such that control characters are freely mixed with numbers resulting in high flexibility and minimum typing for the user. Typically one entire line of commands may be entered for execution. If a mistake is encountered, the program asks the user to retype the command.

The current system allows 10,000 spectra online at any one time. These are located in five files, 3 on disc and 2 on magnetic tape, each containing a maximum of 2000 spectra. A spectrum is accessed by a single letter ID signifying one of the five files and the record number in the file.

Each spectrum record contains 256 real data numbers 32 bits long, plus a header which includes a 296 character manual history (for user comments and large program history requirements), a 60 character program automatic history, a 40 character title and 116 bytes of other information including siderial time, civil or universal time, R.A., Dec., integration time, date, air mass and

other parameters describing typical spectrophotometer data.

The user can select the file protection such as which files are read only, random access read and write, or combinations such as random access read but write sequentially with write protection on existing data as it is added to the file.

IV. HARDWARE AND SOFTWARE REQUIREMENTS

The program is currently about 19,000 lines of FORTRAN IV in length, the load module is 400,000 bytes and includes about 220 subroutines and represents about 3 man-years of work. The program is linked in an overlay structure containing 100 overlays and takes about 21,000 words to run on a Texas Instruments (TI) 980B, a 16 bit word machine. The TI overlay link editor requires 38K words to link the program.

The current hardware system includes a Hewlett Packard 2648A graphics terminal, 2 cipher (800 B.P.I.) nine-track magnetic tape drives, 12 megabytes of disc space (including the load module), a lineprinter, and a Gould 5200 printer-plotter. In the past, the program has used a Tecktronix 4010 storage graphics display.

V. IMPLEMENTATION OF OTHER SYSTEMS

The program is written in ANSI standard FORTRAN IV except for format conversions which the TI FORTRAN compiler accomplishes by writing to logical unit number -1. This could be changed to another number for conversions using a disc file on other systems. A few of the newer routines are written in Structured FORTRAN. The program can be made to run on other 16 bit machines with few modifications. Conversion to 32 bit machines would take more work and to 24 bit machines even more modifications due to the change in FORTRAN format statements and the change in the number of characters per word. In addition, new assign, and I/O routines may need minor modifications for other operating systems. The CRT graphics would require minimal modification for different graphics displays as only scaling factors would need changing to different screen resolutions. However, some text on graphics plots may need slight adjustments. The Gould plotting routines can be easily converted for use on a Calcomp plotter.

The disc space requirements are very flexible. The user can assign tape drives, the lineprinter, and disc files only when he needs

them (so they may be free for use by other people on the time-sharing system). The large disc files for spectra are not needed at all since processing could be performed from magnetic tape. The working data files could all be on floppy discs although the number of spectra on line would be greatly reduced.

VI. CURRENT USE AND FUTURE PLANS

The program has been used for about 7 hours a day, 7 days a week on the average over the last year. Approximately 25 papers which used the program for processing spectral data have been submitted to various journals during 1979. It is felt that this huge program has been worth the effort as it has changed the bottleneck in publication of data from the data reduction and analysis phases to the interpretation and paper writing phase.

Our laboratory is directly involved with the Galileo-NIMS spacecraft experiment and this program will be used in the resulting data analysis. We are currently analyzing spectra from many telescopic and spacecraft instruments which would be difficult and time consuming without a flexible program such as described here.

With our circular variable filter spectrometer which acquires a 120 point spectrum about every two minutes, we can reduce the data from start to the finished plots for publication in about the same time as it took to obtain the data. In the future, we plan to put the program on a Digital Equipment Corp. (DEC) LSI-11/2 or 11/23 minicomputer which will also control the spectro-

meter. We will then be able to process the data as it is taken at the telescope. Such rapid processing of the data will increase the science return and minimize inadvertently wasted telescope time.

ACKNOWLEDGEMENTS

I wish to thank Thomas B. McCord for encouraging this project and for providing the computer facilities and necessary resources to carry out this work. This was was supported by NASA grants No. 7323 and No. 7312.

REFERENCES

Adams, J.B. and McCord, T.B. 1973, Proc. Fourth Lunar Sci. Conf. 1, 163.

Bevington, P.R. 1969, Data Reduction and Error Analysis for the Physical Sciences. (New York: McGraw-Hill).

Carnahan, B. and Wilkes, J.O. 1973, in Digital Computing and Numerical Methods. (New York: Wiley and Sons), 307.

Clark, R.N. 1979, Icarus 40, 94.

Clark, R.N. and McCord, T.B. 1980, Icarus in Press. Thesis I Ch 1

Kaper, H.G., Smits, D.W., Schwarz, U., Takakubo, K. and Van Woerden, H. 1966, Bull. Astr. Inst. Neth, 18, 465.

McCord, T.B. and Clark, R. N. 1979, Pub. A.S.P 91, 571. Thesis App B

McCord, T.B., Charette, M.P., Johnson, T.V., Lebofsky, L.A. and Pieters, C. 1972, J. Geophys. Res. 17, 1349.

McCord, T.B., Clark, R.N. and Huguenin, R.L. 1978, J. Geophys. Res. 83, 5433.

McCord, T.B., Clark, R.N., McFadden, LA., Pieters, C.M., Owensby, P.D. and Adams, J.B. 1979, submitted to J. Geophys. Res.

Figure Caption

Figure 1 Spectrometry data from several authors and at several different spectral resolutions is shown for the Galilean satellite Europa from Clark and McCord (1980). This plot was completely generated by the program in about seven minutes. The user can choose the wavelength interval, scaling, data point type and size, whether or not to connect points or include error bars. The user can also input text at any angle of the plot.

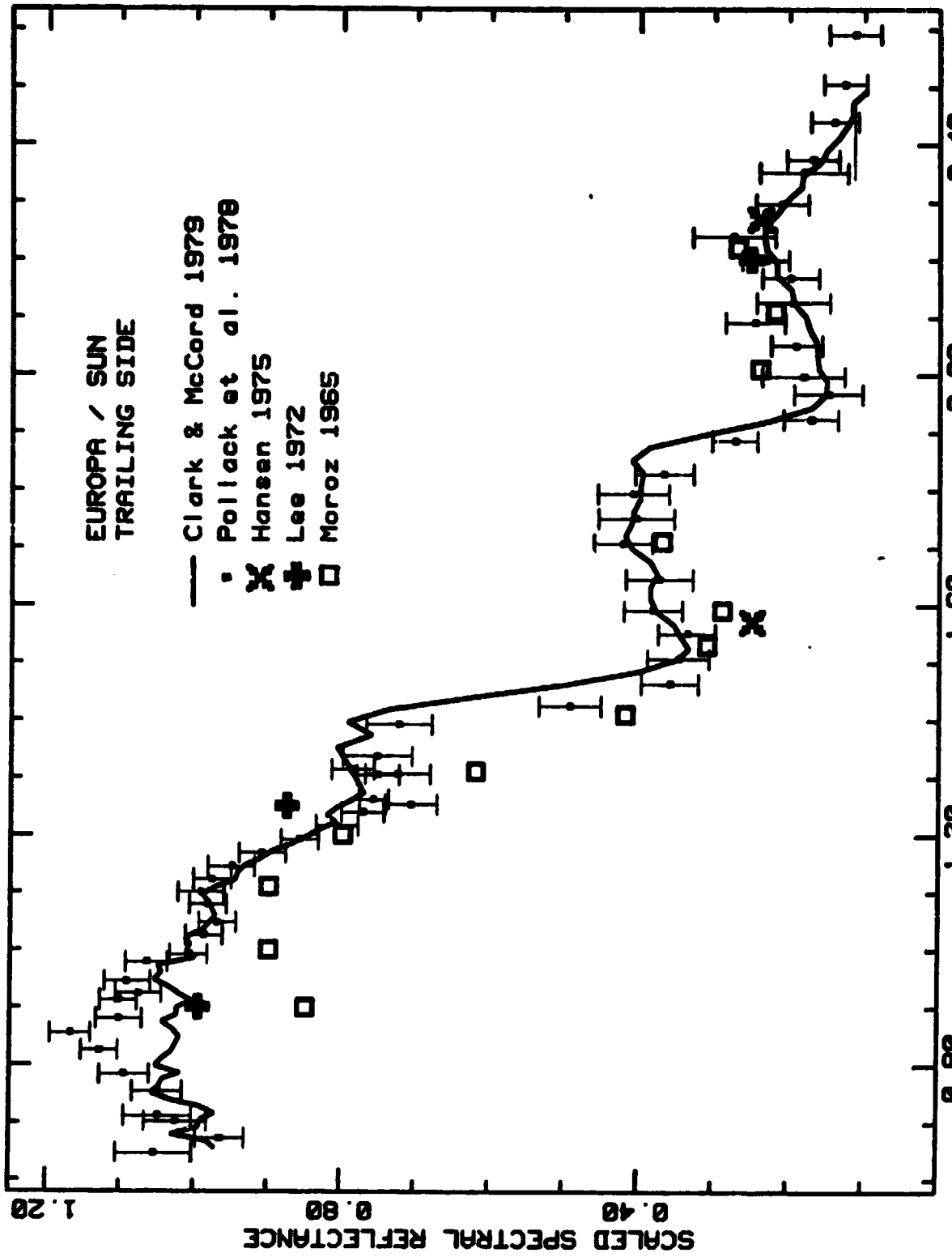

EUROPA / SUN
TRAILING SIDE
Clark & McCord 1979
Pollack et al. 1978
Hansen 1975
Lee 1972
Moroz 1965
SCALED SPECTRAL REFLECTANCE
0.40
0.80
1.20
WAVELENGTH IN MICRONS
0.80
1.20
1.60
2.00
2.40

Figure 1

APPENDIX B

Atmospheric Extinction 0.65-2.50 μm

Above Mauna Kea

Publications of the Astronomical Society of the Pacific
91:571–578, August 1979

ATMOSPHERIC EXTINCTION 0.65–2.50 μm ABOVE MAUNA KEA

THOMAS B. McCORD AND ROGER N. CLARK
Institute for Astronomy, University of Hawaii
Massachusetts Institute of Technology, Department of Earth and Planetary Science

Received 1979 March 19

Observations of the extinction in the spectral range 0.63 to 2.6 μm are presented for Mauna Kea Observatory. It is shown that high-quality photometric data can be obtained even in the intense 1.4 and 1.9 μm telluric water bands. Extinction coefficients (log intensity change per air mass) are presented with 1% spectral resolution.

Key words: extinction—observatories—photometry

I. Introduction

The ability of the terrestrial atmosphere to absorb radiation at certain energies is a well-known and, to the astronomer, an undesirable property. The astronomer must spend a significant fraction and sometimes the majority of his telescope time observing standard sources in order to calibrate out atmospheric extinction and its variations. At some energies and some observing sites, observations cannot be made at all because the extinction is so great.

We have obtained a considerable amount of data on the extinction above Mauna Kea (elevation 4205 meters) between the wavelengths of 0.65 and 2.55 μm, while carrying out spectrophotometric observations. We are publishing a representative sample of these data to give others an indication of the extinction to expect at these wavelengths and to illustrate some of the excellent properties of the Mauna Kea site. Morrison et al. (1973) presented extensive data on the Mauna Kea site in the visible and at infrared wavelengths of 10 μm and longer. This is the first description of extinction in the 0.6 to 2.5 μm region for Mauna Kea.

Extinction (as expressed in astronomy) is given by the relation

$$\log I = \log I_0 - Kx \quad , \tag{1}$$

where I_0 is the intensity outside the atmosphere, I is the corresponding intensity at the observer, x is the path length, and K is the absorption at a single wavelength (Hardie 1962). In magnitude form, equation (1) becomes

$$\begin{aligned} m_0 &= m - 2.5\,Kx \\ &= m - kx \quad . \end{aligned} \tag{2}$$

Thus K represents the absorption per unit path length for monochromatic light. The path length is normally defined in units of the air mass at the zenith of the observer.

II. Observations

A circular variable filter (CVF) spectrometer covering the spectral range 0.65–1.35 μm and 1.32–2.60 μm with about 1.25% resolution at the center of each range is used. The total number of spectral channels is 120. An Insb detector is used with a digital data handling system, and the entire spectrometer and entrance aperture is cooled to LN_2 temperature. The CVF is spun continuously with a period of 10 seconds and the spectrum is coadded, typically for 10 revolutions of the CVF on bright sources. Usually, when making spectrophotometric observations, a bright star or a well-defined area of the moon is observed at least every half hour through the air mass range of the object of scientific interest. The spectrometer and its use is described in more detail in McCord, Clark, and Huguenin (1978).

III. Data Reduction and Analysis

The series of spectra of standard objects is treated, using an interactive computer data reduction system we developed (Clark 1979), to derive extinction coefficients for every spectral channel according to the classical method. This consists of fitting a straight line to the log intensity versus air mass data using a least-squares analysis. The results of each step of the data reduction procedure can be observed on a terminal screen and the extinction coefficient can be displayed in several ways to demonstrate the quality of the observations. Poor observations can then be identified and deleted from the analysis if desired. The observations are treated according to the flow chart shown in Figure 1.

The interpretation of the results is different than in the classical method. Many water bands occur in the infrared portion of the spectrum, and at 1.4 and 1.9 μm these bands are very intense. High-resolution spectroscopy shows very detailed fine structure (e.g., Benedict, Bass, and Plyler 1954; and Woolf, Schwarzchild,

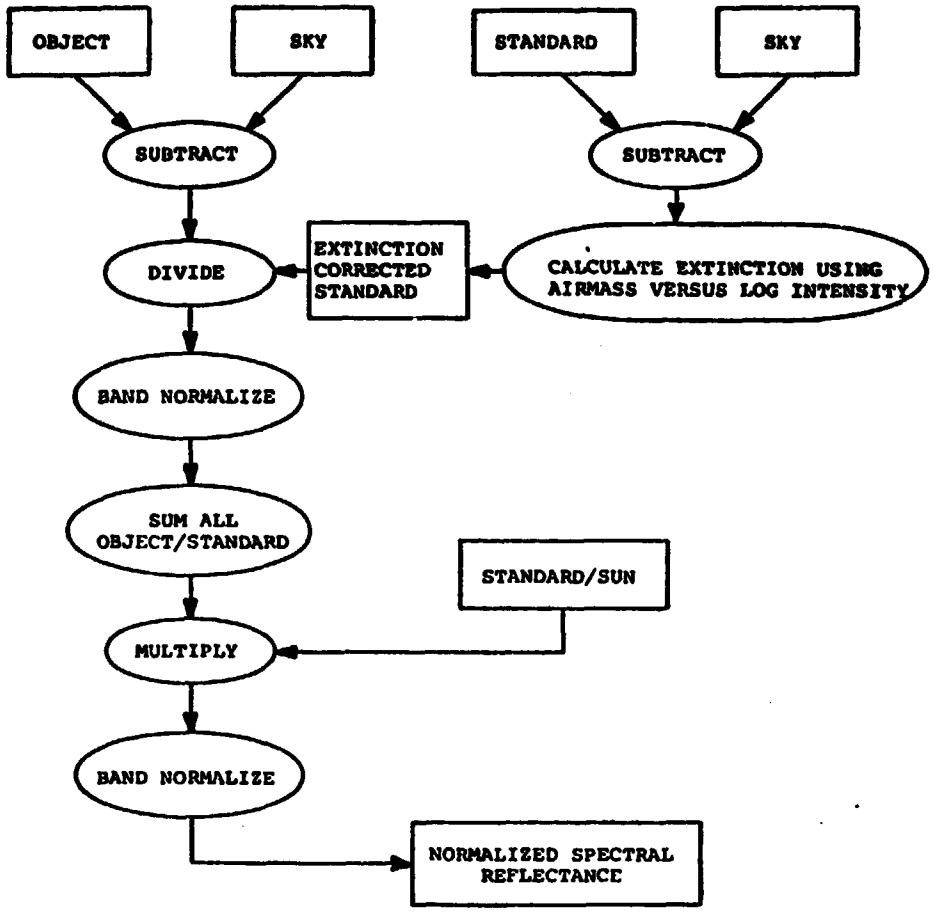


FIG. 1—The data reduction procedure is outlined in this flow chart. The interactive computer data reduction system (Clark 1979) is used to carry out the reduction and to display the results at several stages, if desired.

and Rose 1964), consisting of thousands of narrow absorption lines. Integrated over a hundred angstroms or more, these absorption features transmit a small amount of light if the atmospheric water content is sufficiently low. Since many of the fine structure lines are saturated, we cannot determine the intensity of a celestial object outside the earth's atmosphere in the classical manner as given in equation (1). Thus we modify equation (1) to the form:

$$\log I = \log A - Kx \quad , \tag{3}$$

where A is the intercept of the fitted line (the intensity value extrapolated to zero air mass) from the least-squares analysis of the data. Note that $\log A \neq \log I_0$ in the water-band regions due to the nonlinear effects of band saturation.

The periodic and random-band models (see Goody 1964) can be used to calculate the nonlinear effects in absorption features such as the 1.4 and 1.9 μm water bands. Hoard, Burch, and Williams (1956) found that the random-band model worked well in predicting the transmittance in the 1.1, 1.38, 1.87, 2.7, 3.2, and 6.3 μm water-absorption bands and derived an emperical fit to the theoretical equation of the form

$$I = I_0 \exp\left[\frac{-1.97\ \omega/\omega_0}{(1 + 6.57\ \omega/\omega_0)^{1/2}} \right] , \tag{4}$$

where ω is the absorber concentration (e.g., precipitable microns) and ω_0 is the absorber concentration necessary to give a 50% transmission at a given wavelength. The value of ω_0 is a function of wavelength and pressure. Outside of the absorption bands, ω_0 has a large value thus ω/ω_0 is small and

$$I = I_0 \exp[-1.97\ \omega/\omega_0] \tag{5}$$

In a strong absorption band ω_0 is small and the equation takes the form

$$I = I_0 \exp\left[\frac{-1.97}{6.57} (\omega/\omega_0)^{1/2} \right] \tag{6}$$

as ω/ω_0 becomes large.

If the range of absorber concentration is small enough, the log linear form of equation (3) is equal to equation (6) (within experimental errors) with suitable values of A and K. This is the case for atmospheric extinction observations varying from 1 to 4 air masses as shown in Figure 2. Equation (4) gives the departure from the pure exponential form of equation (1). As ω increases, the intensity will decrease less rapidly than the pure exponential. Thus extrapolating a high air mass observation log-linearly to a low air mass observation will result in an intensity lower than the true value. This is the reason the intercept, A, from equation (3) is not equal to I_0 from equation (1) and thus why we see absorption features in the intercept spectrum in Figure 3. Extinction corrections can then be performed by obtaining the slope $(-K)$ and intercept (A) of a straight line fitted to the log intensity versus air mass plot since the air mass range is not great enough for the band saturation effects (ω/ω_0 becoming large) to depart significantly from the equation (3) log-linear relationship. This assumes that the amount of absorbing materials in the sky does not change with time or azimuth. The results reported here were taken on one such "stable" night.

IV. Results

Figure 3 shows the signal from the star β Gemini at two different air masses as determined from the derived extinction parameters. The intercept, A, still shows very strong H_2O absorption features at 0.95, 1.14, 1.4, and 1.9 μm. Note that we cannot distinguish between apparent absorptions in the intercept spectrum due to the earth's atmospheric or absorptions in the telescope and spectrometer. Thus we cannot determine absolute atmospheric transmittance unless we first determine the telescope-spectrometer response. Figure 4 shows the change in absorption with air mass $(-K)$. Apparent in this spectrum are water absorptions at 0.95, 1.14, 1.4, and 1.9 μm; O_2 at 0.76 μm; and CO_2 at 2.02 μm. The minimum slope in this wavelength region occurs at 1.03 μm with a value of -0.0027/air mass. This is an absorption of about 0.6% at one air mass.

Successful extinction corrections are obtained by dividing the observed object spectrum by the standard spectrum computed from the derived extinction parameters to the same air mass as the object:

$$I_b/I_s = I_b/(A10^{-Kx}) \quad , \qquad (7)$$

where I_b is the intensity of the object at air mass x, I_s is the intensity of the standard computed to air mass x using the slope $(-K)$ and intercept A of the extinction parameters. Examples are shown in Figures 5 and 6. Figure 5 is a reflectance spectrum of Mars from McCord et al. (1978) obtained using the β Gem extinc-

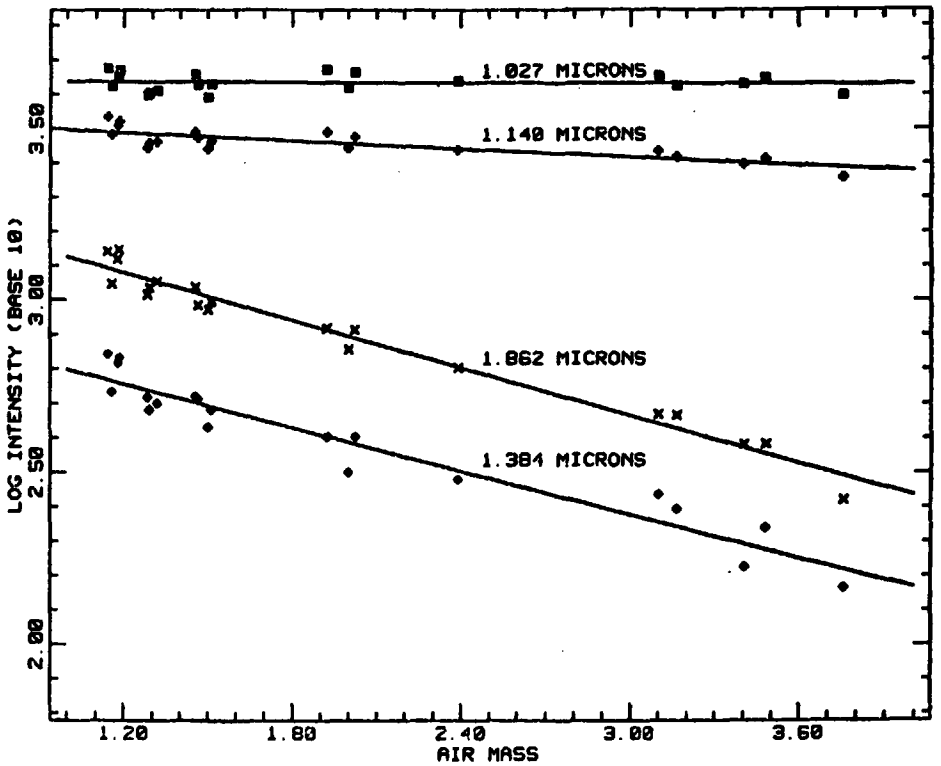


FIG. 2—The air mass versus log intensity is shown at four wavelengths for the β Gem data. The lines represent the least-squares fit. The slope of the line is $-K$ and the intercept at zero air mass is log(A) (see text).

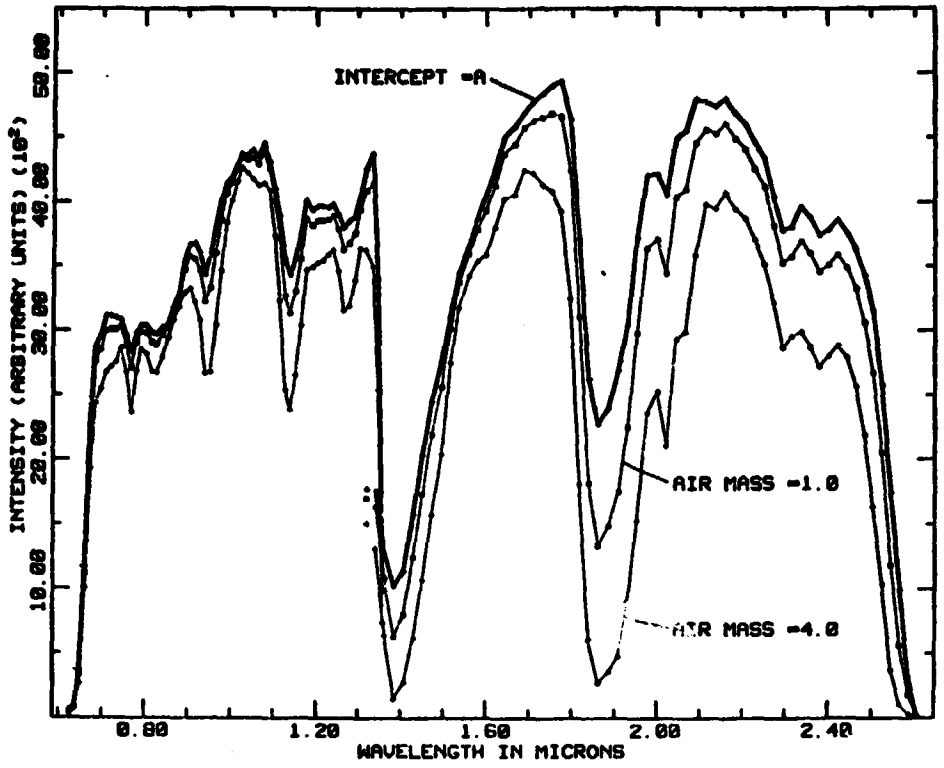


FIG. 3—Beta Gem spectrum is computed from the derived extinction values (slopes from Fig. 2 and intercepts) are shown for two different air mass values. Instrument transfer characteristics are still present as are the effects of saturated absorption lines.

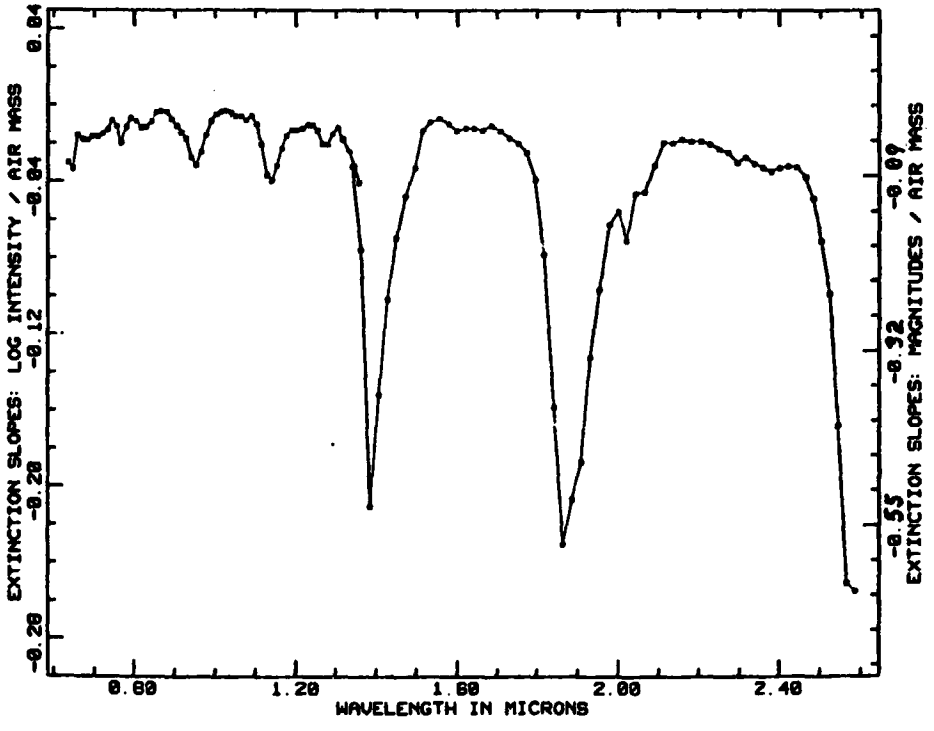


FIG. 4—The slopes ($-K$) of the least-squares line fitted to the air mass versus log intensity data. Ten raised to the $-K$ power gives the decrease in intensity per air mass or $-2.5\,K$ ($\cong -k$) gives the change in intensity per air mass in stellar magnitudes.

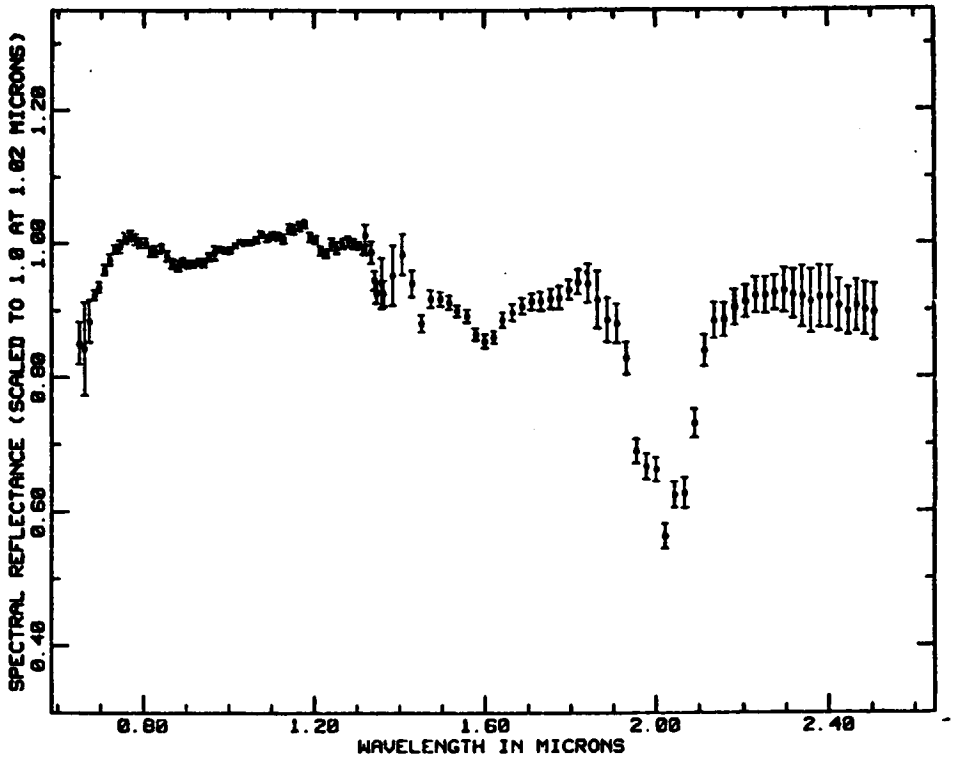


FIG. 5—Martian integral disk reflectance from McCord et al. (1978) shown after correction for telluric absorptions. Note the error bars are larger at 1.4 and 1.9 μm. The absorption at 1.35 μm is real, and is due to atmospheric CO_2 on Mars; it is not an error in removal of telluric H_2O.

tion parameters presented in this paper. The large 2 μm feature is due to Martian atmospheric CO_2 as are the smaller features at 1.3 and 1.6 μm. Errors in telluric water removal are apparent by the slightly larger error bars around 1.4 and 1.9 μm. The extinction parameters were determined from 20 observations on 1976 April 21 using the Mauna Kea Observatory 2.24-m telescope over an air mass range of 1.14 to 3.76.

Figure 6 shows an excellent example of the removal of telluric absorptions. This was done by dividing by the spectrum of a standard area in the lunar crater Copernicus. The reflectance of this standard area, labeled MH0 (for Mare Humorium 0) is known through the Apollo 16 telescopic and laboratory samples (see McCord et al. 1978, 1979*a*,*b*). A β Gem/MH0 ratio was also determined in the same night (1976 April 30). From this, we obtained the Mars/sun ratio via Mars/β Gem ratio. Thus, in order to obtain the Martian spectral reflectance, we had to obtain extinction corrections through four ratios: Copernicus floor/Apollo 16, MH0/Copernicus floor, β Gem/MH0, and Mars/β Gem. The results show that high-quality data can be obtained on Mauna Kea even through the intense 1.4 and 1.9 μm water bands.

These examples also show one motivation for obtaining accurate narrow-band extinction corrections at these wavelengths. Note in Figures 5 and 6, there are absorptions in the reflectance spectrum of areas of the moon and Mars (and other solid solar-system objects) which are weak but which yield a great deal of information about surface composition. The absorptions are due to electronic transitions and they are directly related to the surface mineralogy (e.g. McCord et al. 1979*a*,*b*). The weakness of the absorptions required accurate measurement and calibration.

V. Discussion

In the two years of performing extinction calculations using data from the CVF spectrometer, we have seen a large variation in water content in the atmosphere. The first observing run (April 1976) was so successful that we thought it was easy to perform extinction corrections in this region. The following observing runs proved otherwise. We had intended to publish seasonal variations of the extinction slopes, but we have found that it is not practical. The quality of the observations is highly dependent on the stability of the weather system near the observatory. An approaching storm front (still a couple of hundred miles away) can totally destroy any attempt to derive extinction parameters in the deep water bands. On nights that are fairly stable, the extinction parameters at Mauna Kea

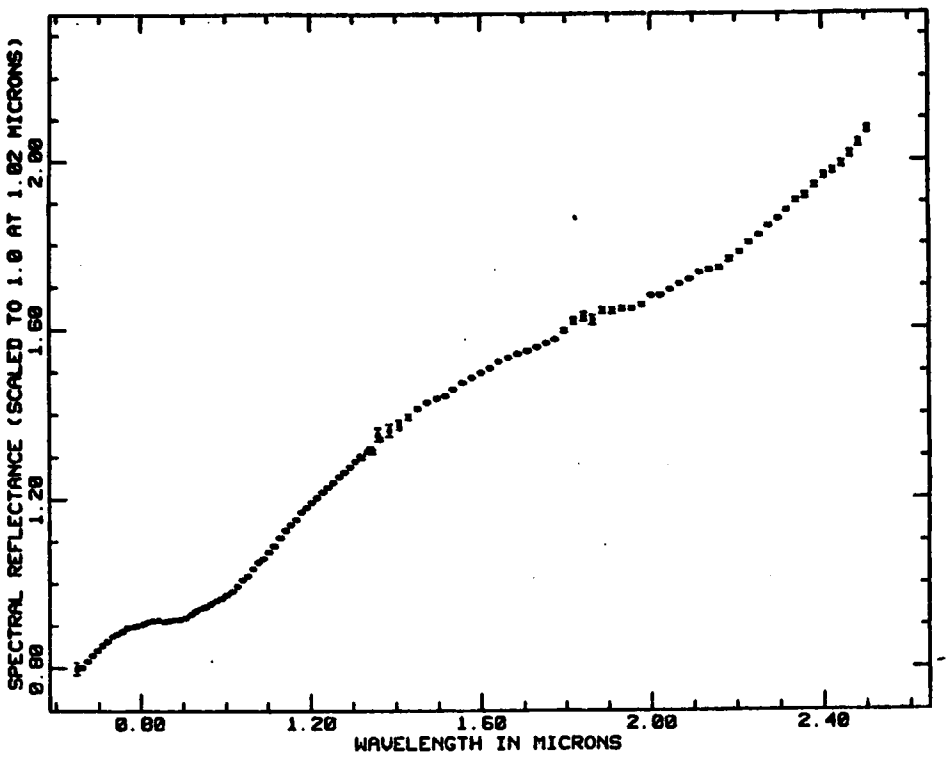


FIG. 6--The spectral reflectance of an area in Mare Humorium on the Moon (McCord et al. 1978, 1979*b*) showing the excellent cancellation of telluric absorptions. The error bars, though too small to be visible on most of the data points, increase at 1.4 and 1.9 μm.

are similar to those published here but the magnitude of the extinction slopes and intercept absorptions vary from night to night.

When obtaining data in the water bands, it is very important, of course, to observe the object and standard as closely as possible in both space and time. For the Mars observations reported here, Mars and β Gem were only 8 degrees apart, and the cycle of Mars, sky, β Gem, sky observations took 30 to 40 minutes. Our recent experience has shown that this time is an upper limit and should probably be cut in half. Our lunar measurements have turned out very well (Fig. 6) because the lunar area and lunar standard are less than 0.5 degree apart and we typically observe two to three lunar areas, the lunar standard and sky every 15 to 20 minutes. Many of our lunar observations have not even required an extinction correction! A carefully planned observing run with good weather can yield useful data down to 3.5 or 4 air masses (e.g. McCord and Clark, 1979) at Mauna Kea. At lower elevations, the water content of the atmosphere is much greater. Data taken at the MIT Wallace Observatory (elevation 100 meters) typically have a transmission in the 1.4 and 1.9 μm water bands between zero and 2% for several of our spectral channels.

REFERENCES

Benedict, W. S., Bass, A. M., and Plyler, E. K. 1954, *N.B.S.J. Res.* 52, 161.

Clark, R. N. 1979, *Pub. A.S.P.* (submitted). Thesis App A

Fink, U., Benner, C. D., and Dick, K. A. 1977, *J.Q.S.R.T.* 18, 447.

Goody, R. M. 1964, *Atmosperic Radiation* (Oxford: Clarendon Press).

Hardie, R. H. 1962, in *Photoelectric Reductions in Astronomical Techniques*, W. A. Hiltner, ed. (London: University of Chicago Press), p. 178.

Howard, J. N., Burch, D. E., and Williams, D. 1956, *J. Opt. Soc. Am.* 46, 334.

McCord, T. B., and Clark, R. N. 1979, *J. Geophys. Res.* (in press).

McCord, T. B., Adams, J. B., and Huguenin, R. L. 1979*a*, *Space Sci. Rev.* (submitted).

McCord, T. B., Clark, R. N., and Huguenin, R. L. 1978, *J. Geophys. Res.* 83, 5433.

McCord, T. B., Clark, R. N., McFadden, L., Pieters, C. M., and Adams, J. B. 1979*b*, *J. Geophys. Res.* (submitted).

Morrison, D., Murphy, R. E., Cruikshank, D. P., Sinton, W. M., and Martin, T. Z. 1973, *Pub. A.S.P.* 85, 255.

Woolf, N. J., Schwarzschild, M., and Rose, W. K. 1964, *A.J.* 140, 883.